THE STRUCTURE, STRATIGRAPHY AND STRAIN HISTORY

OF

THE SEINE GROUP AND RELATED ROCKS

NEAR

MINE CENTRE, NORTHWESTERN ONTARIO

by

Paul Anthony Jackson

Submitted in partial fulfillment

of the requirements for the degree of

Master of Science

Faculty of Science
Lakehead University
Thunder Bay, Ontario, Canada

April, 1982

ABSTRACT

One or possibly two overlapping periods of deformation are responsible for the structures observed in the rocks in the Seine River area. This deformation has resulted in the formation of tight to isoclinal, non-plane approximately cylindrical major F_1 folds with steeply dipping E-W striking axial surfaces. A late stage deformation has resulted in the formation of a crenulation cleavage, kink bands and minor faulting. There is also limited evidence of a possible pre-F_1 folding event.

Two major lithological groups are present in the study area: shallow water metasedimentary rocks of the Seine Group and metavolcanic rocks. The Seine Group metasedimentary rocks are younger than the metavolcanic rocks in the western part of the area but may be older than similar metavolcanic rocks in the eastern part of the area. Two ages of metavolcanic rocks therefore appear to be present: older metavolcanic rocks in the west which underlie the Seine Group, and younger metavolcanic rocks in the east which overlie the Seine Group.

Regional metamorphism to the chlorite to biotite zone greenschist facies was synkinematic with the deformation of the rocks but may have outlasted the folding in places.

Strain analysis from the metasedimentary rocks reveals that the conglomeratic units are more intensely strained than arenite units, although all the strain ellipsoids are of the flattened ($K < 1$) type.

Average shortening in Z ranges from 52% for arenite units to 75% for conglomerate units. A new empirical approach suggested by the writer and Dr. Borradaile for assessing competence contrasts between strain markers and matrix is outlined. This method uses the effects of competent markers on cleavage traces in the matrix of conglomerates.

ACKNOWLEDGEMENTS

This thesis was supervised by Dr. G. J. Borradaile and supported by N.S.E.R.C. grant #A6861 to Dr. G. J. Borradaile; Dr. M. M. Kehlenbeck acted as adviser. Dr. Borradaile visited the author on several occasions in the field, once with Dr. Kehlenbeck. Dr. Borradaile is thanked for his instruction and help in making some preliminary measurements of deformed pebbles and for photographs from which measurements were made. The Seine River Indian Band, in particular, Band Chief Mr. A. Potson, is thanked for permission to work on the Seine River Indian Reserve. Dr. M. Bartley is thanked for his help in arranging this. Sam Spivak provided invaluable advice with drafting problems and helpful criticism.

Many thanks to Taina Baker for typing the manuscript so well.

TABLE OF CONTENTS

	Page
ABSTRACT	i
ACKNOWLEDGEMENTS	iii
INTRODUCTORY STATEMENT	1
CHAPTER 1	
PREVIOUS STUDIES AND AIMS AND OBJECTIVES OF THIS STUDY	2
REGIONAL SETTING	2
PREVIOUS STUDIES	4
AIMS AND OBJECTIVES OF THIS STUDY	7
CHAPTER 2	
STRUCTURE	10
S-SURFACES	10
LINEATIONS	12
YOUNGING INDICATORS	14
1. Sedimentary Rocks	14
2. Pillow Lava	14
MINOR FOLD ASYMMETRY	18
BEDDING-CLEAVAGE RELATIONSHIPS AND STRUCTURAL FACING	18
Application of Techniques: Results of Structural Survey	24
GEOMETRIC RELATIONSHIP BETWEEN S_1 CLEAVAGE AND FOLDING	24
1. Minor Folding	26
2. Intersection Lineations	26
RELIABILITY OF YOUNGING INDICATORS	35

Major Structures 36

MINOR FAULTING AND SHEAR ZONES 36

F_2 STRUCTURES 38

F_1 STRUCTURES 40

Regional Setting of Structural Geology 42

CHAPTER 3

PETROGRAPHY, STRATIGRAPHY AND METAMORPHISM 46

CLASTIC SEDIMENTARY ROCKS 46

(a) Conglomerate 48

- Matrix 48

- Clasts 49

(b) Medium- to Fine-Grained Clastic Sedimentary Rocks 50

(i) Fine-Grained and Argillaceous Sedimentary Rocks 51

(ii) Medium- to Coarse-Grained Arenites 51

- Lithic to Arkosic Greywackes 51
- Medium- to Coarse-Grained Arkoses 52
- Chloritic Greywackes 52

IRON FORMATION 53

VOLCANIC ROCKS 53

INTRUSIVE ROCKS 55

Stratigraphic Relations 55

Metamorphism 58

CHAPTER 4

STRAIN ANALYSIS TECHNIQUES IN CONGLOMERATIC ROCKS 60

DEFORMATION OF NON-SPHERICAL OBJECTS 60

THE R_f/ϕ METHOD OF STRAIN ANALYSIS 63

ELIMINATION OF INITIAL SHAPE FACTOR, R_o 63

MODIFICATIONS OF THE R_f/ϕ TECHNIQUE OF STRAIN ANALYSIS 66

THETA-CURVE METHOD 68

Initial Orientation of Markers 71

Ductility Contrasts 75

(a) Pure Shear Deformation 76

(i) Ellipse Axes Parallel to Strain Axes 76

(ii) Ellipse Axes Not Parallel to Strain Axes 77

(b) Simple Shear Deformation of Elliptical Objects 79

Application of Effects of Ductility Contrasts 82

STRAIN ANALYSIS OF MARKERS OF ANY SHAPE 83

APPROXIMATION TECHNIQUES 85

CHAPTER 5

RESULTS OF STRAIN ANALYSIS 92

APPLICATION OF STRAIN ANALYSIS TECHNIQUES 113

RESULTS 116

Relationship of Strain Ellipsoid Orientation to Major Folds 123

Limitations of Strain Analysis Methods Used 128

DISCUSSION 129

CONCLUSIONS 132

APPENDIX A

DEFORMATION OF CROSSBEDDING AND TROUGH-CROSSBEDDING 134

APPENDIX B

ORIENTATION PLOTS 142

CONGLOMERATE 143

ARENITE 188

REFERENCES 254

LIST OF TABLES

		Page
Table 1-1	Summary of stratigraphic relations from previous workers.	8
Table 2-1	N.T.S. Grid references for localities referred to in the text.	20
Table 5-1a	N.T.S. Grid references for strain localities.	94
Table 5-1	Conglomerate strain ellipsoid ratios.	117
Table 5-2	Sandstone strain ellipsoid ratios.	118
Table 5-3	Restoration of bedding planes.	121
Table 5-4	Results of strain analysis-conglomerate.	126
Table 5-5	Results of strain analysis-sandstone.	127

LIST OF FIGURES

		Page
Figure 1-1	Regional Geological Map.	3
Figure 1-2	Summary of areas studied previously by other authors.	5
Figure 2-1	Effect of competent clast on cleavage traces.	11
Figure 2-2	Minor fold in S_o.	13
Figure 2-3	Crossbedding in Siltstone.	15
Figure 2-4	Crossbedding in Sandstone.	16
Figure 2-5	Younging directions from Pillow lava.	17
Figure 2-6	Outcrop location map.	19
Figure 2-7	Bedding-Cleavage relationships and Minor Fold asymmetry.	21
Figure 2-8	Structural Facing.	23
Figure 2-9	Bedding-Cleavage relationships and transecting cleavage.	25
Figure 2-10	Minor fold in S_o.	27
Figure 2-11	Minor fold in S_o.	28
Figure 2-12	Distribution of Intersection Lineations with axial planar cleavage and transecting cleavage.	29
Figure 2-13	Stereographic projections of F_1 data.	31
Figure 2-14	Stereographic projections of F_1 Linear data.	33

		Page
Figure 2-15	Variation in orientation of Intersection lineation with inaccuracies in S_o and S_1 dip measurements.	34
Figure 2-16	Distribution and orientation of F_2 structural data.	37
Figure 2-17	Stereographic projection of F_2 linear data.	39
Figure 2-18	Hypothetical model to explain downwards Facing Structures in study area.	43
Figure 3-1	Classification of non-carbonate fragmental deposits.	47
Figure 3-2	Classification of Sandstones.	47
Figure 3-3	Aeromagnetic map of the Wild Potato Lake area.	54
Figure 4-1→4-3	Deformation of randomly oriented elliptical objects.	61
Figure 4-4	R_f/ϕ plot for homogeneously deformed ellipses.	65
Figure 4-5	Theoretical R_f/ϕ plots of Dunnet (1969).	65
Figure 4-6	Theoretical θ-curves of Lisle (1977a).	70
Figure 4-7	R_i/θ and R_f/ϕ plots for non-randomly oriented elliptical objects.	73
Figure 4-8	Curves for passive pure shear deformation of ellipses.	73
Figure 4-9	Variation in axial ratio of a non-rigid, initially circular particle during pure shear.	78

		Page
Figure 4-10	Pure shear deformation paths for ellipses with initially 2:1 axial ratios aligned at 45° to the Y' strain axis.	80
Figure 4-11	Simple shear deformation paths for initially circular, non-rigid particles.	81
Figure 4-12	Uniform model of Lisle (1977b) for deformation of elliptical markers.	86
Figure 4-13	Random model of Lisle (1977b) for deformation of elliptical markers.	87
Figure 4-14	Errors involved in using harmonic mean method.	87
Figure 4-15	Orientation fields of deformed markers.	90
Figure 4-16	Flinn diagram for method of Lisle (1979).	90
Figure 5-1	Strain station Location map.	93
Figure 5-2	Indentation relationships between pebbles.	97
Figure 5-3	Determination of shortening for the matrix using Method of Borradaile (1981).	99
Figure 5-4	Determination of competence contrast between competent clast and matrix.	99
Figure 5-5→5-16	Effects of competent clasts on the deformation of a ductile matrix.	100
Figure 5-17	Effects of intermediate volcanic and rhyolite clasts on deformation of matrix.	114
Figure 5-18	Flinn plot.	120
Figure 5-19	Restoration of deformed bedding.	122
Figure 5-20	Stretching Lineation orientations in map area.	124
Figure Ap.-1	Simple shear deformation of troughbedding.	136

		Page
Figure Ap.-2	Pure shear deformation of troughbedding and crossbedding.	137
Figure Ap.-3	2-D deformation of pillow lava by homogeneous pure shear strain.	138
Figure Ap.-4	Effects of deformation on crossbedding.	140
Figure Ap.-5	Effects of deformation on trough-bedding.	141
Figure Ap.-6	Structural Map.	
Figure Ap.-7	Schematic Structural Block diagram.	

LIST OF APPENDICES

		Page
Appendix A	Deformation of Crossbedding and trough-crossbedding.	134
Appendix B	Orientation Plots.	142

INTRODUCTORY STATEMENT

Although the geology in the region of the Seine River area, particularly to the west at Rainy Lake, has been subject to repeated studies throughout the last 95 years, very little work has been conducted directly in the present study area. Further, no structural survey has been carried out prior to this study.

The study area is located approximately 250 kilometres west of Thunder Bay along Highway 11 and is underlain by Archean rocks of the Superior Structural Province of the Canadian Shield. The purpose of this study is twofold: firstly, to unravel the structural geology of the area and thereby add useful data which may help to resolve some of the stratigraphic problems which persist; secondly, to deduce the strain history of the rocks.

CHAPTER 1

PREVIOUS STUDIES AND AIMS AND OBJECTIVES OF THIS STUDY

REGIONAL SETTING

The study area is bounded by two major geological subprovinces or belts of the Superior Province of Northwestern Ontario: the Wabigoon volcanic-plutonic "greenstone" belt to the north and the Quetico gneiss belt to the south (Fig. 1-1). In this region two important faults, the Quetico Fault and the Seine River Fault separate areas of distinctly differing lithology, structural style and metamorphic grade. To the north of the Quetico Fault (Fig. 1-1), metavolcanic rocks and granitoid intrusions predominate while to the south of the Seine River Fault deep water metasedimentary rocks of medium to high metamorphic grade are exposed - these are the 'Quetico' or 'Southern' sediments of the Quetico subprovince. Between the Quetico Fault and the Seine River Fault low grade metavolcanic rocks, which have been correlated by many authors with the Keewatin of Lawson (1888) at Rainy Lake, are intruded by anorthosite and gabbro. These are in turn intruded by granitic rocks, the Laurentian of Lawson (1913). A sequence of low grade, highly-deformed shallow water metasedimentary rocks also occur in the area bounded by the two faults, the study of which forms the basis of this thesis. These rocks are the 'Seine' Group of Lawson (1913). The Quetico Fault and the Seine River Fault merge to the east to form boundaries of the study area.

Fig. 1-1 Regional Geological Map of the Mine Centre area. The study area is bounded by the Quetico Fault and the Seine River Fault.

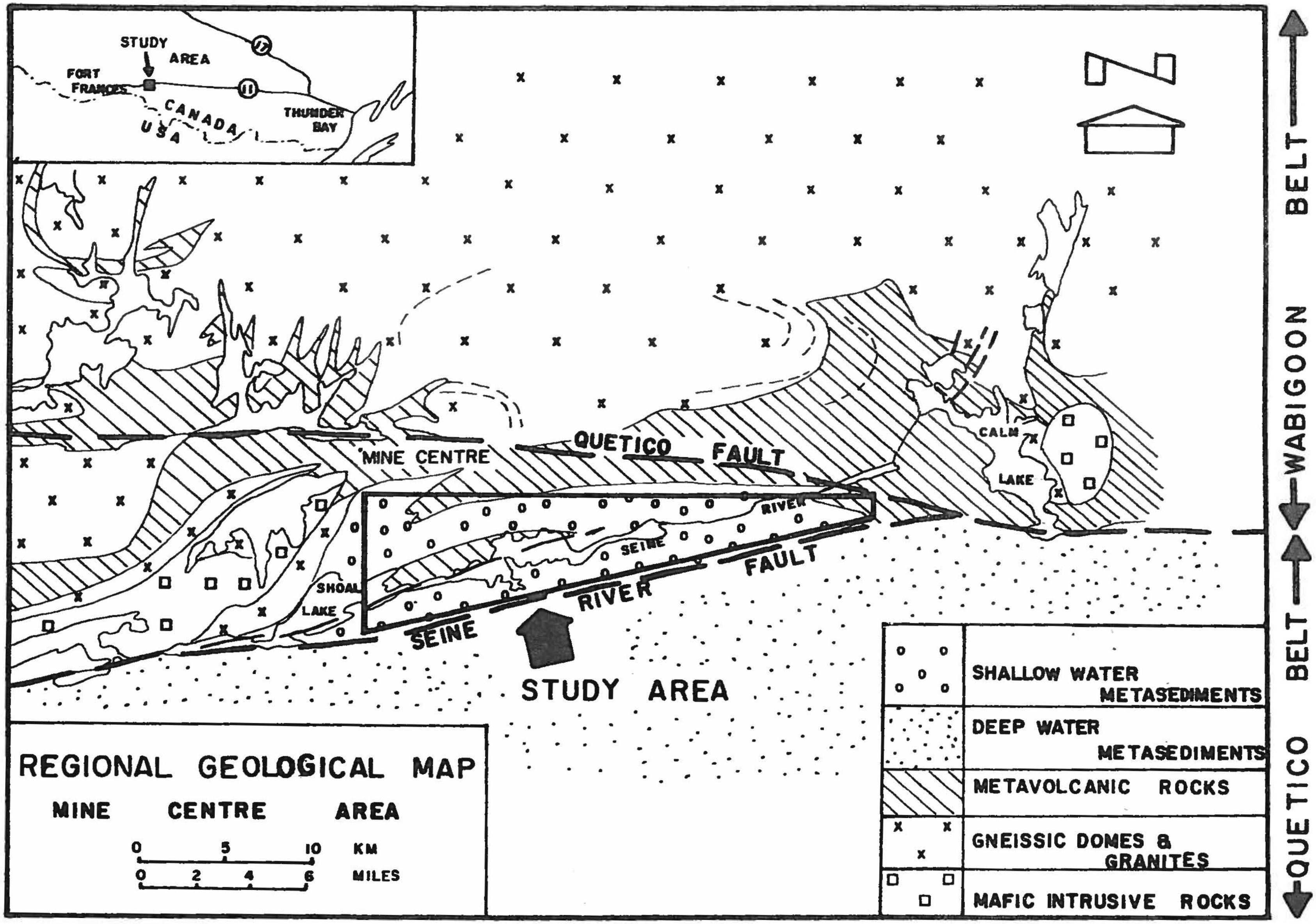

STUDY AREA
FORT FRANCES
CANADA
USA
THUNDER BAY
N
QUETICO FAULT
MINE CENTRE
CALM LAKE
RIVER
SEINE
FAULT
SHOAL LAKE
SEINE RIVER FAULT
STUDY AREA
REGIONAL GEOLOGICAL MAP
MINE CENTRE AREA
0 5 10 KM
0 2 4 6 MILES
SHALLOW WATER METASEDIMENTS
DEEP WATER METASEDIMENTS
METAVOLCANIC ROCKS
GNEISSIC DOMES & GRANITES
MAFIC INTRUSIVE ROCKS
WABIGOON BELT
QUETICO BELT

PREVIOUS STUDIES

Very little work has been conducted directly in the study area and only that of Hsu's (1971) encompasses the whole of the present map area. Figure 1-2 shows the area covered by Hsu as well as the areas covered by other workers previously. The area of the present study is identified by a stipple pattern.

Most of the established geological nomenclature in the region can be attributed to Lawson (1888 and 1913) who carried out much of the initial work in the Rainy Lake area, some 40 km to the west of the present study area, and also (1913) in the western part of the present study area.

He distinguished three major stratigraphic groups:

1. the Coutchiching Group which comprises a thick sequence of metasedimentary mica schists and which he considered to be the oldest rocks in the area,
2. the Keewatin Group which is composed of metavolcanic rocks and was considered by Lawson as younger than the Coutchiching,
3. the Seine Group which consists of shallow water metasedimentary rocks and were thought by Lawson to be unconformable on all the other rocks.

Lawson recognized that the granitic plutonic rocks in the area were of different ages. He concluded that the extensive exposures of Laurentian granite and granite-gneiss were intrusive into both the Coutchiching and the Keewatin. On the other hand, Lawson considered the Algoman plutons of quartz monzonite to granodiorite to be younger than the Seine Group.

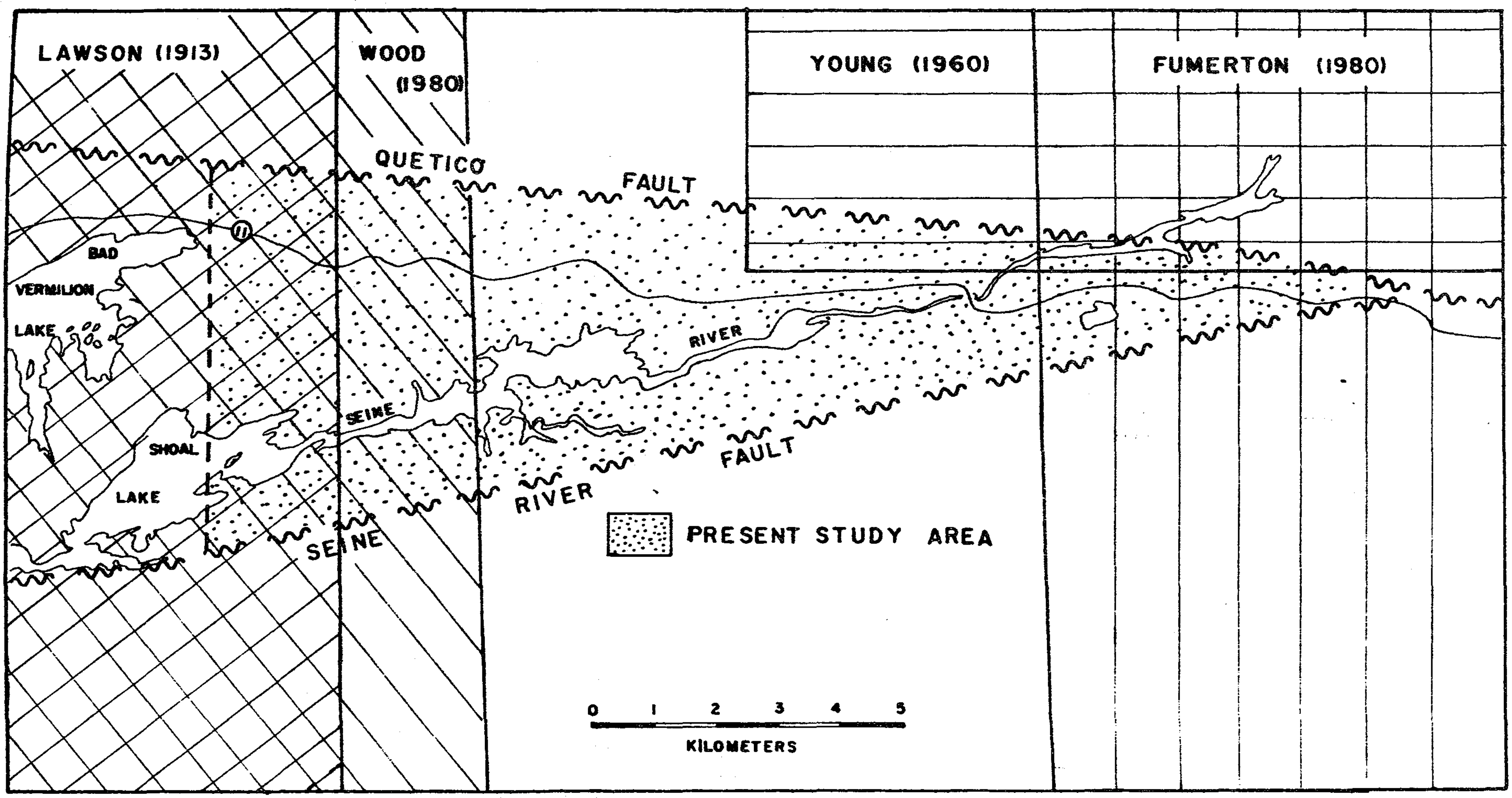

Fig. 1-2 Area Studied by Hsu (1971). Also shown are the areas covered by other workers previously.

Although the terms 'Coutchiching' and 'Keewatin' were used by Lawson in 1888 to describe the lithological units at Rainy Lake, he used the name 'Seine Group' in 1913 to describe the metasedimentary rocks in the present study area. In doing so he correlated the metavolcanic rocks in the present study area with the Keewatin at Rainy Lake and the metasedimentary rocks south of the Seine River Fault with the Coutchiching, which are exposed north of the Seine River Fault at Rainy Lake.

Subsequent work (Poulsen et al., 1980) has revealed that, in the Rainy Lake area, the Coutchiching metasedimentary rocks structurally underlie the Keewatin metavolcanic rocks although they are in fact younger.

Young (1960) working to the east of the present study area (Fig. 1-2) has proposed that the metavolcanic rocks there, which he calls Keewatin, are actually younger than the Seine metasedimentary rocks. He also suggests that there is a genetic relationship between the Seine Group and the metavolcanic rocks. Young suggests that the Seine Group is volcanic in origin and that it represents a sheared volcanic tuff-breccia. He proposes that the finer detrital rocks were incorporated during the time of deposition of the tuffaceous rocks. Young combines the Seine Group and metavolcanic rocks as one formation in which the Seine is considered to be the lowermost member in the area.

Hsu (1971) has suggested that the Coutchiching metasedimentary rocks are older than the Keewatin metavolcanic rocks and that the Seine Group lies stratigraphically between these two. Hsu combines the Coutchiching metasedimentary rocks (Lawson) and the Seine Group as a single formation and regards the Seine as the upper member. Hsu also suggests that deformation, metamorphism and development of penetrative cleavage in the conglomerates of the Seine group post-date folding.

Fumerton (1980), in a provisional report of the same area as that of Young (1960), has distinguished two groups of metasedimentary rocks north of the Seine River Fault. He makes the following correlations:

1. low grade metasedimentary rocks which correspond to the Seine Group of Lawson (1913),
2. medium grade metasedimentary rocks which lie to the north of the present study area. These, according to Fumerton, stratigraphically overlie the metavolcanic rocks and are also tentatively correlated by Fumerton with the Seine Group. Therefore Fumerton disagrees with Young and suggests that the Seine Group here is younger than the metavolcanic rocks.

Wood (1980) mapped in the western part of the study area (Fig. 1-2). He agreed with Lawson's view that the Seine Group unconformably overlies all other rocks in the study area. Wood's interpretation is based on an unconformable contact southeast of Bad Vermillion Lake and north of Shoal Lake (to the west of the present study area). These relationships were also described by Lawson in 1913. Here, according to Wood, conglomerates of the Seine Group overlie subvolcanic granitic rocks and felsic metavolcanic rocks.

These various interpretations are presented in Table 1-1.

AIMS AND OBJECTIVES OF THIS STUDY

From the review of previous studies in and about the present study area, two important considerations emerge:

1. the relative stratigraphic position of the metavolcanic rocks within

TABLE 1-1 - Relative stratigraphic positions of metasedimentary and metavolcanic rocks as interpreted by previous workers

LAWSON (1913)	YOUNG (1960)	HSU (1971)	FUMERTON (1980)	WOOD (1980)	POULSEN ET AL. (1980) (Rainy Lake area)
Seine Group ---	---	---	Seine Group ---	Seine Group	
-unconformity-				-unconformity-	
Keewatin Group ---	{Keewatin Group Seine Group}---	Keewatin Group ---	Keewatin Group ---	Keewatin Group	Coutchiching Group
Coutchiching Group ---	---	{Seine Group Coutchiching Group}			Keewatin Group

this area with the Seine Group is a matter of some controversy.

2. no structural study has been made of the area to date.

The work of Poulsen et al. (1980) in the Rainy Lake area appears to have resolved the Coutchiching-Keewatin problem, at least in that region. However, whether or not the metavolcanic rocks in this study area can be correlated with the Keewatin metavolcanic rocks at Rainy Lake is dubious. Also, no rocks which can be directly traced into the Coutchiching rocks are exposed in the study area. In view of this, the problem of the relative age of the Seine Group and the Coutchiching is left out of this study.

In an area where the rocks are as intensely deformed as those in the present study area, no stratigraphic study can possibly be carried out unless the structure is well understood first. Therefore, this study deals primarily with elucidating the structure of the Seine Group with a view towards contributing some useful data to the stratigraphic problems outlined above. The second half of the study is concerned with the strain of the rocks in the area.

CHAPTER 2

STRUCTURE

Various structural elements were observed in the field and recorded. These include S-surfaces, lineations, minor fold asymmetry, bedding-cleavage relations, younging indicators and structural facing directions.

S-SURFACES

Two types of S-surface are commonly observable in outcrops: bedding in the sedimentary rocks, which is designated S_0 and cleavage, designated S_1, which is found within all the rock units.

Bedding is best preserved in the medium to fine-grained clastic sedimentary rocks, while in the conglomerate it is defined by 15 to 30 cm thick steeply dipping sandstone or greywacke layers.

One dominant penetrative cleavage (S_1), which dips steeply towards the north or south, is especially well developed within the conglomerate. In typical outcrops the cleavage appears to form closely spaced discrete parallel surfaces within the matrix although on a smaller scale it is seen to be deflected around large competent clasts (Fig. 2-1). In thin section a strong preferred orientation of phyllosilicates defines the cleavage. Less competent clasts are aligned with their long and intermediate axes within the cleavage planes.

The S_1 cleavage is also well developed within the more argillaceous, medium- to fine-grained clastic sedimentary rocks, but is not so well developed in the less argillaceous arkoses and sandstones. In these

Fig. 2-1 Detailed sketch to illustrate how cleavage is deflected around competent clasts in the conglomerate. Outcrop No. 29 (Fig. 2-6).

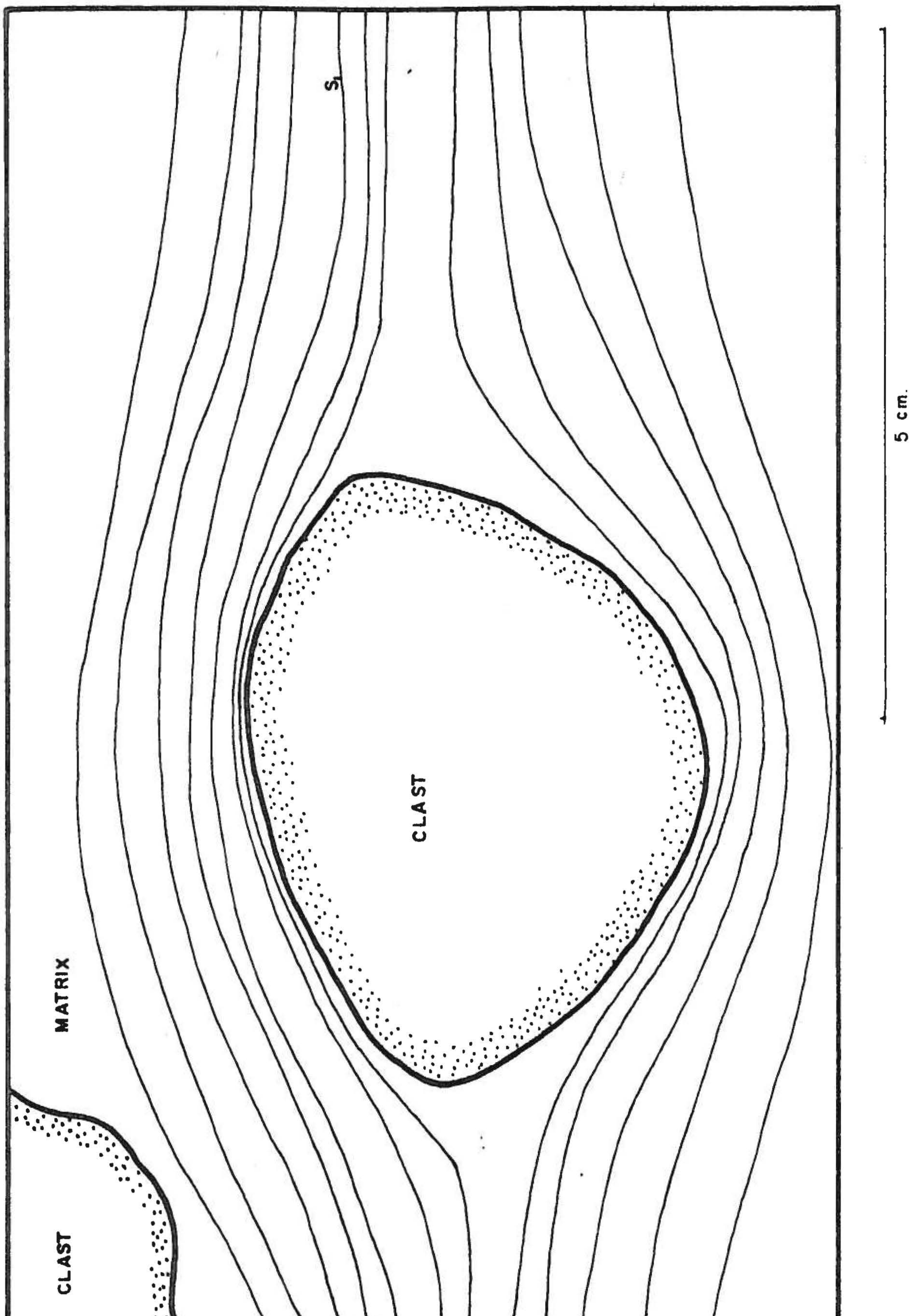

S1
MATRIX
CLAST
CLAST
5 cm.

rocks the cleavage results from a preferred alignment of quartz and feldspar clasts and from the preferred orientation of phyllosilicates confined to thin discrete layers.

In individual outcrops S_1 appears to be axial planar to minor folds.

At the eastern margin of the area the rocks possess a crenulation cleavage, S_2, the strike of which is at a low angle to S_1. S_2 surfaces are closely spaced, less than 1 cm apart and commonly discrete, resulting from a crenulation of S_1.

LINEATIONS

A number of linear elements were observed and measured. These include minor fold axes, intersection lineations of S_1 and bedding, and stretching lineations.

Minor folding is often found within the fine-grained clastic sedimentary rocks (Fig. 2-2) and is usually of low amplitude (less than 5 cm) and wavelength (up to 15 cm). No larger scale minor folding is observed. Fold axes have variable plunge amounts and trend either east or west. Steeply plunging kink folds are also common throughout the area and are found in all the different rock units where S_1 is well developed.

Stretching lineations in the sedimentary rocks were measured and commonly found to be inclined to the major fold axes, as discussed in Chapter 5.

Fig. 2-2 Minor folding in S_0, North Shore of Wild Potato Lake, Outcrop No. 94

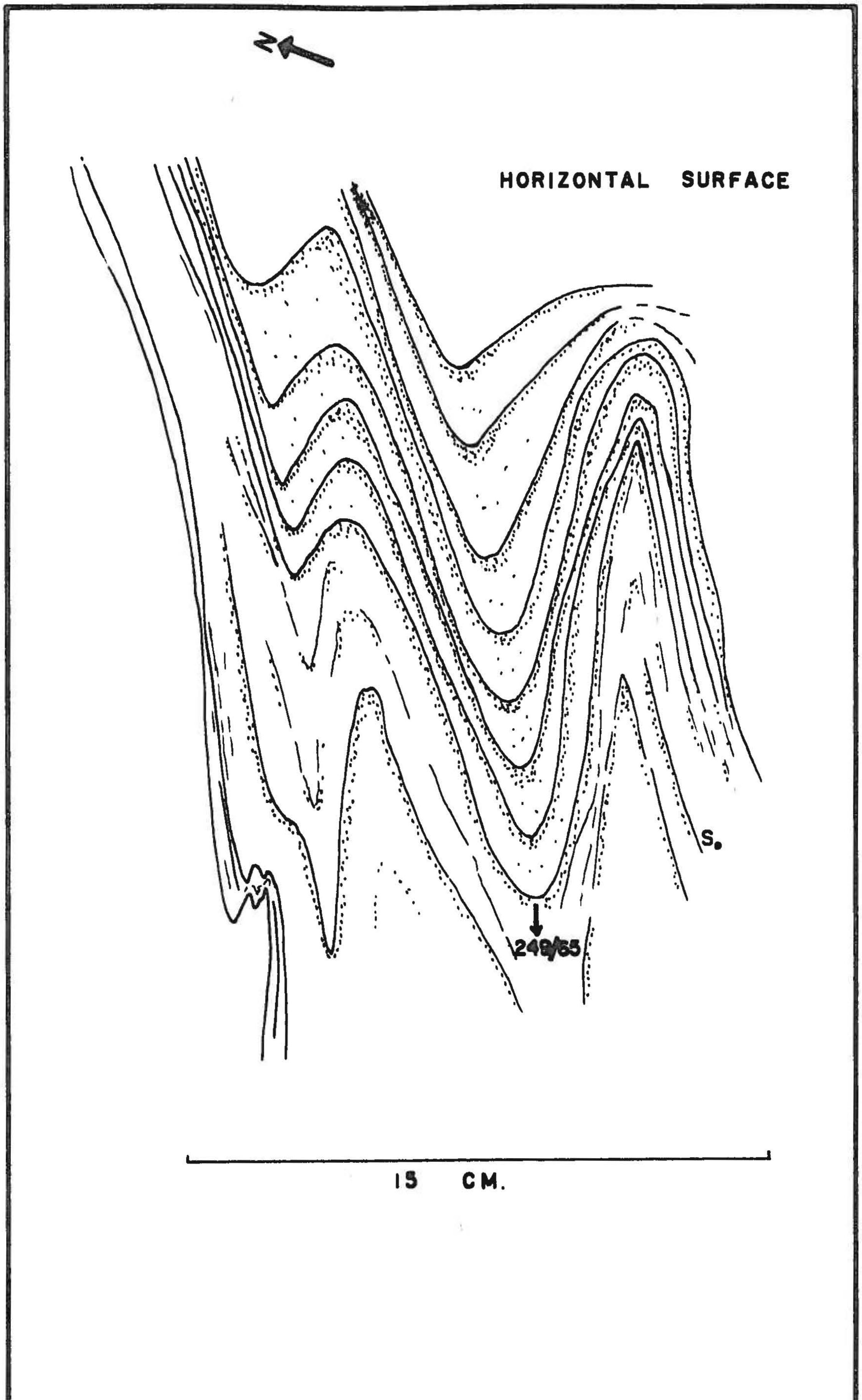
N
HORIZONTAL SURFACE
S₀
249/65
15 CM.

YOUNGING INDICATORS

1. Sedimentary Rocks

Within the sedimentary units two types of younging indicator are observed: cross-bedding, which is common in the medium- to fine-grained clastic sedimentary rocks (Figs. 2-3 and 2-4) and grading, which is found in sandstone and greywacke beds within the conglomerate. Crossbedding and trough-crossbedding are believed to be very reliable and are both therefore considered to give true indications of local younging directions. However, reversals in grading are known to exist (Bishop and Force, 1969) especially within shallow marine or fluvial sequences, as with this sequence. In their study, Bishop and Force suggest that most of the reversals in grading occur either in groups of small sets, or as large scale grading within conglomerates.

In this study, such grading has been treated with extreme caution and only well-defined sandstone or greywacke units have been used where no other younging indicator was present.

2. Pillow Lava

Pillow lavas are found in many exposures of basic volcanic units, particularly along the north shore of Wild Potato Lake.

In the undeformed state, pillow lavas can be used to determine younging directions from their "stacked" appearance (Fig. 2-5a). However, the situation becomes more complex after deformation as Borradaile and Poulsen (1981) show. Depending on the orientation of the strain ellipsoid relative to the pillow long axis, the bedding trace S_0 may become lost and since S_0 is needed to determine the precise younging direction, which is perpendicular to S_0, no such observation can be made.

Fig. 2-3 Crossbedding in Siltstone, North of Wild Potato Lake, Outcrop No. 60 (Fig. 2-6). Younging is towards the North.

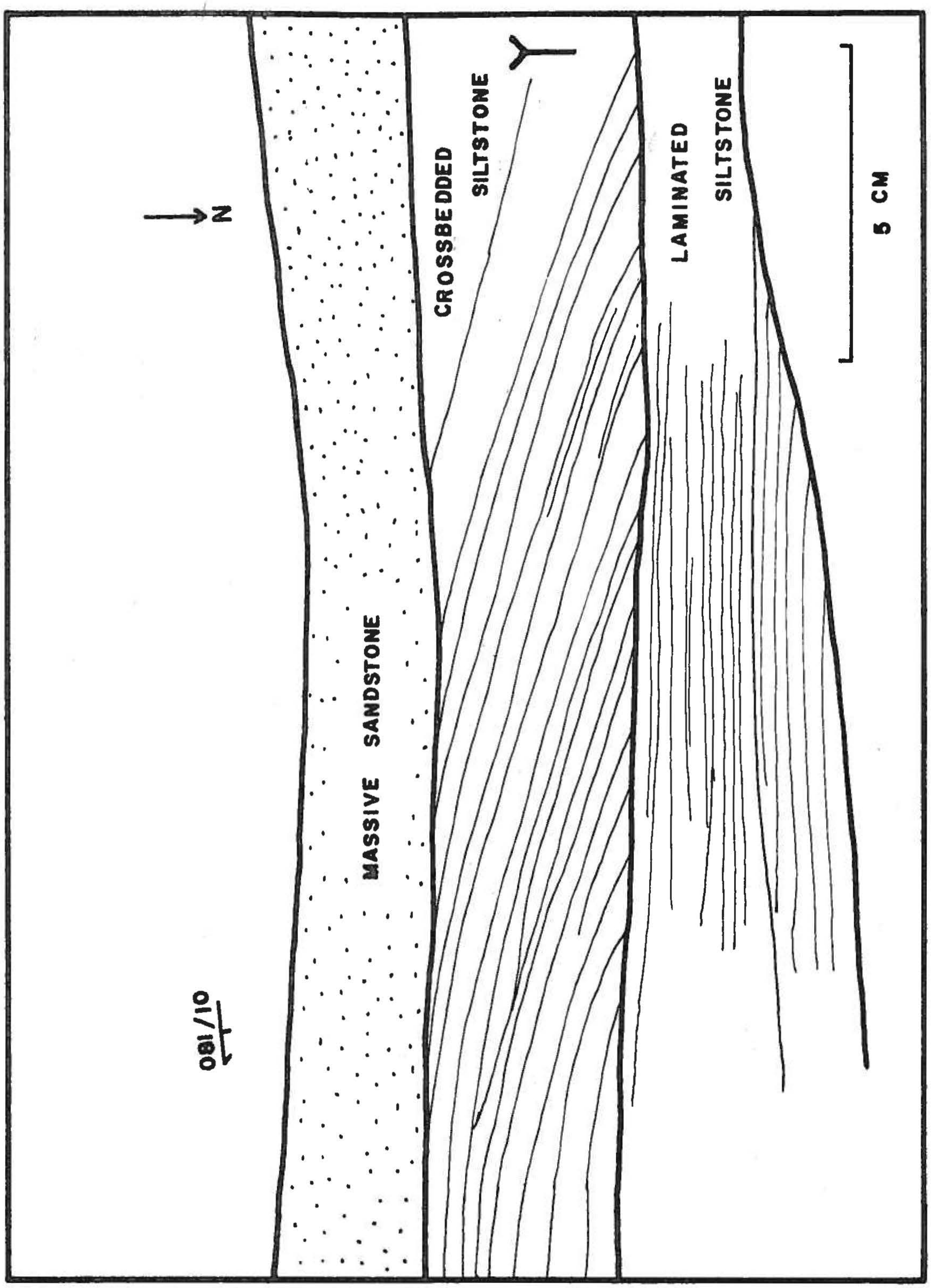
N
01/180
MASSIVE SANDSTONE
CROSSBEDDED SILTSTONE
LAMINATED SILTSTONE
5 CM

Fig. 2-4 Crossbedding in sandstone unit, south of Sturgeon Falls, locality 64 (Fig. 2-6).

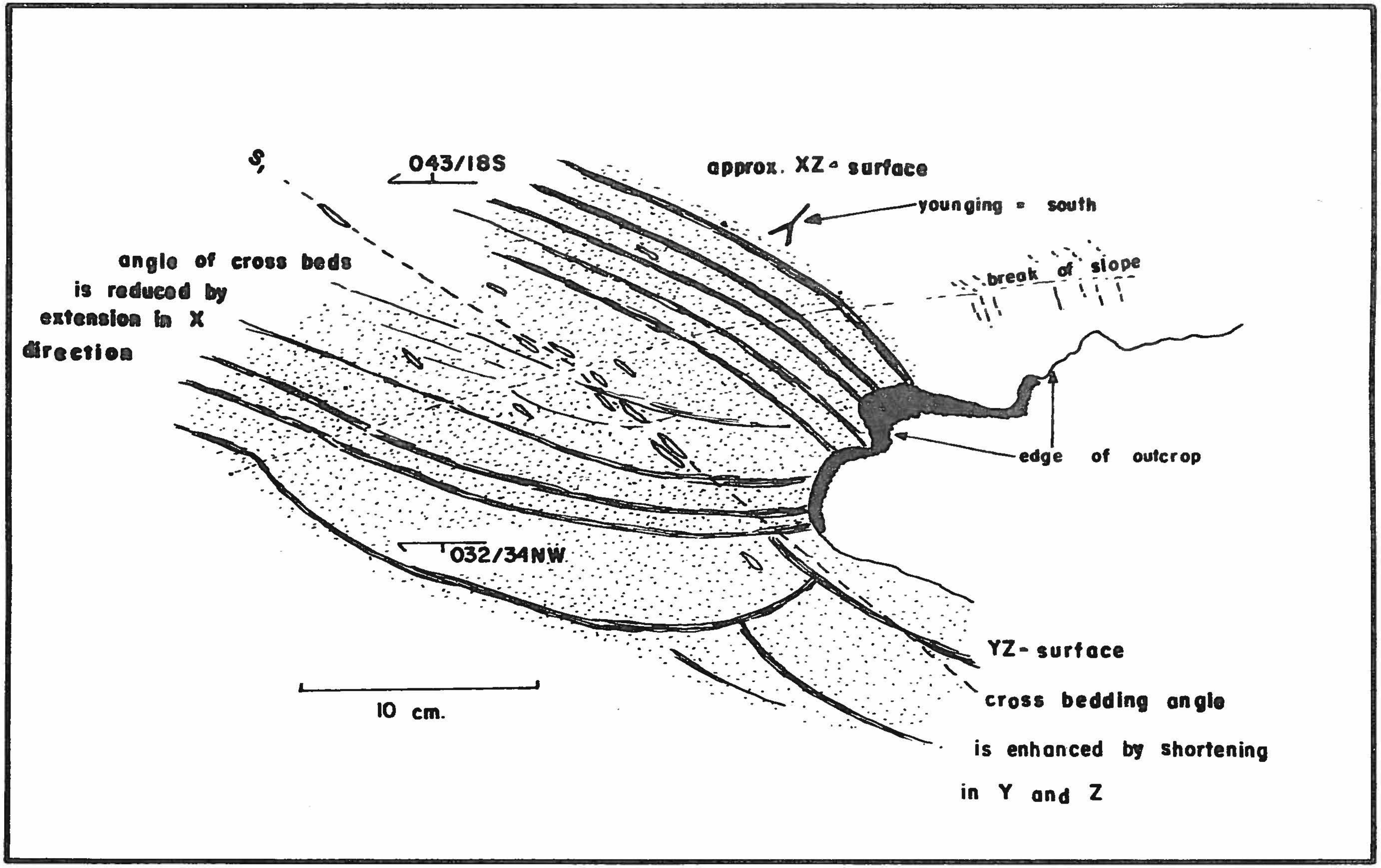

S_1
043/18S
approx. XZ - surface
younging = south
break of slope
angle of cross beds
is reduced by
extension in X
direction
edge of outcrop
032/34NW
YZ- surface
cross bedding angle
is enhanced by shortening
in Y and Z
10 cm.

Fig. 2-5 Younging directions from pillow lava

a. Theoretical 'stacked' appearance yielding younging direction towards top of page.

b. Deformed pillow lavas from the North Shore of Wild Potato Lake, Locality 85 (Fig. 2-6), giving a wide range of possible directions for younging.

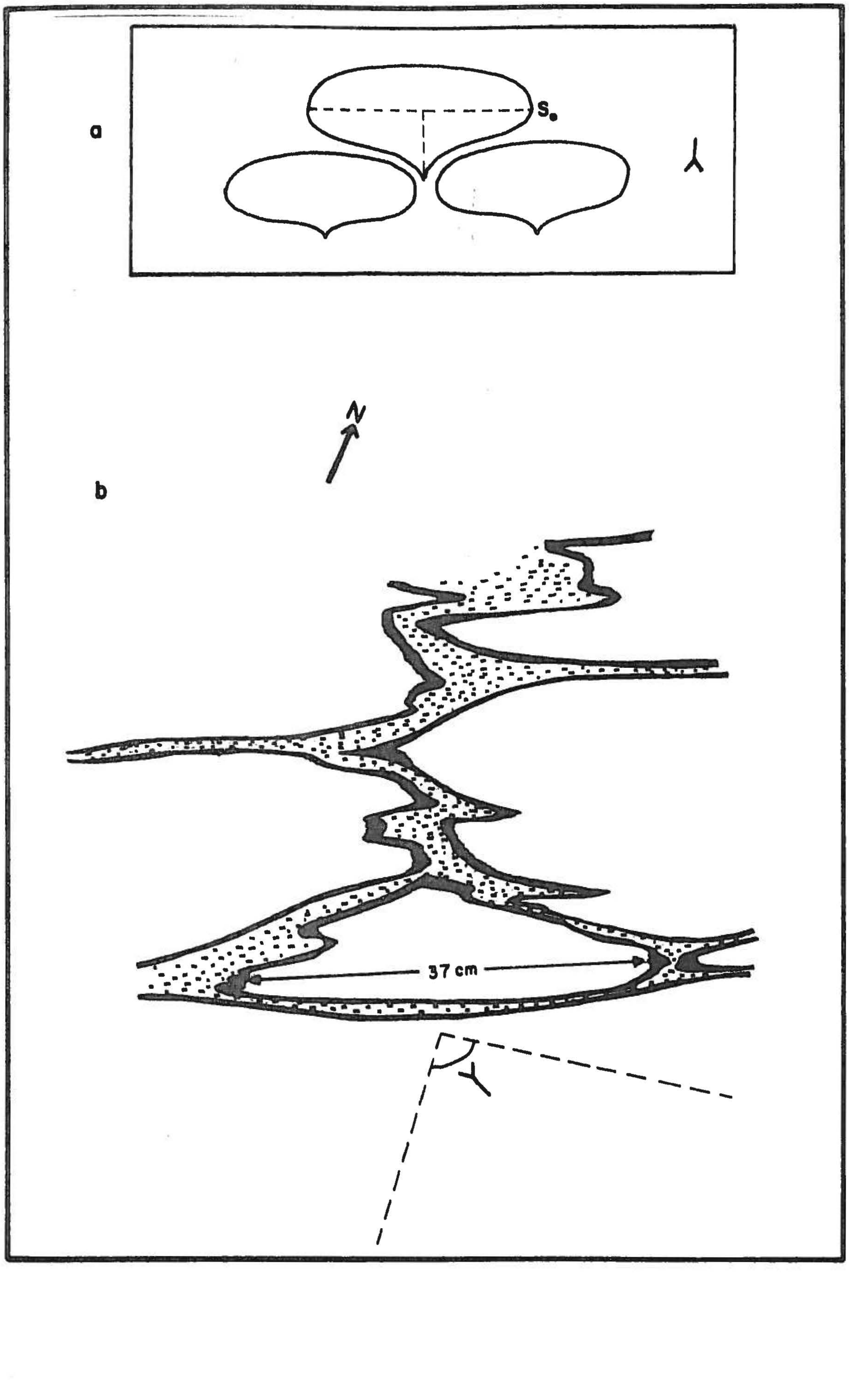
a
S_0
b
N
37 cm

Only in cases where the principal plane of the strain ellipsoid is parallel to either of the pillow axes will the long axis of the pillow remain parallel to bedding.

In none of the outcrops were these conditions met and only at one locality (locality 85, Fig. 2-6) was it possible to make an approximate estimate of younging direction (Fig. 2-5b).

MINOR FOLD ASYMMETRY

Where minor folds were observed in the field, the type of fold asymmetry was recorded. Figure 2-7b illustrates the type of fold asymmetry and the nomenclature used.

In cases where the symbols 'S', 'Z', 'M' and 'W' are used to describe minor fold asymmetry, great care must be taken always to view the minor folds down-plunge. Where fold axes are horizontal, observations should always be made in the same direction (Teaching manual, Borradaile).

BEDDING-CLEAVAGE RELATIONSHIPS AND STRUCTURAL FACING

In an area where there is little topographic relief and limited lithological influence on topography, bedding-cleavage relationships will play an extremely important role in elucidating the structure. If it can be shown that cleavage is axial planar to the major folds being considered, then the geometrical relationship between bedding and cleavage will show the relative position of the outcrop to the major fold as shown in Figure 2-7a.

'Facing', as defined by Shrock (1948), was first applied to structural geology by Cummins and Shackleton (1955), and Shackleton (1958) subsequently changed its use to determine the structure of a large area

Fig. 2-6 Outcrop location map.

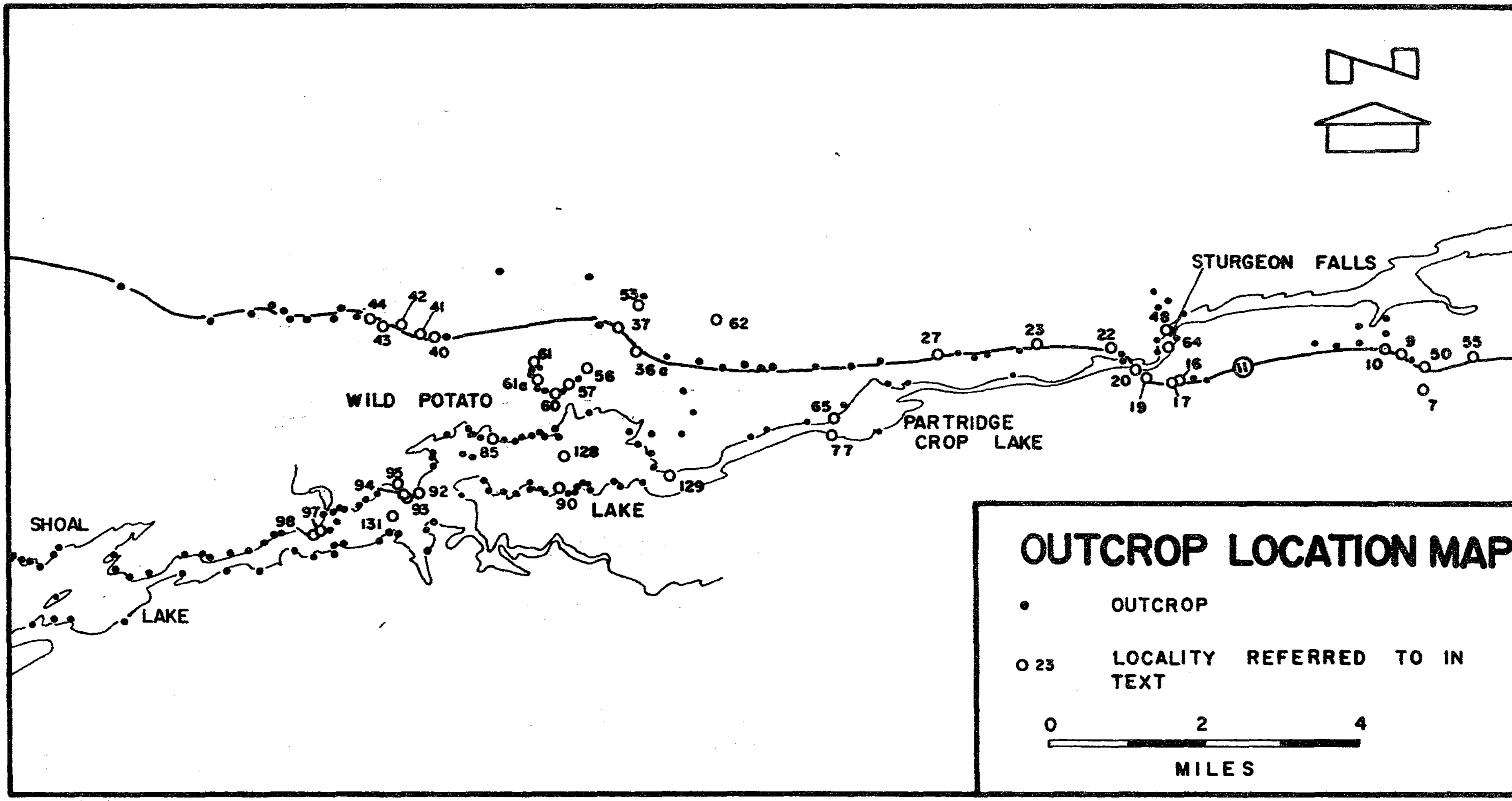

TABLE 2-1

N.T.S. GRID REFERENCES FOR LOCALITIES REFERRED TO IN THE TEXT.

OUTCROP NUMBER	EASTING	NORTHING
55	558450E	5398500N
50	558050E	5398411N
7	557800E	5398200N
9	557450E	5398750N
10	557100E	5398850N
16	552950E	5398050N
17	552750E	5398100N
19	551850E	5398250N
20	551850E	5398450N
22	551550E	5398850N
23	550050E	5398950N
27	547850E	5398550N
36A	541200E	5398500N
37	540400E	5399150N
40	537000E	5398900N
41	536600E	5398900N
42	536400E	5398100N
43	535750N	5399350N
44	535400E	5399450N
48	552600E	5399150N
56	540350E	5398550N
57	540200E	5398350N
60	539850E	5398100N
61	538950E	5398600N
61A	539200E	5398200N
62	543600E	5399200N
64	552600E	5398450N
65	545600E	5397200N
77	545550E	5396900N
85	538300E	5396700N
53	541400E	5399550N
90	539700E	5399550N
92	536950E	5395550N
93	536750E	5395400N
94	536550E	5395450N
95	536400E	5395600N
97	534850E	5394450N
98	534800E	5394550N
128	539800E	5396450N
129	542000E	5395900N
131	536000E	5395000N

Fig. 2-7

a. Bedding-cleavage relationships, viewed normal to the intersection lineation.

b. Minor fold asymmetry, viewed parallel to the fold axis.

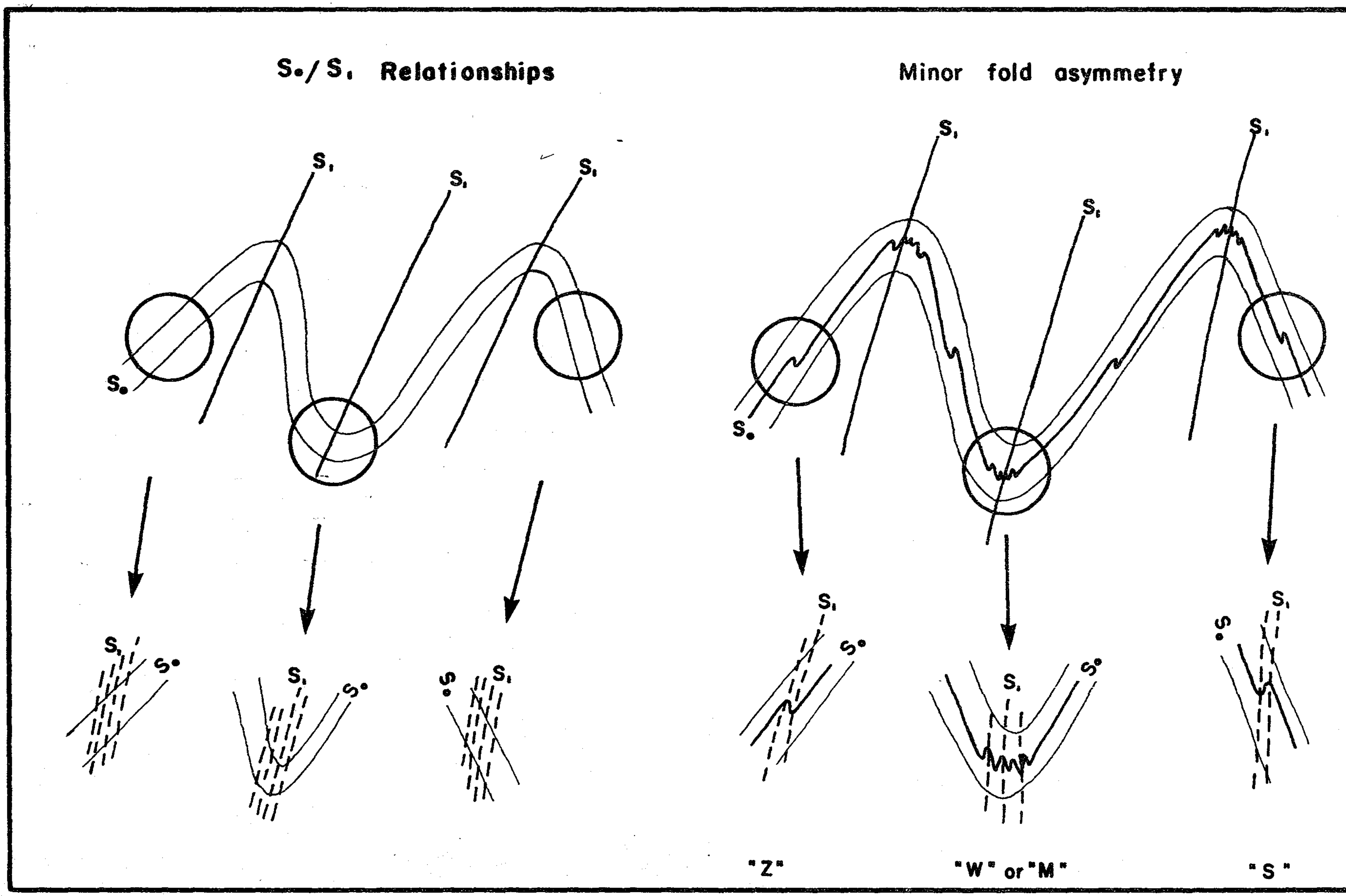
S₀/S₁ Relationships
Minor fold asymmetry
S₁
S₀
"Z"
"W" or "M"
"S"

of the Southwestern Highlands of Scotland. Shrock (1948) used the term 'to face' rather than 'to young' to describe the way in which a sedimentary layer is deposited. In his definition a layer is deposited facing upwards so that, after any subsequent readjustment of attitude, it always faces towards the side which was originally upwards. With structural facing, or "Shackleton's rule", a fold is said to face towards the younger beds in a direction normal to the fold axis along the axial plane (Cummins and Shackleton, 1955). Furthermore, where folds are absent, this is extended (Borradaile, 1976) to beds which then have structural facing directions in the plane of cleavage normal to the intersection lineation between bedding and cleavage, towards the younger strata. As the intersection lineation is parallel to the fold axis, where cleavage is axial planar to the folds, the structural facing direction of the beds will be parallel to that of the folds (Fig. 2-8) as defined by Shackleton.

As can be seen from Figure 2-8, a clear advantage in using structural facing over simply using younging directions of strata alone is that, in a folded sequence, where the younging directions of individual beds generally have a great variation in orientation, the structural facing direction will have a constant orientation. This is, of course, provided the folds are plane cylindrical (as defined by Turner and Weiss, 1963) in their geometry.

Therefore, using bedding-cleavage relationships and structural facing, one can determine the position of the major fold axial traces and the younging direction of the stratigraphy as a whole.

Fig. 2-8 Structural facing in layers where younging directions are known. Where folds have a plane cylindrical geometry, structural facing directions are always constant despite variations in local younging directions. (After Poulsen et al, 1980).

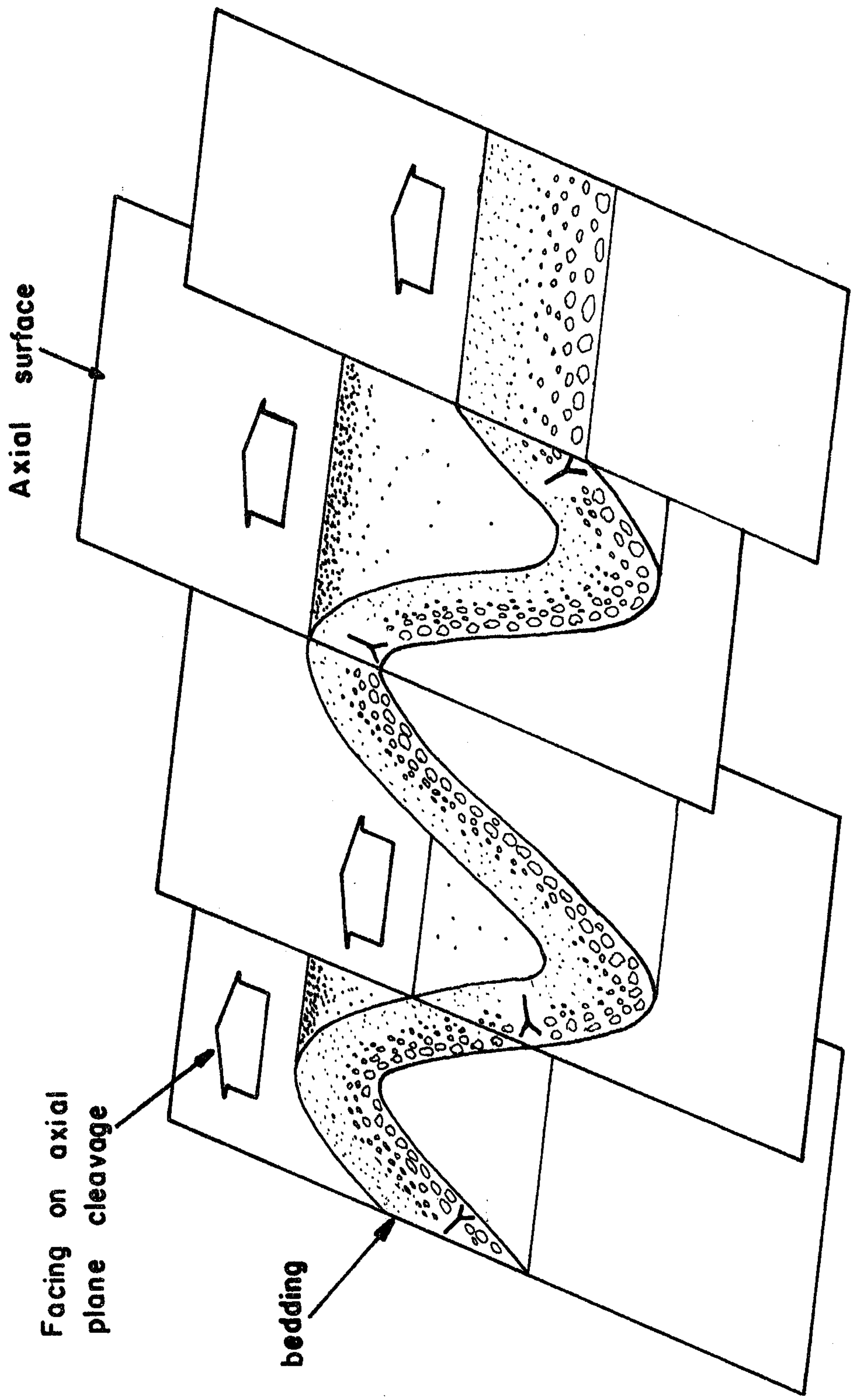
Axial surface
Facing on axial plane cleavage
bedding

From the above discussion, it should be apparent that caution must be exercised when applying 'Shackleton's rule' and bedding-cleavage relationships. The rule relies on the geometric relationship between folding and axial plane cleavage and clearly will not work if the folds are transected by the cleavage (Powell, 1974; Borradaile, 1978). The relationship between bedding and cleavage can be applied however if the major folds are transected, provided cleavage does not cut both limbs of the fold in the same sense (Fig. 2-9). Also, the folds and cleavage must be of the same generation (Borradaile, 1976) and lastly, the younging indicators must be reliable. Application of this technique recently resolved some stratigraphic problems near the present area (Poulsen et al., 1980).

Application of Techniques: Results of Structural Survey

The relative age of S_1 to the major folding is difficult to establish. Based on the minor structures however only one dominant folding episode appears to be present which is accompanied by one penetrative cleavage, S_1. S_1 is also axial planar to the minor folds in the area and so would appear to be of the same general age as the folding.

GEOMETRIC RELATIONSHIP BETWEEN S_1 CLEAVAGE AND FOLDING

It has been pointed out in the previous section that a major condition for using bedding-cleavage relationships and structural facing is that cleavage must be axial planar to the folds being considered. There are two principal ways in which this can be tested: firstly, by

Fig. 2-9 Bedding-cleavage relationships and transecting cleavage.

a

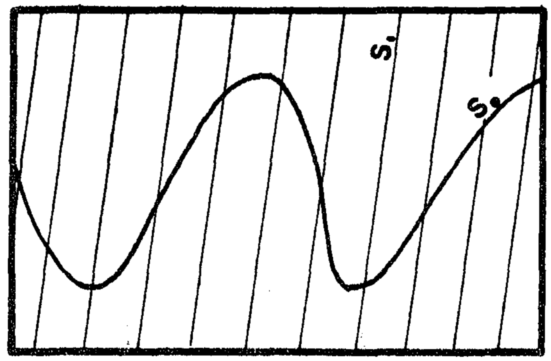

a. S_1 is axial planar to folds. S_0 - S_1 relationships can be applied.

b

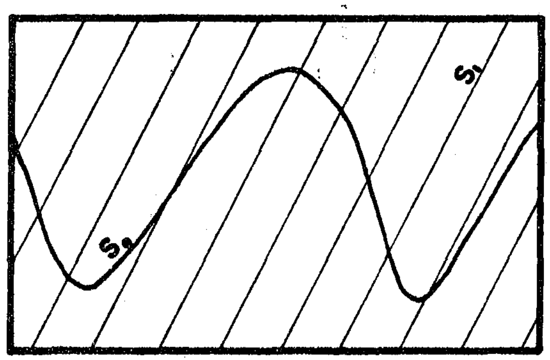

b. S_1 is not axial planar to folds, but still cuts both limbs in opposite senses. S_0 - S_1 relationships can be applied.

c

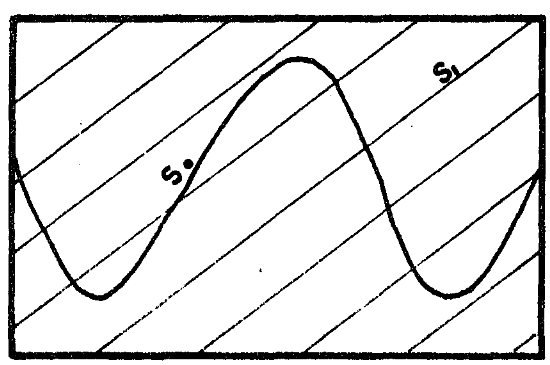

c. S_1 is transecting folds and cuts both limbs in the same sense. S_0 - S_1 relationships cannot be applied.

direct observation of the relationships between cleavage and minor folds, and secondly, by analysis of the intersection lineations of bedding and cleavage.

1. Minor Folding

A total of 15 minor folds in S_0 were observed in the field and in cases where it was possible to establish the relationships, the S_1 cleavage appeared to be axial planar to the folds (Figs. 2-10 and 2-11). In a few cases cleavage could not be identified in the fold closure, but in all of these the asymmetry of the minor folds agreed with the general angular relationship between bedding and cleavage in the rest of the outcrop.

2. Intersection Lineations

Consider the case represented in Figure 2-12a where a plane, S_0, is folded with a plane of symmetry S_A, so S_A is the axial surface of the fold. In this case the intersection lineation of S_0 and S_A is always constant and parallel to the fold axis, as shown in the accompanying stereographic projection.

Figure 2-12b shows the case of the same fold now cut obliquely by the plane S_T, as might be the case with a transecting cleavage. In this case we see that the intersection of S_0 and S_T is never parallel to the fold axis and plots along a great circle, which is the plot of S_T.

Therefore, if cleavage is transecting the major folds in this manner, then we should see a great circle distribution of intersection lineations along the cleavage plot. However, this is so in the case where there is only an F_1 event and S_0 is originally planar. A similar situation may arise if we are dealing with an F_2 event after F_1 or an F_1 event where S_0 is not planar.

Fig. 2-10 Minor F_1 fold in S_0 with an axial planar S_1, eastern end of Wild Potato Lake at locality 129 (Fig. 2-6). The fold is plunging towards the SW and has a 'Z' asymmetry indicating that the axial trace of a major synform lies to the SE of the outcrop. Note the minor fault to the east of the fold.

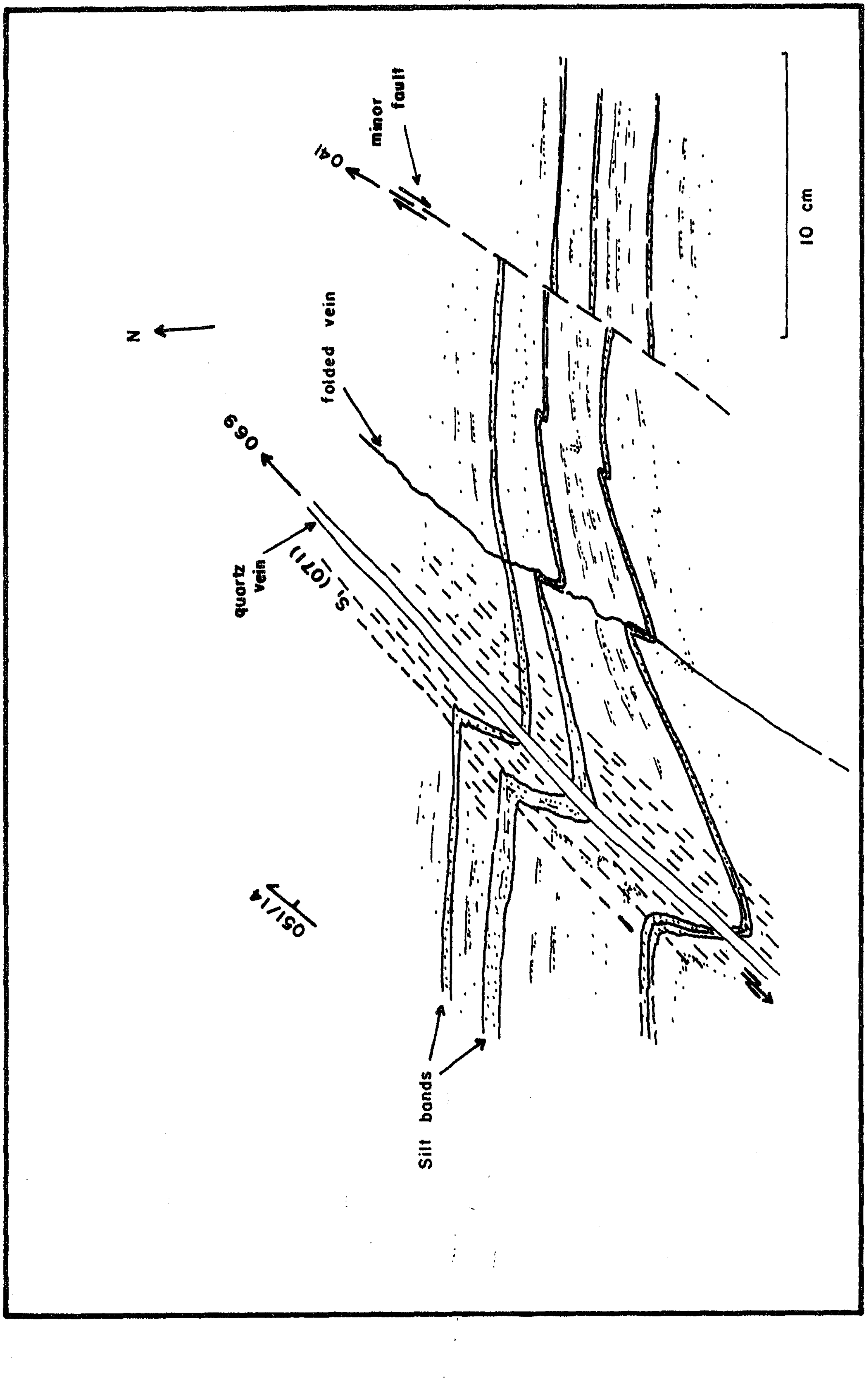
minor fault
041
10 cm
N
folded vein
069
quartz vein
S_1 (071)
051/14
Silt bands

Fig. 2-11 Minor F_1 folding in S_0 with an axial planar S_1, North Shore of Wild Potato Lake, outcrop no. 92 (Fig. 2-6). Asymmetry is 'S'-type and the folds are plunging steeply towards the west, so the outcrop is to the north of the axial trace of a major antiform.

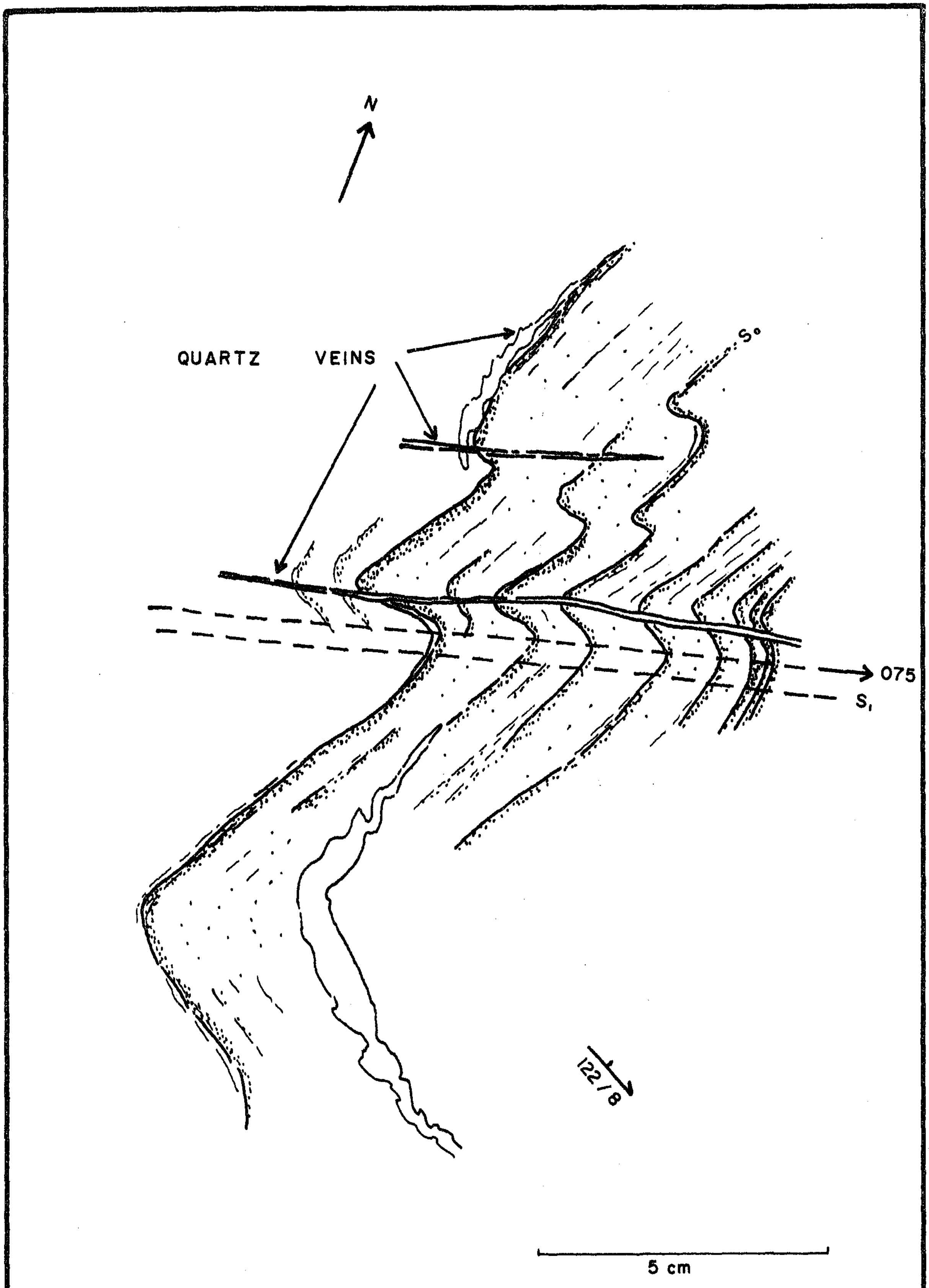
N
QUARTZ VEINS
So
075
S1
122/8
5 cm

Fig. 2-12 Orientation of Intersection Lineation where cleavage is axial planar (a) or transecting (b)

a. S_0 folded with a plane of symmetry S_A parallel to the axial surface of the fold. The intersection of S_0 and S_A is always constant and parallel to the fold axis as shown on the accompanying stereographic projection.

b. The fold is now cut obliquely by a plane S_T. The intersection of S_0 and S_T is never parallel to the fold axis and plots along a great circle, which is the plot of S_T, on the stereonet.

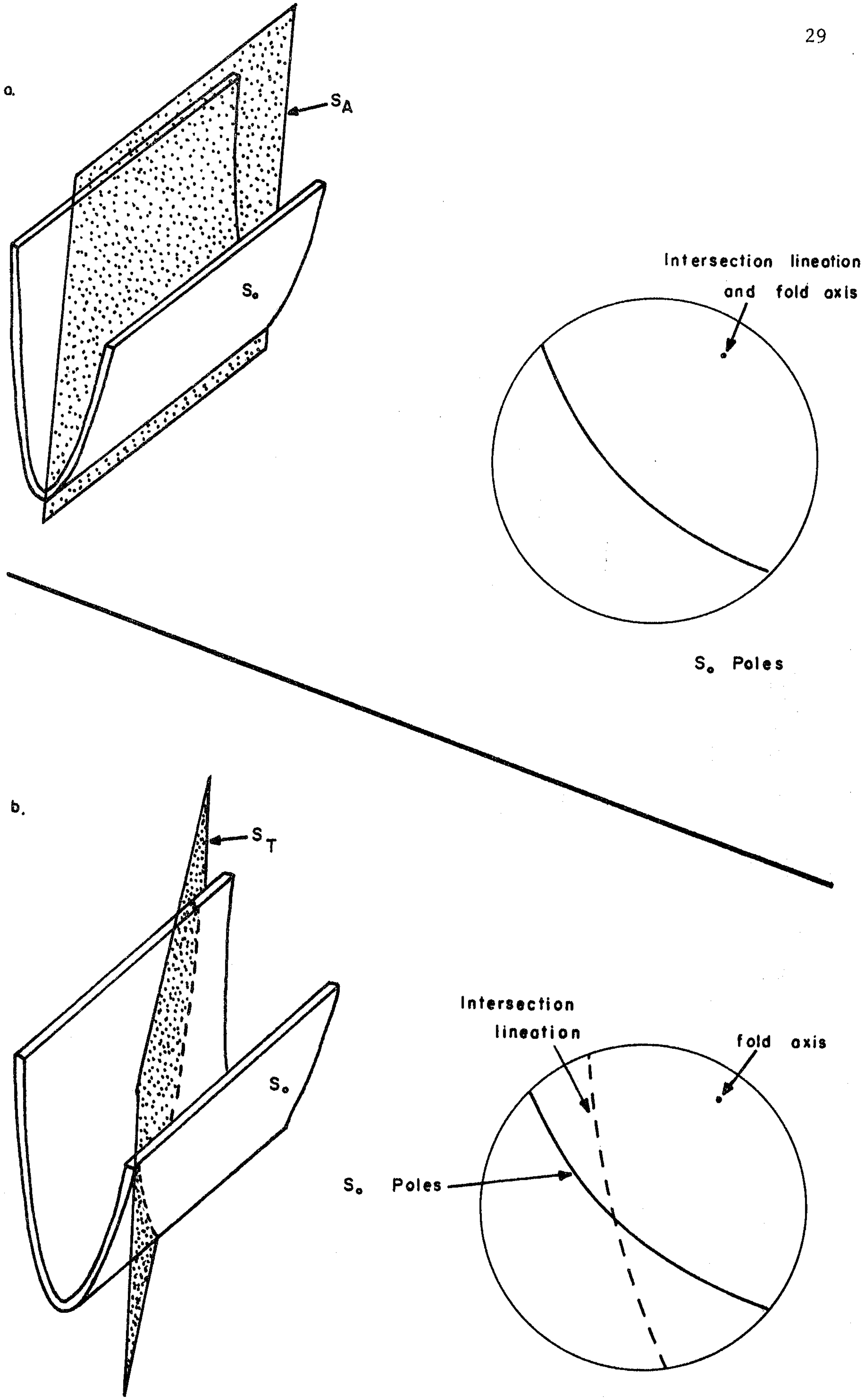

a.
S_A
S_o
Intersection lineation
and fold axis
S_o Poles
b.
S_T
S_o
Intersection
lineation
fold axis
S_o Poles

In the case of an F_2 event after an F_1 event, the intersections of S_0 and the axial plane cleavage to F_2, which would be S_1 here, would show a distribution similar to that in the example above, except that they would be parallel to F_2 minor fold axes. Depending on the mechanism of the F_2 folding, F_1 lineations would be redistributed along small circles, in the case of flexural-slip folding, or great circles, in the case of slip folding (Turner and Weiss, 1963). However, if no pre-S_1 cleavage developed associated with the proposed F_1 fold event, then no F_1 intersection lineations would form.

The abundance of crossbedding and trough-crossbedding (see Chapter 3) suggests a high energy, shallow water environment for at least much of the area. The conglomerate has also been interpreted as an alluvial fan type deposit (Wood, 1980) and the large size of clasts within this unit might suggest rapid uplift and erosion at the source and thus fairly steep palaeoslopes. Thus, the likelihood that S_0 was planar originally appears to be minimal.

Stereographic projections of S_0 poles, S_1 poles, intersection lineations and minor folds have been constructed for different parts of the area. These stereographs are reproduced in Figure 2-13.

Throughout much of the study area it was often very difficult to see and measure the intersection of bedding and S_1 cleavage. However, along the shore of Wild Potato Lake intersection lineations could be measured (Fig. 2-13c). From this projection S_0 - S_1 intersections plot in a fairly tight cluster, plunging at a moderate angle to the west. There is also a close agreement between the intersection lineations and

Fig. 2-13 Equal area projections to the lower hemisphere of F_1 data for different parts of the study area.

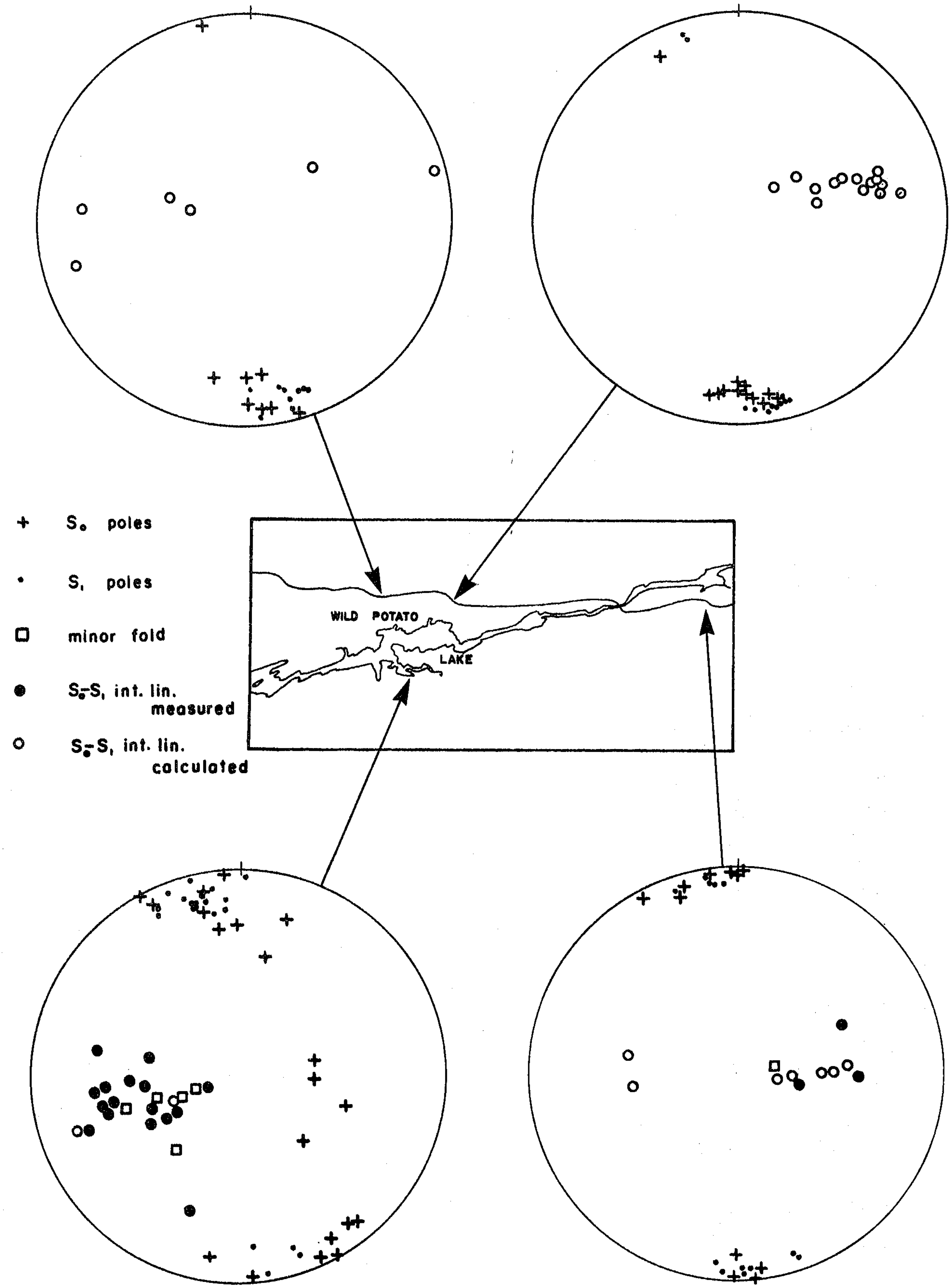

+ S_o poles
• S_1 poles
□ minor fold
● S_o-S_1 int. lin. measured
○ S_o-S_1 int. lin. calculated
WILD POTATO
LAKE

the minor fold axes trends and plunges which were observed in the area. Thus, at least here, cleavage appears to be axial planar to the folding. In both Figures 2-13b and 2-13d we see again that the intersections of S_0 and S_1 plot in a cluster, this time plunging to the east. S_0 - S_1 intersections in Figure 2-13a however plot along a great circle.

Based on this data, it appears that cleavage is more or less axial planar to the major folding everywhere except in the area represented by Figure 2-13a. However, if we now plot all the linear data for the whole area on a single stereographic projection (Fig. 2-14) we see that there is a general circular arc distribution of S_0 - S_1 intersections. This is also true for minor fold trends and plunges. Perhaps then cleavage is axial planar to the folding in the area covered by Fig. 2-13a and the data supports a pre-F_1 event or a non-planar S_0?

A note of caution should be added here. Where the intersection of bedding and cleavage can be measured directly, then accuracy of measurement to within ±5° is acceptable. However, if the intersection cannot be measured directly, it has to be derived through stereographic projection. Now, if the angle between S_0 and S_1 is large, then inaccuracies in their measurement will not produce highly significant inaccuracies in their derived intersection. But if the angle is small, as is the case in most of the study area, then such inaccuracies can result in a very wide range of possibilities for the intersection lineation, of the order of 70° (Fig. 2-15). In this figure, typical bedding and cleavage measurements have been plotted on a stereonet. Assuming that strike was measured accurately and that dip was measured to within ±3°, the variation of the intersection lineation, L, is shown in dark stipple and if

Fig. 2-14 Equal area projection to the lower hemisphere of F_1 linear data for the whole study area.

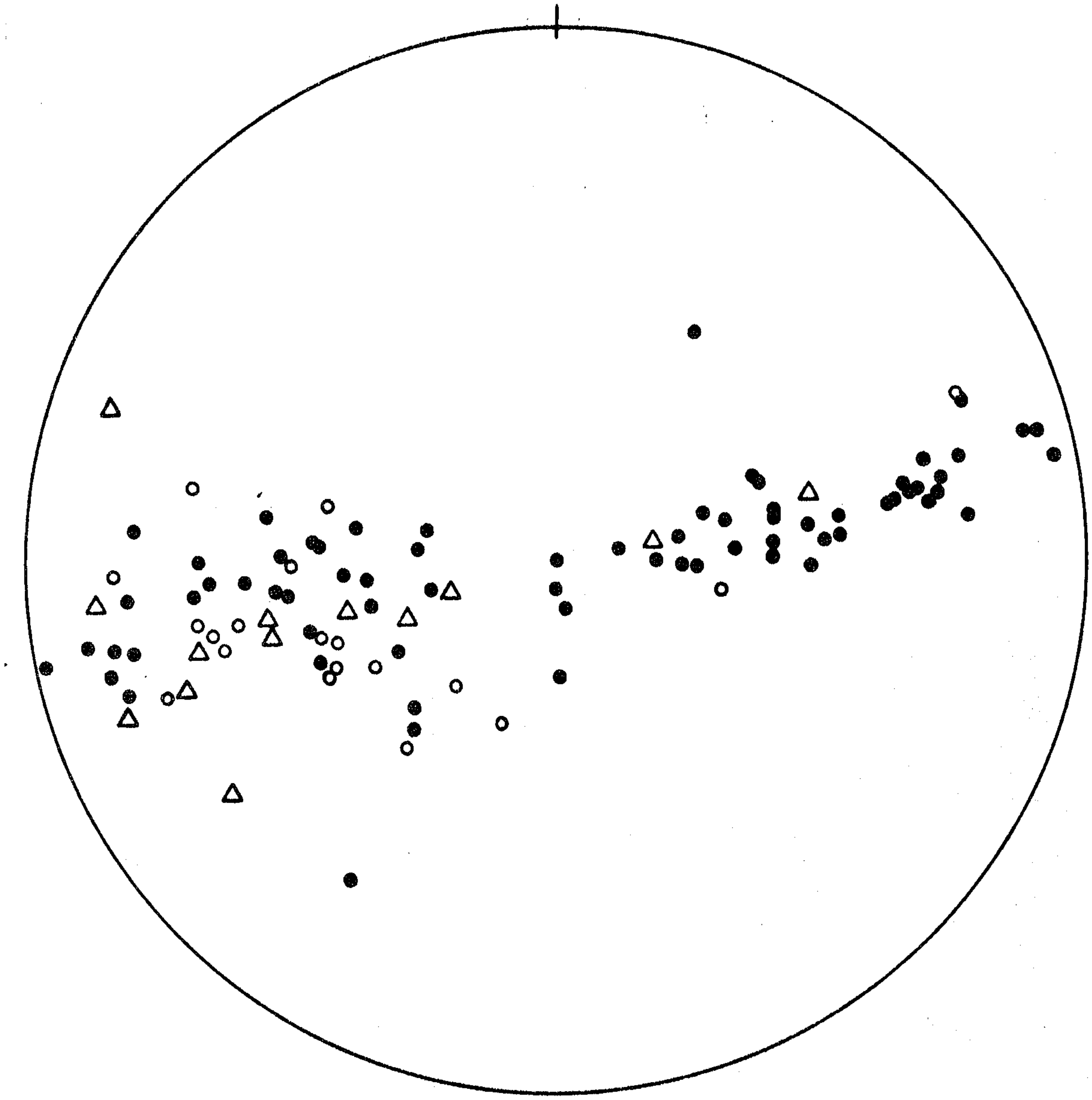

○ S_0/S_1 INTERSECTION - measured

● S_0/S_1 INTERSECTION - calculated

△ MINOR FOLD AXIS

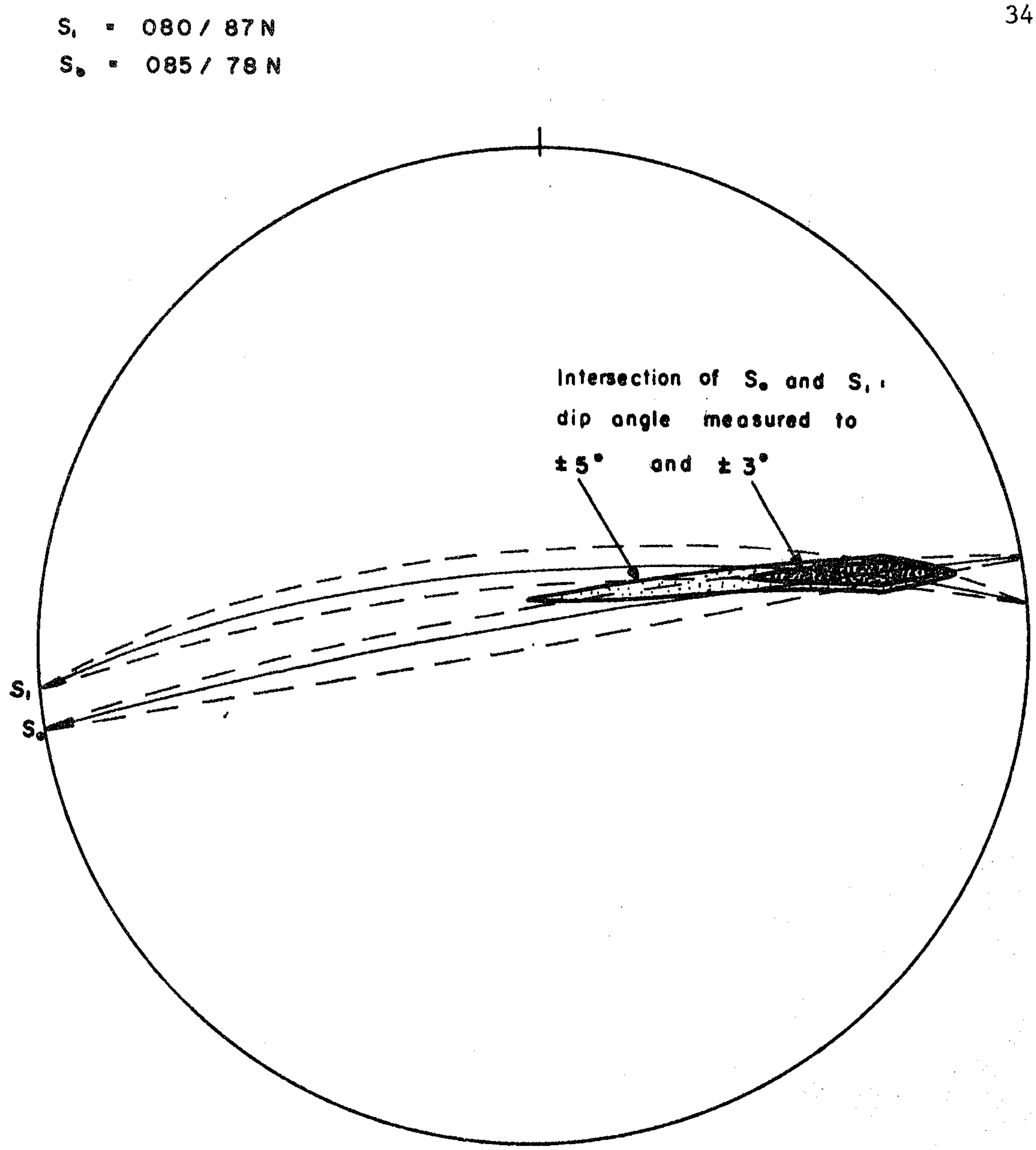

Fig. 2-15 Variation in orientation of intersection lineation with inaccuracies in S_0 and S_1 dip measurement. Assuming strike is measured accurately and that dip is measured to within ±3°, the variation in orientation of the intersection lineation, L, is shown in dark stipple. If dip is measured to ±5, the variation in L is shown in light stipple.

dip was measured to within ±5°, the variation in L is shown in light stipple. Clearly the situation would deteriorate even further if one also considered inaccuracies in the measurement of strike.

With this in mind, it should be added that the intersection lineations plotted in Figure 2-13a were derived by plotting S_0 and S_1 rather than by direct field measurement.

Therefore, based on the evidence, it would appear that in at least some parts of the area (Fig. 2-13a) the cleavage may not be parallel to the axial surfaces of the folds.

RELIABILITY OF YOUNGING INDICATORS

Crossbedding and trough-crossbedding appear to give reliable indications of younging directions, although some problems arise when these features are deformed by analogy with the deformation of pillows (see Appendix A). However, where they were used it is felt they gave reliable younging directions for the beds. Pillow lavas, also sensitive to the effects of deformation, were not used to determine younging. Grain size gradations, on the other hand, can be identified even if the strata have been deformed. As already pointed out however, reverse grading can occur in shallow water environments.

In general, it is considered that the younging indicators used to determine structural facing of folds were reliable. Where crossbedding and grading was observed in the same outcrop, agreement between the two was routinely checked. At some outcrops, only grading was observed and at these several sets were used in order to establish the younging. No outcrops were found in which graded beds yielded opposing younging directions. However, adjacent outcrops did occasionally yield conflicting data (see section on structural facing, page 41).

Major Structures

The results of the structural survey are presented on the structural map and schematic structural diagram (in the rear folder of this volume) which show the attitudes of the main structural elements observed in the field.

It is proposed that one dominant period of deformation is responsible for the structures which are present in the area. Major folds and minor folds in S_0 with S_1 cleavage as axial surfaces are designated F_1 structures. Other structures, such as kink folds and crenulations which affect F_1 structures, are designated F_2 structures and are recorded in Figure 2-16. Also recorded in Figure 2-16 are minor faults and shear zones which affect F_1 structures. However, while F_2 structures certainly do affect S_0 and S_1, the symbols F_1 and F_2 do not necessarily imply strict age relationships. F_2 structures are clearly not pre-F_1 structures but whether or not they represent a distinctly different period of deformation, or even a period of folding, is not clear.

MINOR FAULTING AND SHEAR ZONES

Minor faulting (Fig. 2-10) was observed at 4 localities (9, 16, 64 and 129, Fig. 2-6) within fine-grained silty horizons. Minor faulting was not observed in any other rock unit. In all cases the relative sense of movement of the faults was dextral with apparent displacements along strike of 2 to 10 cm - S_0 and S_1 cleavage were both displaced by the faults.

At localities 19, 20, 23 and 53 (Fig. 2-6) larger scale shear zones were observed in which relative motion was sinistral except at locality 53

Fig. 2-16 Distribution and orientation of F_2 structural data.

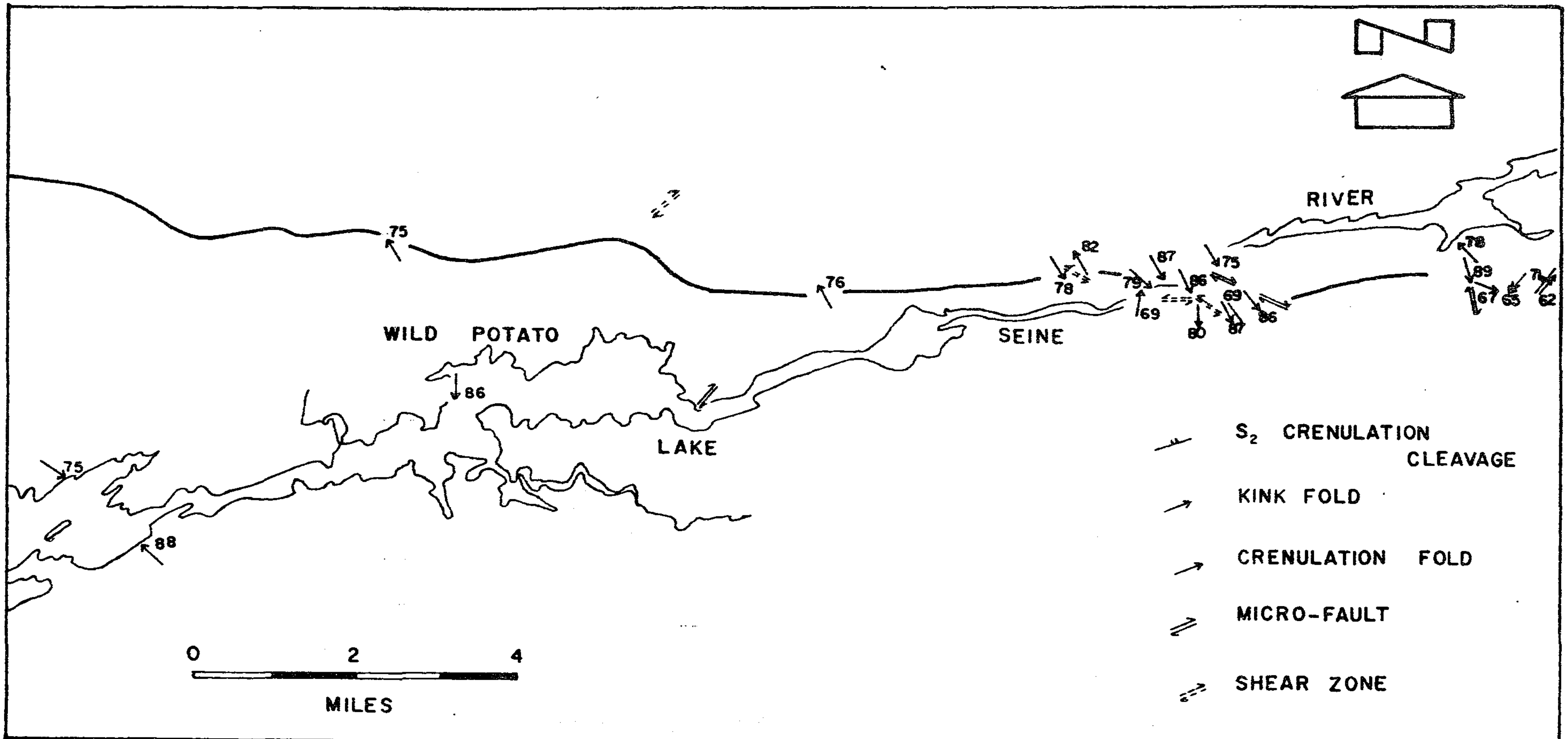

where a small dextral shear zone was observed. At localities 19 and 23, where a vertical cut as well as the horizontal could be observed, the shear zones were found to be steeply dipping to the southwest (at locality 19) and to the northeast (at locality 23) and both had strikes of 124°. Slickensides on the shear zone wall at locality 19 pitched at 40° from the northwest, while those at locality 23 pitched at 48° from the northwest. The shear zone at locality 23 was about 50 cm wide and appeared to be later than the kink folding which was affected by the shearing.

F_2 STRUCTURES

The most common and widespread F_2 structures are small kink folds which occur as discrete bands about 3 to 5 cm in width and are the result of kinking of S_1 and S_0. They are found within all the rock types in the study area where S_1 is well developed. Figure 2-17 is a stereographic projection of the trends and plunges of the kink folds which clearly plunge steeply northwest or southeast.

Crenulation cleavage and folding is only observed at the easternmost portion of the study area at localities 7, 50 and 55 (Fig. 2-6) where they occur as discrete slip planes, about 1 to 2 cm apart, at low strike angles to S_1. At locality 55, S_1 cleavage planes are seen folded about an S_2 crenulation cleavage associated with small F_2 crenulation folds plunging steeply to the northeast. At this outcrop S_0 can also be seen oblique to and refolded with S_1.

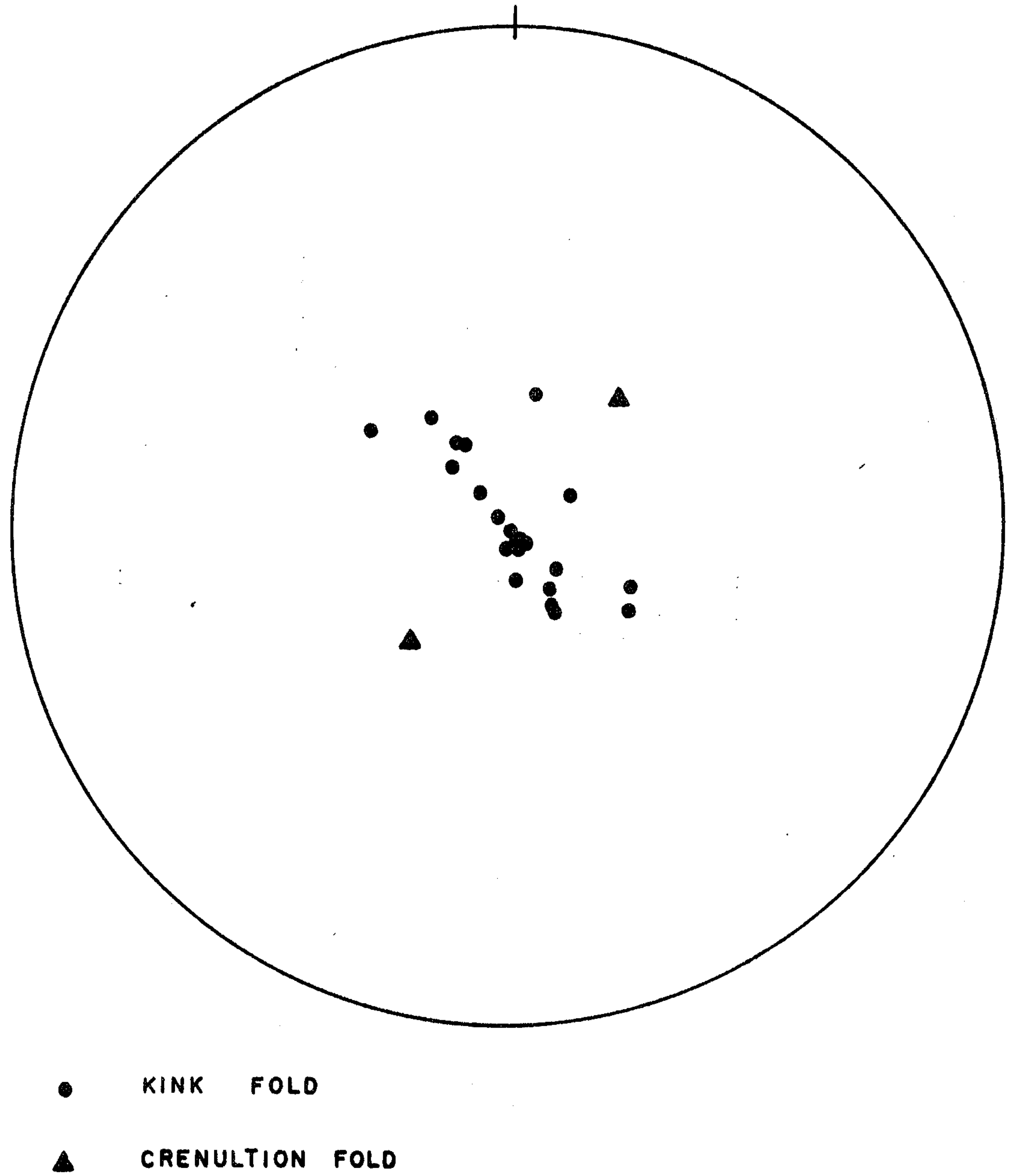

Fig. 2-17 Equal area projection to lower hemisphere of orientation of F_2 fold hinges.

F_1 STRUCTURES

The structural map and schematic structural diagram in the rear folder show the distribution, orientation and geometry of the F_1 structures as interpreted from the data collected. The two dominant structures are numerous F_1 minor folds and a penetrative cleavage, S_1. Detailed field sketches of F_1 minor folds are shown in Figures 2-2, 2-10 and 2-11 where original sedimentary layering, S_0, has been folded about an axial planar cleavage, S_1. The mutual intersection of S_0 and S_1 has also resulted in the formation of a lineation, L_1. From the structural map it is seen that, in general, S_0 and S_1 tend to strike at very low angles to one another and are also both generally steeply dipping. However, along the southern shore of Wild Potato Lake, bedding dips gently and strikes at a much greater angle to S_1.

From the geometric relationship between S_0 and S_1 and from the asymmetry of F_1 minor folds, the locations and orientations of the F_1 major fold axial traces have been determined as shown on the structural map. The intersection of S_0 and S_1 and the orientations of F_1 minor fold axes also reflects the orientation of F_1 major fold axes. The structural map shows a series of tight to isoclinal, inclined folds with steeply dipping ENE/WSW striking axial surfaces and curvilinear hinge lines. This is illustrated on the accompanying schematic structural diagram. Thus, while the minor F_1 folds are apparently plane cylindrical in geometry, the major folds tend to be non-plane approximately cylindrical although the axial surface is also slightly curving in both strike and dip. At Wild Potato Lake the major folds are more open and disharmonic and plunge more uniformly towards the WSW approximating to plane cylindrical in geometry. The major F_1 folds are also upwards facing or sometimes sideways facing and can thus be called anticlines and synclines. The variation in orientation of the structural facing directions reflects the variation in plunge direction of the major fold axes.

The "blacked-in" heavy structural facing arrows on the structural map represent downwards facing structures and thus warrant some further explanation. There are three general ways in which it is possible to produce downwards facing structures:

1. The sedimentary structures used show the reverse of the true younging direction. As discussed earlier, reversed graded bedding can develop under certain conditions. However, at one downwards facing outcrop (locality 42, Fig. 2-6) crossbedding was used to indicate the local younging direction and at other localities, several graded beds for each outcrop were observed, all giving the same result.
2. The folds may be transected by cleavage. If cleavage cuts both limbs of a fold in the same sense (Fig. 2-9c) then the structural facing direction on one limb of the fold will be the opposite from the other. We have seen that S_1 may well be transecting in the area shown in Figure 2-13a. On the structural map this area shows structural facing directions which are not consistent. In an area such as this, where the angle between S_0 and S_1 is very low, local departures from an axial planar relationship of cleavage to folds could well result in such a situation. However, in the area covered by Figure 2-13b, cleavage does appear to be axial planar to the folding.
3. There may have been a pre-tectonic overturning of strata or a pre-F_1 deformation event. If originally upside-down strata were

folded, then the resultant folds would face downwards after deformation. If this overturning of beds was on a large scale, one might expect to find large areas of downwards facing folds. Similarly, if it was a tectonic event there should be other evidence for it such as a remnant pre-S_1 cleavage, if it formed, or refolded pre-F_1 minor fold closures. None of these were observed in the study area although, as suggested earlier, the distribution of S_0 - S_1 intersection lineations and F_1 minor fold axes may support a pre-F_1 folding event. It is possible however that a smaller scale overturning occurred through, for example, slump folding which did not result in the formation of associated cleavage development. Figure 2-18 illustrates a model which fits all the data obtained in the field.

Therefore, of the three above possibilities, it seems likely that either cleavage is locally transecting or that there was some form of local overturning of strata prior to the F_1 deformation.

Regional Setting of Structural Geology

Schwerdtner et al. (1979) suggest that two principal periods of deformation are responsible for the present structures observed in the Archean in Northwestern Ontario. The first, and major deformation was caused by the emplacement of massive diapiric bodies which resulted in a lateral crustal shortening of the more ductile supracrustal masses giving rise to the major folding seen in the area. The second period of deformation caused major easterly trending dextral (Schwerdtner et

Fig. 2-18 Hypothetical model to explain the downwards facing structures in the NW part of the study area.

Upper diagram: a pre-cleavage overturning of S_0 by, for example, slump-folding is not accompanied by significant deformation.

Lower diagram: later folding accompanied by the development of an axial planar cleavage results in the present distribution of downwards facing structures. Locally, for example in the NW part of the section, cleavage may be transecting.

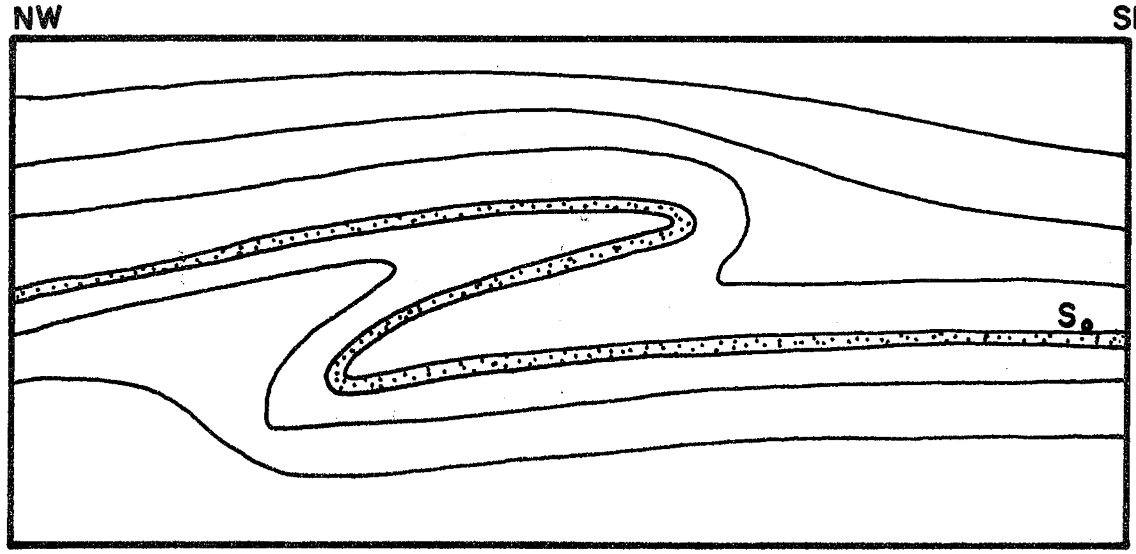

pre - cleavage

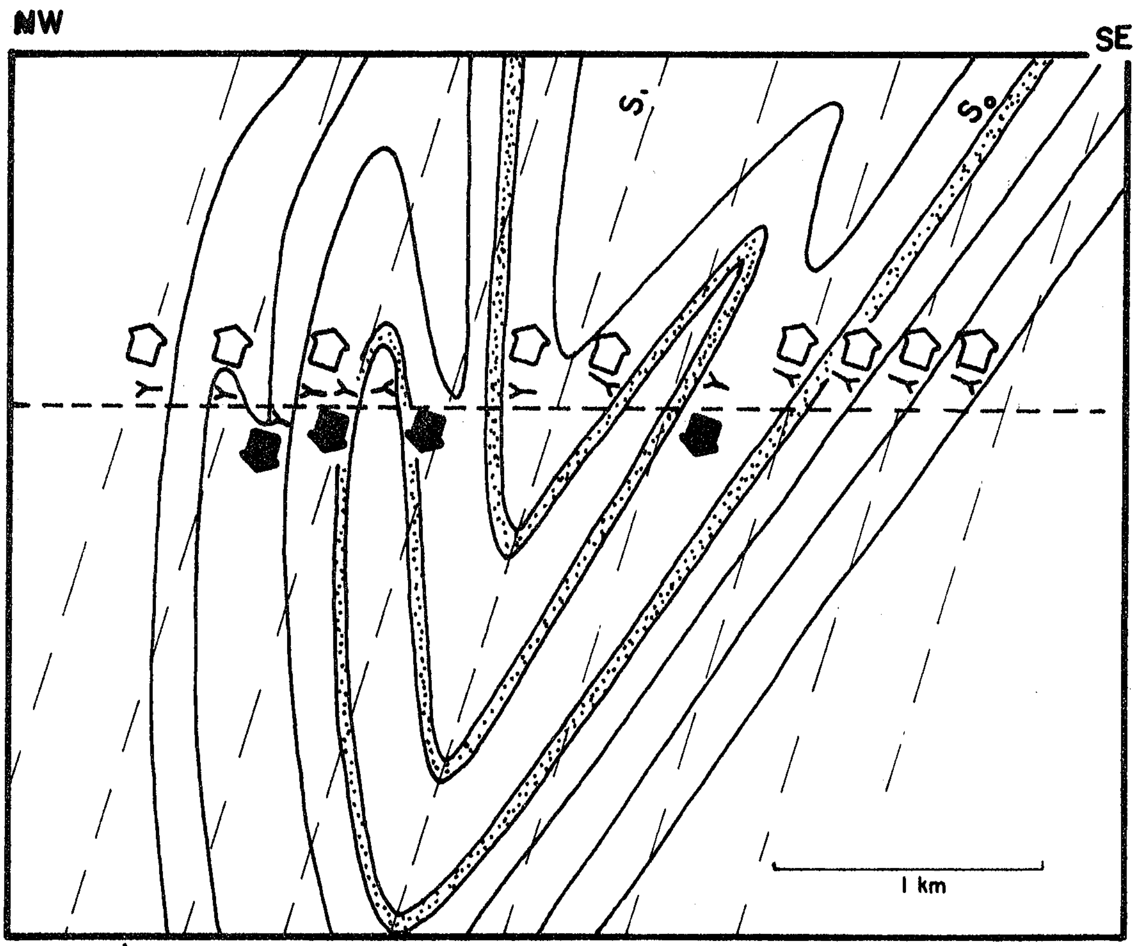

post - cleavage

al., 1979) transcurrent faults of which the Quetico fault, just to the north of the study area, is an example. Schwerdtner et al. also suggest that the effect of these faults on the surrounding supracrustal rocks was to cause kinking and crenulation in those rocks.

It is difficult to assess this study area in terms of the model of Schwerdtner et al. for the following reasons:

1. Although there is limited evidence for two, possibly overlapping deformations, the geology to the north and to the south bears little resemblance to that within the study area. Here the geology is dominated by shallow water metasedimentary rocks and volcanic rocks. To the north are found principally gneissic bodies (possible diapirs) and supracrustal rocks of the Wabigoon belt while to the south is a monotonous sequence of deep-water turbidite metasediments, the "Quetico sediments" or "Southern sediments" of the Quetico belt. Thus one might ask the question, if the subdivision of the Superior Province into structural belts is justified, to which belt does this study area belong? In terms of lithology and paleo - sedimentary environment, neither seems likely.
2. To the north and south, the study area is bounded by major faults - the Quetico fault to the north and the Seine River fault to the south. Assuming these faults are major transcurrent faults as Schwerdtner et al. suggest and furthermore, that movement along the faults was initiated after the emplacement of the diapiric bodies presently north of the area, then any correlation between diapirism and deformation in the study area is impossible. This is because the relative position of the study area to the diapirs at their time

of uprise cannot be known, unless the amount of transcurrent motion along the faults is known. It is possible and perhaps likely that the minor faulting and shearing in the study area is related to the movement of the faults. If this is the case, then the relative movement of the minor faulting supports the suggestion of Schwerdtner et al. that the relative motion along the Quetico fault is dextral. However, the relative motion of the minor shear zones in the study area is predominantly sinistral. Perhaps then the Quetico fault has experienced a pulsating history with relative motion in opposite senses, although the pursuit of such a supposition is beyond the bounds of this study.

CHAPTER 3

PETROGRAPHY, STRATIGRAPHY AND METAMORPHISM

Figure 1-1 is a regional geological map of the Mine Centre area. A more detailed geological map of the study area accompanies the structural map in the rear folder. As can be seen from this map two characteristic lithologies are exposed: metavolcanic rocks and clastic metasedimentary rocks. The main objective of this study is to determine the structure and strain history of the rocks and consequently description of lithological units is kept general in nature. All of the rocks have been subjected to low-grade metamorphism, although one unmetamorphosed diabase dyke was observed. However, for the purposes of description and to avoid repetition, the prefix 'meta' is dropped from specific rock names.

CLASTIC SEDIMENTARY ROCKS

On the basis of clast size these rocks can be divided broadly into two types: coarse-grained rudites (conglomerates) and medium- to fine-grained clastic sedimentary rocks.

Grain size classification, nomenclature and compositional classification of the clastic sedimentary rocks follows that outlined by Greensmith (1978) as far as possible. Figure 3-1 outlines the Wentworth classification by size of non-carbonate fragmental deposits and Figure 3-2 illustrates the classification by composition used for the arenites. The degrees of original roundness and shape of clasts are difficult to assess due to post-depositional deformation of clasts.

Fig. 3-1 Size classification and nomenclature of non-carbonate fragmental deposits. (From Greensmith, 1978).

Fig. 3-2 Classification of Sandstones. (from Greensmith, 1978).

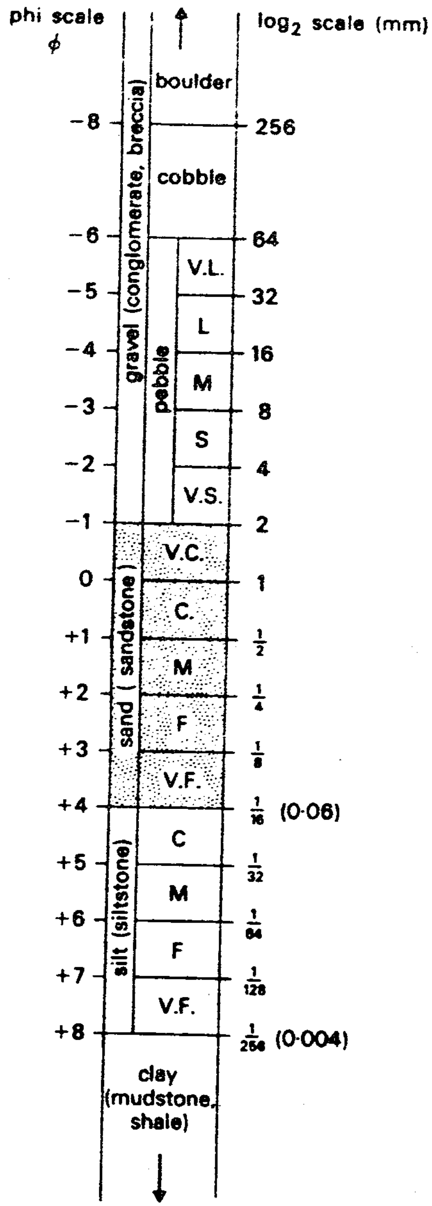

phi scale
ϕ
$\log_2$ scale (mm)
boulder
cobble
pebble
V.L.
L
M
S
V.S.
gravel (conglomerate, breccia)
sand (sandstone)
V.C.
C.
M
F
V.F.
silt (siltstone)
C
M
F
V.F.
clay (mudstone, shale)
−8
−6
−5
−4
−3
−2
−1
0
+1
+2
+3
+4
+5
+6
+7
+8
256
64
32
16
8
4
2
1
$\frac{1}{2}$
$\frac{1}{4}$
$\frac{1}{8}$
$\frac{1}{16}$ (0·06)
$\frac{1}{32}$
$\frac{1}{64}$
$\frac{1}{128}$
$\frac{1}{256}$ (0·004)

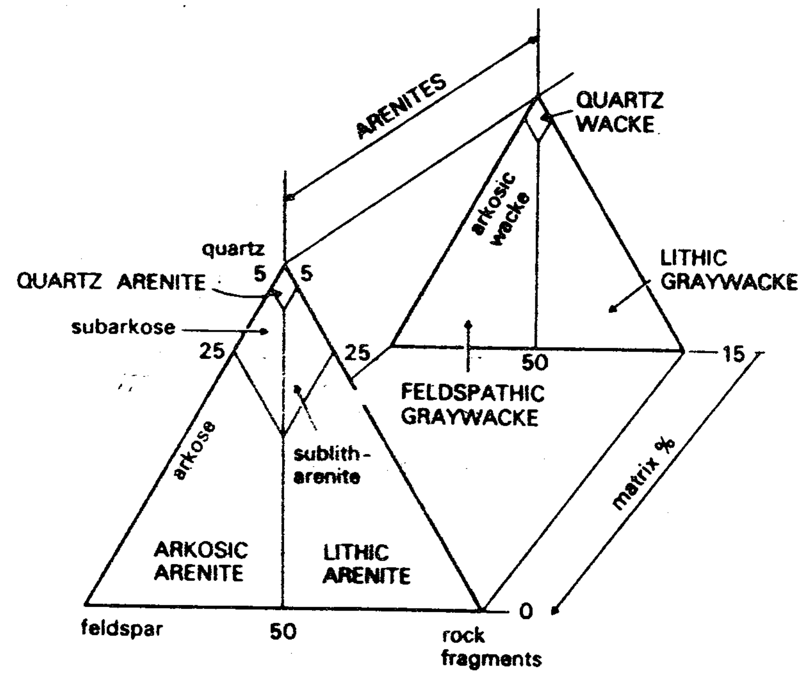

ARENITES
QUARTZ WACKE
arkosic wacke
LITHIC GRAYWACKE
quartz
QUARTZ ARENITE
subarkose
5
5
25
25
50
15
FELDSPATHIC GRAYWACKE
sublith-arenite
arkose
matrix %
ARKOSIC ARENITE
LITHIC ARENITE
feldspar
50
rock fragments
0

(a) Conglomerate

This unit is extensively exposed along Highway 11 and is occasionally seen as thin, up to a metre thick, granule to pebble clast size beds along the south shore of Wild Potato Lake. It is also exposed as a cobble to boulder clast size unit, in which bedding is not obvious, on the northern shore of Shoal Lake. At most localities along the highway the clasts in the conglomerate are cobble to boulder size. At these localities thin, up to 30 cm thick, beds of greywacke are commonly observed in the unit. The greywacke beds are typically graded yielding younging directions and attitude for the conglomerate as a whole. Compositionally the conglomerate is polymictic and appears to be clast-supported although it is often difficult to differentiate between chlorite schist clasts, which might represent altered basic volcanic fragments and true matrix.

- Matrix

In general, the matrix is composed of very fine-grained sericite and chlorite, muscovite, occasional biotite and fine-grained quartz. The phyllosilicates show a strong preferred alignment which defines the schistosity of the rock. Thin dark wavy bands in thin section are commonly oriented approximately parallel to schistosity and possibly result from the accumulation of insoluble material at pressure solution surfaces. Sericite is commonly found to have grown along fractures in quartz and feldspar clasts while chlorite and calcite commonly occur in pressure shadows of large competent clasts. Occasionally the matrix is composed of alternating layers of very fine-grained sericite and chlorite, with fine-grained quartz layers.

- Clasts

In the conglomerate clasts vary in size from granule to boulder. Variations in clast composition are also common. The most commonly observed clasts are granitoids, with compositions typical of quartzolite, granodiorite, tonalite and granite (Streckeisen, 1976). Of these, quartzolite clasts are the most common. Tonalite clasts are sometimes porphyritic. In general, all the granitoid clasts are devoid of amphibole or pyroxene - also micas are rare although the presence of chlorite as overgrowths may have resulted from the alteration of mica. Quartz and feldspar are thus the main mineral constituents of the granitoid clasts. Quartz is usually sutured and may show shadowy extinction. It is commonly intergrown in a myrmekitic texture with feldspar. Graphic intergrowths also occur in some localities. Calcite overgrowths on quartz grains are fairly common. Occasionally quartz grains are fractured or boudinaged, a possible indication of cataclastic deformation. The feldspar is dominantly plagioclase (oligoclase to andesine - no albite compositions have been found) with lesser amounts of microcline and micro-perthite. Chlorite and sericite within the granitoid clasts show a preferred orientation parallel to S_1 and are most probably metamorphic in origin. Small amounts of epidote are also observed in some granitoid clasts.

Rhyolite clasts in the conglomerate are readily identified because of their light colour. In thin section they are usually composed of a fine-grained mass of sutured quartz and sericite needles, strongly aligned parallel to S_1. Some carbonate is also present. Poorly-oriented plagioclase in the porphyritic rhyolite clasts form the large crystals - this low degree of orientation of plagioclase crystals is probably due to deformation of the rhyolite clasts, which are often seen in both thin section and on an outcrop scale deflected around more competent granitoid clasts. In some porphyritic rhyolites remnant quartz and feldspar 'megacrysts' are overgrown and pseudomorphed by calcite.

Intermediate and basic volcanic clasts are usually difficult to distinguish from the matrix in both handspecimen and thin section. Basic volcanic clasts are altered to chlorite schists and occur as very fine-grained chlorite and quartz aggregates, in which chlorite shows a strong preferred orientation parallel to S_1.

In most outcrops all ranges of clast size from granule to boulder can be observed suggesting that sorting was poor. Original roundness of clasts within the conglomerate is difficult to establish due to the effects of deformation on the clasts. However, 'fish-mouth' textures in a few rhyolite clasts do indicate that at least some of the clasts were originally angular in shape (Borradaile and Jackson, 1982 - in press).

(b) Medium- to Fine-Grained Clastic Sedimentary Rocks

These rocks are extensively exposed across much of the study area, especially along the banks of the Seine River and along the south shore and parts of the north shore of Wild Potato Lake. They are also exposed around the shores of Shoal Lake. Primary sedimentary structures such as bedding, crossbedding, trough-crossbedding and graded bedding are common to all the silt- and sand-sized sedimentary rocks. Crossbedding and trough-crossbedding angles vary from very shallow, less than 5° in cross-bedded units, to very steep and have been modified by deformation (see Appendix A). Bedding thickness varies from a few centimetres in the finer grained sedimentary rocks to tens of centimetres in the coarser units: massive beds of arkose and greywacke are not uncommon.

(i) Fine-Grained and Argillaceous Sedimentary Rocks

Fine-grained semi-pelitic siltstones and clay-rich sedimentary rocks are commonly interbedded with coarser-grained greywackes. These relationships occur extensively along the north shore of Wild Potato Lake, notably at localities 92, 93, 94 and 97 (Fig. 2-6). Here fine-grained, well-laminated siltstones, composed of about 60 to 80% fine-grained quartz with a few larger clasts of quartz and feldspar, are found. The rest of the rock is composed of fine-grained biotite, minor muscovite and sericite. The quartz in the matrix shows a strong preferred orientation of grains and the micas are well aligned, occurring in discrete layers where they define S_1. Both quartz grains and clasts are sutured. Occasionally, for example at locality 97 (Fig. 2-6), there is a poorly-defined layering comprising layers of quartz, which is dominant, biotite and muscovite alternating with biotite and sericite layers. At locality 98 (Fig. 2-6) the siltstone contains less clay and is slightly coarser than at other localities. Here the matrix is made up mostly, about 90%, of fine sutured quartz grains and some feldspar with discrete layers of coarser mica, almost all of which is biotite. The clasts are mostly quartz and make up about 20% of the rock.

Notably, chlorite is rare or absent in all these rocks.

(ii) Medium- to Coarse-Grained Arenites

These rocks are abundant, particularly along the shoreline of Wild Potato Lake.

- Lithic to Arkosic Greywackes. To the south of the localities mentioned above, along the south shore of Wild Potato Lake, considerably coarser arenaceous sedimentary rocks are exposed. In the outcrops the matrix is composed of fine- to medium-grained quartz, minor feldspar and large amounts of fine-grained sericite, muscovite and some biotite, showing a strong preferred alignment parallel to S_1. Biotite, however, generally occurs as larger laths, sometimes with muscovite, overgrowing quartz and feldspar clasts. The clasts are relatively coarse and are composed mainly of quartz, feldspar and some cordierite. Some calcite, minor apatite and epidote are present. At locality 90 (Fig. 2-6) biotite appears to pseudomorph quartz. In this outcrop the matrix is composed of fine-grained quartz, muscovite, biotite and sericite while the clast composition is mostly quartz, some cordierite, perthite and fragments of quartzolite. Within the biotite pseudomorphs are found zircons which are surrounded by pleochroic haloes.

- <u>Medium- to Coarse-Grained Arkoses</u>. These rocks occur commonly along the Seine River and the shoreline of Wild Potato Lake. A good example can be seen at locality 65 (Fig. 2-6). Here, the matrix is composed of fine-grained biotite, muscovite and sericite with later overgrowths of carbonate. Clasts are mostly quartz and plagioclase feldspar.

- <u>Chloritic Greywackes</u>. Where arenites are found within or near conglomerate horizons or close to the contact with volcanic rocks, chlorite becomes a dominant matrix constituent. Here the matrix constitutes up to 40% of the rock and is composed of chlorite, fine-grained muscovite and sericite, which have a strong preferred alignment parallel to S_1, and fine-grained quartz. Clasts are mostly quartz and feldspar although small quartzolite and rhyolite fragments are also found. Quartzolite clasts are sometimes boudinaged and the boudin necks are infilled with calcite. At one locality (43, Fig. 2-6), which is close to the contact with volcanic rocks at the northwest extent of the area, the matrix is made up almost entirely of dark green chlorite and minor quartz. One or two dark green chloritic schist clasts were also observed in thin section from this outcrop.

In thin section many of the rocks display prominent dark brown wavy bands which approximately parallel the cleavage. In some cases these bands appear to truncate clasts and may be the result of the accumulation of insoluble material along pressure solution surfaces.

IRON FORMATION

Several outcrops of magnetite iron formation were found (localities 77, 93, 128 and 131, Fig. 2-6). The iron formation was generally found in dark brown to green, often chlorite-rich, fine-grained rocks as thin laminated layers (locality 128, Fig. 2-6) or as a mass of fine-grained magnetite (locality 77, Fig. 2-6). At this latter outcrop the rock was composed of fine-grained chlorite and quartz aggregate with abundant fragments of magnetite. Biotite laths were also observed pseudomorphing quartz clasts.

An aeromagnetic map of the Wild Potato Lake and Partridge Crop Lake area (Fig. 3-3) clearly reflects the presence of the iron formation in the discrete positive anomalies. The trends of the anomalies closely conform to the structure as interpreted in the area.

VOLCANIC ROCKS

Two principal types of volcanic rock occur in the study area. Firstly, mafic volcanic rocks, commonly pillowed or massive and secondly, pyroclastic units. Although pillowed lavas are common in the mafic

Fig. 3-3 Aeromagnetic map of the Wild Potato Lake area. The presence of iron formation is reflected in the discrete positive anomalies. (From OGS 1980: Airborn Electromagnetic and Total Intensity Magnetic Survey, Atikokan-Mine Centre Area, Western Part, District of Rainy River; by Quester Surveys Limited for the Ontario Geological Survey, Geophysical/Geochemical Series, Maps 80505 and 80507, Scale 1:20,000. Survey and Compilation, December 1979 to April 1980).

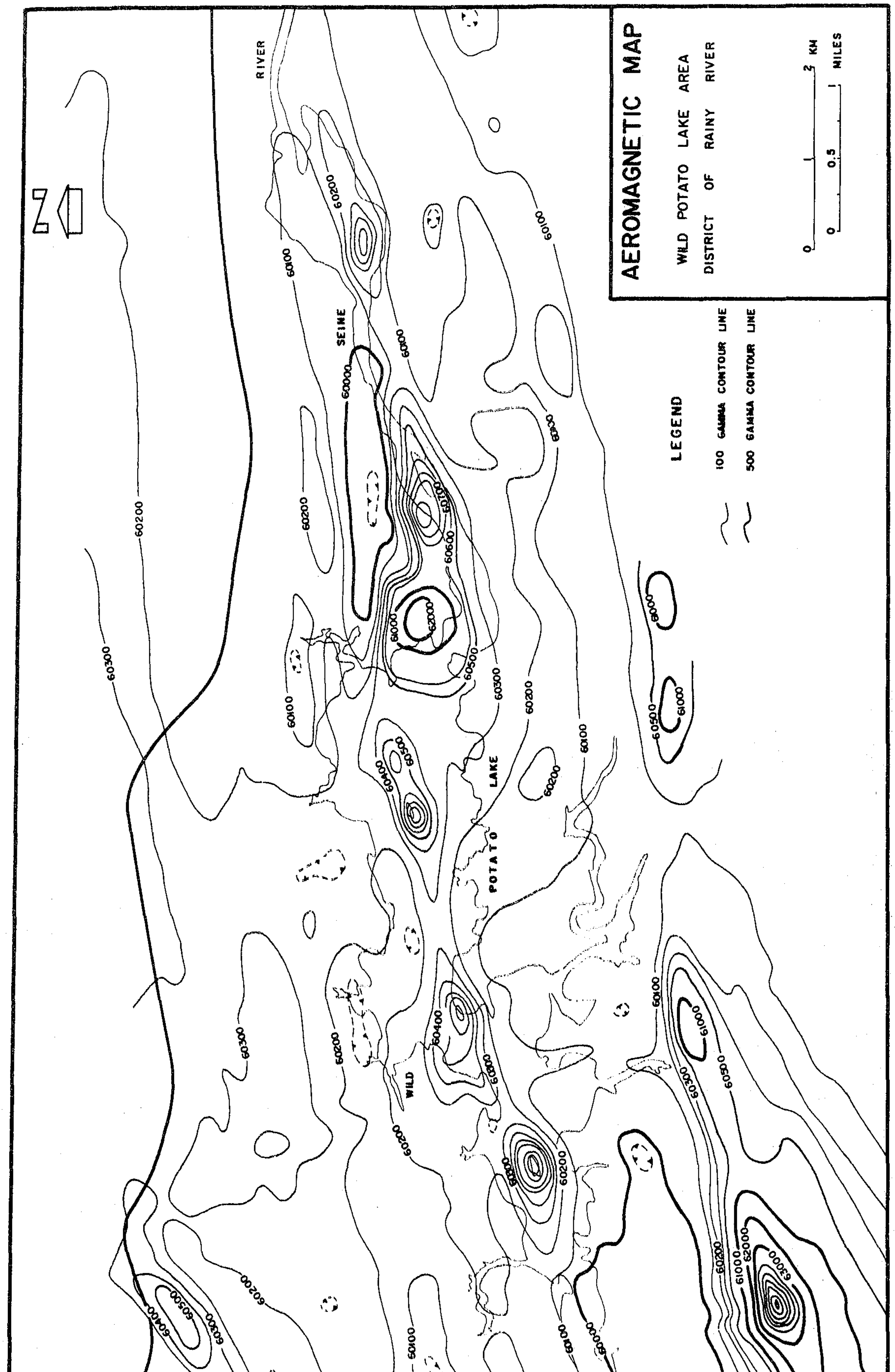
AEROMAGNETIC MAP
WILD POTATO LAKE AREA
DISTRICT OF RAINY RIVER
0 1 2 KM
0 0.5 1 MILES
LEGEND
100 GAMMA CONTOUR LINE
500 GAMMA CONTOUR LINE
SEINE
RIVER
WILD
POTATO
LAKE
N

volcanic rocks deformation of the pillows is such that younging directions are questionable (see Appendix A). At one outcrop (locality 43, Fig. 2-6) a small exposure of amygdaloidal basalt, about 5 metres thick, was found enclosed by sedimentary rocks, near the contact with the volcanic rocks. The pyroclastic volcanic rocks tend to be more massive and are commonly composed of large feldspar fragments, with some aggregates of feldspar and quartz, set in a matrix of highly-deformed chlorite, calcite and quartz.

INTRUSIVE ROCKS

A small undeformed north-south trending quartz-diabase dyke was found at outcrop 95 (Fig. 2-6) and was composed of large crystals of plagioclase, augite and quartz with a random orientation.

Stratigraphic Relations

In the western part of the map area, Wood (1980) suggests that the sedimentary rocks of the Seine Group unconformably overlie the volcanic rocks which Lawson (1913) correlated with the Keewatin at Rainy Lake. Wood also suggests that the conglomerate is a basal conglomerate and thus underlies the finer-grained clastic sedimentary rocks. In the northwest part of the map area the volcanic rocks do appear to be older than the sedimentary rocks although contacts are not exposed. Strong evidence to support this is provided at localities 40 to 44 (Fig. 2-6). At localities 40, 41, 42 and 43 sedimentary rocks consistently young to the south. At locality 44, north of the above localities, grading in silt horizons within volcanic rocks also yields younging directions towards the south, towards the sedimentary rocks. Further, as shown on the structural map in the rear folder, the axial trace of a major E-W trending syncline lies to the south of all these localities. Therefore, at least in this area, the volcanic rocks both structurally and stratigraphically underlie the sedimentary rocks. Whether or not the contact is unconformable is debatable however as it appears to be somewhat gradational in places. This is especially evident along Highway 11, again around locality 43 (Fig. 2-6), where thin layers of sandstone and volcanic rocks are interbedded.

At the eastern extent of the map area there is limited evidence to suggest that the sedimentary rocks there are older than the volcanic rocks. At locality 7 (Fig. 2-6) finely-laminated interbedded silts and chloritic tuffs young towards the south - both crossbedding and grading in the silts yield the same younging direction for the rocks. Further, S_0 - S_1 relations and minor folding imply that this locality is on the southern limb of an E-W trending anticline. To the north of this locality are found sedimentary rocks while to the south are found volcanic rocks. However, no younging indicators were found in the volcanic rocks east along Highway 11, stratigraphically south of this locality.

It is likely then that more than one sequence of volcanic rocks exist in the study area: older volcanic rocks in the west which underlie the Seine sedimentary rocks, and younger volcanic rocks in the east which overlie the same sediments.

Within the sedimentary units, field evidence suggests that conglomerate and sandstone in general are interbedded regardless of location. At Shoal Lake the sandstones young towards the northwest, away from the conglomerate and thus appear to be younger than the conglomerate. Along Highway 11 however, sandstone units at localities 42 and 43 (Fig. 2-6) young to the south towards locality 41 (conglomerate) which also youngs to the south. As mentioned above, these localities are on the northern limb of an E-W trending syncline. The position of the axial trace of this syncline is fixed by localities 61 and 37, on the northern limb and localities 56, 36A and 62 on the southern limb - these are all outcrops of conglomerate. At locality 60, north of Wild Potato Lake, crossbedded siltstone and sandstone young towards the north. Immediately to the north, at localities 61a and 59 are found north-younging conglomerate units. Thus the conglomerate appears to form the core of the syncline flanked to the north and south by older sandstones.

The axial trace of a major anticline can be located from the eastern end of Wild Potato Lake, north of the Seine River to the Hydro-electric dam at Sturgeon Falls (locality 48). Eastwards, along the highway from locality 36A a series of conglomerate outcrops all young towards the north, as far as the contact with the sandstone at locality 27. Further to the east the road bends northwards and the conglomerate appears again at locality 23. Stratigraphically to the south of the conglomerate is older northwards younging sandstone, which forms the core of the anticline. At locality 22, which is on the south limb of the anticline a small outcrop of conglomerate is found. The conglomerate is not found to the west along the Seine River or at Partridge Crop Lake so it appears to wrap around the nose of the fold and pinch out along strike to the west.

To the east however, a contact between conglomerate and sandstone is observed at locality 48, above Sturgeon Falls. Here conglomerate is in contact with sandstone to the south - younging from the sandstone is to the south. S_0 - S_1 relations also show that this locality is on the southern limb of the anticline. To the north are numerous conglomerate outcrops while to the south are a series of sandstone outcrops. Thus the sandstone here appears to be younger than the conglomerate. Bedding in the sandstone at locality 20 is sub-horizontal and is close to the core of a syncline.

At locality 19, sandstone shows a transition eastwards and southwards into conglomerate, but no younging indicators are observed. At locality 17 however, just southeast of locality 19, younging in the conglomerate is towards the north and $S_0 - S_1$ relations show that the outcrop is on the north limb of an E-W trending anticline. The conglomerate here shows a transition into sandstone to the east which now youngs towards the south (locality 14). $S_0 - S_1$ relations here show that the locality is now on the south limb of the anticline, so the sandstone is older than the conglomerate and forms the core of the anticline. The conglomerate can be traced along the highway eastwards as far as locality 10. At locality 9, a 6-metre thick layer of conglomerate is interbedded with sandstone.

Therefore the suggestion that the conglomerate is basal and hence older than the finer-grained clastic sediments can only hold true for the Shoal Lake area. Elsewhere, the units appear to be interbedded in a more complex way and do not tend to be persistent along strike for any great distance.

Metamorphism

The abundance of pelitic rocks in the study area provides a good indication of the grade of metamorphism. Common metamorphic assemblages of biotite, muscovite, sericite, quartz and chlorite with occasional carbonate suggest that the metamorphic grade falls into the chlorite to biotite zone of the Greenschist Facies. Also the persistence of these assemblages throughout the whole area implies a more or less uniform distribution of temperature and pressure.

In general these metamorphic minerals, especially the phyllosilicates, exhibit a high degree of preferred orientation parallel to the axial trace of major folds, which would imply a syntectonic metamorphism and development of cleavage. However biotite, and locally muscovite, chlorite and calcite commonly pseudomorph clastic grains and also randomly cut across all other metamorphic phyllosilicates, suggesting that they were formed later than the development of cleavage. Therefore metamorphism appears to have been generally synkinematic with the folding but in places may have outlasted it.

CHAPTER 4

STRAIN ANALYSIS TECHNIQUES IN CONGLOMERATIC ROCKS

DEFORMATION OF NON-SPHERICAL OBJECTS

Cloos (1947), from the study of the 'fluctuation in orientation' of the major axes of elliptical sections of deformed ooids, first made the observation that perhaps some of the unusually high variations in orientation at low strains could be due to original eccentricity and that the ooids initially deviated from a perfect spherical form. Serious consideration to the problem was given by Ramsay (1967) and thus much of the initial part of this chapter follows his work.

Consider the effect on an initially non-circular shape on the resulting form after a coaxial strain history, assuming passive behaviour of the objects, no volume change and that the objects are initially elliptical in shape.

The shape and orientation of the final ellipses will depend on three factors:

1. the ratios of the principal axes of the original ellipses,
2. the ratio of the principal tectonic strain axes,
3. the orientations of the axes of the original ellipses with respect to the principal strain directions.

In Figure 4-1 a series of undeformed elliptical markers with variable shape but similar initial axial ratio are randomly oriented. Figures 4-2 and 4-3 show the effects of successive coaxial strain increments on the

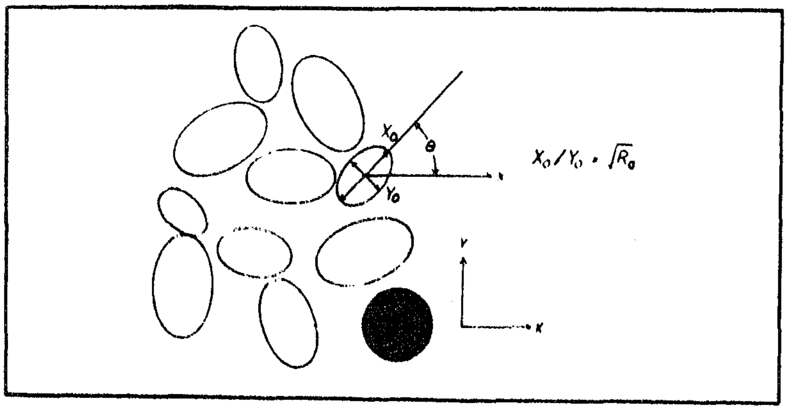

Fig. 4-1 Suite of elliptical objects with constant axial ratio and variable orientation. (From Ramsay, 1967).

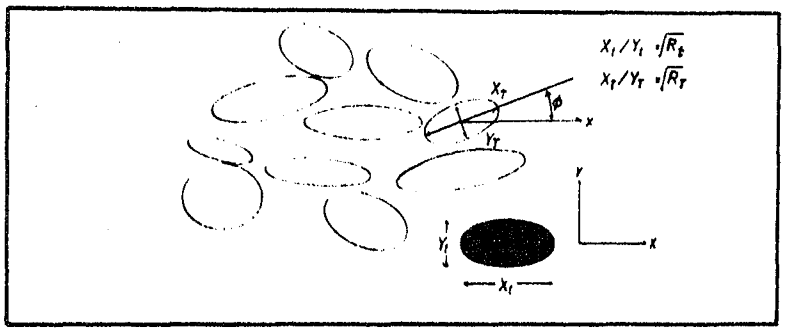

Fig. 4-2 Ellipses from Figure 4-1 deformed by a homogeneous strain $(R_T)^{\frac{1}{2}}$. (From Ramsay, 1967).

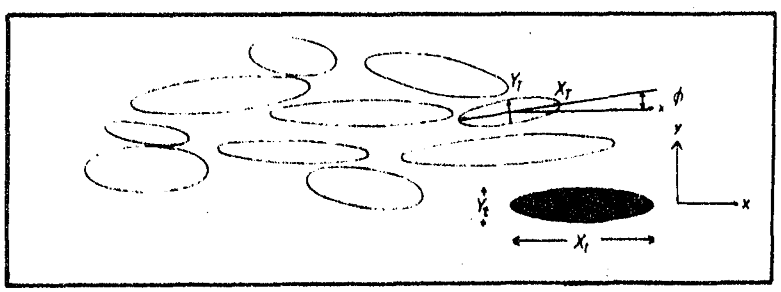

Fig. 4-3 Ellipses from Figure 4-2 further modified by a greater homogeneous strain than that for the deformation in Figure 4-2. The resulting ellipses show a great variation in axial ratio and fluctuation is decreased. (From Ramsay, 1967).

markers - notice that the markers apparently change shape and thus orientation of long axes.

Ramsay (1967) has shown that it is possible to establish the resulting shape and orientation of the final ellipse knowing the shape and orientation of the original ellipse and of the tectonic ellipse, such that: if

ϕ is the orientation of the final deformed ellipse,

$R_t^{\frac{1}{2}}$ is the axial ratio of the tectonic strain ellipse,

θ is the orientation of the original undeformed ellipse with respect to the principal extension direction, λ_1, of the tectonic ellipse,

$R_o^{\frac{1}{2}}$ is the axial ratio of the original undeformed ellipse,

then

$$\tan 2\phi = \frac{2R_t^{\frac{1}{2}}(R_o - 1)\,\mathrm{Sin}\,2\theta}{(R_o + 1)(R_t - 1) + (R_o - 1)(R_t + 1)\,\mathrm{Cos}\,2\theta} \qquad \text{4-1 (Ramsay, eq. 5-22)}$$

This relates the orientation of the final ellipse (ϕ) to the axial ratio of the tectonic strain ellipse ($R_t^{\frac{1}{2}}$) and the orientation (θ) and axial ratio of the original ellipse ($R_o^{\frac{1}{2}}$).

From equation 4-1 it is possible to establish the orientation of the final ellipse. Ramsay (1967) has also derived equations which relate the final shape of the ellipse ($R_T^{\frac{1}{2}}$) to the orientation (ϕ), the tectonic strain ellipse shape ($R_t^{\frac{1}{2}}$) and the original ellipse shape ($R_o^{\frac{1}{2}}$).

$$R_T = \frac{\tan^2\phi\,(1 + R_o\tan^2\theta) - R_t\,(\tan^2\theta + R_o)}{R_t\tan^2\phi\,(\tan^2\theta + R_o) - (1 + R_o\tan^2\theta)} \qquad \text{4-2 (Ramsay, eq. 5-27)}$$

THE "R_f/ϕ" METHOD OF STRAIN ANALYSIS

Equations 4-1 and 4-2 form the basis of perhaps the most widely used technique of strain analysis in conglomeratic rocks, as put forward by Ramsay (1967). The technique depends upon establishing graphs of "fluctuation" (ϕ) versus final pebble shape ($X_f/Y_f = R_T^{\frac{1}{2}}$ or R_f), in order to determine how the ratios of the axes of the deformed ellipses vary with the orientations of their long axes.

Field measurements of long and short axes of pebbles and the orientation (α) of the long axes relative to some arbitrary line in space can be made on joint surfaces. Graphs of axial ratio against α can then be plotted. If the strain is homogeneous and the markers had an initially random fabric, then the plot should be symmetrical about some value of α (Figure 4-4).

ELIMINATION OF INITIAL SHAPE FACTOR R_o

Figure 4-4 will yield a maximum R_T value and a minimum R_T value depending on the initial orientation of the markers. When $\theta = 0$, R_T = max. and when $\theta = 90$, R_T = min. (where θ is the angle between the undeformed pebble long axis and the principal extension direction).

Consider when $\theta = 0$:

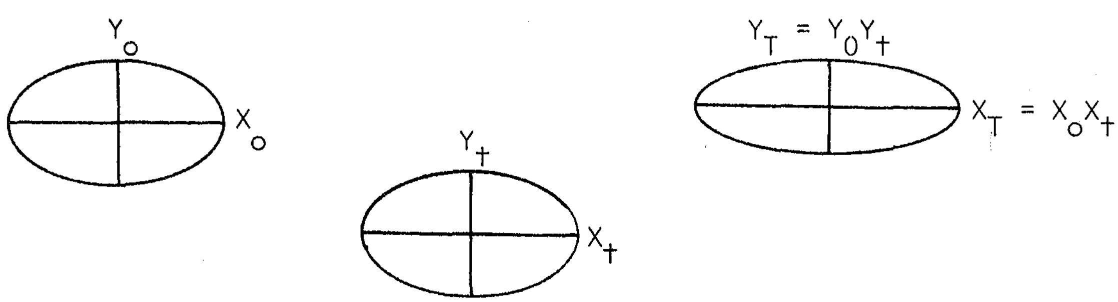

$$(R_{Tmax})^{\frac{1}{2}} = X_T/Y_T = X_oX_t/Y_oY_t = (R_oR_t)^{\frac{1}{2}}$$

$$\therefore\ (R_{Tmax})^{\frac{1}{2}} = (R_oR_t)^{\frac{1}{2}} \text{ and } \theta = 0 = \phi$$

Consider when $\theta = 90$: if $R_t = R_o$

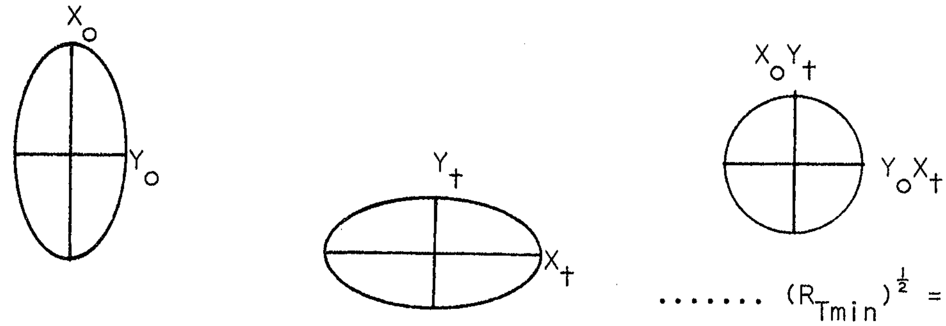

.... $(R_{Tmin})^{\frac{1}{2}} = 1$

if $R_t < R_o$

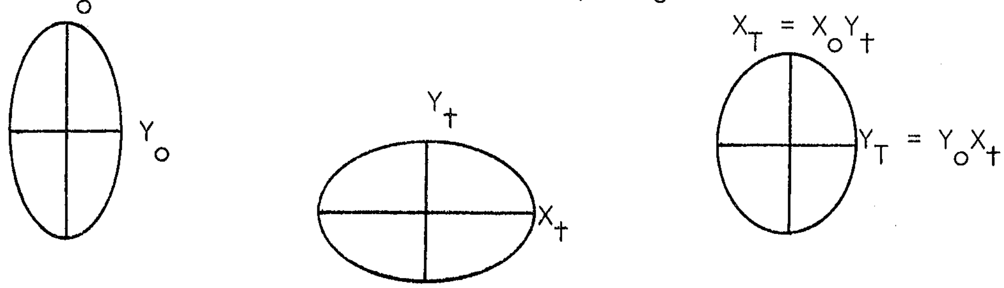

$(R_{Tmin})^{\frac{1}{2}} = X_oY_t/Y_oX_t = (R_o/R_t)^{\frac{1}{2}}$ and $\phi = 90$.

if $R_t > R_o$

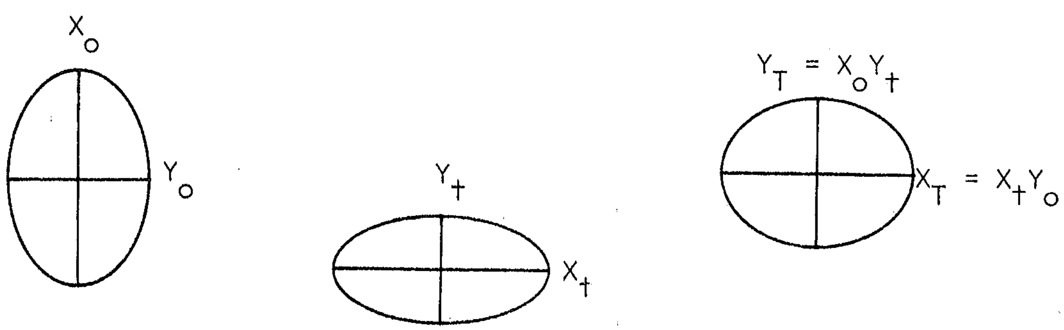

$(R_{Tmin})^{\frac{1}{2}} = Y_oX_t/X_oY_t = (R_t/R_o)^{\frac{1}{2}}$ and $\phi = 0$.

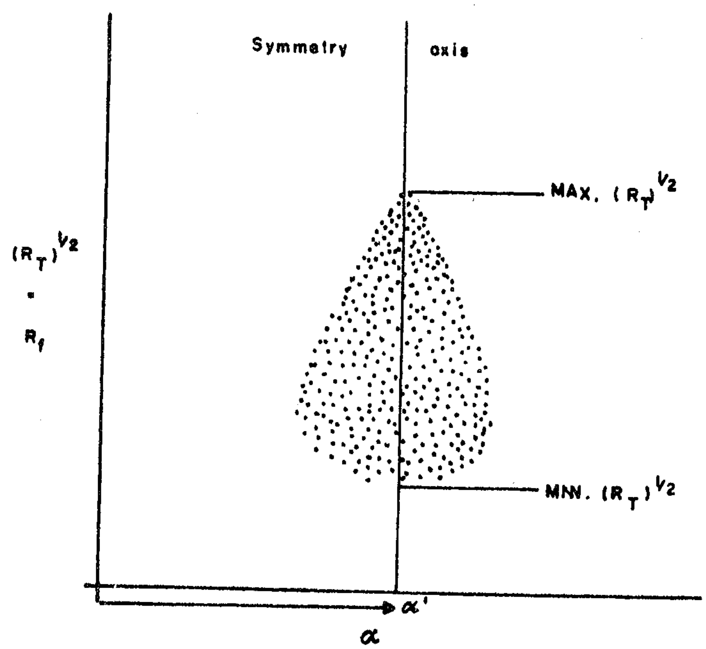

Fig. 4-4 Plot of final shape (R_T) against orientation (α) for homogeneously deformed ellipses which originally had variable axial ratios. (After Ramsay, 1967).

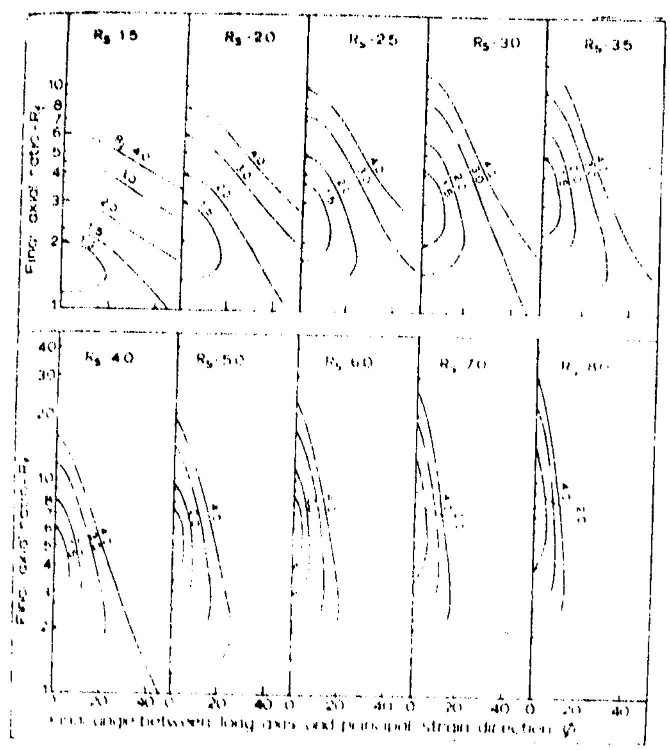

Fig. 4-5 Curves of variation in R_f/ϕ for initial ellipse ratios, R_i, subject to various finite strain ratios, R_s. The curves are symmetric about the 0° ϕ axis. (From Dunnet, 1969).

Therefore,

1. $(R_{Tmax.})^{\frac{1}{2}} = (R_o R_t)^{\frac{1}{2}}$ when $\theta = \phi = 90$

2. $(R_{Tmin.})^{\frac{1}{2}} = (R_t/R_o)^{\frac{1}{2}}$ when $\theta = 90,\ \phi = 0$ and $R_t > R_o$

   $(R_{Tmin.})^{\frac{1}{2}} = (R_o/R_t)^{\frac{1}{2}}$ when $\theta = 90,\ \phi = 90$ and $R_t < R_o$

So two cases of $R_{Tmin.}$ exist depending on whether $R_t > R_o$ or $R_t < R_o$. By multiplying or dividing $R_{Tmax.}$ by $R_{Tmin.}$, R_t or R_o can be obtained alone.

By application of this method on three mutually perpendicular planes cut through a deformed conglomerate, or more easily, on sections parallel to the principal planes of the strain ellipsed, it is possible to isolate R_t in each section and thus determine the tectonic strain, as described by Ramsay (1967, p. 199-200). This forms the basis for the R_f/ϕ method.

MODIFICATIONS OF THE R_f/ϕ TECHNIQUE OF STRAIN ANALYSIS

In Ramsay's (1967) equations 5-22 and 5-27, equations 4-1 and 4-2 here, we have seen that he was able to derive functions in the form:

$$\tan 2\phi = f(R_i,\ R_s,\ \phi) \qquad 4\text{-}3$$

and

$$R_f = f(R_i,\ R_s,\ \theta,\ \phi) \qquad 4\text{-}4$$

where

R_i = original undeformed particle axial ratio = $R_o^{\frac{1}{2}}$

R_f = final deformed particle axial ratio = $R_T^{\frac{1}{2}}$

R_s = finite strain axial ratio = $R_t^{\frac{1}{2}}$

θ = angle between R_i long axis and principal strain direction

ϕ = angle between R_f long axis and principal strain direction.

Adopting the same assumptions as Ramsay, that is:

1. the initial suite of elliptical markers is randomly oriented,
2. no ductility contrast exists between markers and matrix, so the markers deform homogeneously with the matrix,
3. the strain history is coaxial,
4. there is no volume change.

Dunnet (1969) has suggested that another relationship must exist of the form:

$$R_f = f(R_i, R_s, \phi) \qquad 4\text{-}5$$

because θ and ϕ are not independent.

This relates the two final parameters, R_f and ϕ, to the two controlling parameters, R_i and θ.

Dunnet's (1969) equation 16 is reproduced below:

$$\text{Cos } 2\phi = \frac{R_i(R_f^2 + 1)(R_s^2 + 1) \pm 2(R_i^2 + 1)R_s \times R_f}{R_i(R_f^2 - 1)(R_s^2 - 1)} \qquad 4\text{-}6$$

For any set values of R_i and R_s the locus of R_f/ϕ will reflect only the variation in initial orientation (θ) of the particles (Dunnet, 1969). Therefore, a suite of particles of constant initial shape, but variable orientation will have, after deformation, R_f/ϕ parameters which lie on a hyperbolic curve around the finite strain value. Dunnet has constructed theoretical curves from equation 4-6 and similar equations (Dunnet 1969, eq. 28) which can be directly compared with R_f/ϕ diagrams collected from field data. Field measurement of axial ratio and orientation of long axis can be carried out in the same way as Ramsay (1969) suggested. Some of these theoretical curves are illustrated in Figure 4-5 - the curves are plotted on log/linear graph paper to produce plots which are symmetric about the strain ratio R_s.

One of the main limitations of this method is immediately apparent in that it relies on a visual best fit of data to theoretical curves. Therefore, there is no statistical way of assessing accuracy, which is mainly due to the fact that nothing is known, or assumed about the initial shape (R_i) of the elliptical markers.

THETA-CURVE METHOD

In view of this problem Lisle (1977a) has modified Ramsay's equations in order to be able to introduce statistical criteria for curve - matching and therefore to provide for a measure of 'goodness of fit' for the data. Lisle's analysis was conducted on clastic grains from a competent greywacke bed within the Aberystwyth Grits at Cwm Tydi, Cardinganshire, Wales, but is just as easily applicable to deformed elliptical markers within a conglomerate.

By combining Ramsay's (1967) two basic equations for R_f and ϕ (eq. 5-22 and 5-27, or equations 4-1 and 4-2 here),

$$\tan 2\phi = \frac{2R_s(R_i^2 - 1)\sin 2\theta}{(R_i^2 + 1)(R_s^2 - 1) + (R_i^2 - 1)(R_s^2 + 1)\cos 2\theta} \qquad 4\text{-}1$$

and

$$R_f = \left[\frac{\tan^2\phi\,(1 + R_i^2 \tan^2\theta) - R_2^2\,(\tan^2\theta + R_i^2)}{R_s^2 \tan^2\phi\,(\tan^2\theta + R_i^2) - (1 + R_i^2 \tan^2\theta)} \right]^{\frac{1}{2}} \qquad 4\text{-}2$$

R_i is eliminated to give:

$$R_f = \left[\frac{\tan 2\theta(R_s^2 - \tan^2\phi) - 2R_s \tan \phi}{\tan 2\theta(1 - R_s^2 \tan^2\phi) - 2R_s \tan \phi} \right]^{\frac{1}{2}} \qquad \text{4-7}$$

(Lisle, 1977a p. 385)

So R_f is thus related to ϕ and θ. For a given strain, R_s, equation 4-7 allows the construction of the locus on an R_f/ϕ diagram of all ellipses with a particular original orientation θ (Lisle, 1977a). Lisle calls these curves "Theta-curves".

Figure 4-6a shows a set of vertical lines, for the undeformed state, set out in 9° intervals. These are lines of constant angle with reference to an arbitrary line $\theta = 0$. The vertical scale represents initial shape, R_i, so that the dotted horizontal lines are lines of constant R_i. If a suite of undeformed elliptical markers with a perfectly random orientation is plotted on the diagram, each vertical column should contain equal numbers of data (5%). Figure 4-6b shows the shape adopted, after a deformation such that $R_s = 2.2$, by the curves of constant R_i and θ (θ-curves). On this diagram we would expect the now deformed groups of θ-curves still to contain equal numbers of data points.

The value of R_s using this method, like the R_f/ϕ technique of Dunnet (1969), depends on finding the best fit set of theoretical curves to the R_f/ϕ data derived from field measurements. The difference here is that we now have a statistical test which can be applied; that is, the "Chi-squared" test. From the number of data collected, the expected number of points to fall in each sub-area can be calculated. These can then be compared with the observed number of data points in each sub-area.

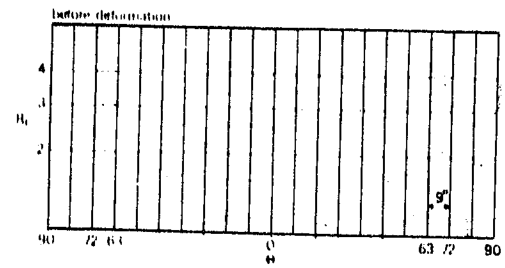

Fig. 4-6a. R_i/θ diagram. If there is no preferred orientation before deformation, each subarea of 9° width will be expected to contain 9/180 = 5% of the total number of markers. (From Lisle, 1977a).

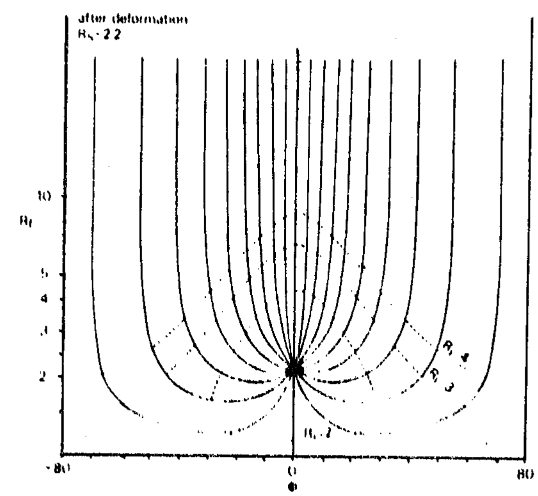

Fig. 4-6b. R_f/ϕ diagram for R_s = 2.2 showing the shapes adopted, after deformation, by the curves of constant R_i and constant θ (θ-curves). (From Lisle, 1977a).

Therefore, for each family of θ-curves, we can calculate χ^2 (Chi-squared):

$$\chi^2 = \sum_{i=1}^{i=n} \frac{(O_i - E)^2}{E} \tag{4-8}$$

where

O_i is the observed number of points in the i^{th} area

n is the number of sub-areas

E is the expected number of points in each area.

The family of θ-curves giving the lowest value of χ^2 is then taken to indicate the best fit R_s value. The value of χ^2 at best fit will also give an indication of the "goodness of fit" of the data.

The above methods of strain analysis all relate the final shape and orientation of the marker to the shape and orientation of the strain ellipsoid and the orientation and/or shape of the original marker. The basic limitations of these techniques lie in two very important assumptions which they all make, namely:

1. the initial orientation of the markers is random,
2. no ductility contrast exists between marker and matrix. This means that the markers will behave as passive objects and will deform homogeneously with the matrix.

They also assume constant volume deformation and a coaxial strain history.

1. Initial Orientation of Markers

Any sedimentary fabric which results in a preferred orientation of markers symmetrical about, for example, a bedding plane will yield an

R_i/θ distribution in the undeformed state closely resembling the "onion" curves of Dunnet (1969) on the R_f/ϕ diagrams for the deformed state. When the markers are subsequently deformed, it will be difficult to separate the pretectonic sedimentary fabric from the tectonic strain. Sedimentary compaction or successive increments of strain will yield similar distributions.

Undeformed conglomerates and sandstones commonly show some form of preferred orientation of pebbles or clasts. Generally, the shortest axes of the clasts line up approximately perpendicular to bedding, or occasionally there may be an additional preferred alignment of clast long axes about some preferred direction within or at an angle to the bedding trace.

In Figure 4-7a (taken from Ramsay, 1967, Fig. 5-38), axial ratios of markers, which have a variable orientation up to ±10° to a bedding trace, are plotted against long axis angle with bedding. The distribution is remarkably similar to the R_f/ϕ plots of Dunnet (1969). If the markers are deformed now with the matrix by a homogeneous finite strain, R_s, they will all change their shape and orientation depending on the axial ratio and orientation of the strain ellipse. The resultant R_f/ϕ plot for the deformed markers is shown in Figure 4-7b.

Two important observations are obvious immediately from Figure 4-7b. Firstly, the distribution of deformed markers is asymmetric about the bedding trace. Secondly, the distribution is offset with respect to the principal axis of the strain ellipse.

Therefore, on an R_f/ϕ plot from measured data, asymmetry of this kind will be indicative of a pre-tectonic sedimentary fabric, or of the superposition of successive strain increments.

Fig. 4-7 (a) R_i/θ plot for undeformed ellipses which have a preferred alignment of long axes symmetrical about a bedding trace. (After Ramsay, 1967).

(b) R_f/ϕ plot for ellipses in Figure 4-7(a) after a homogeneous strain, R_s. (After Ramsay, 1967).

Fig. 4-8 Curves for passive pure shear deformation of ellipses. Solid lines are strain paths, broken lines are curves of equal strain increments. The lower diagram is an example of the transformation of a line element S, and a suite of ellipses, abcd, by deformation through $R_S^{\prime}$ to $R_S^{\prime\prime}$. (From Dunnet and Siddans, 1971).

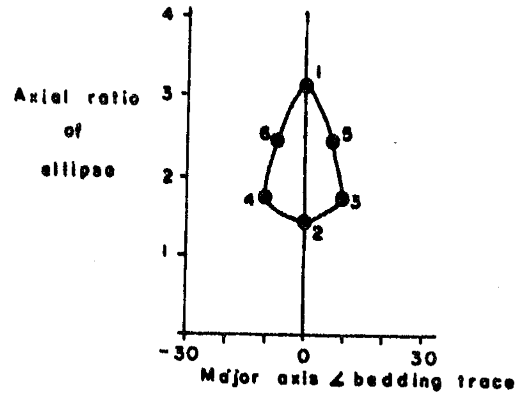
Axial ratio of ellipse
Major axis ∠ bedding trace

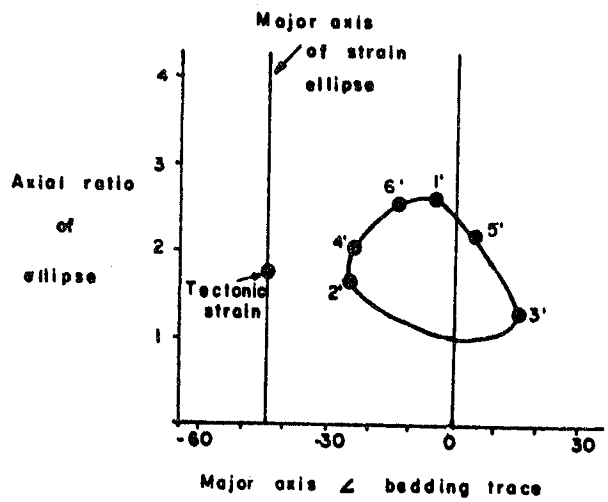
Major axis of strain ellipse
Axial ratio of ellipse
Tectonic strain
Major axis ∠ bedding trace

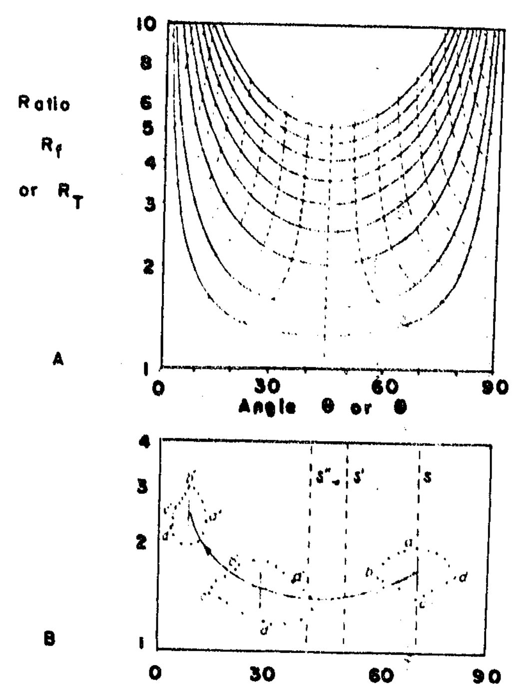
Ratio R_f or R_T
A
Angle θ or ϕ
B

Gay (1968a, fig. 6) has presented a graph of deformation paths (change of ellipse ratio and long axes orientation) of passive (no ductility contrast) elliptical objects subjected to progressive pure shear. The graph is reproduced in Figure 4-8 - solid lines are strain paths and broken lines are curves of equal strain increments. Any point on the graph represents an ellipse with coordinates R_i, θ, which when deformed will move along the appropriate deformation path, through a specific number of increments of strain, to a new ratio and orientation R_f/ϕ (Dunnet and Siddans, 1971). A suite of ellipses of constant initial axial ratio but variable orientation will move along different deformation paths to lie on a curve of R_f/ϕ given by the equation (Dunnet, 1969, eq. 28),

$$\text{Cos } 2\theta = \frac{\text{Cosh } 2\,\varepsilon f \text{ Cosh } 2\varepsilon s - \text{Cosh } 2\,\varepsilon i}{\text{Sinh } 2\varepsilon f \text{ Sinh } 2\varepsilon s} \qquad 4\text{-}9$$

where εf, εs and εi are the logarithmic ellipse ratios ($\varepsilon = \ln(1 + e)$).

The lower diagram in Fig. 4-8 illustrates how a field of elliptical markers (abcd), with a preferred orientation symmetrical about a bedding plane, S, is deformed along specific strain paths, through intermediate fields, a'b'c'd', to new ratios and orientations in the field a"b"c"d".

The bedding trace, S, is changed in its orientation during the deformation through S' to S" as the tectonic strain ratio increases through R_s' to R_s'' governed by the equation (Ramsay, 1967, eq. 3-4),

$$R_s \tan \alpha' = \tan \alpha \qquad 4\text{-}10$$

which relates line elements in the deformed and undeformed states (where α and α' are the angles between the undeformed and deformed line elements and the principal extension direction). The change of ellipse long axis is governed by the relationships in equation 4-9. During deformation the long axes of the particles will apparently migrate towards the principal tectonic extension direction. Thus, even if the undeformed elliptical particles were symmetric about the bedding trace, they will become tectonically "imbricated". In the resultant fabric, the mean ellipse axes, the deformed bedding trace and the local tectonic extension direction will all be oblique to one another.

As a consequence of this observation, Dunnet and Siddans (1971) have proposed an extension to the R_f/ϕ technique of strain analysis on 2-dimensional sections, to incorporate some non-random sedimentary fabrics. If the elliptical markers were initially symmetric about the bedding trace, the strain could be removed systematically from the deformed ellipse fabric until the mean of the ellipse long axes and the bedding trace coincide. In this way a measure of the strain may be estimated. This can be done graphically, using the pure shear strain paths for the suite of ellipses and by use of equation 4-10. Alternatively, the strain may be removed from each R_f/ϕ data point individually, in successive increments, to where the field of data (R_i/θ) is symmetric about the undeformed bedding trace. Dunnet and Siddans (1971) have developed computer programs for the latter method.

Where the bedding trace is parallel or at a low angle to the principal strain direction, the method does not work or is inaccurate.

2. Ductility Contrasts

So far it has been assumed that we have been dealing with a totally homogeneous rock in which there is no ductility contrast either between markers, or between markers and matrix. Clearly however this assumption is not valid in most conglomerates - firstly, there is usually a wide range of pebble types and secondly, the matrix material is seldom of the same composition as the pebbles.

Gay (1968b) has discussed the progressive deformation of inhomogeneous materials by pure shear and simple shear, assuming both the markers and the matrix behave as viscous fluids. The model Gay used was that of a Newtonian fluid matrix in which were embedded elliptical particles. These particles were also assumed to be Newtonian bodies but differing from the matrix in coefficient of viscosity.

(a) Pure Shear Deformation

(i) Ellipse Axes Parallel to Strain Axes

Gay considered first the pure shear deformation of a single elliptical particle with its axes parallel to the strain axes and derived the following equation (Gay, 1968b, eq. 16) for the change in particle axial ratio during deformation:

$$\ln (X_f/Y_f) = \ln (X_i/Y_i) + (5/(2R + 3)) \ln (\lambda_1/\lambda_2)^{\frac{1}{2}} \qquad 4\text{-}11$$

where

X_f and Y_f are the major and minor axes of the resultant ellipse,

X_i and Y_i are the major and minor axes of the original ellipse,

R is the viscosity ratio between the particle and the matrix,

$(\lambda_1)^{\frac{1}{2}}$ and $(\lambda_2)^{\frac{1}{2}}$ are the principal extensions of the strain ellipse.

The viscosity ratio, R, is defined as the ratio of the coefficient of viscosity of the particle to the coefficient of viscosity of the matrix.

Equation 4-11 is plotted in Figure 4-9 for initially circular ($X_i/Y_i = 1$) particles and different values of R ranging from 0 to 50.

Clearly, equation 4-11 has the form:

$$y = nx + c$$

which is the equation for a straight line where, $(5/(2R + 3)) = n$, or the gradient of the line. Thus the factor $(5/(2R + 3))$ is a viscosity factor which controls the change in particle shape during the pure shear deformation of the system.

It is also apparent, from the graph in Figure 4-9, that for an increase in viscosity ratio, R, the amount of strain required to cause a change in shape increases greatly. Further, for a value of R greater than about 10, the particle-matrix system has to experience very large strains to achieve a significant increase in the particle axial ratio.

(ii) Ellipse Axes Not Parallel to the Strain Axes

From previous discussion of homogeneous deformation (where R = 1), this case will result in an "apparent rotation" of principal axes of the particle towards the principal tectonic extension direction, as well as a change of shape. It has also been shown how we can predict the new orientation and shape of the deformed particle using the equations of Ramsay (1967, eq. 5-22 and 5-27, eq. 4-1 and 4-2 here). However, if the particle differs in competence from the matrix (so now $R \neq 1$), the deformation will also impart a component of rigid body rotation to the particle (Gay 1968b).

To deal with this problem, Gay (1968b) has presented a numerical solution which involves the summing of infinitesimal strains to obtain a finite pure shear.

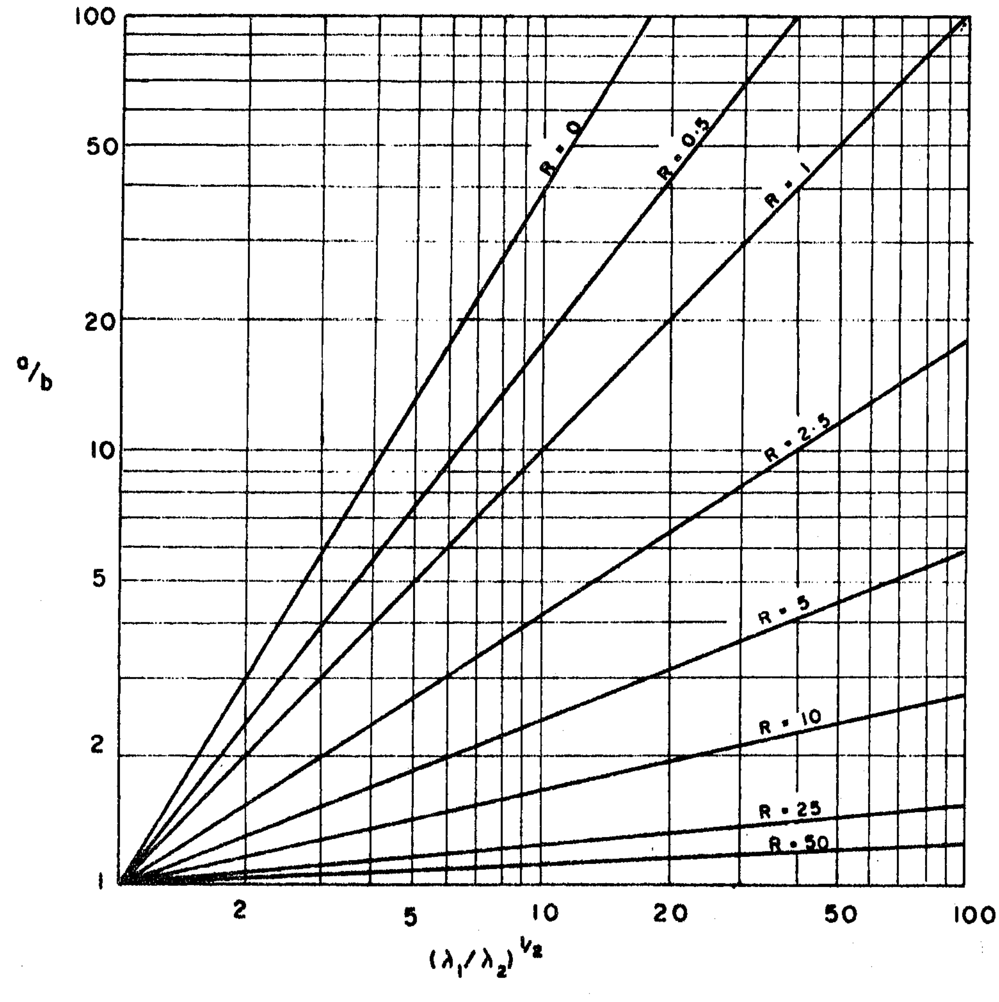

Fig. 4-9 Variation in the axial ratio of a non-rigid, initially circular particle during pure shear. (After Gay, 1968b).

The results of Gay's calculations are presented in Figure 4-10 which represents the pure deformation paths for initially 2:1 ellipses aligned at $\phi = 45°$ to the Y strain axis. This graph should be compared with Figure 4-8 (upper) which represents pure shear deformation paths for R = 1 ellipses. From Figure 4-10 it is apparent that, with increasing R, there is a rapid decrease in the change in particle shape and orientation.

(b) Simple Shear Deformation of Elliptical Objects

Simple shear is generated by displacing all points in a direction parallel to one axis, the amount of shear being proportional to the distance of the points from the other axis (Gay, 1968b).

Figure 4-11 represents simple shear deformation paths for initially circular, non-rigid particles with different values of viscosity ratios (shown by the solid lines). The dashed lines are lines of equal simple shear.

The first point to note from the graph is that, with increasing shear, the particles deform and rotate towards the shearing direction. The particles were originally at 45° to the shearing direction and ϕ on the diagram is the orientation of the particle long axis with respect to the Y' simple shear axis. Secondly, for values of viscosity ratio, R, less than one, the deformation is intense with increasing shear. However, the rate of rotation decreases with decreasing R, so that, only after considerable deformation will the particle become aligned parallel to the X' shearing direction. With increasing R however, rotation becomes very rapid, even for moderate changes of particle shape.

Therefore, if we consider a large aggregate of different particles each with different coefficients of viscosity, the amount of deformation

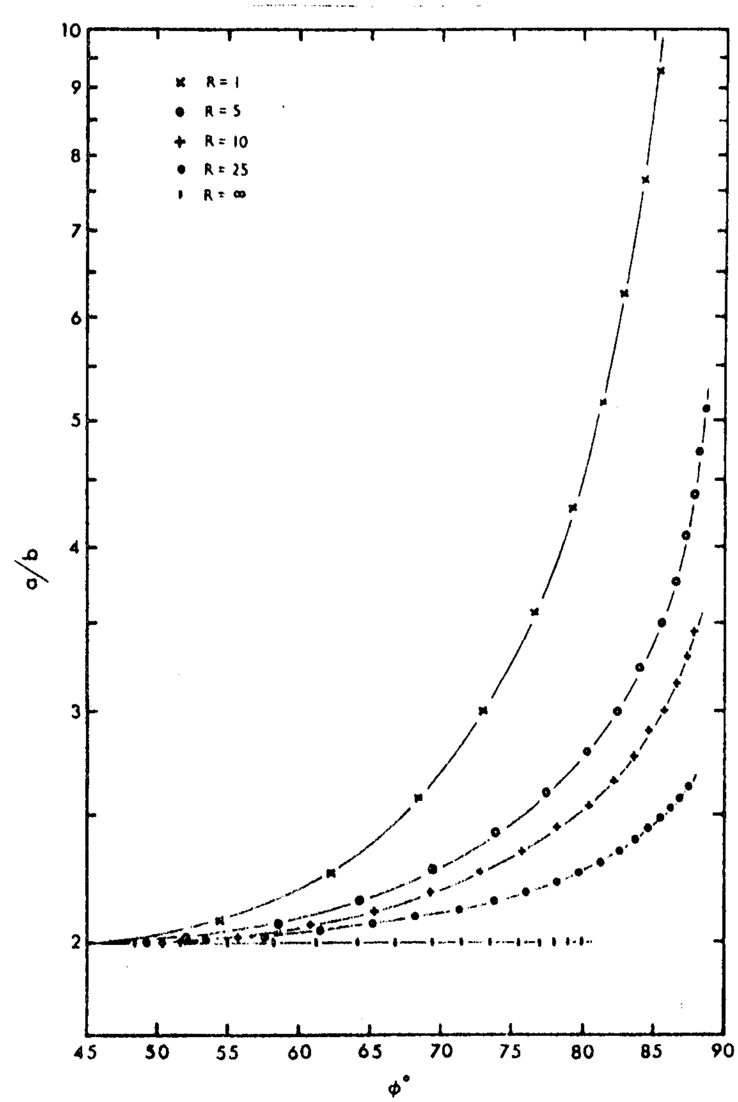

Fig. 4-10 Pure shear deformation paths for ellipses with initially 2:1 axial ratios aligned at 45° to the Y' strain axis. (From Gay, 1968b).

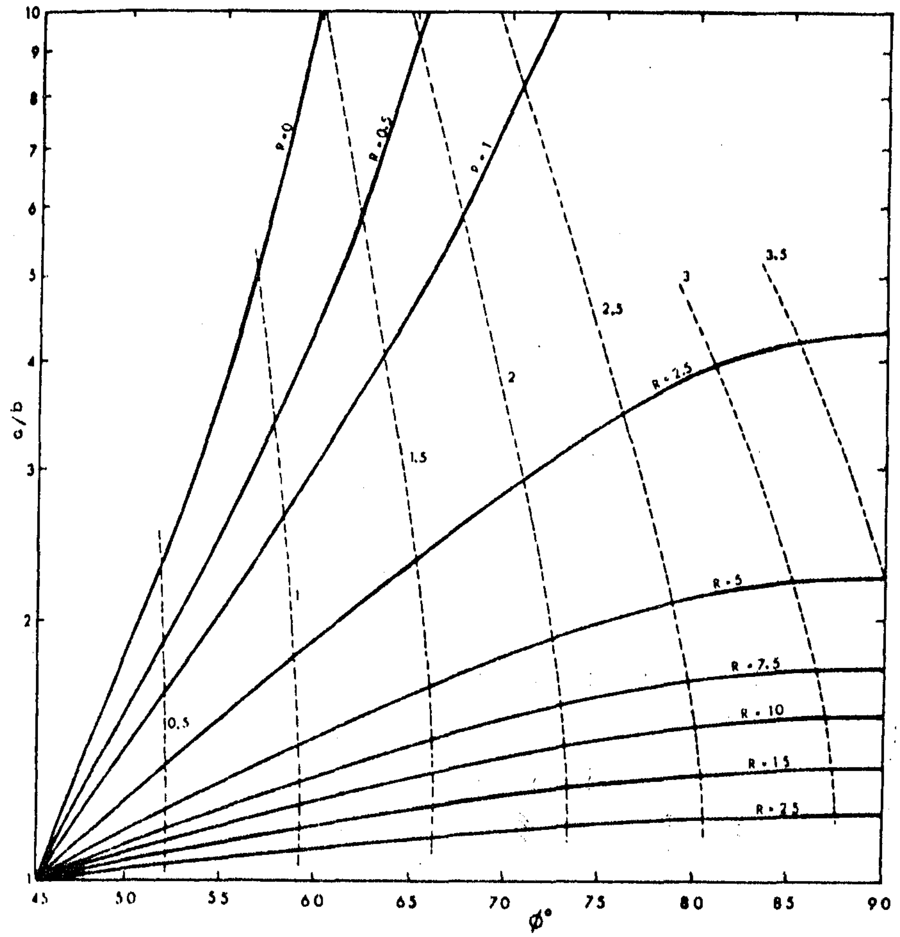

Fig. 4-11 Simple shear deformation paths for initially circular, non-rigid particles. Solid curves are deformation paths and dashed curves are lines of equal simple shear. (From Gay, 1968b).

and rate of rotation will be a function of the viscosity ratio, R, between the particle and the surrounding material. Particles with large viscosities compared with the matrix will rotate rapidly towards and conceivably through the shearing direction. Particles with moderate or similar viscosities compared with the matrix, on the other hand, will rotate more slowly, but will also deform more rapidly. If the viscosity of the particle is less than that of the matrix, so $R < 1$, then from Fig. 4-11, rotation becomes minimal and deformation is intense.

During this type of deformation, the particle axial ratio is likely to reach a maximum while aligned parallel to the shearing direction.

Application of the Effects of Ductility Contrasts

From the above discussion, the amount of deformation and the rate of rotation of a particle, both during pure shear and simple shear, will depend to a large extent on the viscosity ratio (R) of the particle to the matrix material. However, the mean viscosity of a particle-matrix system containing a large number of particles will depend on the concentration of the particles (Gay, 1968b). Gay (1968b) has derived an equation which relates the viscosity of the system to the volume concentration of the particles:

$$\mu_m = \mu'[1 + 5\psi C_v (R - 1)/(2R + 3)] \qquad \text{4-12}$$

(Gay, 1968b, eq. 25)

where

μ_m is the mean viscosity of the system,

C_v is the volume concentration of the particles in the system,

ψ is an interaction factor allowing for the interaction between the flow fields around individual particles and is dependent on C_v,

μ' is the viscosity of the particle.

Equation 4-12 can be modified to

$$R_m = R/[1 + 5\psi C_v\ (R - 1)/(2R + 3)] \qquad \text{4-13}$$

(Gay 1968b, eq. 26)

where $R_m = \mu'/\mu_m$ = the viscosity ratio.

So, if $R > 1$, $R_m < 1$ and R_m decreases with increasing ψ or C_v. Therefore, if something is known about the actual value of R_m, C_v can be calculated from perpendicular sections, a value of relative viscosity, R_a can be found from equation 4-13.

Equation 4-11 can be rewritten:

$$\ln\ (\lambda_1/\lambda_2)^{\frac{1}{2}} = ((2R_a + 3)/5)[\ln\ (X_f/Y_f - \ln\ (X_i/Y_i)] \qquad \text{4-14}$$

X_i/Y_i can be estimated from measurements of undeformed conglomerates and X_f/Y_f can be measured directly.

Clearly, competency contrasts between pebbles and matrix and between pebbles of different composition will be of prime importance in any estimation of strain from a deformed polymict conglomerate. It is felt that a true estimation of strain in such a rock should include strain estimates for each individual component summed up in some way so as to give the total strain of the rock as a whole.

STRAIN ANALYSIS OF MARKERS OF ANY SHAPE

Robin (1977), adopting a quite different approach, has developed a method of strain analysis using randomly oriented markers which can be of any shape. It is based on finding the centre of the deformed markers and measuring the ratios of the lengths of the diameters parallel to the tectonic strain axes. Robin makes the same general assumptions as those made by previous methods:

1. there is no competency contrast between marker and matrix,
2. the markers had an initially random orientation,
3. the rock underwent no volume change,
4. the strain history is coaxial.

There is however no restriction on the shape of either the initial or the deformed marker (so they do not necessarily have to be ellipsoidal). In a group of randomly-oriented markers, if a_j and c_j are the diameters of the markers parallel to the future principal strain axes λ_1 and λ_3 and intersect at the centres of the markers, then

$$\prod_{j=1}^{n} \frac{a_j}{c_j} = \frac{a_1}{c_1} \times \frac{a_2}{c_2} \times \frac{a_3}{c_3} \times \ldots\ldots\ldots\ldots \frac{a_j}{c_j} \times \ldots\ldots\ldots \frac{a_n}{c_n} \cong 1 \qquad 4\text{-}15$$

In the strained state a_j and c_j become a_j' and c_j' such that

$$a_j' = (\lambda_1)^{\frac{1}{2}} a_j \qquad 4\text{-}16$$

and

$$c_j' = (\lambda_3)^{\frac{1}{2}} c_j \qquad 4\text{-}17$$

Therefore,

$$\prod_{j=1}^{n} \frac{a_j'}{c_j'} = [(\lambda_1/\lambda_2)^{\frac{1}{2}}]^n \prod_{j=1}^{n} \frac{a_j}{c_j} \qquad 4\text{-}18$$

$$= ((\lambda_1/\lambda_3)^{\frac{1}{2}})^n$$

or

$$\prod_{j=1}^{n} \ln \frac{a_j'}{c_j'} = n \ln (\lambda_1/\lambda_2)^{\frac{1}{2}} \qquad 4\text{-}19$$

(Robin 1977, eq. 3b)

APPROXIMATION TECHNIQUES

Lisle (1977b) has showed that, where fluctuation is low, which is one of the constraints of the R_f/ϕ techniques, and strain is moderately high, another constraint of the R_f/ϕ techniques, the strain of randomly oriented elliptical markers is given simply by the harmonic mean of the clasts' shapes. Again, it is also assumed that the clasts behave as passive markers.

There are three types of mean of R_f (final shape) which can be used as an approximation of R_s (strain ellipse shape):

1. Arithmetic mean, ($\bar{R}$)

$$\bar{R} = \frac{\Sigma R_f}{n} \qquad 4\text{-}20$$

2. Geometric mean, (G)

$$G = n(R_{f_1} \times R_{f_2} \times R_{f_3} \times \ldots\ldots\ldots\ldots R_{f_n})^{\frac{1}{2}} \qquad 4\text{-}21$$

3. Harmonic mean, (H)

$$H = \frac{n}{\Sigma 1/R_f} \qquad 4\text{-}22$$

Figures 4-12 and 4-13 show the results of two mathematical models presented by Lisle (1977b), each consisting of variably oriented elliptical markers of axial ratio R_i, deformed by a homogeneous pure shear strain to give final axial ratios R_f. The first model (Fig. 4-12) consists of 89 markers with constant R_i and uniform orientation distribution (1 to 80 degrees to the principal strain direction) which are deformed by various values of R_s. In the second model (Fig. 4-13), markers with variable R_i between 1.1 and 2.5 with a random orientation are considered.

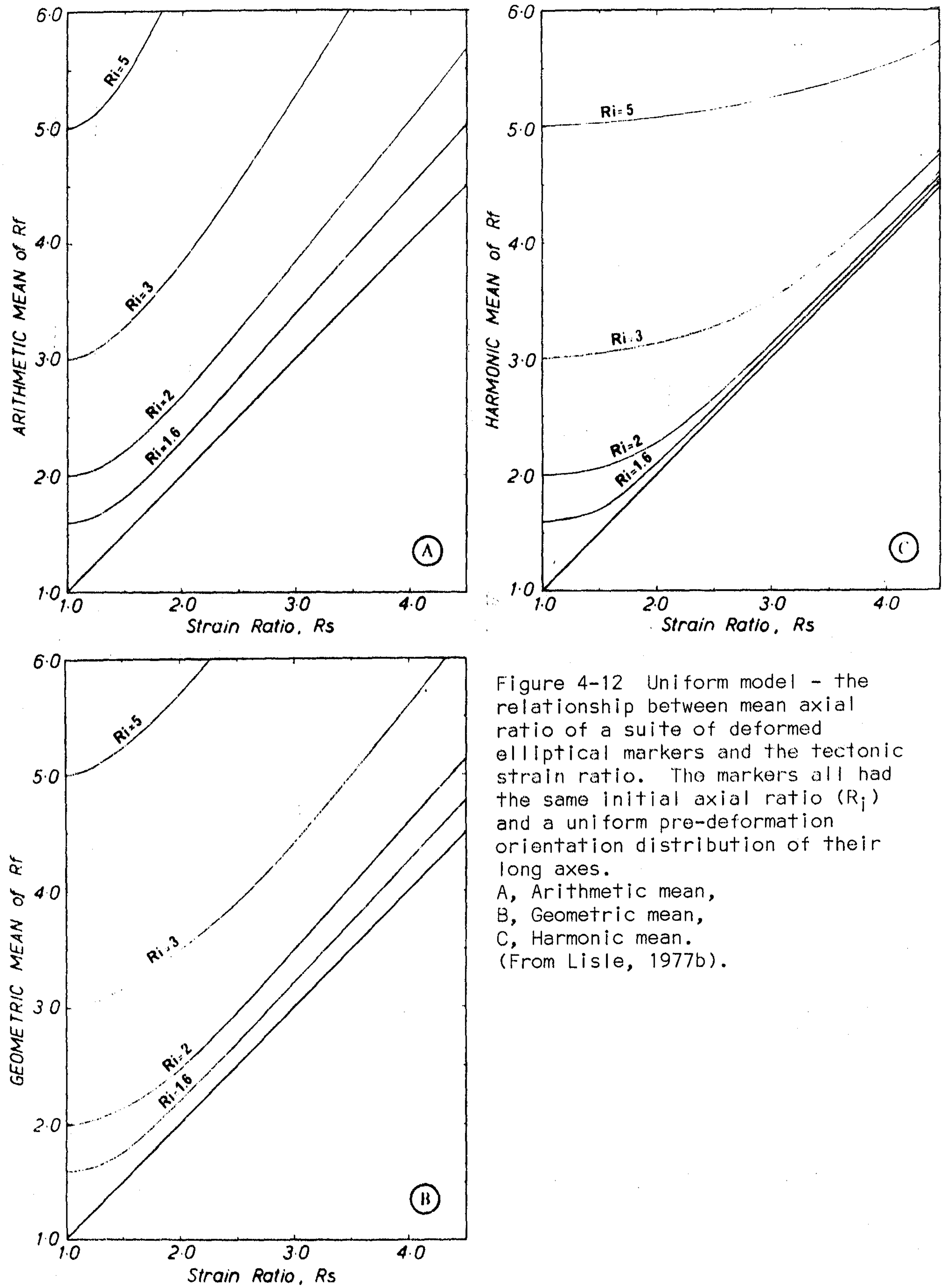

Figure 4-12 Uniform model - the relationship between mean axial ratio of a suite of deformed elliptical markers and the tectonic strain ratio. The markers all had the same initial axial ratio (R_i) and a uniform pre-deformation orientation distribution of their long axes.
A, Arithmetic mean,
B, Geometric mean,
C, Harmonic mean.
(From Lisle, 1977b).

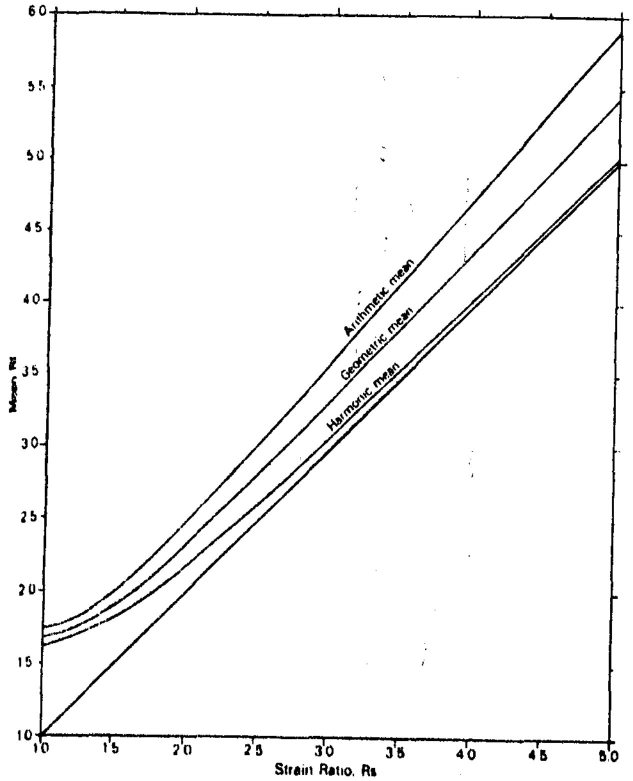

Fig. 4-13 Random model - the relationship between mean axial ratio of a suite of deformed elliptical markers and the tectonic strain ratio. Predeformation shapes and orientations of the markers are random. (From Lisle, 1977b).

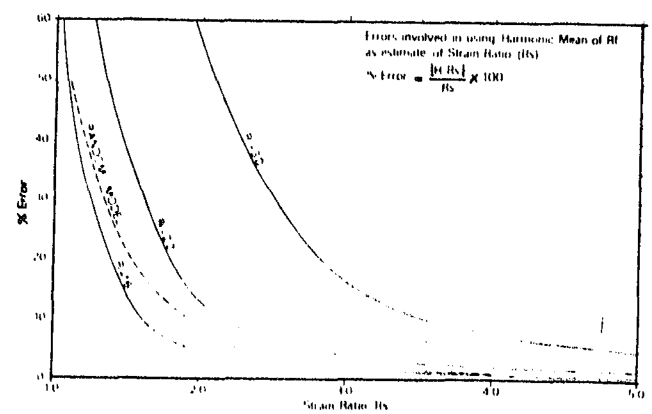

Fig. 4-14 Departure of the harmonic mean (H) of final ellipse shapes from the strain ratio as predicted by the uniform model (solid lines) and random model (dashed lines). (From Lisle, 1977b).

From Figures 4-12 and 4-13, although each of the means does not directly yield exact values of R_s when $R_i \neq 1$, the harmonic mean gives the closest approximation.

Figure 4-14 shows the percentage error for the harmonic mean from the two models where:

$$\% \text{ error} = \frac{|\text{mean} - R_s|}{R_s} \times 100 \qquad 4\text{-}23$$

This graph illustrates two points:

1. The harmonic mean gives greater accuracy at higher strains,
2. As R_i increases, so the accuracy of the harmonic mean decreases.

Therefore, the percentage error in estimating R_s using the harmonic mean of final pebble shapes is dependent on the R_i/R_s ratio, which is related to the maximum range of final marker orientations ($2\phi_{max.}$) as follows (Lisle, 1977b):

$$\text{Sin } 2\phi_{max.} = \frac{R_i - 1/R_i}{R_s - 1/R_s} \qquad 4\text{-}24$$

Thus, as the ratio R_i/R_s decreases (that is, with increasing strain) so $2\phi_{max.}$ decreases and so also does the percentage error from the harmonic mean. It should be remembered here that, where fluctuation, ϕ, is low, the application of the R_f/ϕ technique becomes more and more difficult and accuracy is reduced. Apparently then, for moderate to high strain values, the harmonic mean will provide at least as good an estimate of tectonic strain, if not better than the R_f/ϕ methods.

Lisle (1979) has proposed another simple approximation technique which uses the final pebble orientation. After a homogeneous strain of passive, randomly-oriented markers the long, intermediate and short axes of the markers will plot in orientation fields on a stereonet about the principal strain axes (Fig. 4-15). In Figure 4-15, α, β and γ are the maximum fluctuation angles of the pebble axes in the respective principal planes of the strain ellipsoid. Lisle expresses these orientation fields as ratios:

for the long axes $p = \text{Sin } 2\alpha/\text{Sin } 2\gamma$ 4-25

for the intermediate axes $q = \text{Sin } 2\beta/\text{Sin } 2\alpha$ 4-26

for the short axes $r = \text{Sin } 2\beta/\text{Sin } 2\gamma$ 4-27

where,

$$p = \frac{\sinh 2\varepsilon s_{XZ}}{\sinh 2\varepsilon s_{XY}} = \frac{\frac{1}{2}(ab - a/ab)}{\frac{1}{2}(a - 1/a)} \qquad 4\text{-}28$$

(Lisle 1979, eq. 11)

where $a = R_{s_{XY}}$ and $b = R_{s_{YZ}}$

ε = logarithmic tectonic extension.

Lisle has plotted curves of constant p and q on a Flinn diagram where,

$$a = [(p - 1/b)/(p - b)]^{\frac{1}{2}} \qquad 4\text{-}29$$

(Lisle 1979, eq. 12)

for curves of equal p; and

$$a = \frac{q(b - 1/b) + (q^2(b - 1/b)^2 + 4)^{\frac{1}{2}}}{2} \qquad 4\text{-}30$$

(Lisle 1979, eq. 13)

for curves of equal q.

The Flinn plot is shown in Figure 4-16.

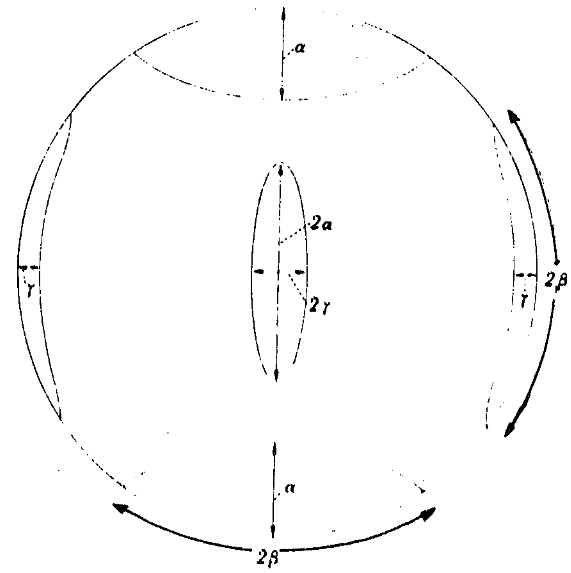

Fig. 4-15 Angular dimensions of the orientation fields containing the long axes (approx. vertical), intermediate axes (N-S horizontal) and short axes (E-W horizontal) of deformed markers. (From Lisle, 1979).

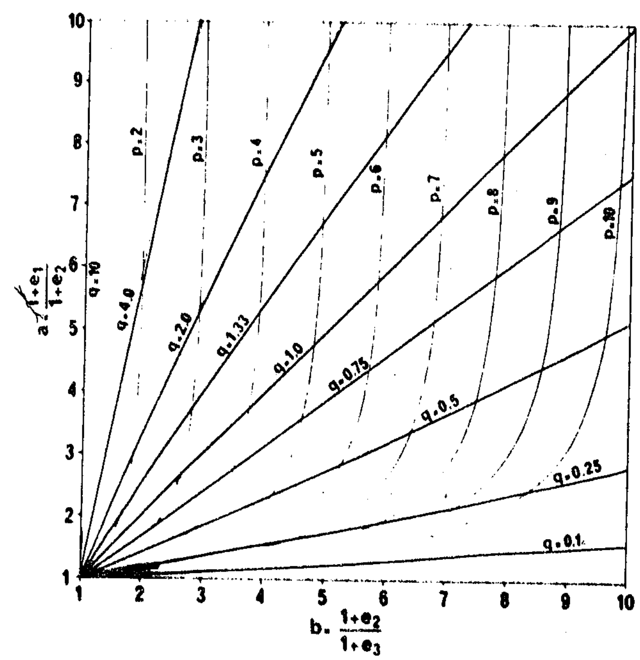

Fig. 4-16 Flinn diagram to show how the ratios p and q are related to the strain ellipsoid shape. Parameters p and q describe the shape, on a stereogram, of the orientation fields occupied by the pebble long axes and the pebble intermediate axes, respectively. (From Lisle, 1979).

Provided α, β and γ are all less than 45°, this method provides a quick approximation of tectonic strain by the intersection of the appropriate p and q curves on the Flinn diagram.

In this review of strain determination in conglomerates, we have discussed the main methods of analysis which have been developed over the last 15 years since Ramsay (1967) first drew attention to the problem. Indeed Ramsay's concept of combining pebble ratio, fluctuation and original fabric, has formed the basis for much of the later work in the area. Gay (1968 a, b, c and 1969) and Gay and Jaegar (1975) have made valuable advances with regard to the problem of ductility contrasts between markers and the marker/matrix system.

Lisle (1977b), on the other hand, has shown that, where strain is moderate or high, the simple approach of using the harmonic mean of pebble shapes appears to give the best approximation of strain. Using this method also allows a greater number of strain estimates to be made as the application is not as long and arduous as some of the other methods. Used in conjunction with the R_f/ϕ methods, as a check for original preferred fabrics of the markers, and the ideas of Gay, Lisle's approximation technique is considered to be a valuable tool in the estimation of strain in conglomeratic rocks.

CHAPTER 5

RESULTS OF STRAIN ANALYSIS

In Chapter 4 techniques of strain analysis as applied to deformed conglomeratic rocks are reviewed. The present discussion deals with the application of the selected techniques and presents the results of the strain analysis.

Within the conglomerate the lengths of principal axes of clasts and their orientations were measured at various exposures (Fig. 5-1) and axial ratios calculated (see Appendix B). Where possible, measurements were taken from joint surfaces and the attitude of these surfaces was also recorded (Appendix B). In addition, a suite of oriented samples of coarse-grained arenite was obtained from various outcrops (Fig. 5-1). Subsequently, two thin sections were made from each sample. One was parallel to the stretching lineation and perpendicular to S_1, the other was perpendicular to both stretching lineation and S_1.

The different methods of strain analysis described in Chapter 4 rely to varying degrees on several assumptions:

1. that the strain history is coaxial,
2. that no volume change is experienced by the markers during deformation,
3. that the initial orientation of the markers is random,
4. that no ductility contrast exists between the marker and its matrix, so the marker deforms homogeneously with the matrix.

Fig. 5-1 Location of conglomerate and sandstone outcrops used for strain estimates.

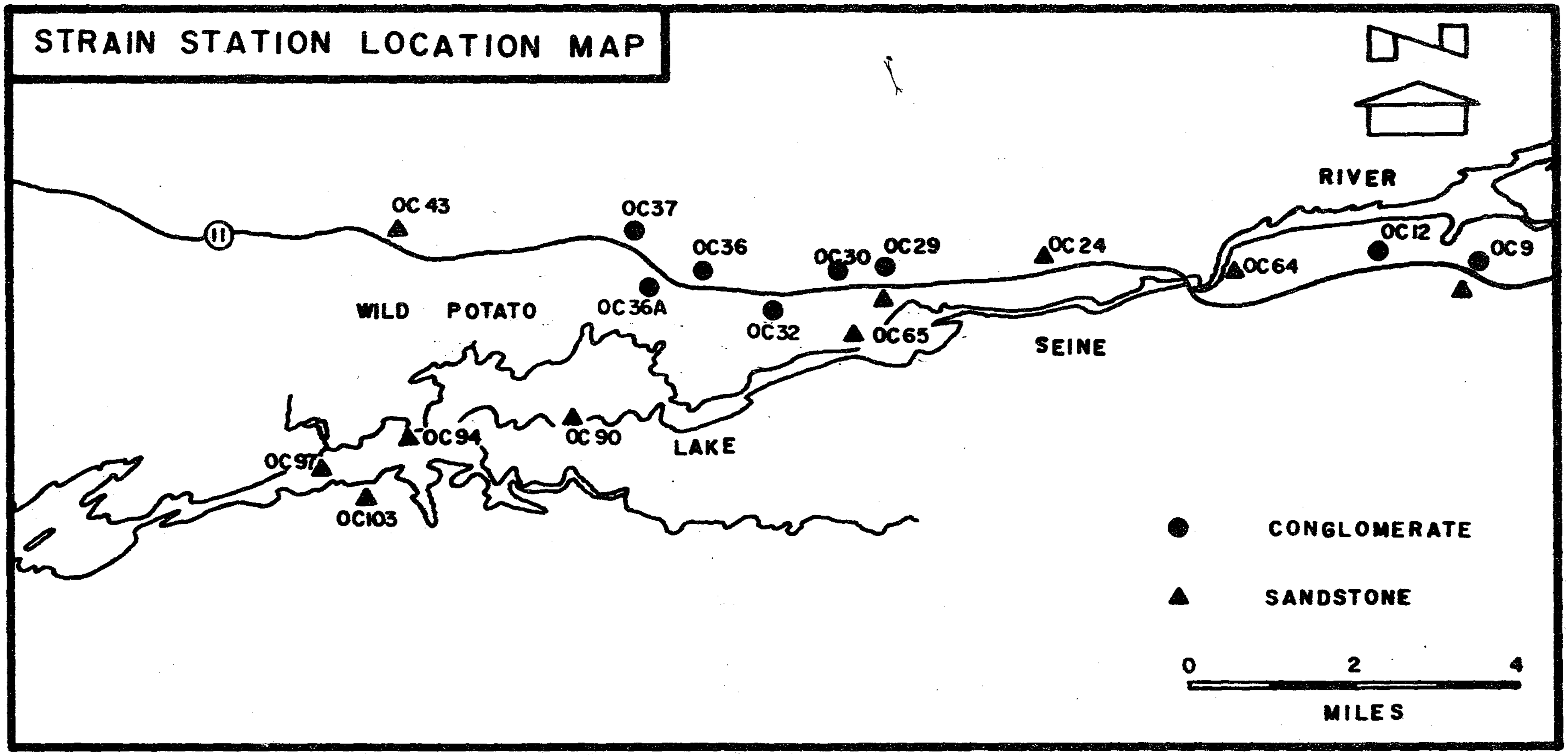

TABLE 5-1a

N.T.S. GRID REFERENCES FOR STRAIN LOCALITIES IN FIG.5-1

OUTCROP NUMBER	EASTING	NORTHING
9	557450E	5398750N
12	556150E	5398850N
24	549500E	5398750N
29	545950E	5398450N
30	544350E	5398250N
32	543500E	5398200N
36	541700E	5398400N
37	540400E	5399150N
43	535750E	5399350N
64	552600E	5398450N
65	545600E	5397200N
90	539700E	5395650N
94	536550E	5395450N
97	534850E	5394450N
103	535950E	5394400N

1. Whether or not the strain history is coaxial is difficult to assess. However, Durney and Ramsay (1973) suggest that curving pressure shadows are a good indication of a non-coaxial strain history. No such textures, either in outcrop, or in thin section, have been observed in the present study.

2. There is limited evidence to suggest that some volume change may have been experienced by the rocks during deformation, as a result of pressure solution.

Pressure solution is described by Sorby (1908) as "the dissolution and removal of mineral substance at a grain contact subjected to 'pressure'". The term 'pressure' is usually regarded as promoting the process (Durney, 1976). Also, from Sorby's definition, pressure solution is a process of dissolution only and does not include any crystallization processes so therefore, in itself, it is not truly a deformational process. In view of this, Durney (1972) and Bathurst (1975) favour the term 'solution transfer' to describe the combined action of pressure solution followed by precipitation.

Pressure solution, or solution transfer, as a deformational process in pitted conglomerates, was first put forward by Sorby (1865) and McEwen (1978) has suggested that large volume losses of up to 50% can occur by pitting of limestone pebbles with no visible sign of plastic deformation of the remaining pebbles. Mosher (1981), working on the Purgatory conglomerate from Rhode Island has described three major 'pressure solution features' which are characteristic of that conglomerate:

(i) adjacent pebbles show indentation relationships with no change in quartz fabrics within the individual pebbles,

(ii) insoluble material is concentrated between the pebbles in mutual contact, both in the matrix and within the outer margins of the pebbles,

(iii) quartz overgrowths are found at the long axis terminations of the pebbles.

Some granitoid clasts in the conglomerate show indentation relationships with adjacent granitoid clasts (Fig. 5-2). In thin section dark brown wavy layers are common in samples from the conglomerate and arenite. These may represent stylolite surfaces or may be the result of the metamorphic breakdown of detrital feldspar to produce quartz and illite (Beach, in McClay, 1977). Pressure shadows adjacent to competent clasts commonly are occuped by quartz and calcite grains. However, it is difficult to assess from the available observations whether these minerals are a product of pressure solution or represent recrystallized matrix.

In general therefore, pressure solution may well be responsible, at least in part, for some of the deformation observed in the rocks and the assumption that no volume change has been experienced by the strain markers may not be wholly valid.

3. The importance of initial orientation of markers on the resulting deformed fabric has been reviewed in Chapter 4. For each locality R_f/ϕ plots have been constructed and these are presented in Appendix B. From these plots, there is a symmetry of points about the S_1 traces. This implies one of two things: either the initial orientation of markers was random and S_1 corresponds with the XY plane of the strain ellipsoid, or there was a preferred initial fabric which was close in orientation

Fig. 5-2 Indentation relationships between adjacent granitoid clasts at locality 16 (Fig. 2-6). Such relationships are a possible indication of pressure-solution.

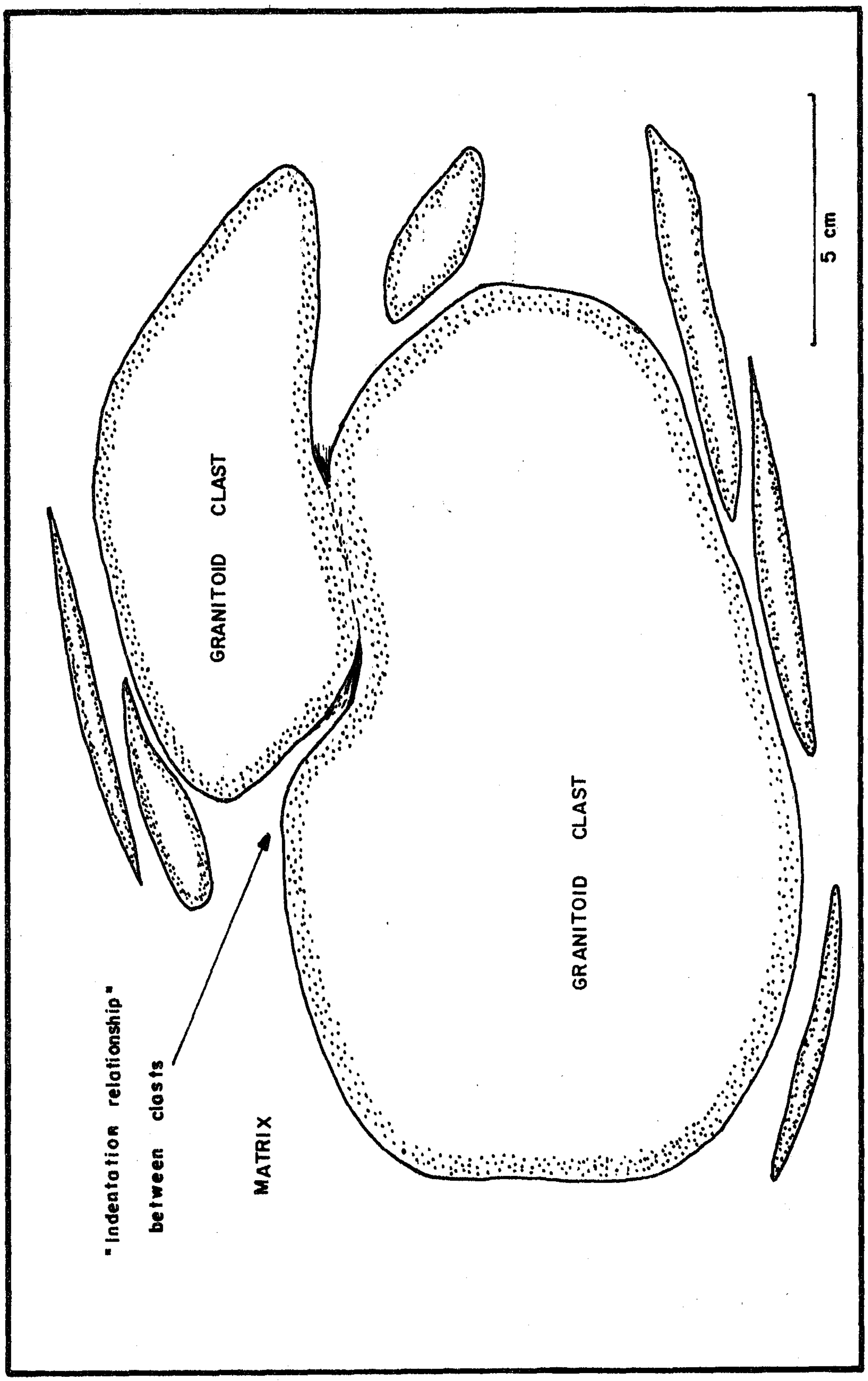

GRANITOID CLAST
GRANITOID CLAST
5 cm
"Indentation relationship"
between clasts
MATRIX

to the future XY plane of the strain ellipsoid. Such might be the case if S_0 in the underformed state was sub-parallel to the future XY plane and there was an original preferred orientation of clasts about S_0.

4. Ductility contrasts between marker and matrix are of extreme importance in deducing the bulk strain in a rock. Gay has dealt with the problem mathematically and derived equations (Gay 1968b, eq. 16) which take into account the relative viscosity ratios between different markers.

Borradaile (1981) however, has proposed a simple approximation technique of strain analysis which relies on competency contrasts between rigid clasts and matrix. The method uses the form of strain shadows about rigid clasts. In Figure 5-3, the length L represents the original distance from the centre of the clast to the cleavage trace which just grazes the side of the clast (as the clast is rigid and therefore not itself deformed). The length L' represents the shortened distance, not affected by the clast. Thus the shortening for the matrix is simply given by:

$$\lambda_3 = \left(\frac{L'}{L}\right)^2 \qquad 5\text{-}1$$

This idea has been extended following a suggestion from Dr. Borradaile. Ideally the nearest cleavage trace to the clast should be used. However, if we measure the ratio L/L' for cleavage traces successively further away from the clast (eg., 1 to 4 in Fig. 5-3) and calculate the percentage of matrix to clast in the cleavage-normal direction, then we estimate the effect of the clast on the deformation of the matrix. Graphs have been plotted of L/L' versus percentage matrix for several competent clasts (Figs. 5-5 to 5-16), from which the following observations can be made:

Fig. 5-3 Determination of shortening for the matrix using the method of Borradaile (1981). The length, L, represents the original distance from the centre of the rigid clast to the cleavage trace which just grazes the side of the clast. L' represents the shortened distance, not affected by the clast.

So, $\lambda_3 = (\frac{L'}{L})$

Fig. 5-4 Determination of competence contrast between competent clast and matrix. Two cleavage traces, distance, b, apart, become wrapped around the clast, with a new spacing $(a_1 + a_2)$. The competence contrast between clast and matrix, c, is given by:

$$c = \frac{b}{a_1 + a_2}$$

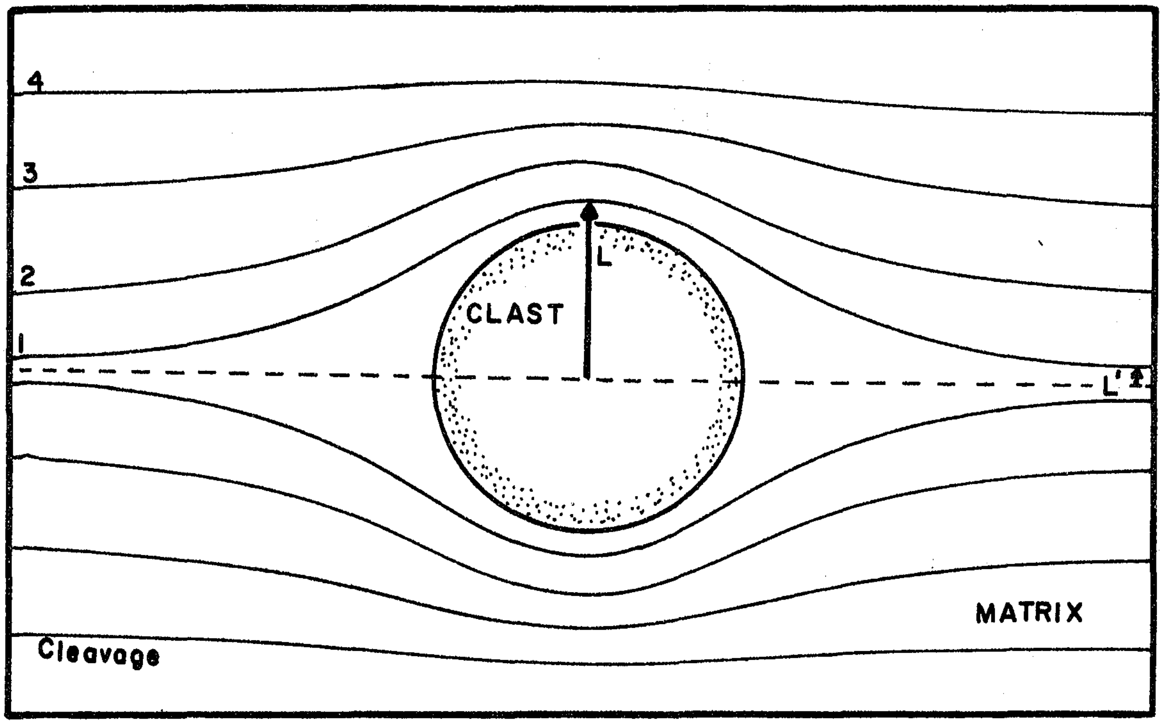
4
3
2
1
CLAST
L
L'
MATRIX
Cleavage

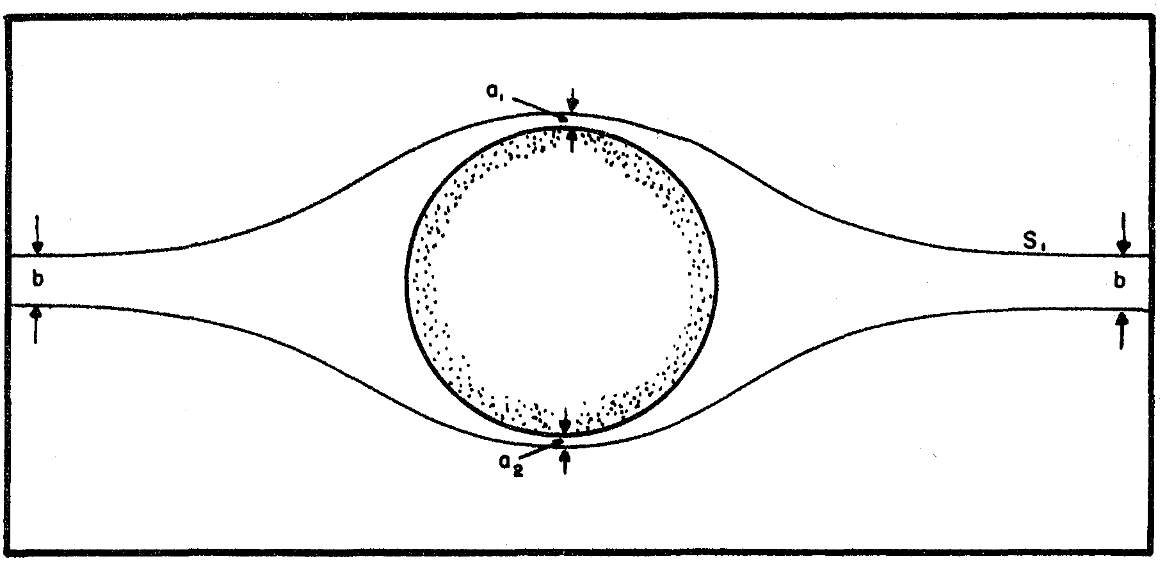
a_1
b
S_1
b
a_2

Fig. 5-5 to 5-16

Effects of competent clasts on the deformation of a ductile matrix. For each clast, L and L' have been measured for cleavage traces successively further away from the clasts, and percentage matrix to clast, in the cleavage-normal direction, calculated. The graphs are plots of L/L' versus percentage matrix of each clast.

The graphs show that, where the percentage matrix is greater than about 30%, the clasts have little effect on the deformation of the matrix.

FIG. 5-5 · Pebble sketch no. 1

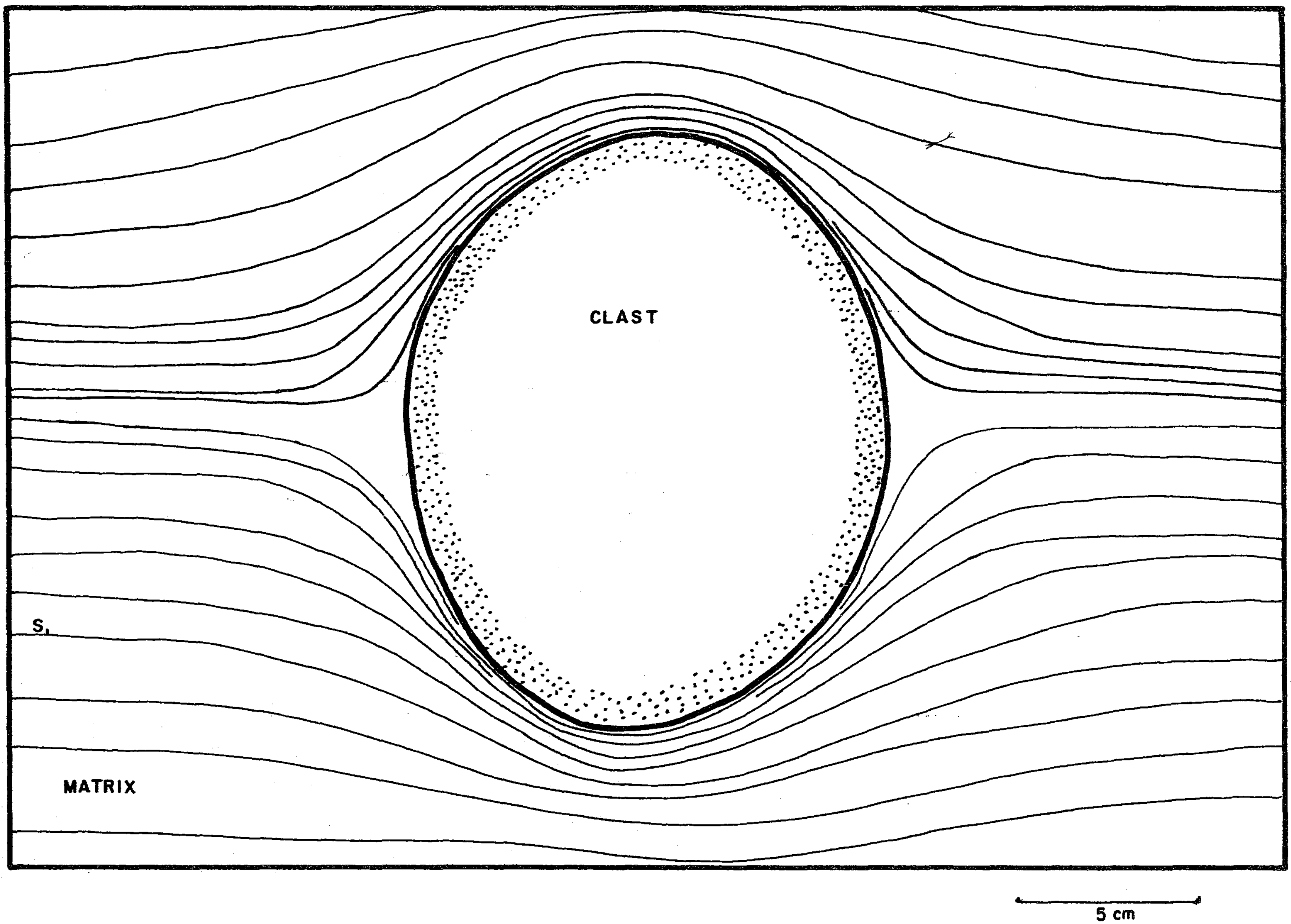

FIG. 5 - 6 : Plot of (L/L') / % matrix for Fig. 5 - 5

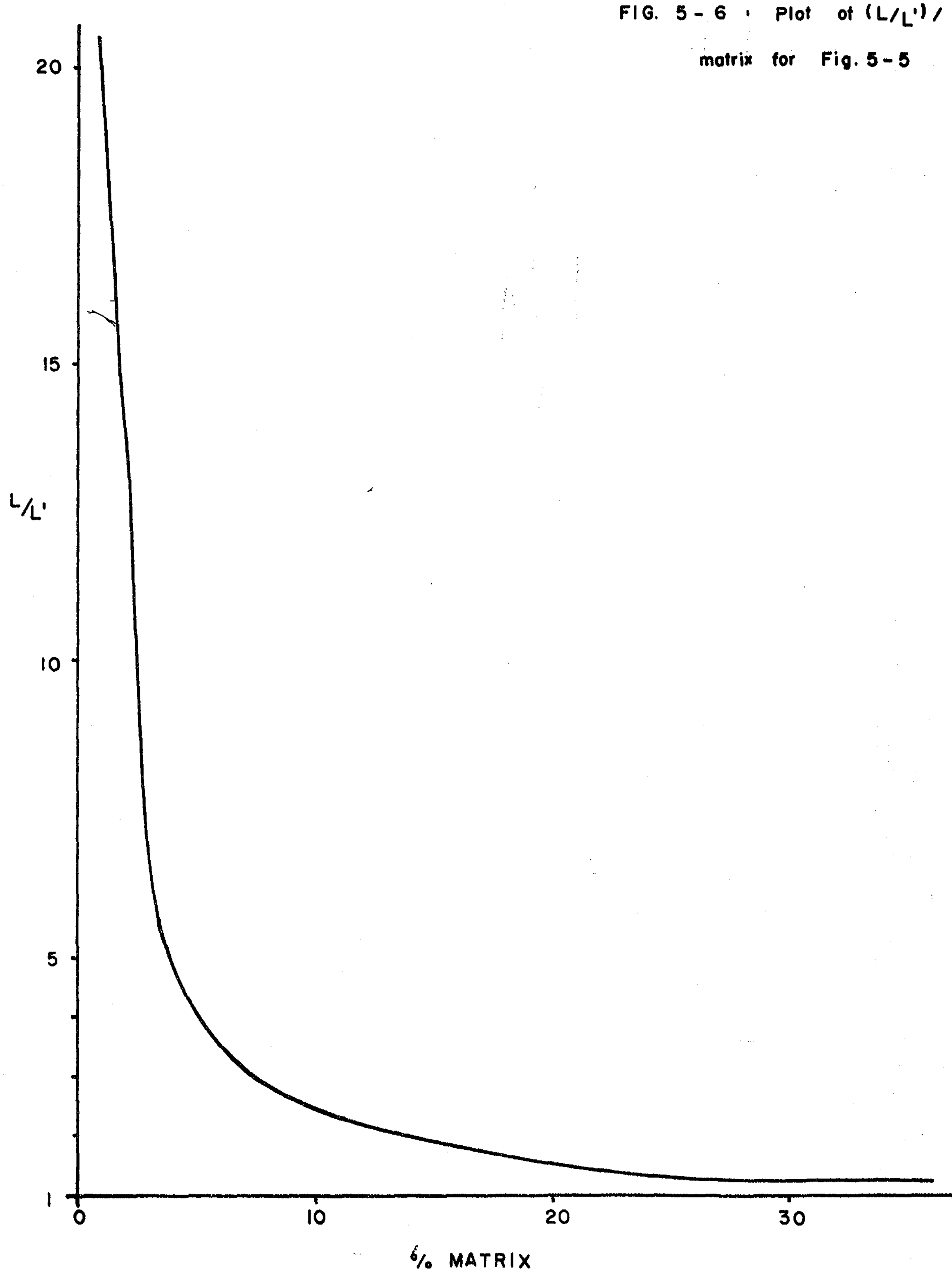

FIG. 5-7 · Pebble sketch no. 2

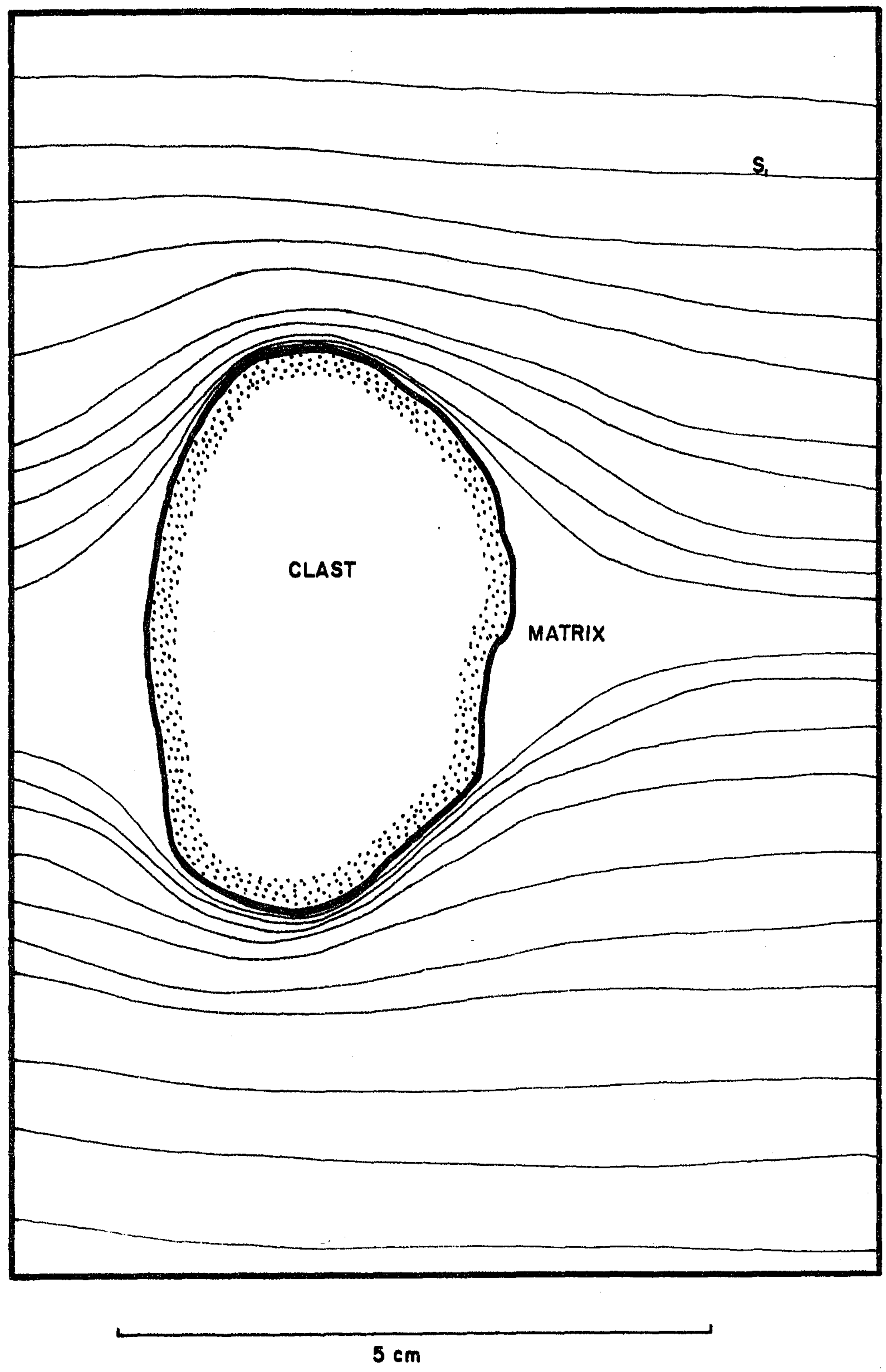

FIG. 5-8 : Plot of (L/L') ∤ % matrix for Fig. 5-7

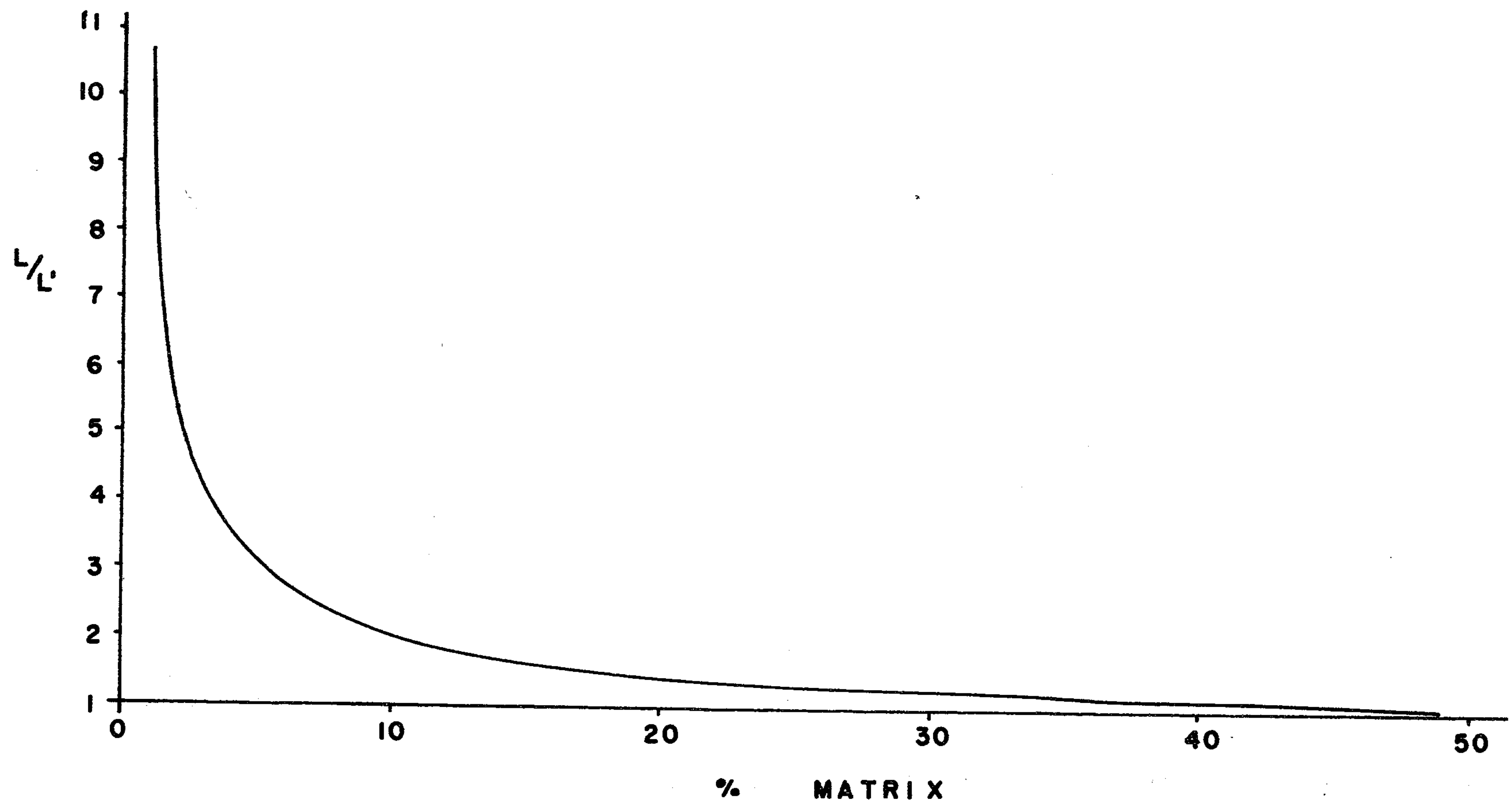

FIG. 5-9 : Pebble sketch no. 3

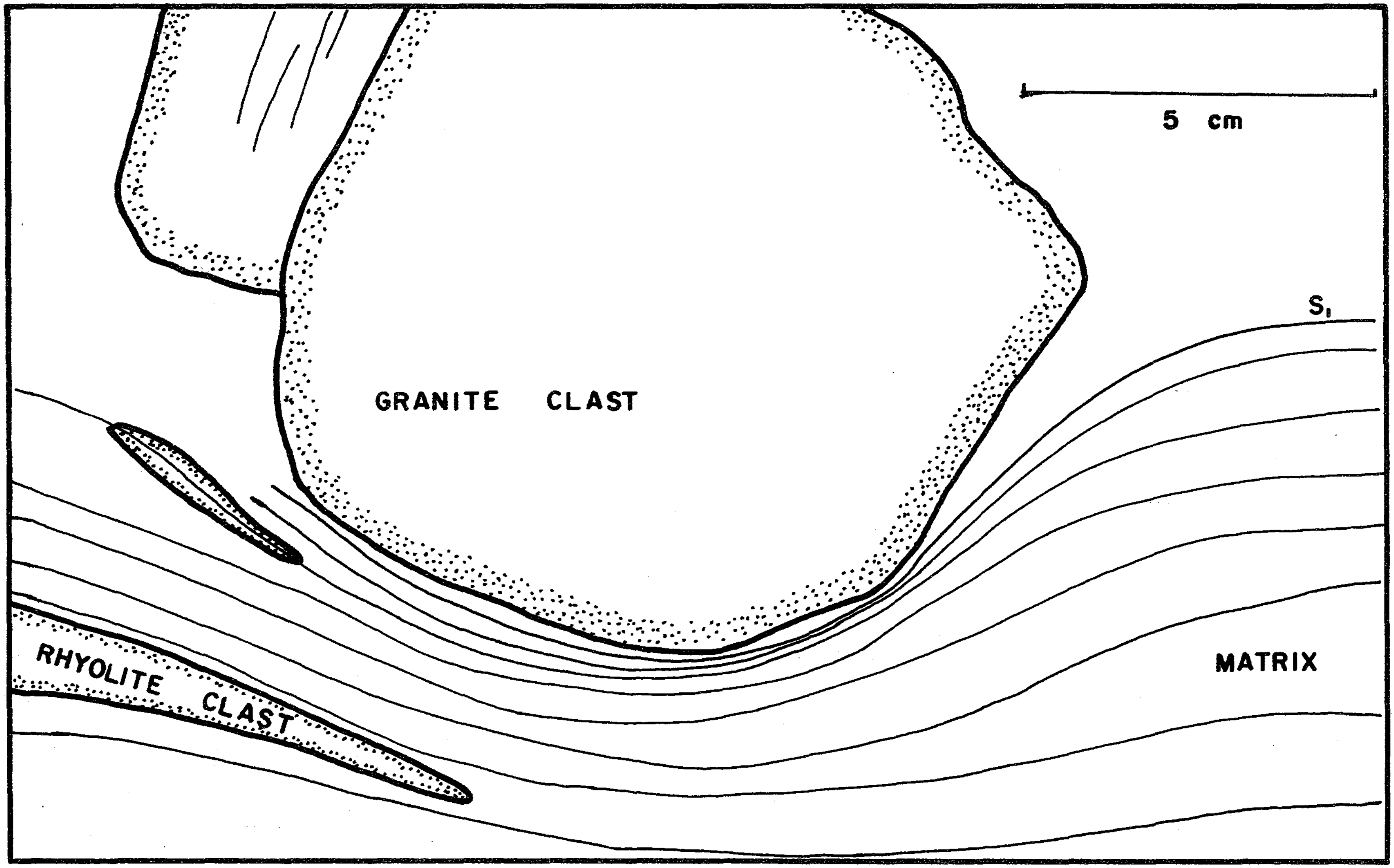

FIG. 5-10 . Pebble sketch no. 4

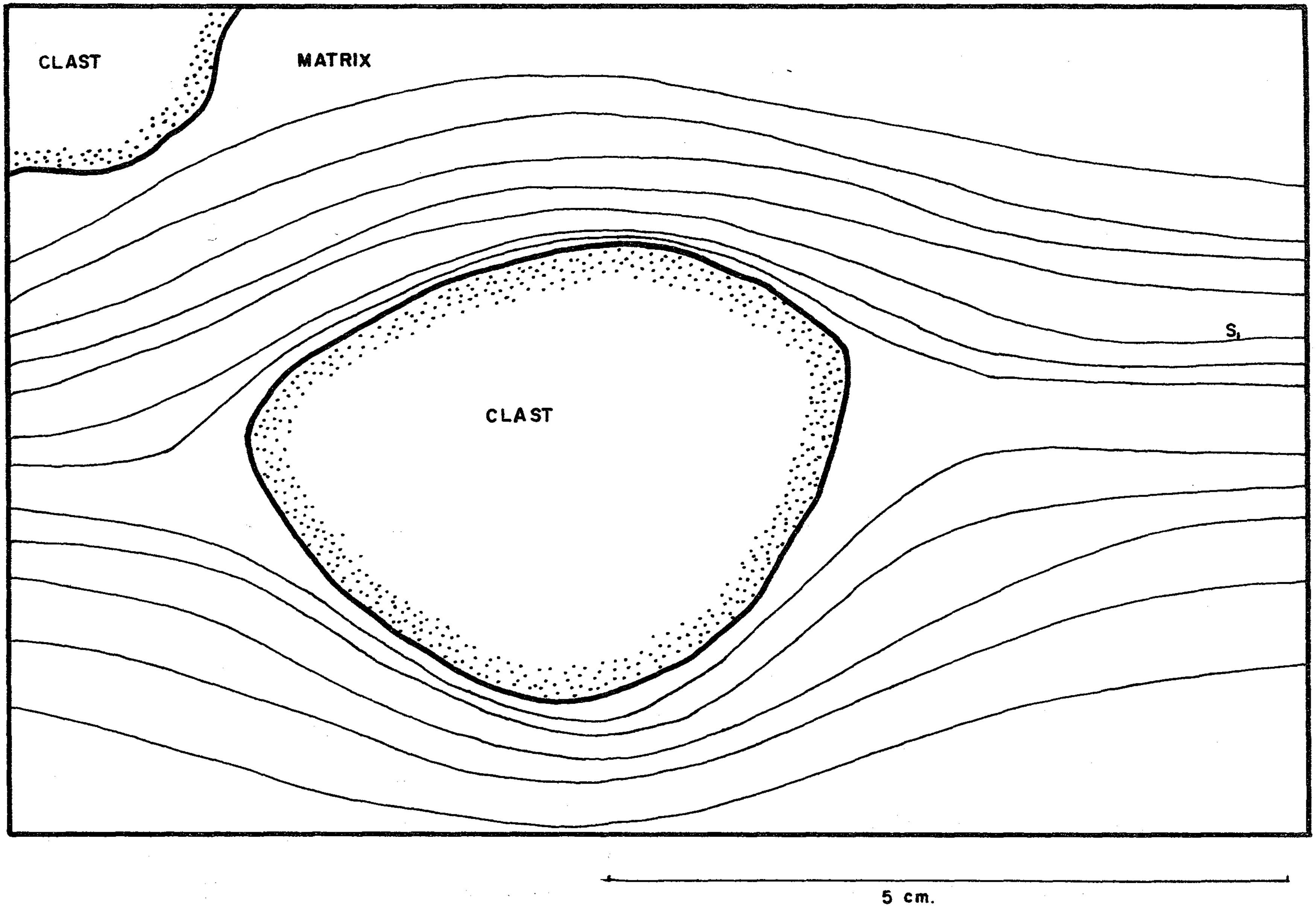

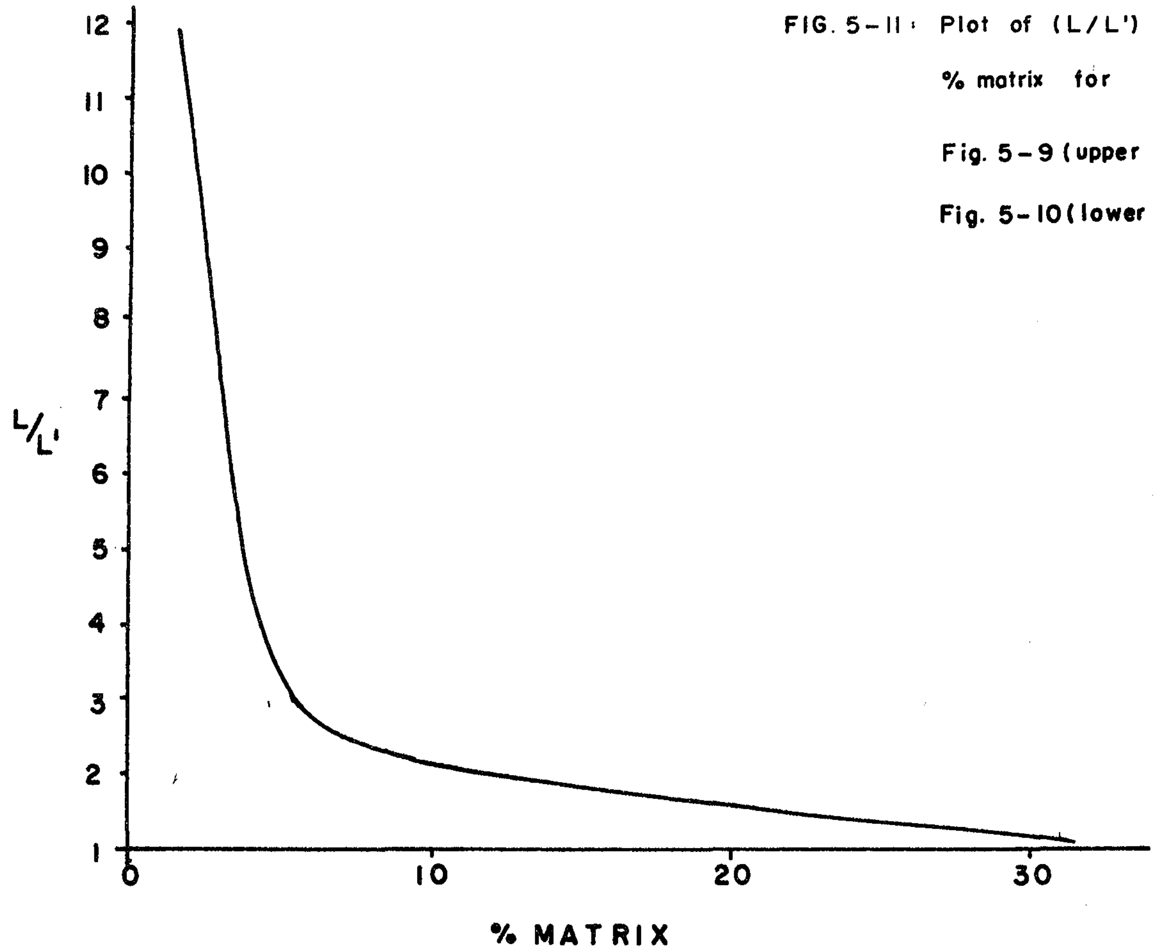

FIG. 5-11: Plot of (L/L') / % matrix for Fig. 5-9 (upper plot) & Fig. 5-10 (lower plot)

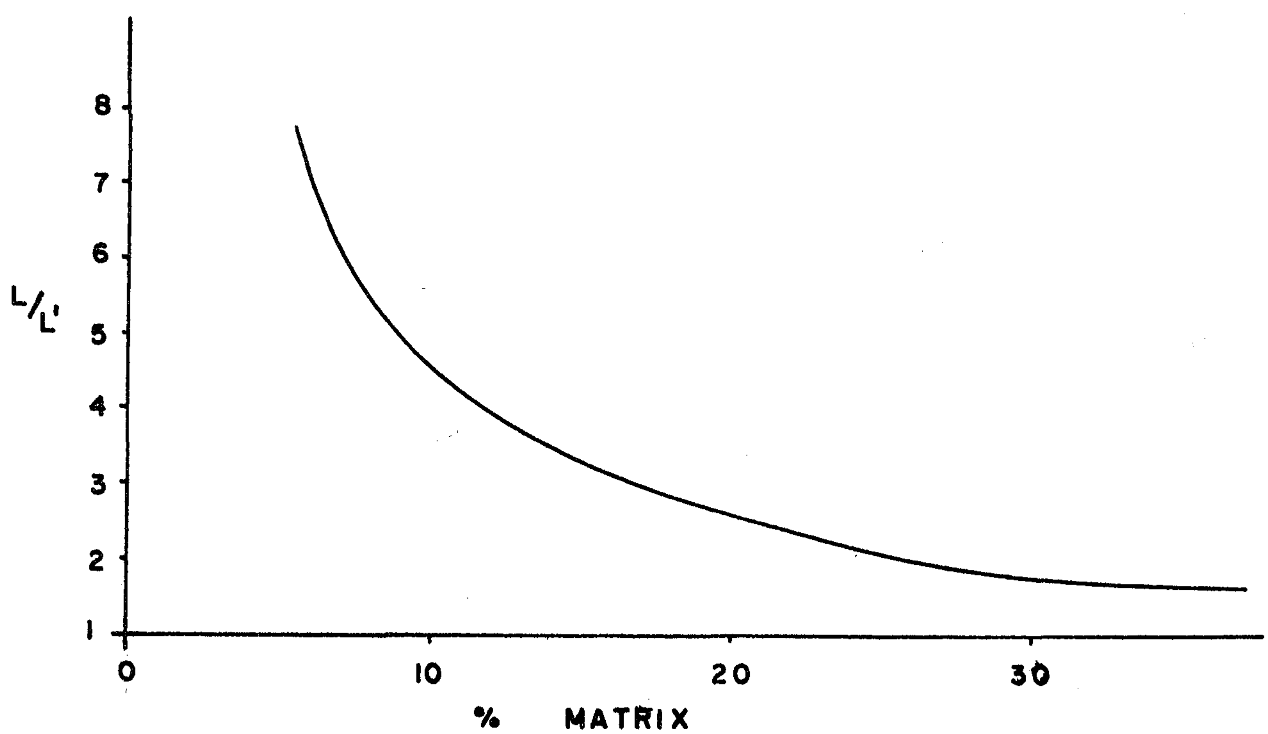

FIG. 5 - 12 · Pebble sketch no. 5

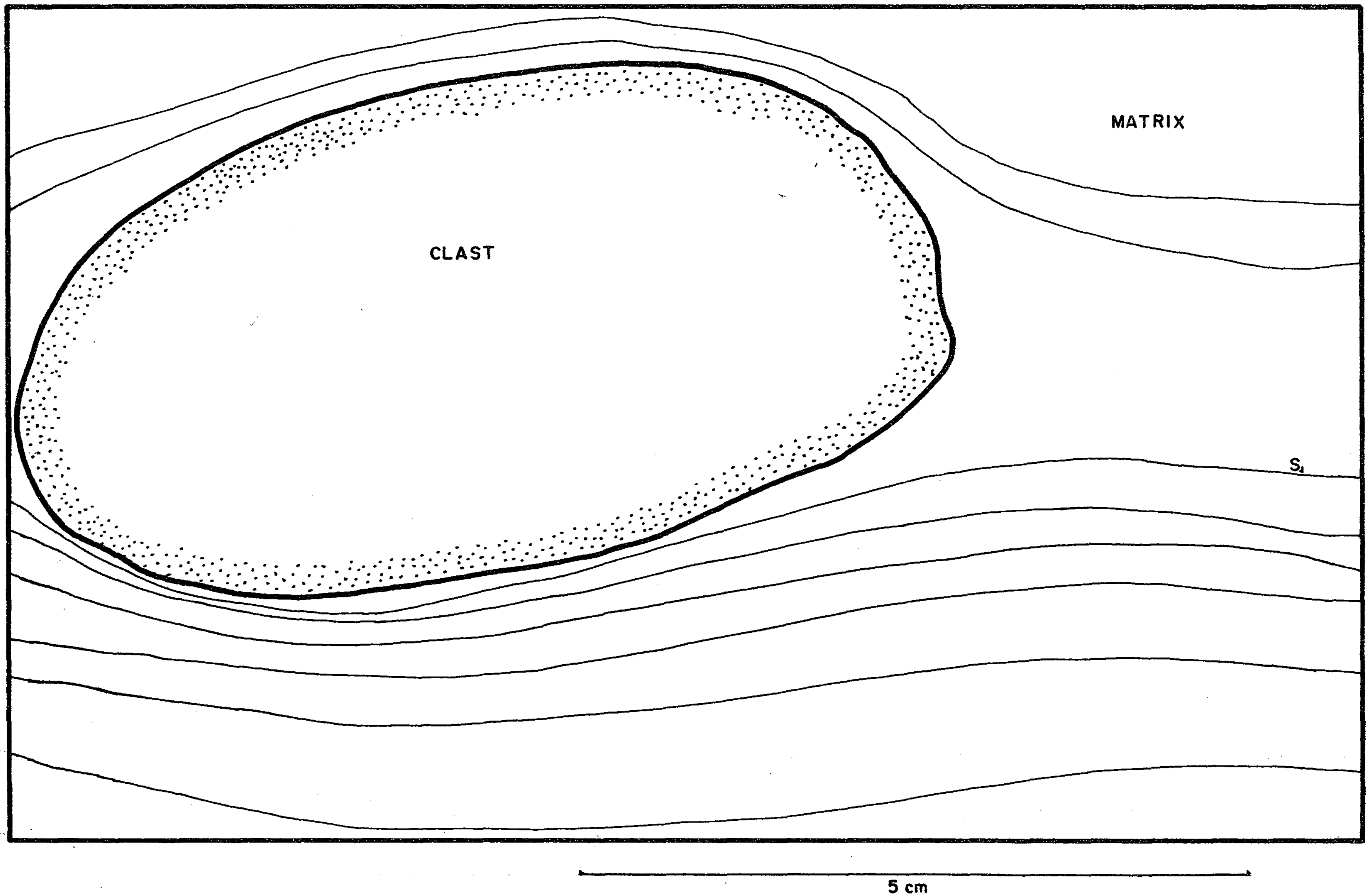

FIG. 5 - 13 : Pebble sketch no. 6

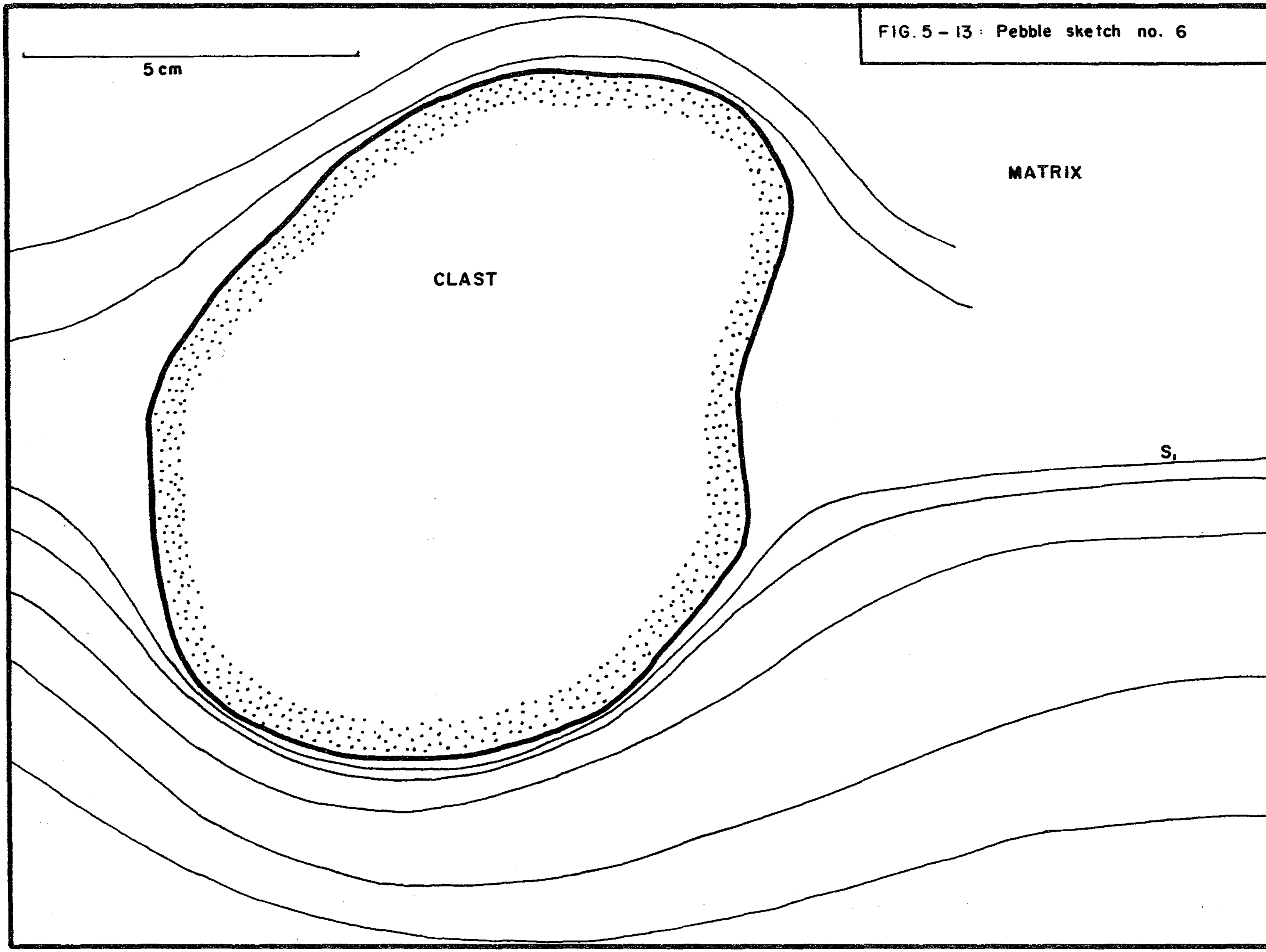

FIG. 5-14 : Plot of (L/L') / % matrix for Fig. 5-12 (lower) & Fig. 5-13 (upper)

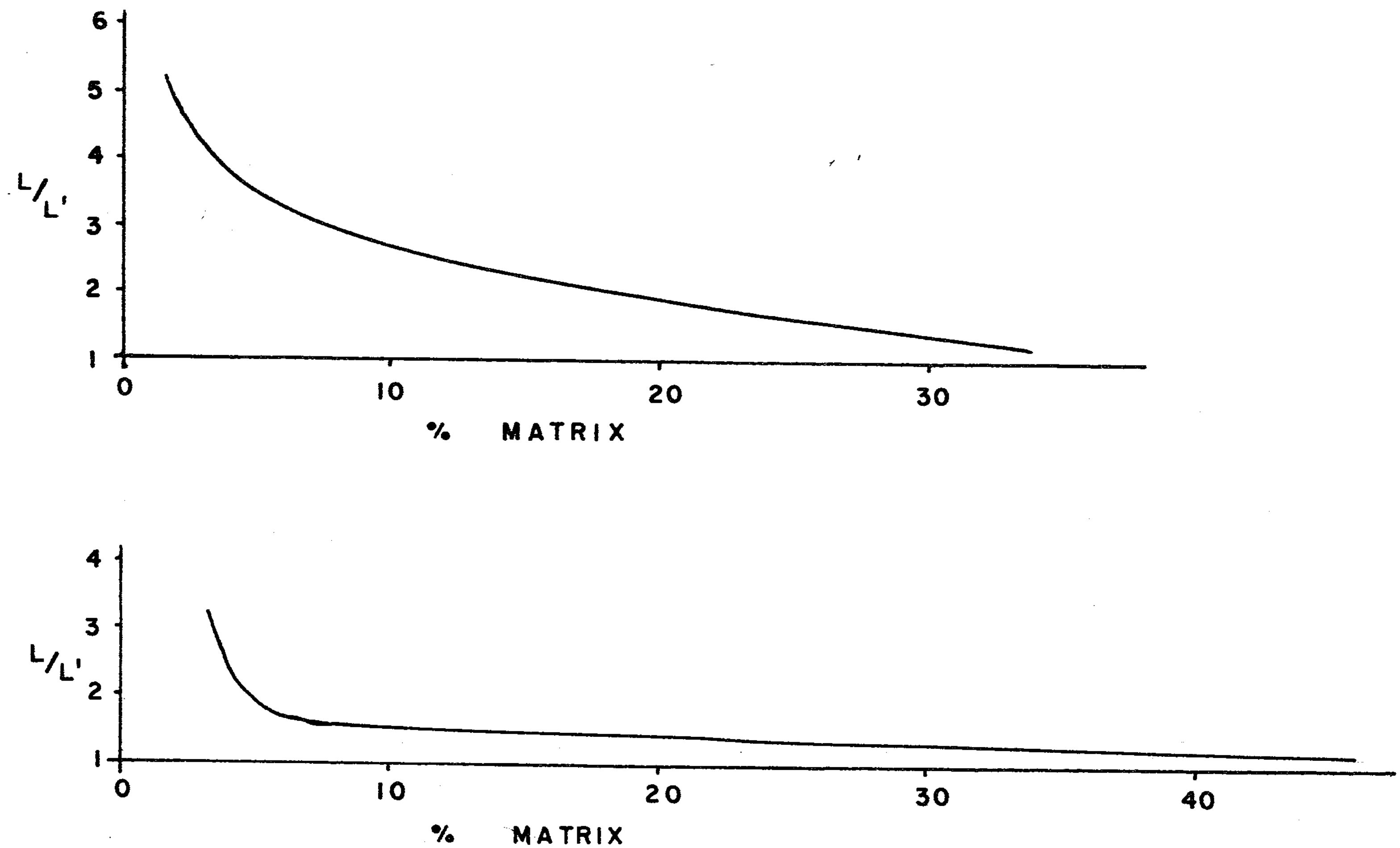

FIG. 5-15 : Pebble sketch no. 7

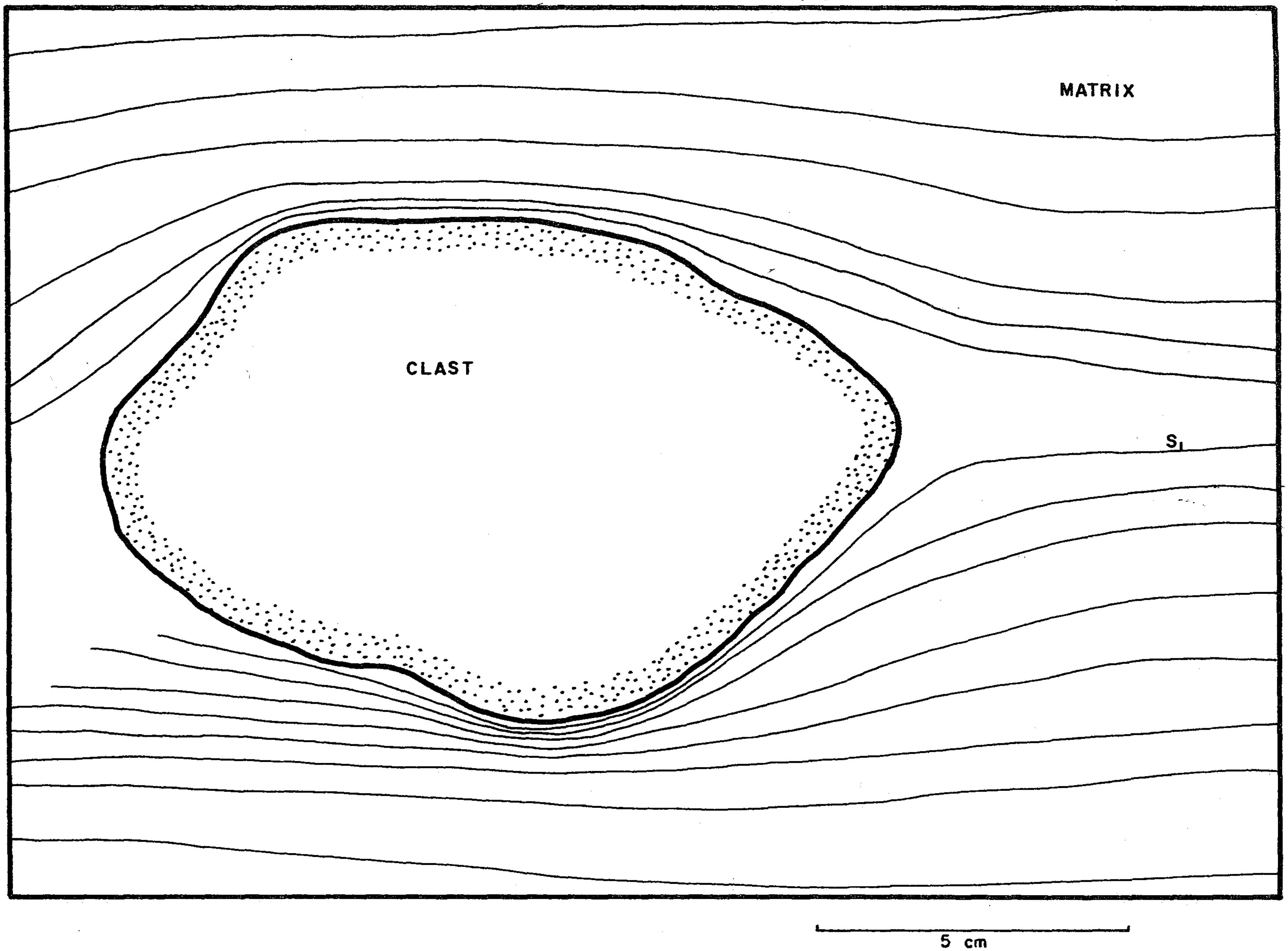

FIG. 5-16: Plot of (L/L') / % matrix for Fig. 5-15

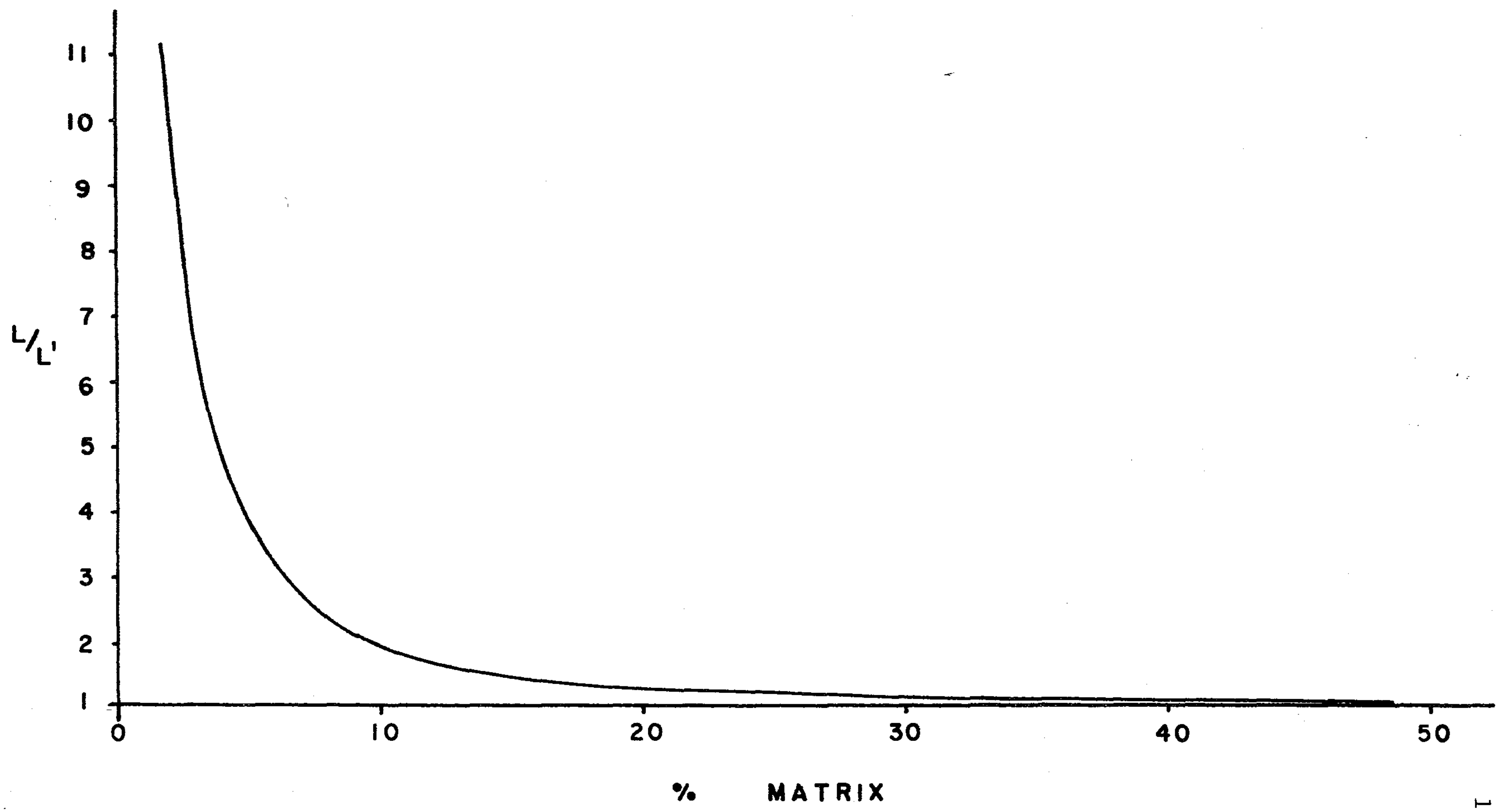

(i) there is a rapid decrease in the ratio L/L' with increasing percentage matrix,

(ii) as the proportion of matrix increases beyond 30%, the ratio L/L' approaches 1, where the clast has no "strain-shadow" effect on the matrix. This implies that, in order for a set of competent clasts (such as the granitic clasts in the study area) to have an appreciable effect on the bulk strain of the rock, their percentage concentration must be greater than about 70%.

Borradaile's technique can be extended further in order to evaluate the competency contrast between clast and matrix. If the strain in the rock as a whole can be considered to be homogeneous on a large scale, i.e., scale of an outcrop, then cleavage traces on any surface should be approximately parallel. Consider now the effect of a hypothetical, competent clast on the matrix (Fig. 5-4). Two cleavage traces, distance b apart, will become wrapped around the clast so that their new separation by the matrix material will be $(a_1 + a_2)$. If the clast had no effect on the matrix (i.e., no competence contrast), then b should be equal to $(a_1 + a_2)$. If this is not the case then b will not equal $(a_1 + a_2)$. Thus we can define a ratio, c, which will be a measure of the competency contrast between clast and matrix:

$$c = \frac{b}{a_1 + a_2} \qquad 5\text{-}2$$

where c increases with the competency contrast. The method fails where the clast is less competent than the matrix - for example, this might be the case in a sandy sediment containing mud pellets. Where c = 1, no competency contrast exists.

Values of c were measured and calculated in the vicinity of several granitoid clasts and were found to range from 5 to over 11. Intermediate volcanic clasts and their matrix gave c values of 1.9 to 1.95 while rhyolite clasts and their matrix had average c values of 1.4. Figure 5-17 illustrates the effects of two intermediate volcanic clasts and a rhyolite clast on the cleavage traces, which are minimal in the case of rhyolite clasts (Fig. 5-17c).

This method yields an empirical value of competency contrast and can easily be applied, either from direct measurement in the field or from photographs.

APPLICATION OF STRAIN ANALYSIS TECHNIQUES

Two important implications arise from the preceding discussion. Firstly, in order for competent clasts to have an appreciable effect on the strain of the rock as a whole, their percentage concentration must be greater than about 70%. Where such clasts make up less than 70% of the rock they can effectively be ignored in a strain estimate. Within the study area, granitoid clasts make up less than 25% of the rocks observed at each conglomerate outcrop. Secondly, competence contrasts can be determined rapidly by the empirical method outlined. But how can these values be combined with the strain analysis techniques discussed in Chapter 4?

We have seen in Chapter 4 that the approach of Lisle (1977b), using the harmonic mean of clast shapes, is likely to yield the simplest and quickest approximation of strain where no ductility contrasts exist. Where such a ductility contrast does exist, this method will yield a strain estimate for the clasts alone. However, combined with the equations

Fig. 5-17

(a) & (b) Effects of intermediate volcanic clasts on the matrix. C = 1.9 and 1.95.

(c) Effect of rhyolite clast on the matrix. C = 1.4.

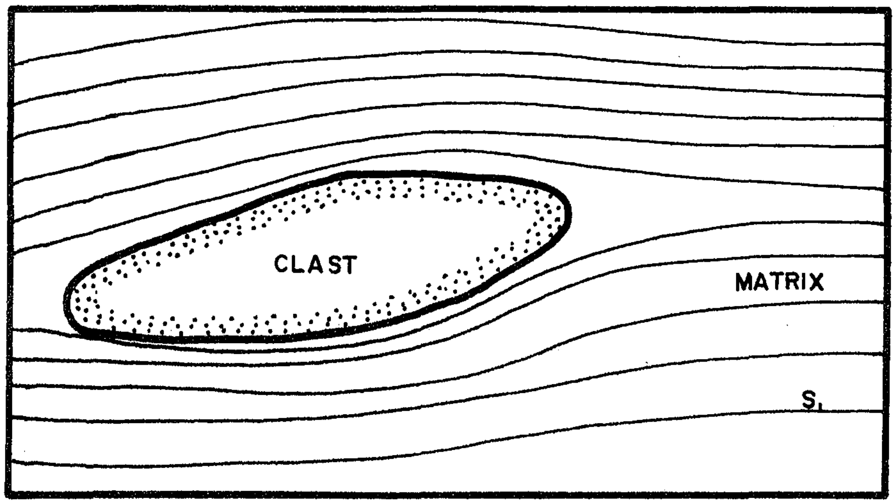

a. Intermediate volc. clast

5 cm

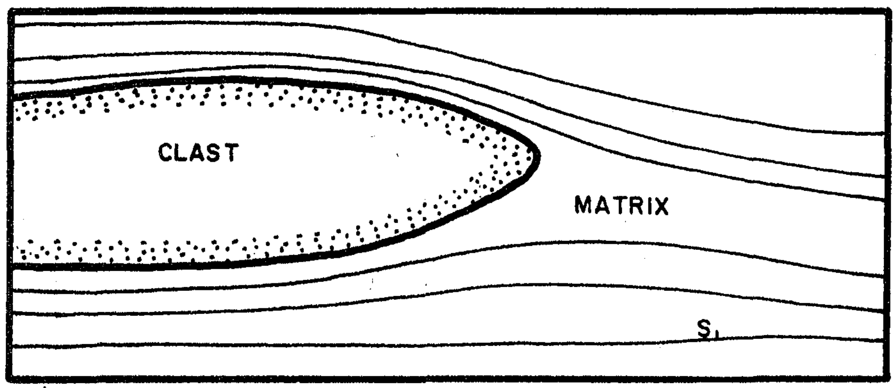

b Intermediate volc. clast

5 cm

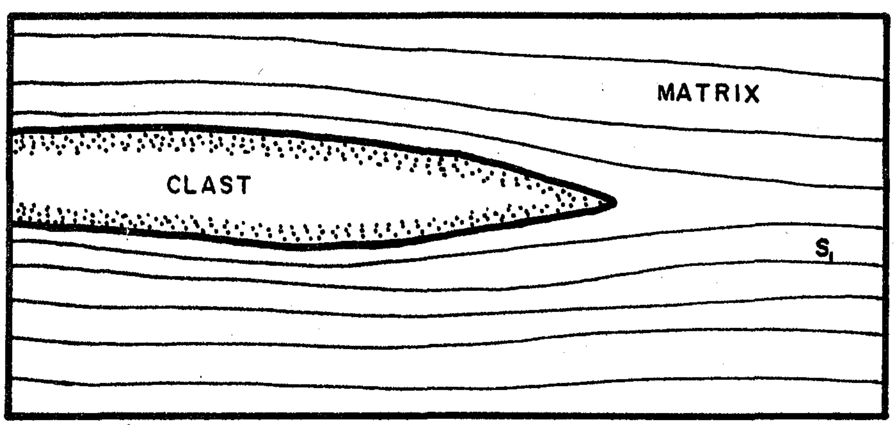

c Rhyolite clast

5 cm

of Gay (1968b) it is possible to determine the bulk strain of the rock as a whole.

Consider equation 4-14

$$\log (\lambda_1/\lambda_2)^{\frac{1}{2}} = ((2R_a + 3)/5)[\log (X_f/Y_f) - \log (X_i/Y_i)] \qquad 4\text{-}14$$

If $R_a = 1$, i.e., there is no viscosity contrast between clast and matrix, then the factor $((2R_a + 3)/5) = 1$. In this case

$$\log (\lambda_1/\lambda_2)^{\frac{1}{2}} = \log (X_f/Y_f) - \log (X_i/Y_i) \qquad 5\text{-}3$$

This is the condition (i.e., homogeneous deformation of passive markers) for which the various methods discussed in Chapter 4, including Lisle's harmonic mean method, calculate strain.

Therefore, if the strain is calculated by one of these methods, then the function $((2R_a + 3)/5)$ can simply be applied to the "apparent strain" of the clasts in order to obtain an estimate for the rock as a whole.

R_a in equation 4-14 is a viscosity ratio for the particle to matrix system and is equivalent to c in this discussion. Using rhyolite clasts, which are the most easily identified of all clasts in the field and have the lowest value of c of those measured, we can substitute in a value of 1.4 for c or R_a:

the factor $((2R_a + 3)/5)$ becomes $((2 \times 1.4 + 3)/5 = 1.16$

Therefore, by using rhyolite clasts, we are approaching the condition of no ductility contrast between markers and matrix. This means that an estimate of the bulk strain of the rock as a whole can be obtained simply by calculating the harmonic mean of rhyolite clast shapes.

RESULTS

Tables 5-1 and 5-2 show the results of the strain analysis, using the harmonic mean method of Lisle (1977b). For each locality (Fig. 5-1) within the conglomerate, clasts were separated according to lithology and plots of R_f against ϕ were constructed for each lithology (see Appendix B). R_f/ϕ plots were also made for the arenite. From these plots there appears to be no pre-tectonic preferred fabric of clasts and S_1 also appears to correspond with the XY plane of the strain ellipsoid. The effects of such fabrics could conceivably be masked by high strains - however, R_f/ϕ plots for granitoid clasts, which yield low strain values, are also symmetrical about S_1 traces. Thus, stretching lineations measured, which are contained in S_1, are considered to coincide with the principal extension directions of the strain ellipsoid. For each lithology in the conglomerate exposures and for each arenite outcrop the harmonic mean of clast shapes was calculated (see Appendix B), which represents an estimate of the principal strain ratios, and these values are summarized in Tables 5-1 and 5-2.

The R_f/ϕ plots (Appendix B) and the data of Tables 5-1 and 5-2 illustrate the variation in strain characterized by clasts of different composition. From the preceding discussion we can use strain values obtained for rhyolite clasts in the conglomerate to give an indication of the strain in the rock as a whole, for competent granitoid clasts make up less than 25% of the rock. Arenite samples are more homogeneous in composition and thus strain estimates from clasts using the harmonic mean method of Lisle (1977b) approximate to the bulk strain of the whole rock.

TABLE 5-1

CONGLOMERATE

O/C	CLAST TYPE	STRAIN ELLIPSOID RATIOS X : Y : Z	N(XZ)	N(YZ)
9	Granitic	2.60 : 2.05 : 1	10	36
	Acid Volcanic	21.65 : 10.96 : 1	4	20
	Int. Volc.	6:39 : 4.12 : 1	3	3
12	Granitic	1.84 : 1.82 : 1	38	30
29	Granitic	4:15 : 2.86 : 1	20	11
	Acid Volcanic	11.93 : 3.16 : 1	7	8
	Int. Volcanic	18.52 : 3.32 : 1	2	7
30	Granitic	3.87 : 2.77 : 1	31	15
	Acid Volcanic	11.44 : 8.72 : 1	26	27
	Int. Volcanic	9.45 : - : 1	6	-
	Basic Volcanic	12.92 : - : 1	1	-
32	Granitic	3.84 : 2.19 : 1	20	36
	Acid Volcanic	8.11 : 5.36 : 1	20	20
	Basic Volcanic	27.0 : - : 1	5	-
36	Granitic	2.30 : 2.17 : 1	27	26
	Acid Volcanic	8.51 : 6.28 : 1	15	25
	Basic Volcanic	13.18 : - : 1	3	-
36A	Granitic	1.67 : 1.67 : 1	29	26
	Acid Volcanic	10.22 : 4.36 : 1	10	20
	Int. Volcanic	4.33 : - : 1	5	-
	Basic Volcanic	17.05 : - : 1	3	-
37	Granitic	2.39 : 2.37 : 1	52	23
	Acid Volcanic	10.93 : 7.08 : 1	20	21
	Int. Volcanic	- : 5.90 : 1	-	9
	Basic Volcanic	20.33 : - : 1	5	-

TABLE 5-2

SANDSTONE

SAMPLE NO.	O/C	STRAIN ELLIPSOID RATIOS X : Y : Z	N(XZ)	N(YZ)
PJ81-60	9	2:46 : 2.09 : 1	70	70
PJ81-58	24	2.75 : 2.28 : 1	70	70
PJ81-62	29	2.21 : 1.90 : 1	120	90
PJ81-57	43	2.53 : 1.63 : 1	70	70
PJ81-16	64	2.63 : 1.94 : 1	70	70
PJ81-13B	65	2.11 : 1.76 : 1	50	50
PJ81-26	90	2.89 : 2.00 : 1	70	70
PJ81-39	94	2.71 : 1.63 : 1	70	70
PJ81-42	97	3.32 : 2.38 : 1	70	70
PJ81-43	98	3.00 : 1.91 : 1	70	70
PJ81-47	103	2.36 : 2.01 : 1	70	45

Figure 5-18 is a Flinn plot of strain values obtained for conglomerate (using rhyolite clasts) and arenite localities, most of which fall into the flattening (1 > K ≧ 0) field, assuming no volume change. At locality 94 (Fig. 5-1) a strain ellipsoid with a K-value almost equal to unity was obtained and at only one locality (29, Fig. 5-1) was a value of K > 1 obtained.

In general, strain values for arenite localities are much lower than for conglomerate outcrops, which is to be expected when one considers the differences in competencies between the two. The conglomerate is composed of a ductile argillaceous matrix in which clasts of different lithologies are embedded. It is therefore highly susceptible to deformation. The arenites behave more rigidly because they are composed of quartz and feldspar clasts set in a quartz-rich matrix.

Using the method outlined by Ramsay (1967, p. 129→) bedding planes at individual strain localities have been restored to their pre-strain attitudes and the results are presented in Table 5.3. Figure 5-19 is an example of how the technique has been applied. From the data in Table 5-3 it can be concluded that bedding planes were not horizontal in their unstrained state. Restored bedding planes in the conglomerate are less steeply dipping than restored bedding planes for the arenite layers. This obviously warrants further explanation:

(i) strain estimates may be underestimates,

(ii) deformation of the rocks may have begun at a late stage or later than the main folding,

(iii) the original bedding was not horizontal, which would have the same effect as (ii).

Fig. 5-18 Flinn plot for strain estimates made at localities shown in Fig. 5-1.

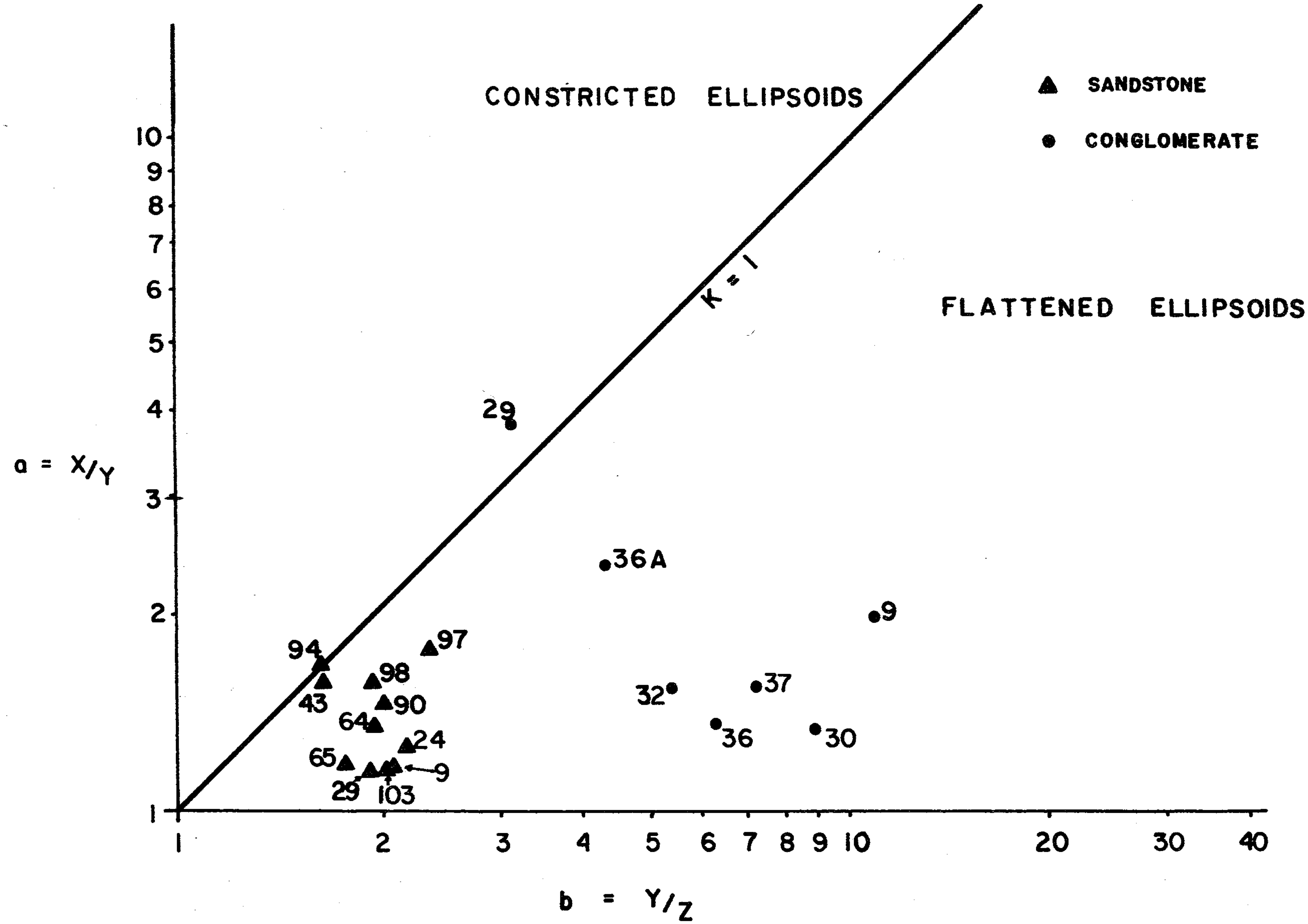
CONSTRICTED ELLIPSOIDS
FLATTENED ELLIPSOIDS
SANDSTONE
CONGLOMERATE
K = 1
a = X/Y
b = Y/Z
10
9
8
7
6
5
4
3
2
1
1
2
3
4
5
6
7
8
9
10
20
30
40
29
36A
9
97
94
98
43
90
64
24
65
9
29
103
32
37
36
30

TABLE 5-3

RESTORATION OF BEDDING PLANES

Conglomerate

Outcrop No.	S_0' (Deformed)	S_0 (Undeformed)
9	083/87°S	051/57°SE
29	075/74°N	031/32°NW
30	070/85°N	036/39°NW
32	082/52°N	111/ 3°N
36	090/74°N	104/32°NE
36A	088/72°N	126/61°NE
37	078/83°N	046/68°SE

Sandstone

Outcrop No.	S_0' (Deformed)	S_0 (Undeformed)
24	083/77°N	097/57°N
43	075/89°N	078/82°S
64	079/85°N	072/86°S
65	077/87°S	072/84°S
94	050/81°N	040/75°NW
97	059/82°N	045/71°NW
103	071/72°S	038/82°SE

OC 32

X : Y : Z = 8·11 : 5·36 : 1

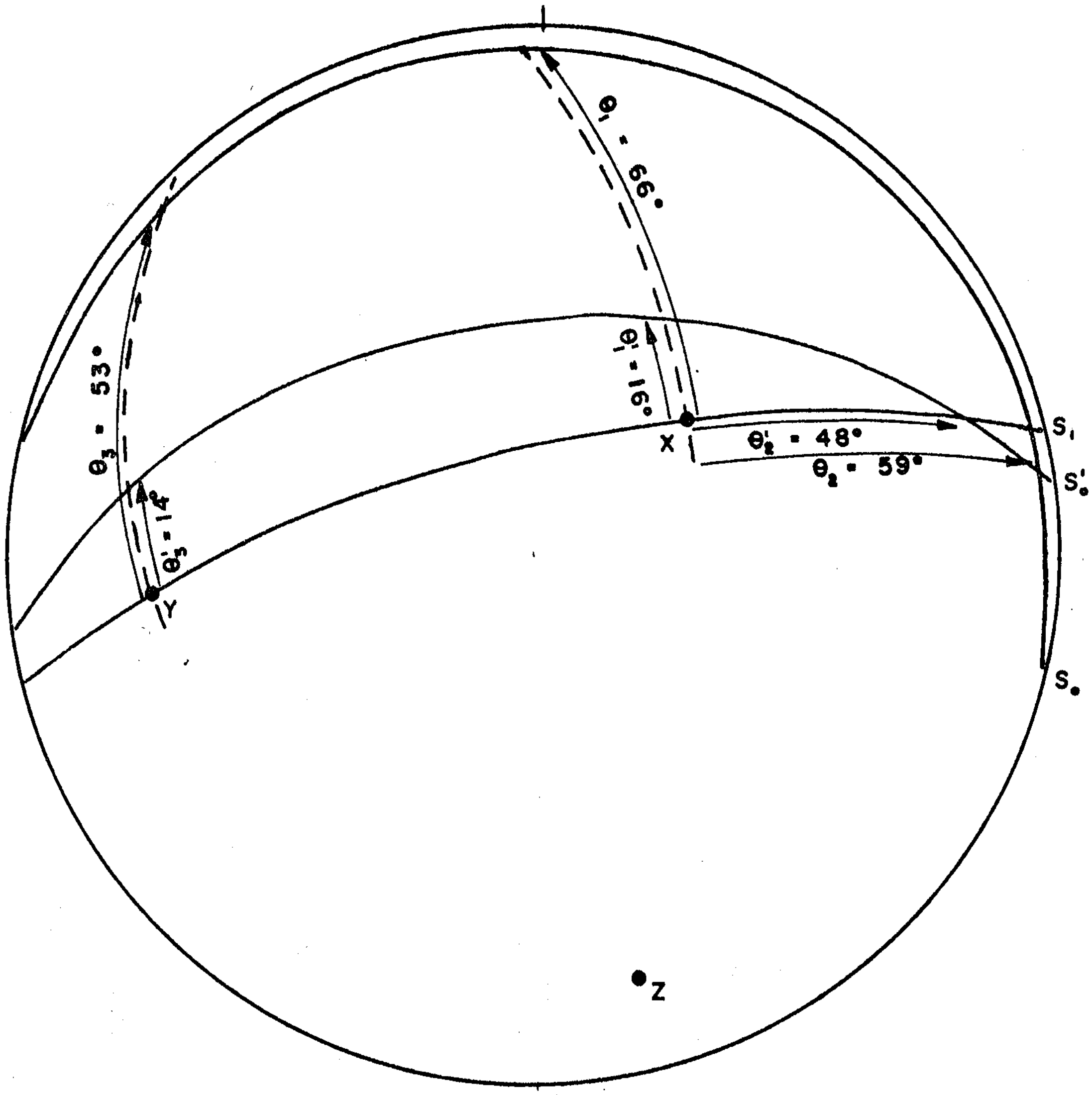

Z/X	= 0·123	Y/X	= 0·661	Z/X	= 0·187
θ_1'	= 16°	θ_2'	= 48°	θ_3'	= 14°
θ_1	= 66°	θ_2	= 59°	θ_3	= 53°

S_0' = 082 / 52N - deformed

S_0 = 111 / 3 N - undeformed

Fig. 5-19 Restoration of bedding at locality 32 (conglomerate) using the method of Ramsay (1967, p. 129→).

Strain estimates are likely to be minimum estimates because ductility contrasts do exist between rhyolite clasts and the matrix. Even though these are small, they are likely to affect the strain value determined. Also joint surfaces measured were only approximately parallel to the principal planes of the strain ellipsoid because no such surfaces were observed and thus pebble long axes are likely to be underestimates. Thirdly, there is some evidence that pressure solution was at least in part responsible for some of the deformation, as discussed earlier.

It is a distinct possibility that deformation might be a late stage event in the regional folding. In this case the deformation which caused the straining of the rocks could have caused a tightening of folds about their axial surfaces and resulted in the present isoclinal fold structures which are inferred from field data.

The original attitude of bedding may have deviated from the horizontal as discussed in Chapter 2, but is unlikely to have been as steeply dipping as is suggested by the restorations in Table 5.3.

Thus, none of these three possibilities can be ruled out entirely - a more likely explanation for the unstrained attitude of bedding is a combination of all three.

<u>Relationship of Strain Ellipsoid Orientations to Major Folds</u>

Stretching lineations in the rock units were measured at numerous localities and some of these are presented in Figure 5-20. This figure also shows the trend of cleavage traces and the trend and plunge of F_1 fold axes.

Assuming that the stretching lineations observed reflect the orientation of the principal extension direction, X, of the strain ellipsoid

Fig. 5-20 Stretching lineation orientations across the map area. F_1 fold axes are also shown as well as the trend of cleavage traces.

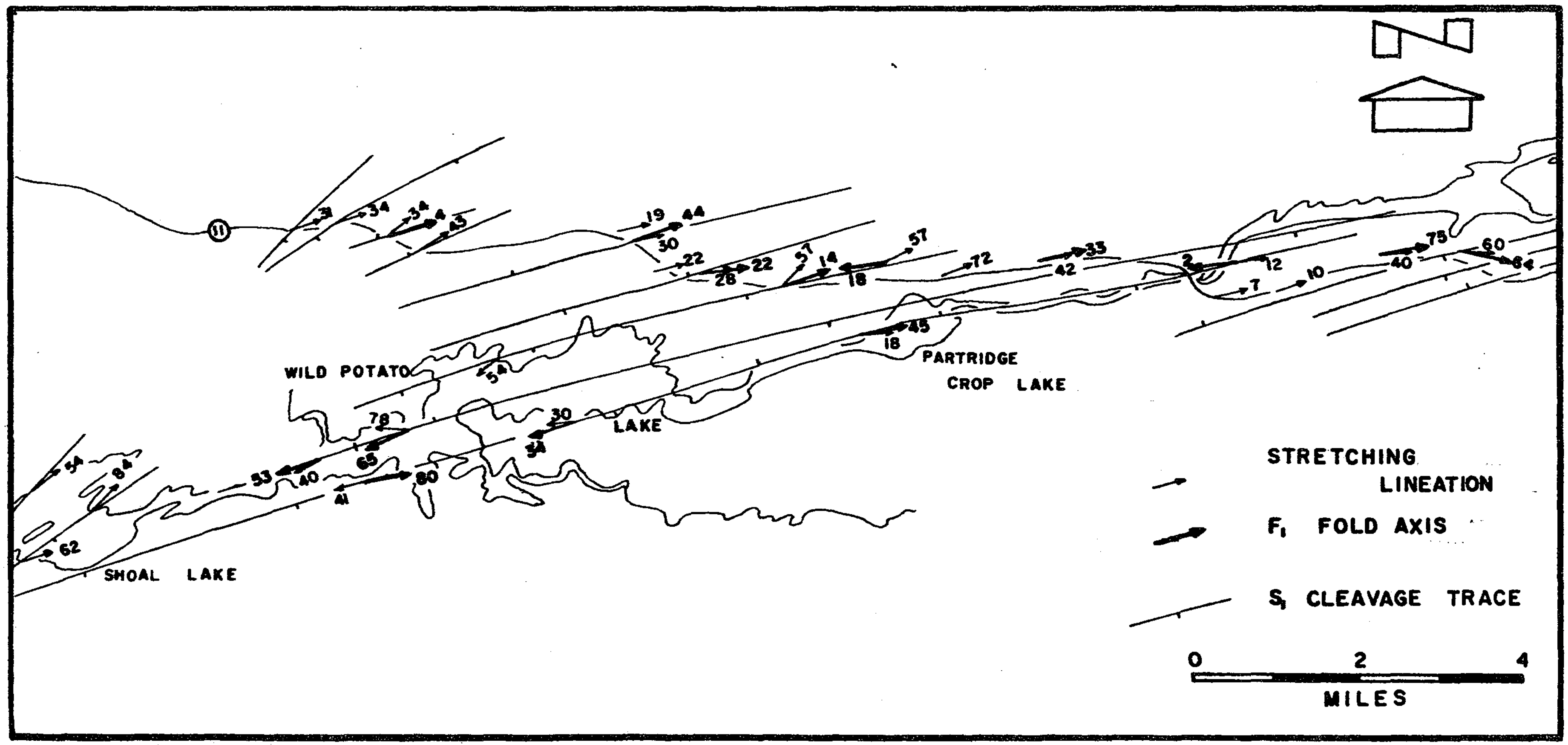

at individual localities, then from Figure 5-20, the principal extension direction for the main part of the area trends towards the ENE with a variable plunge. Along Highway 11, at the eastern extent of the map area, the plunge of X is steep (60°). It becomes gradually shallower further to the west, steepens again north of Partridge Crop Lake, shallows north-east of Wild Potato Lake and again becomes steeper towards the western part of the map. Along the shores of Wild Potato Lake however, X plunges at varying angles towards the west. At Shoal Lake, it again plunges steeply towards the east.

In relation to F_1 fold axes the orientation of the strain ellipsoid ranges from sub-parallel, at the eastern extent of the map area and along the south shore of Wild Potato Lake, up to nearly 80° difference in plunge, north of Partridge Crop Lake. Therefore, there appears to be no immediate relationship between F_1 fold axes and the orientation of the strain ellipsoid. Perhaps this is because the main deformation of the strain markers was later than the folding.

From the values of X/Z and Y/Z in Tables 5-1 and 5-2, values of X, Y and Z and the percentage extension/shortening they represent have been calculated, assuming constant volume strain (Flinn, 1962). The results are presented in Tables 5-4 and 5-5.

Within all the rocks used for the strain analysis there is generally extension in both X and Y except at locality 94 in the arenite and locality 29 in the conglomerate. The latter outcrop is interesting because a strain analysis was made using both arenite and conglomerate. This gave different types of strain ellipsoid, constricting ($K > 1$) in the case of the conglomerate and flattening ($K < 1$) from the arenite.

TABLE 5-4

CONGLOMERATE - RHYOLITE CLASTS

Outcrop	X	Y	Z	Extension/Shortening X	Y	Z	$k=\frac{(X/Y-1)}{(Y/Z-1)}$	X x Y x Z
9	3.50	1.77	0.16	+250%	+77%	-84%	0.098	0.9912
29	3.56	0.94	0.30	+256%	- 6%	-70%	1.287	1.0039
30	2.46	1.88	0.22	+146%	+88%	-78%	0.040	1.0175
32	2.30	1.53	0.29	+130%	+53%	-71%	0.117	1.0205
36	2.27	1.67	0.27	+127%	+67%	-73%	0.068	1.0235
36A	2.88	1.23	0.28	+188%	+23%	-72%	0.399	0.9919
37	2.56	1.66	0.24	+156%	+66%	-76%	0.089	1.0199

Ave. Ext. in X = 179% S' = 50.39

Ave. Ext. in Y = 52.57% S' = 30.58

Ave. Short. in Z = 74.86% S' = 4.55

TABLE 5-5

SANDSTONE

Outcrop	X	Y	Z	Extension/Shortening X	Y	Z	$k=\frac{(X/Y-1)}{(Y/Z-1)}$	X x Y x Z
9	1.43	1.21	0.58	+43%	+21%	-42%	0.165	1.0036
24	1.50	1.24	0.54	+50%	+24%	-46%	0.164	1.0044
29	1.37	1.18	0.62	+37%	+18%	-38%	0.178	1.0023
43	1.58	1.02	0.62	+58%	+ 2%	-38%	0.873	0.9992
64	1.53	1.13	0.58	+53%	+13%	-42%	0.383	1.0028
65	1.36	1.14	0.65	+36%	+14%	-35%	0.263	1.0078
90	1.61	1.11	0.56	+61%	+11%	-44%	0.450	1.0008
94	1.65	0.99	0.61	+65%	- 1%	-39%	1.048	0.9964
97	1.67	1.19	0.50	+67%	+19%	-50%	0.290	0.9937
98	1.66	1.07	0.56	+66%	+ 7%	-44%	0.626	0.0947
103	1.40	1.20	0.60	+40%	+20%	-40%	0.168	1.0080

Ave. Ext. in X = 41.64% S' = 4.05

Ave. Ext. in Y = 13.64% S' = 7.36

Ave. Short. in Z = 52.36% S' = 11.35

The variation in extension and shortening is large for both arenite and conglomerate exposures.

Because the folds in the area are so tight, all the strain estimates made coincide with the flanks of folds, which probably explains why nearly all of the strain ellipsoids fall into the K < 1 flattening field on the Flinn diagram (Fig. 5-18).

Limitations of the Strain Analysis Methods Used

The basic limitations of the methods used lie in the assumptions they make. Firstly, it is difficult to assess whether or not the strain history was coaxial. Secondly, some volume loss by the strain markers is likely, due to the effects of pressure solution, which would result in an underestimate of strain by the methods used. Thirdly, original sedimentary fabrics will only appear as skewed R_f/ϕ plots for the deformed state where the symmetry element was at a high angle to the present XY plane of the strain ellipsoid. Where the angle was low, or if the strain was sufficiently high, then the R_f/ϕ plots may not be sensitive to the original symmetry. This could result in an overestimate of strain. The methods of Gay and the ideas outlined in this discussion attempt to minimize the problem of competency contrasts. The advantage with the present method is that it is easy to apply and yields an empirical value of competency contrast. Thus, used in combination with the harmonic mean method of Lisle and the equations of Gay, although not perhaps giving an exact estimate, this approach is considered to yield at least a realistic approximation of strain where competency contrasts exist (as is the norm rather than the exception in natural conglomerates).

DISCUSSION

STRUCTURE

From the evidence in Chapter 2, there appears to have been one dominant period of deformation resulting in the major F_1 fold structures illustrated on the structural map in the rear folder. Small kink folds and isolated crenulation folds probably represent a second phase of folding but whether or not these structures represent a distinct deformation period is unclear.

Poulsen et al. (1980) have demonstrated that a large scale overturning of strata occurred prior to the dominant folding at Rainy Lake, 40 km west of the present study area. They suggest that the development of nappe structures was responsible for this overturning. Downwards facing structures are observed in the present study area, but these are localized and probably do not represent any major pre-F_1 folding. Thus the lateral geographic extent of the overturning of strata at Rainy Lake cannot be traced as far east as the present area.

STRATIGRAPHY

The field evidence outlined in Chapter 3 supports the supposition that two ages of metavolcanic rocks are present in the study area: younger metavolcanic rocks which overlie the Seine metasedimentary rocks at the eastern margin of the area and older metavolcanic rocks which underlie the same metasedimentary rocks in the west. The metavolcanic rocks to the west have been correlated by many authors (eg., Lawson, 1913 and Wood, 1980) with the Keewatin metavolcanic rocks at Rainy Lake. Young (1960) has also correlated the metavolcanic rocks at the eastern margin of the map area with the Keewatin at Rainy Lake. These views are apparently in contradiction with the results of the present study.

The significance of such ambiguities is that lateral stratigraphic correlations, even across relatively small distances, are difficult to establish in the Archean in Northwestern Ontario, unless the regional structure is well understood first.

METAMORPHISM

Temperature and pressure conditions appear to have been more or less uniform during the regional metamorphism of the rocks, as evidenced by the consistency of the metamorphic assemblages across the area. This metamorphism was also synkinematic with the deformation and development of cleavage. However late stage overgrowths of biotite and muscovite which have a random orientation may suggest that the metamorphism outlasted the folding in places.

STRAIN HISTORY

In all the localities studied, the principal shortening direction, Z, was subhorizontal and N-S (perpendicular to cleavage). At most outcrops, cleavage and bedding are also subparallel to one another so Z is more or less normal to bedding. The principal extension direction, X, has a variable plunge angle within the plane of cleavage.

From Chapter 5 the strain ellipsoids for the various localities studied are dominantly of the flattening type with average shortening for the conglomerates of 75% and 53% for the arenites. The cause of the deformation and folding is uncertain because the area is bounded by major transcurrent faults. However, diapiric uprise on the scale suggested by Schwerdtner et al. (1979) could well result in such a high degree of lateral shortening in the rocks.

The timing of the deformation relative to the folding is also uncertain. However, there is some evidence to suggest that the deformation may have been a late stage event in the regional folding (Chapter 5). In this case, the "straining" of the rocks would have caused a tightening of major folds resulting in the present subparallel attitude of bedding and cleavage and the high degree of shortening in the limbs of the folds.

In this study an attempt has been made to provide structural data which may help to resolve some of the stratigraphic problems which still persist and secondly to quantify the strain in the rocks. The importance of these two fields cannot be underestimated in understanding the stratigraphic relations in any deformed area, but particularly in Archean terrains. Only when the structure is understood clearly can stratigraphic relations be deduced.

This study also underlines the importance of using bedding-cleavage relations and structural facing to determine the positions of major fold axial traces in areas of limited lithological variety. Without the use of these techniques, no structural survey would have been possible in this area.

CONCLUSIONS

From the evidence provided by this thesis, the following conclusions can be drawn:

1. One or possibly two overlapping periods of deformation are responsible for the present structures in the study area.
2. The structure is dominated by major F_1 folds. Geometrically these folds are tight to isoclinal, non-plane approximately cylindrical, slightly inclined. Axial traces are approximately east-west trending and 1 to 2 km apart with fold amplitudes of up to several kilometres.
3. Small kink folds and crenulation folds represent a late stage deformation.
4. There is limited evidence for a pre-F_1 folding event.
5. Two ages of metavolcanic rocks are present, separated by the Seine Group metasedimentary rocks.
6. The metasedimentary rocks are subdivided into conglomerate and fine- to medium-grained arenites. These units are interbedded with each other across the whole area.
7. Crossbedding and trough-crossbedding is common in the areneous deposits suggesting a shallow water, high energy environment of deposition. Sp
8. Regional metamorphism to the chlorite to biotite zone greenschist facies was synkinematic with the deformation.

9. Strain analysis reveals that the conglomerate units are more intensely strained than arenite units. The strain ellipsoids for individual outcrops are of the flattening type with average shortening of 75% for conglomerates and 53% for arenites.

APPENDIX A

DEFORMATION OF CROSSBEDDING AND TROUGH-CROSSBEDDING

APPENDIX A

DEFORMATION OF CROSSBEDDING AND TROUGH-CROSSBEDDING

Many primary sedimentary structures are susceptible to the effects of deformation. Crossbedding and trough-crossbedding are examples. These structures are also common in the study area and so some further explanation is required.

Simple experiments have been conducted to model the deformation of these sedimentary structures by pure shear and simple shear. Simple shear deformation was simulated by the use of a card-deck model while a stretched rubber sheet simulated two-dimensional, homogeneous pure shear. Results are presented in Figures Ap. 1 and 2.

In the undeformed state, the symmetry of troughs can be used as a guide to the orientation of bedding, which is likely to be tangential to the inflection point on the trough. However, as suggested by Dr. Borradaile in the field and shown in Figure Ap. 1, during both simple and pure shear, this symmetry is lost: during pure shear, only where bedding is parallel or perpendicular to the principal extension direction is the symmetry retained. This is analogous to the deformation of pillow lava (Borradaile and Poulsen, 1981), illustrated in Figure Ap. 3, where the pillow symmetry is lost in all cases except when the long axis is parallel or perpendicular to the principal extension direction.

Crossbedded units are also subject to the effects of deformation, as illustrated in Figure Ap. 2. Flattening where $\theta = 0$ and steepening

Fig. Ap.-1 Simple shear deformation of troughbedding. Shear directions are parallel to length of page. Values of simple shear (ψ) are given and θ is the original angle between S_0 and the simple shear axes.

SIMPLE SHEAR

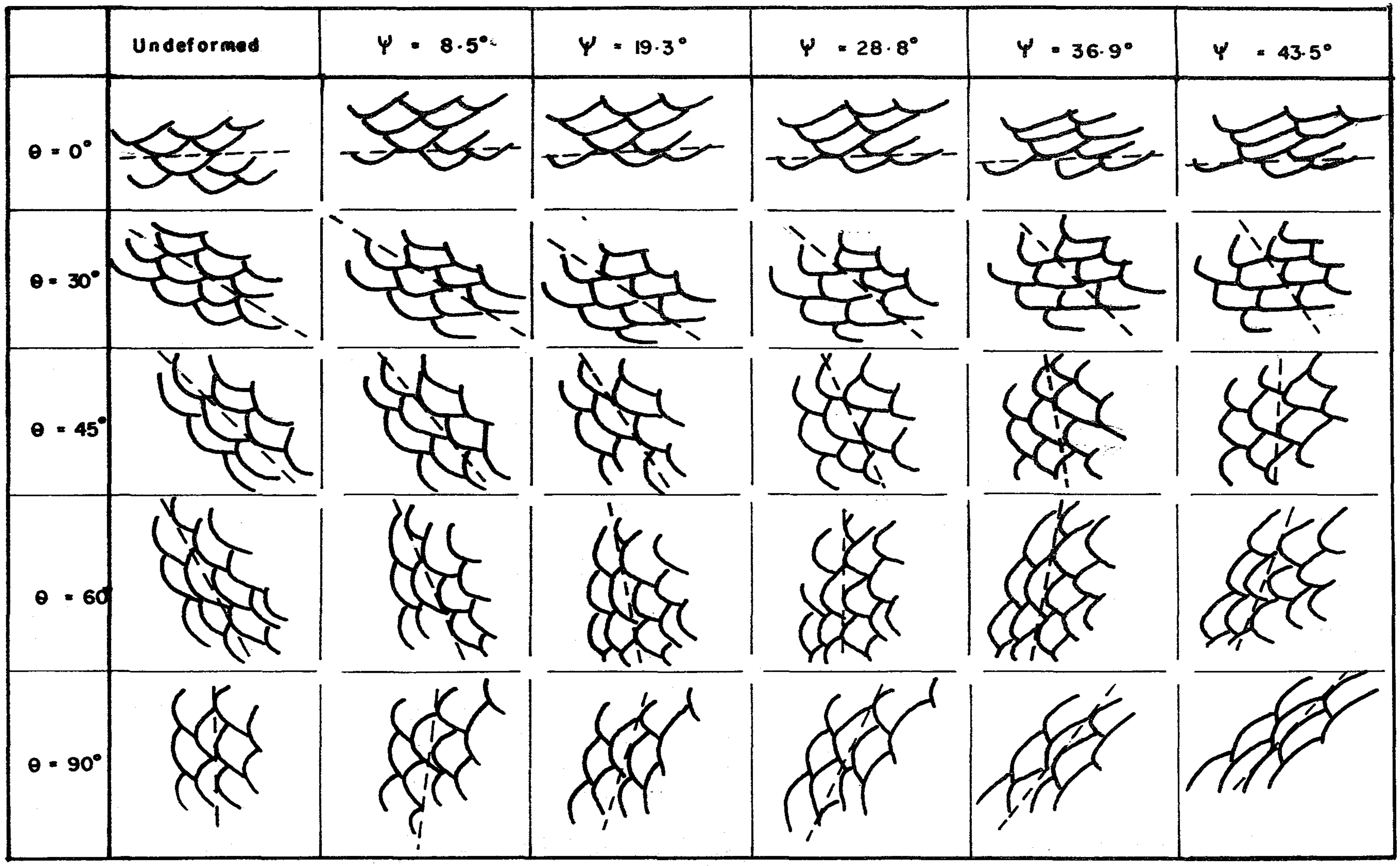

Fig. Ap.-2 Pure shear deformation of trough-crossbedding (lower) and crossbedding (upper). $\lambda_1/\lambda_2 = 1.44$. θ is the angle between the undeformed bedding trace, S_0 and the extension direction λ_1.

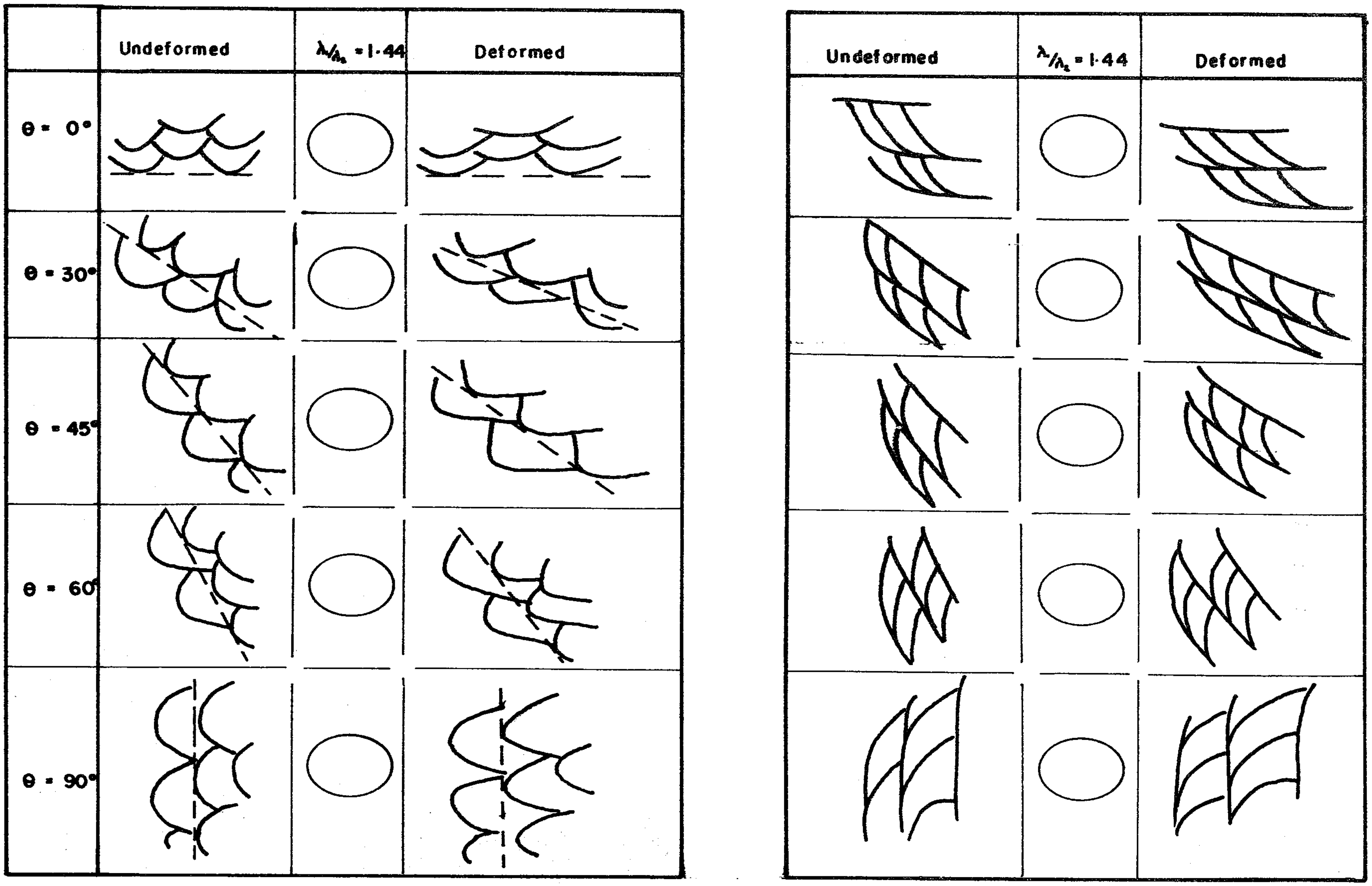

Undeformed
$\lambda_1/\lambda_2 = 1{\cdot}44$
Deformed
θ = 0°
θ = 30°
θ = 45°
θ = 60°
θ = 90°
Undeformed
$\lambda_1/\lambda_2 = 1{\cdot}44$
Deformed

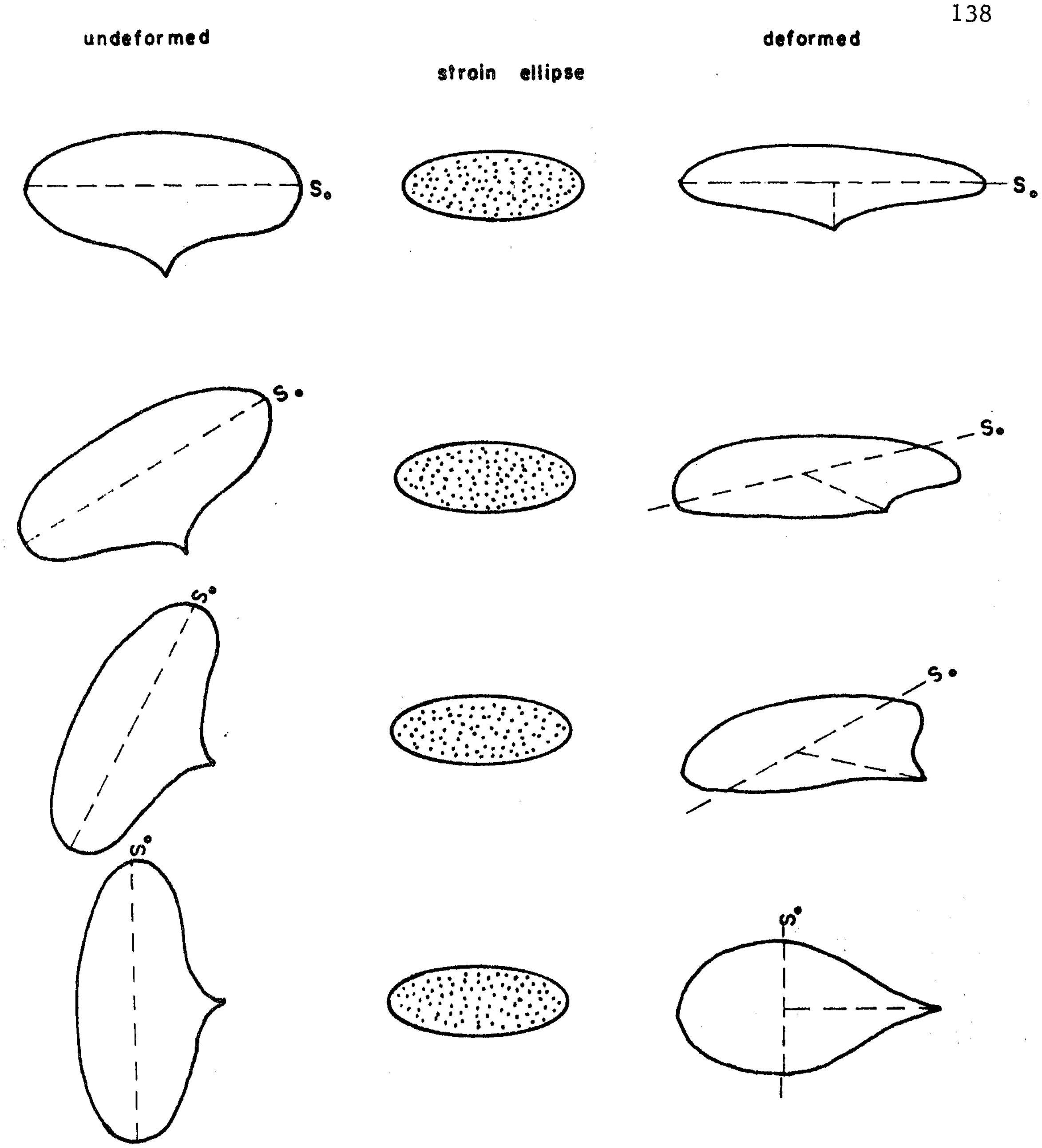

Fig. Ap.-3 2-D deformation of pillow lava by homogeneous pure shear strain. (After Borradaile and Poulsen, 1981).

of cosets for other orientations is pronounced even for such low strains (λ_1/λ_2 = 1.44 here). Where θ is large, strain is high and the cosets are originally at high angles, it is possible that shortening could cause the sets to oversteepen and thus mimic trough-crossbedding.

Thus caution must be exercised when crossbeds or trough-crossbeds are used to determine bedding or younging in deformed terrains.

A good example of deformed crossbeds is shown in Figure Ap. 4. Cosets are steepened in the YZ plane but flattened in the XZ plane to the extent where truncations are not readily observable.

Deformed trough-crossbedding is common in the map area particularly around the shores of Wild Potato Lake. An example is illustrated in Figure Ap. 5. Shortening on the YZ surface has caused a steepening of troughs; however, extension on the XY surface has drawn the scours out so they now appear similar to crossbeds. Extension on the XZ surface has also drawn the structures out resulting in curious 'canoe'-shaped troughs.

Fig. Ap.-4 Effects of deformation on crossbedding, at locality 64, South of Sturgeon Falls.

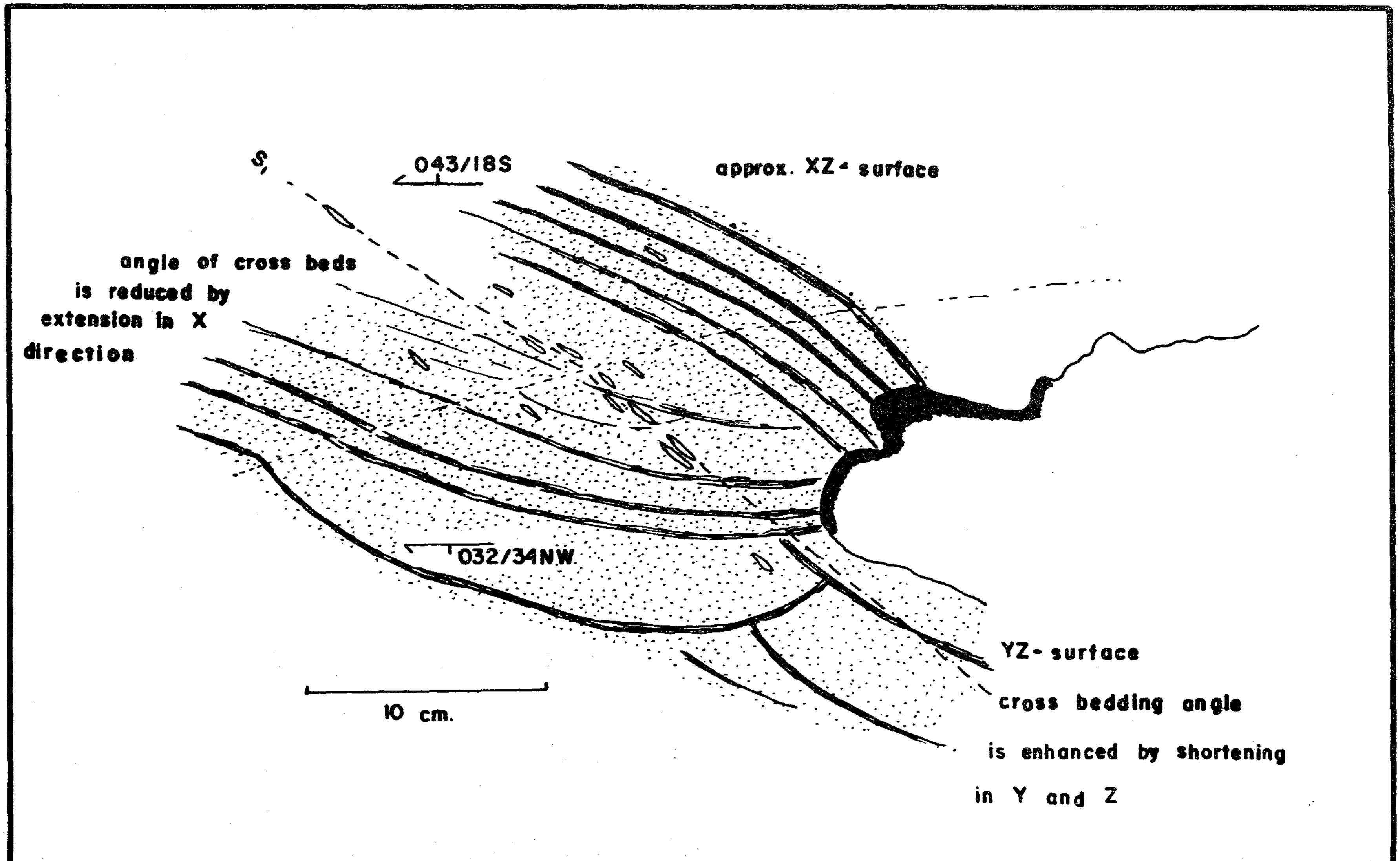

S_1
043/18S
approx. XZ- surface
angle of cross beds
is reduced by
extension in X
direction
032/34NW
10 cm.
YZ- surface
cross bedding angle
is enhanced by shortening
in Y and Z

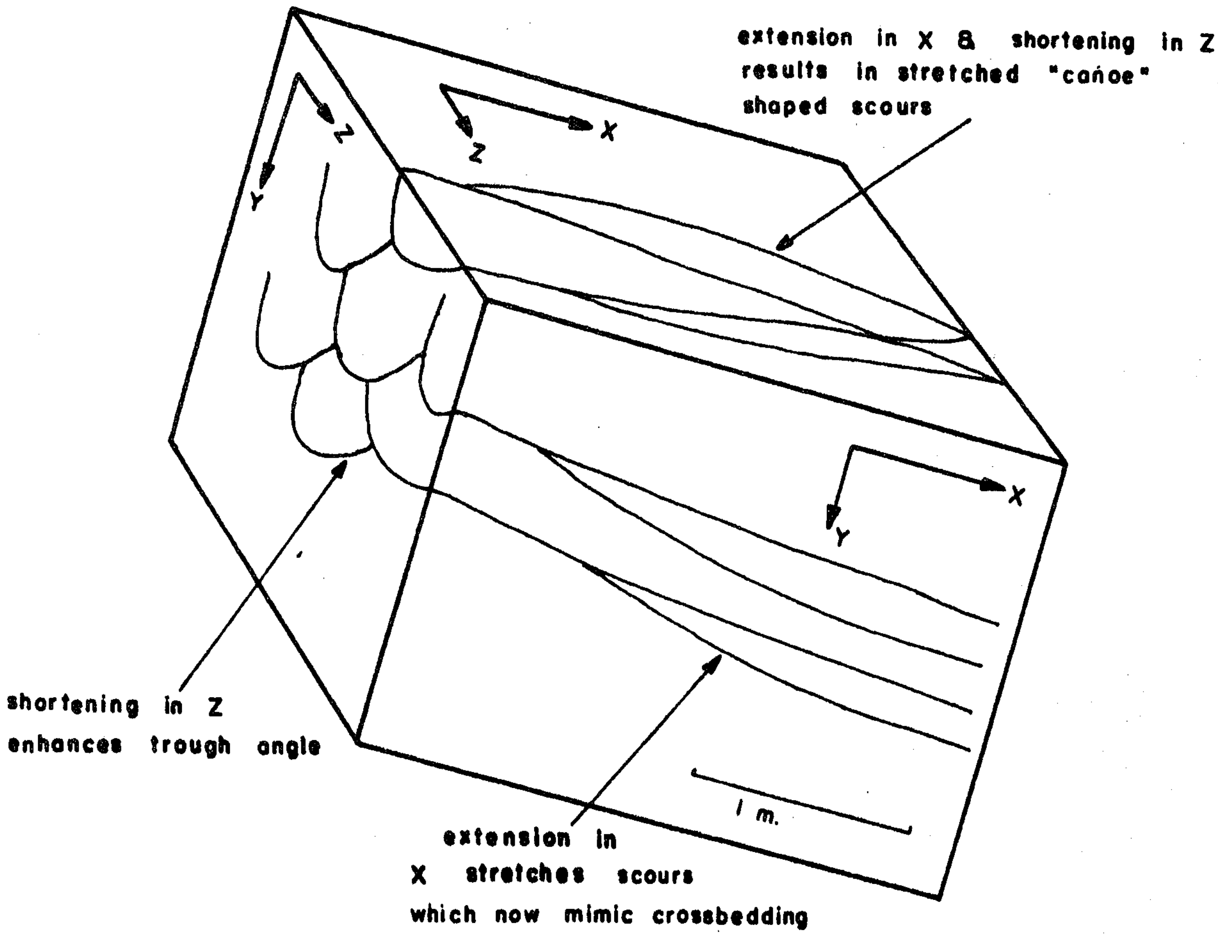

Fig. Ap.-5 Effects of deformation on trough-bedding at outcrop no. 129, North Shore of Wild Potato Lake.

APPENDIX B

ORIENTATION PLOTS

CONGLOMERATE

Location - OC 9 XZ - surface

Orientation of S_1 = 086/82S
Orientation of stretching lineation = 091/60
Orientation of joint surface = 016/ 56E

GRANITOID CLASTS

Long-axis pitch, α	Axial ratio, R_f	$1/R_f$
72N	5.200	0.192
65N	1.486	0.673
84N	3.647	0.274
74N	2.118	0.472
84N	1.628	0.614
82N	6.700	0.149
87N	4.400	0.227
77N	6.818	0.147
88S	1.231	0.813
84N	3.533	0.283

$\Sigma 1/R_f$ = 3.844
$N/(\Sigma 1/R_f)$ = 2.601
N = 10

ACID VOLCANIC (RHYOLITE) CLASTS

Long-axis pitch, α	Axial ratio, R_f	$1/R_f$
84N	45.250	0.022
84N	12.400	0.081
83N	19.800	0.051
84N	31.667	0.032

$\Sigma 1/R_f$ = 0.185
$N/(\Sigma 1/R_f)$=21.645
N = 4

INTERMEDIATE VOLCANIC CLASTS

Long-axis pitch, α	Axial ratio, R_f	$1/R_f$
83N	5.385	0.186
85N	4.067	0.246
84N	26.667	0.038

$\Sigma 1/R_f$ = 0.470
$N/(\Sigma 1/R_f)$= 6.390

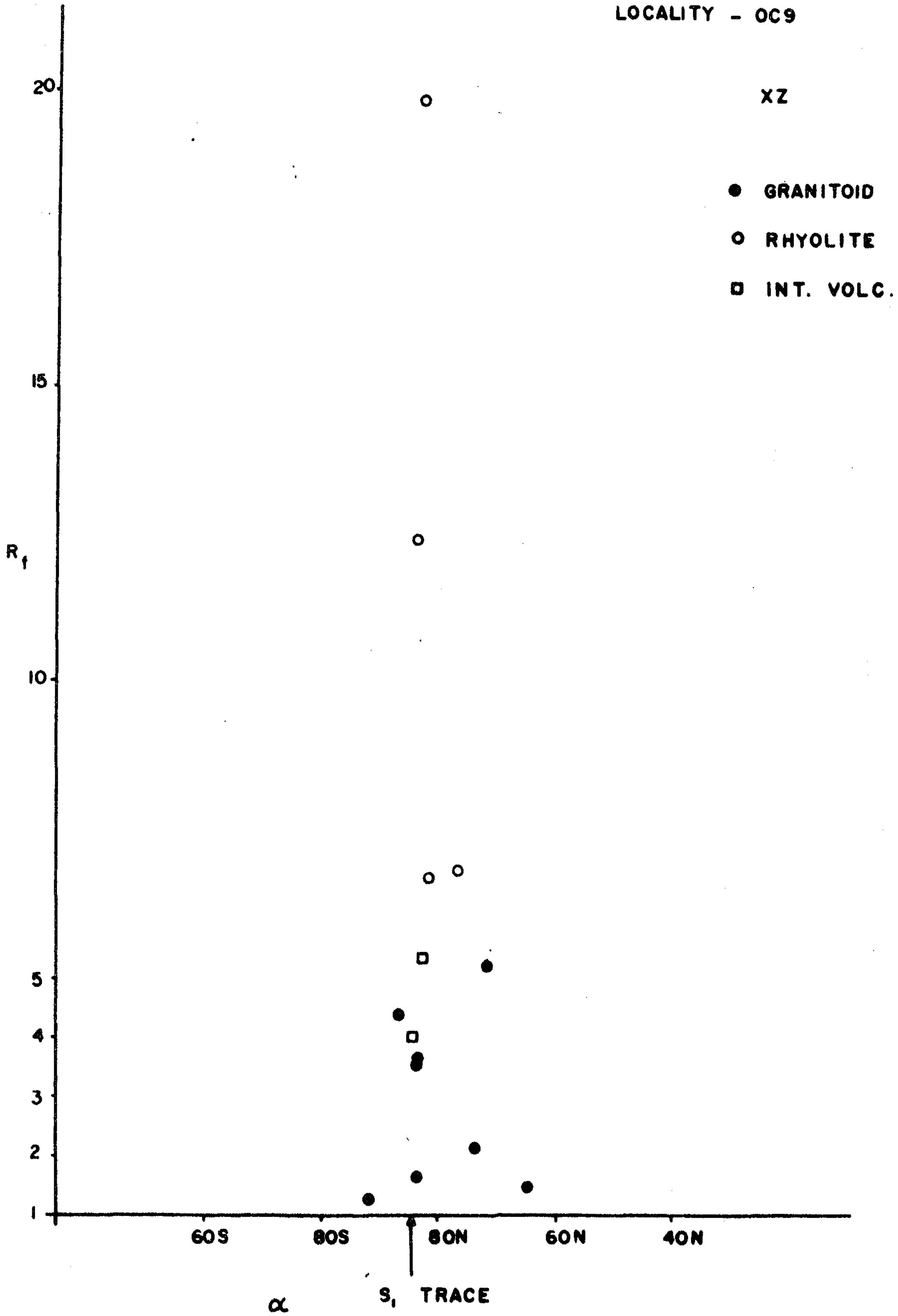

LOCALITY - OC9
XZ
GRANITOID
RHYOLITE
INT. VOLC.
20
15
10
5
4
3
2
1
R_f
60S
80S
80N
60N
40N
S_1 TRACE
α

Location - OC 9 YZ - surface

Orientation of joint surface = 016/30W

GRANITOID CLASTS

Long-axis orient., α	Axial ratio, R_f	$1/R_f$
101	1.214	0.824
081	1.848	0.541
080	2.500	0.400
085	2.105	0.475
083	3.100	0.323
098	1.095	0.913
142	1.510	0.662
076	2.625	0.381
081	2.293	0.436
086	3.889	0.257
085	1.971	0.507
076	2.727	0.367
079	3.100	0.323
083	1.789	0.559
086	2.136	0.468
084	3.111	0.321
087	3.889	0.257
084	3.500	0.286
081	3.389	0.295
085	3.077	0.325
063	1.259	0.794
082	1.813	0.552
089	2.409	0.415
084	2.852	0.351
087	1.933	0.517
101	1.714	0.583
075	2.737	0.365
090	2.750	0.364
080	1.619	0.618
080	1.639	0.610
091	1.541	0.649
077	2.765	0.362
087	1.714	0.583
096	1.579	0.633
096	1.478	0.676
078	1.656	0.604

$\Sigma 1/R_f$ = 17.596

$N/(\Sigma 1/R_f)$ = 2.046

N = 36

ACID VOLCANIC (RHYOLITE) CLASTS

Long-axis orient., α	Axial ratio, R_f	$1/R_f$
086	19.000	0.053
081	12.600	0.071
087	13.000	0.077
084	21.750	0.046
084	9.714	0.103
087	9.143	0.109
083	5.833	0.171
087	15.667	0.064
087	15.200	0.066
084	18.000	0.056
085	9.222	0.108
086	31.333	0.032
088	17.333	0.058
086	7.000	0.143
087	12.000	0.083
086	11.500	0.087
085	5.500	0.182
085	11.750	0.085
086	9.125	0.110
087	8.889	0.113

$\Sigma 1/R_f = 1.824$

$N/(\Sigma 1/R_f) = 10.964$

$N = 20$

INTERMEDIATE VOLCANIC CLASTS

Long-axis orient., α	Axial ratio, R_f	$1/R_f$
080	4.222	0.237
086	6.714	0.149
083	2.917	0.343

$\Sigma 1/R_f = 0.729$

$N/(\Sigma 1/R_f) = 4.115$

$N = 3$

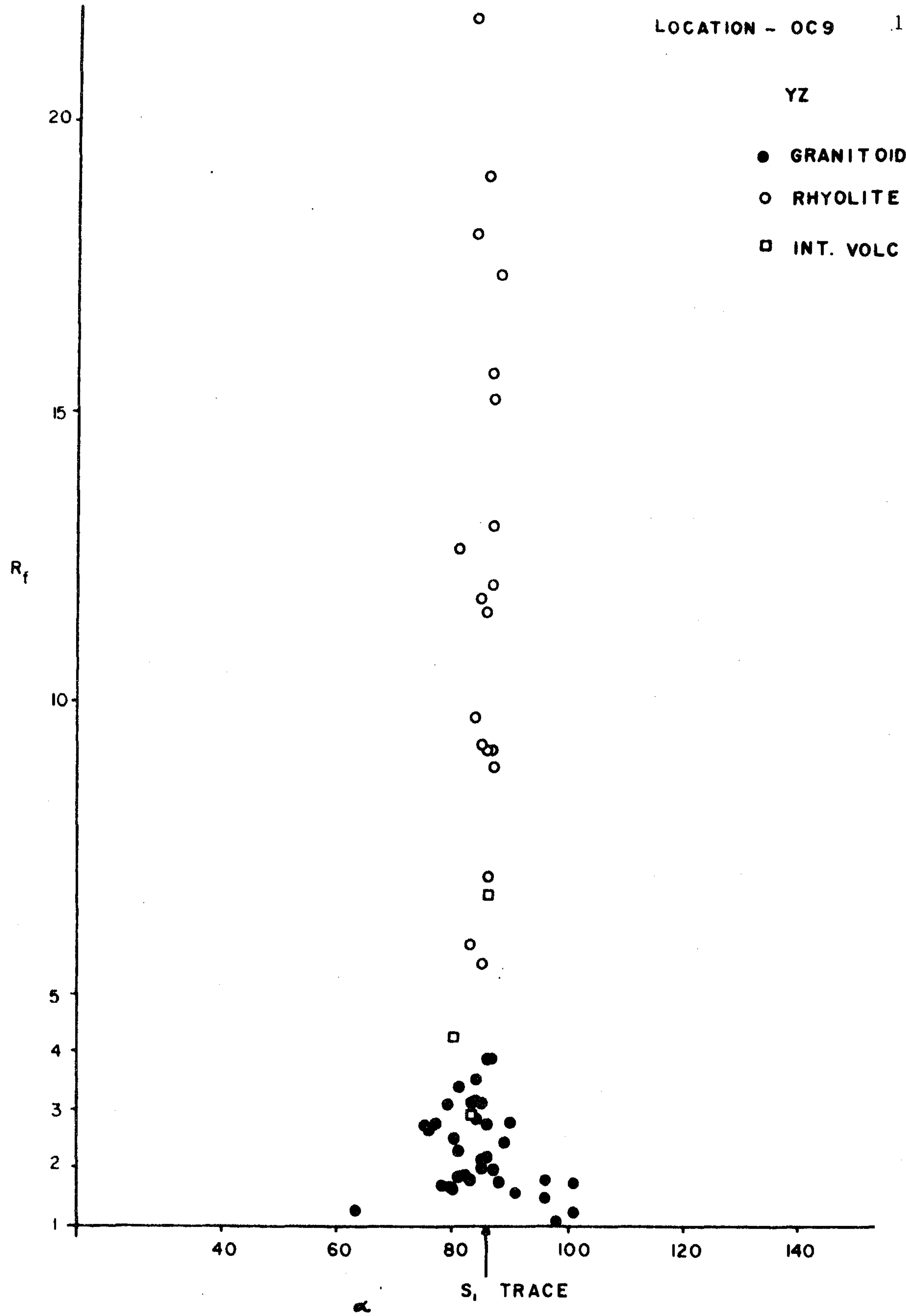
LOCATION - OC9
YZ
GRANITOID
RHYOLITE
INT. VOLC
R_f
20
15
10
5
4
3
2
1
40
60
80
100
120
140
S_1 TRACE
α

Location - OC 12 XZ - surface

Orientation of S_1 = 081/76S
Orientation of stretching lineation = 081/16
Orientation of joint surface = 052/5SE

GRANITOID CLASTS

Long-axis orient., α	Axial ratio, R_f	$1/R_f$
069	2.178	0.459
131	1.361	0.735
083	1.762	0.568
091	2.042	0.490
090	1.656	0.604
098	1.739	0.575
080	2.636	0.379
076	2.200	0.455
166	1.690	0.592
068	2.278	0.439
131	1.429	0.700
070	1.619	0.618
066	1.300	0.769
077	2.692	0.371
176	1.482	0.675
078	1.750	0.571
101	1.750	0.571
129	1.269	0.788
064	4.231	0.236
088	1.682	0.595
056	2.187	0.457
088	1.767	0.566
093	2.750	0.364
075	1.579	0.633
086	2.154	0.464
087	2.400	0.417
168	1.114	0.897
065	2.000	0.500
098	1.333	0.750
078	2.042	0.489
090	3.222	0.310
064	1.308	0.765
076	1.889	0.529
076	2.519	0.397
072	2.059	0.486
081	3.059	0.327
085	2.304	0.434
094	1.412	0.708

$\Sigma 1/R_f$ = 20.683

$N/(\Sigma 1/R_f)$ = 1.837

N = 38

Location - OC 12 YZ - surface

Orientation of joint surface = 007/89E

GRANITOID CLASTS

Long-axis pitch, α	Axial ratio, R_f	$1/R_f$
73S	2.857	0.350
89S	1.500	0.667
69N	1.147	0.872
VERT.	2.464	0.406
87N	3.545	0.282
73N	1.310	0.763
83N	2.353	0.425
84S	1.512	0.662
89N	1.632	0.613
82N	3.400	0.294
77S	1.714	0.583
VERT.	1.750	0.571
85N	1.765	0.567
81N	2.880	0.347
86S	3.429	0.292
80N	2.000	0.500
86N	1.636	0.611
86N	1.364	0.733
75N	1.833	0.545
VERT.	1.270	0.787
83N	1.765	0.567
89N	1.864	0.537
88S	2.540	0.394
88N	1.478	0.676
89N	1.778	0.563
88N	3.077	0.325
84S	1.650	0.606
84N	1.867	0.536
87S	1.429	0.700
82S	1.400	0.714

$\Sigma 1/R_f = 16.488$

$N/(\Sigma 1/R_f) = 1.820$

$N = 30$

LOCATION - OC12

XZ

GRANITOID CLASTS

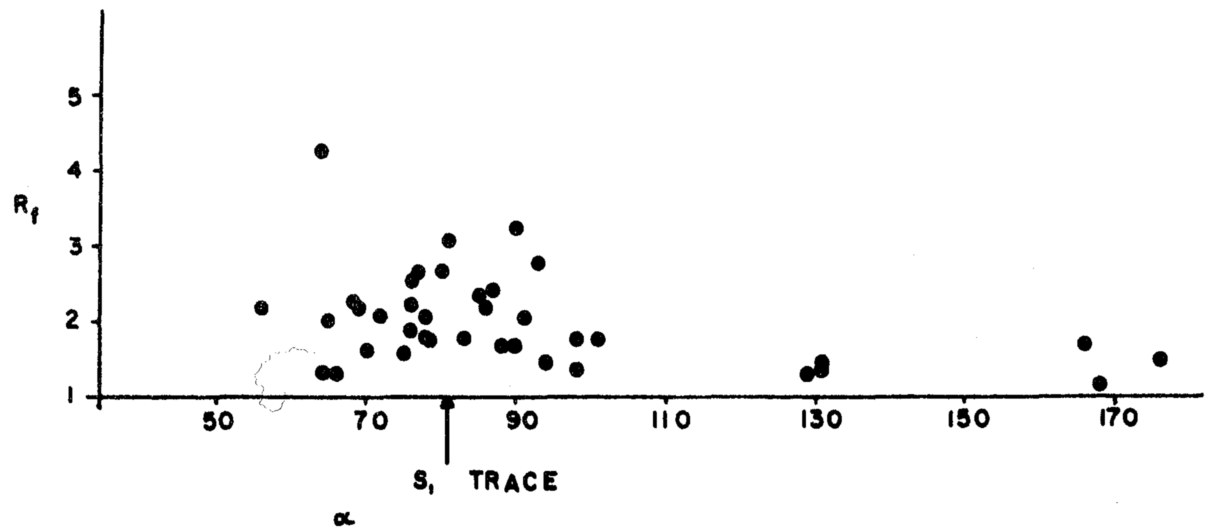

YZ

GRANITOID CLASTS

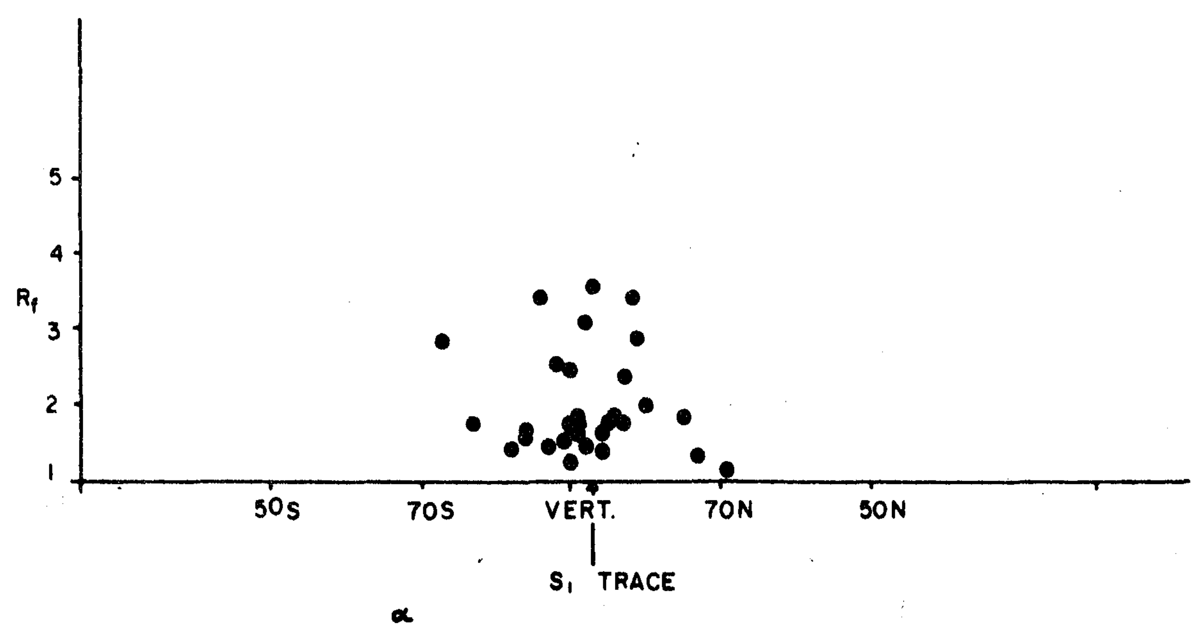

Location - OC29 XZ - surface

Orientation of S_1 = 074/78N
Orientation of stretching lineation = 067/57
Orientation of joint surface = 026/48E

GRAITOID CLASTS

Long-axis orient., α	Axial ratio, R_f	$1/R_f$
244	4.462	0.224
236	2.600	0.385
251	2.250	0.444
250	3.077	0.325
235	3.067	0.326
239	2.429	0.412
254	4.600	0.217
235	4.583	0.218
271	1.400	0.714
249	2.769	0.361
251	4.719	0.212
252	4.889	0.205
250	2.571	0.388
252	9.000	0.111
250	7.121	0.140
240	3.052	0.327
248	4.000	0.250
256	6.846	0.146
250	6.666	0.150
258	3.000	0.333

$\Sigma 1/R_f$ = 4.819
$N/(\Sigma 1/R_f)$ = 4.150
N = 20

ACID VOLCANIC (RHYOLITE) CLASTS

Long-axis orient., α	Axial ratio, R_f	$1/R_f$
260	11.250	0.088
250	17.250	0.057
255	15.142	0.066
248	15.333	0.065
250	12.800	0.078
255	5.238	0.190
251	22.857	0.043

$\Sigma 1/R_f$ = 0.587
$N/(\Sigma 1/R_f)$ = 11.925
N = 7

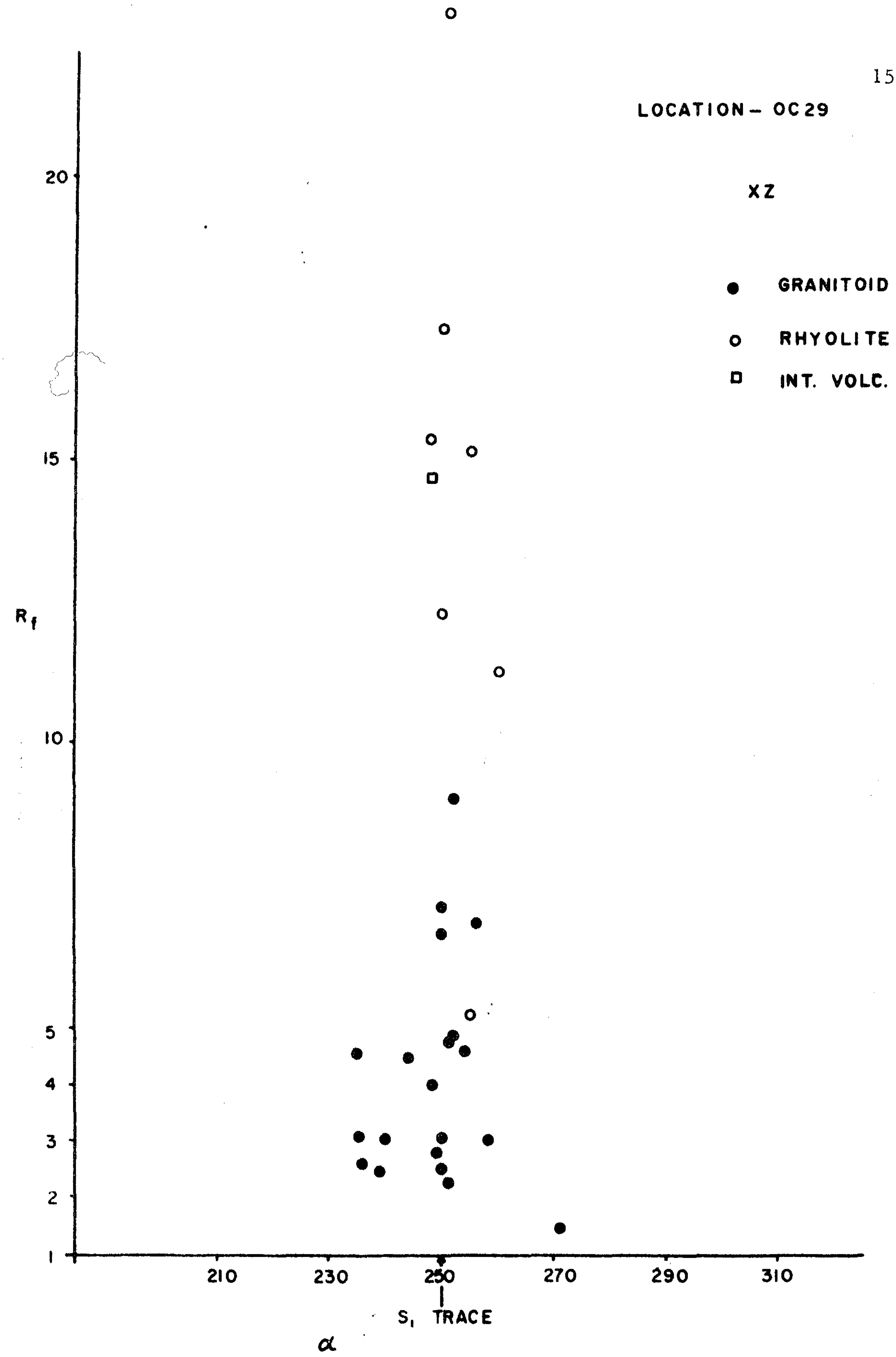

LOCATION – OC29
XZ
GRANITOID
RHYOLITE
INT. VOLC.
R_f
20
15
10
5
4
3
2
1
210
230
250
270
290
310
S_1 TRACE
α

INTERMEDIATE VOLCANIC CLASTS

Long-axis orient., α	Axial ratio, R_f	$1/R_f$
243	24.642	0.040
248	14.667	0.068

$\Sigma 1/R_f = 0.108$

$N/(\Sigma 1/R_f) = 18.520$

$N = 2$

YZ - surface

Orientation of joint surface = 122/33SW

GRANITOID CLASTS

Long-axis orient., α	Axial ratio, R_f	$1/R_f$
270	3.222	0.310
280	2.474	0.404
264	3.333	0.300
254	1.800	0.555
256	4.143	0.241
256	2.830	0.353
270	3.143	0.318
268	3.412	0.293
273	4.385	0.228
259	2.182	0.458
250	2.611	0.382

$\Sigma 1/R_f = 3.842$

$N/(\Sigma 1/R_f) = 2.863$

$N = 11$

ACID VOLCANIC (RHYOLITE) CLASTS

Long-axis orient., α	Axial ratio, R_f	$1/R_f$
254	2.560	0.390
276	3.145	0.317
282	2.080	0.480
273	2.286	0.437
266	10.000	0.100
268	2.609	0.383
268	7.810	0.128
293	3.410	0.293

$\Sigma 1/R_f = 2.528$

$N/(\Sigma 1/R_f) = 3.164$

$N = 8$

INTERMEDIATE VOLCANIC CLASTS

Long-axis orient., α	Axial ratio, R_f	$1/R_f$
282	3.846	0.260
256	4.388	0.227
265	9.688	0.103
287	2.763	0.361
258	1.350	0.740
263	4.263	0.234
264	5.364	0.186

$\Sigma 1/R_f = 2.111$

$N/(\Sigma 1/R_f) = 3.315$

$N = 7$

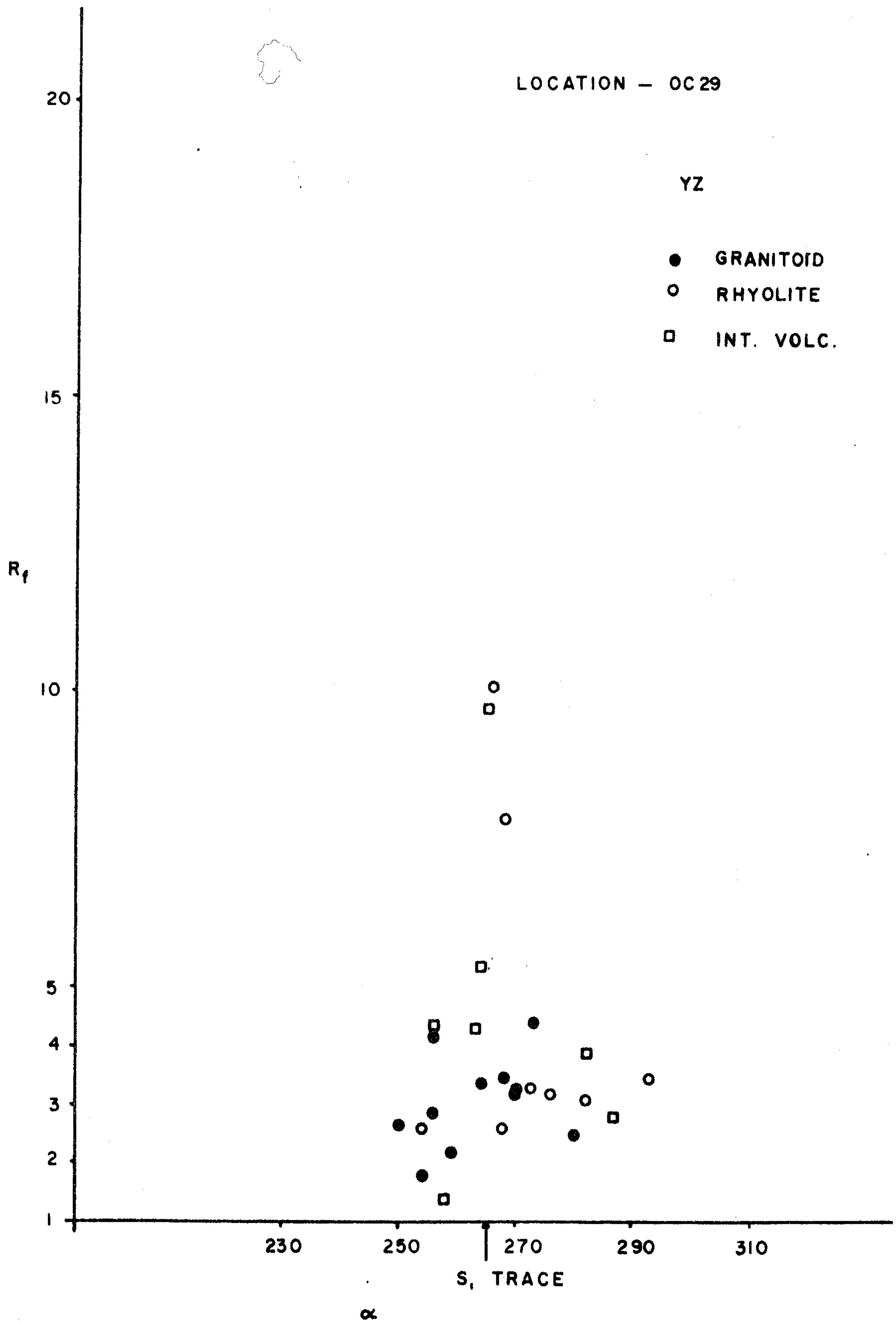
LOCATION — OC29
YZ
GRANITOID
RHYOLITE
INT. VOLC.
R_f
20
15
10
5
4
3
2
1
230
250
270
290
310
S_1 TRACE
α

Location - OC30 XZ - surface

Orientation of S_1 = 073/88N
Orientation of stretching lineation = 078/40
Orientation of joint surface = 010/34E

GRANITOID CLASTS

Long-axis orient., α	Axial ratio, R_f	$1/R_f$
244	5.000	0.200
252	3.375	0.296
254	4.050	0.247
243	3.045	0.328
246	3.545	0.282
246	6.433	0.155
254	14.000	0.071
253	9.286	0.108
256	3.400	0.294
243	3.371	0.297
254	2.300	0.435
223	1.250	0.800
245	7.000	0.143
239	1.766	0.566
246	3.235	0.309
245	1.974	0.507
248	3.400	0.291
245	5.500	0.182
246	2.794	0.358
257	1.950	0.513
250	13.643	0.073
260	5.889	0.170
255	7.841	0.128
245	6.429	0.156
255	7.000	0.143
230	2.500	0.400
254	11.974	0.084
248	23.765	0.042
258	4.480	0.223
250	13.000	0.077
248	7.963	0.126

$\Sigma 1/R_f$ = 8.004

$N/(\Sigma 1/R_f)$ = 3.873

N = 31

Location - OC30 XZ - surface (cont.)

ACID VOLCANIC (RHYOLITE) CLASTS

Long-axis orient., α	Axial ratio, R_f	$1/R_f$
252	14.000	0.071
249	15.857	0.063
252	32.778	0.031
253	9.500	0.105
253	37.000	0.027
254	8.214	0.122
252	6.364	0.157
255	16.083	0.062
249	10.429	0.096
249	16.619	0.062
253	20.714	0.048
254	16.750	0.060
253	18.000	0.056
255	10.857	0.092
256	6.364	0.157
256	12.182	0.082
255	10.857	0.092
251	28.429	0.035
251	9.167	0.109
249	7.294	0.137
258	14.181	0.070
245	16.000	0.062
252	16.000	0.062
252	5.444	0.183
251	17.667	0.056
245	5.700	0.175

$\Sigma 1/R_f = 2.272$

$N/(\Sigma 1/R_f) = 11.444$

$N = 26$

Location - OC30 XZ - surface (cont.)

INTERMEDIATE VOLCANIC CLASTS

Long-axis orient., α	Axial ratio, R_f	$1/R_f$
240	5.541	0.180
248	21.304	0.046
245	17.304	0.058
245	12.800	0.078
255	4.315	0.231
245	24.583	0.040
	$\Sigma 1/R_f$ =	0.633
	$N/(\Sigma 1/R_f)$ =	9.477
	N =	6

BASIC VOLCANIC CLASTS

Long-axis orient., α	Axial ratio, R_f	$1/R_f$
248	12.916	0.077

YZ - surface

Orientation of joint surface = 132/54SW

GRANITOID CLASTS

Long-axis orient., α	Axial ratio, R_f	$1/R_f$
066	2.711	0.369
080	2.690	0.372
081	2.000	0.500
073	4.118	0.243
072	3.000	0.333
061	1.621	0.617
033	2.833	0.353
071	3.000	0.333
072	4.712	0.212
069	5.222	0.192
084	1.867	0.536
072	4.333	0.231
094	1.900	0.526
068	5.067	0.197
078	2.500	0.400
	$\Sigma 1/R_f$ =	5.414
	$N/(\Sigma 1/R_f)$ =	2.771
	N =	15

ACID VOLCANIC (RHYOLITE) CLASTS

Long-axis orient., α	Axial ratio, R_f	$1/R_f$
065	7.647	0.131
073	13.391	0.075
072	14.111	0.071
075	15.700	0.064
074	6.522	0.153
075	15.143	0.066
071	10.000	0.100
070	10.500	0.095
076	9.286	0.108
075	9.000	0.111
076	6.000	0.166
076	16.800	0.056
075	11.667	0.086
074	13.571	0.074
070	6.063	0.165
075	8.909	0.122
068	17.000	0.058
070	11.043	0.090
070	11.750	0.085
065	6.785	0.147
075	20.500	0.048
080	5.000	0.200
065	4.600	0.217
088	3.437	0.290
074	7.250	0.137
076	9.642	0.103
073	13.333	0.075

$\Sigma 1/R_f = 3.095$

$N/(\Sigma 1/R_f) = 8.723$

$N = 27$

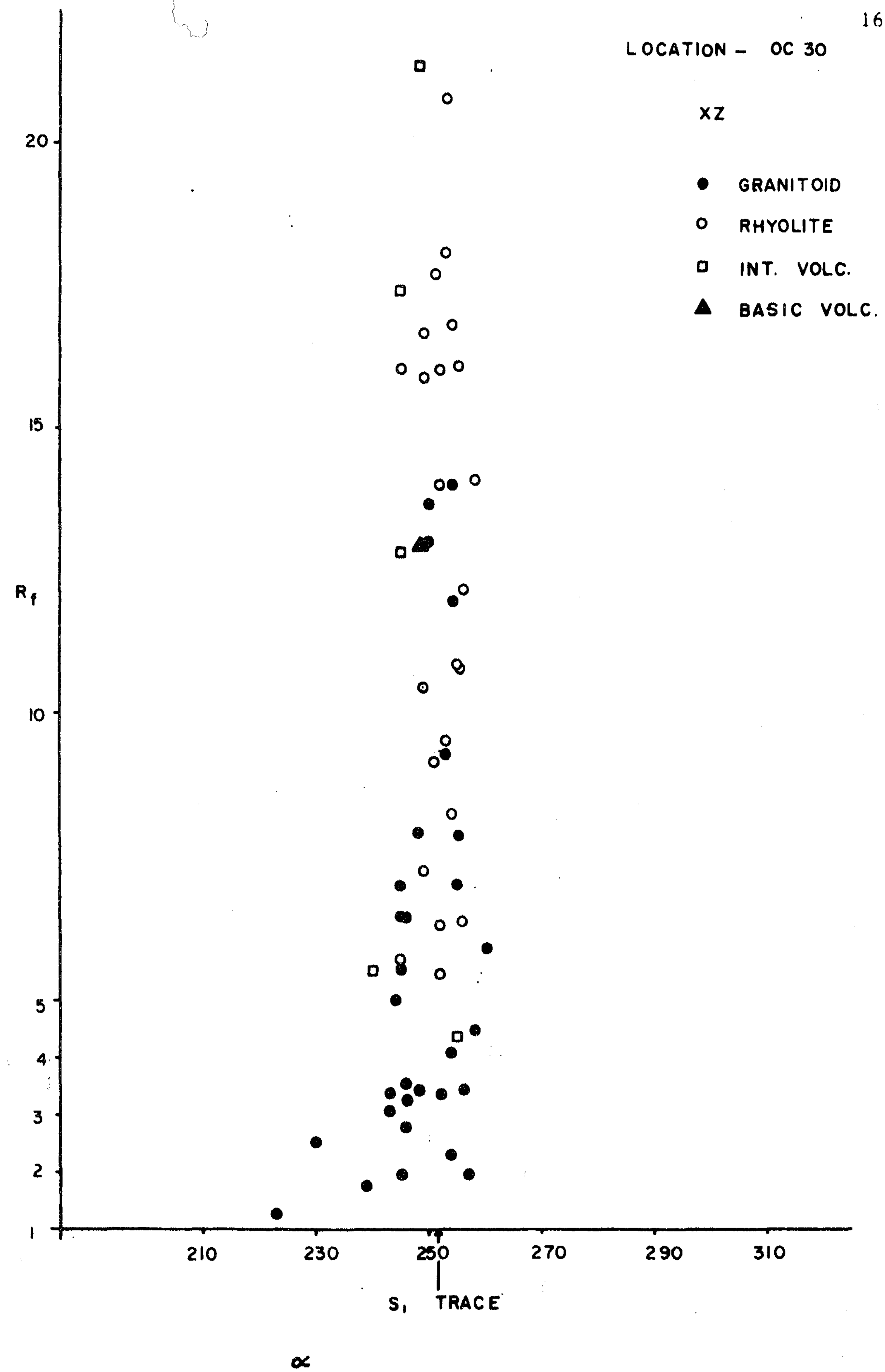
LOCATION - OC 30
XZ
GRANITOID
RHYOLITE
INT. VOLC.
BASIC VOLC.
20
15
10
5
4
3
2
1
R_f
210
230
250
270
290
310
S_1 TRACE
∝

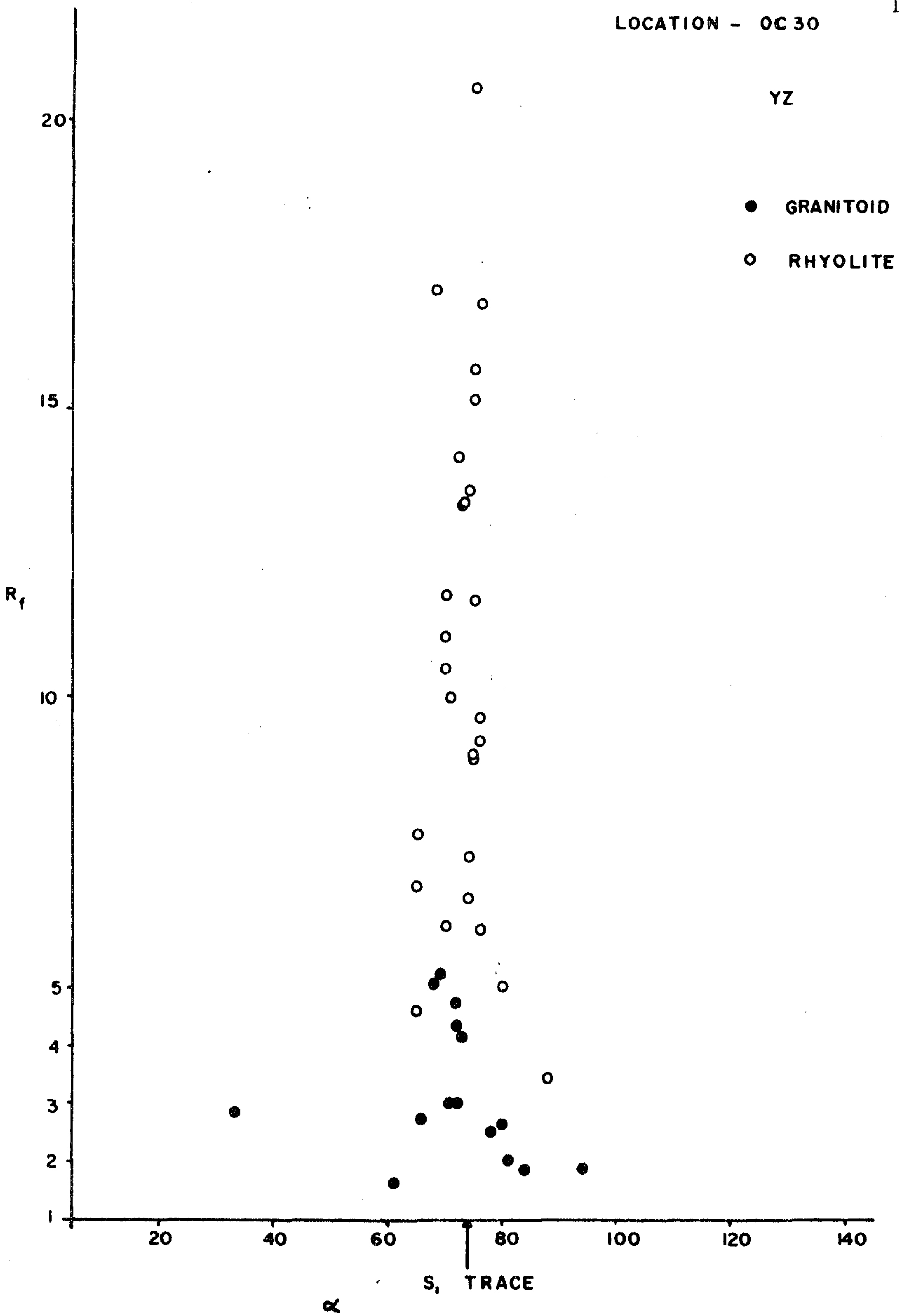

LOCATION - OC 30
YZ
GRANITOID
RHYOLITE
R_f
20
15
10
5
4
3
2
1
20
40
60
80
100
120
140
S_1 TRACE
α

Location - OC 32 XZ - surface

Orientation of S_1 = 076/72N
Orientation of stretching lineation = 046/57
Orientation of joint surface = 035/40SE

GRANITOID CLASTS

Long-axis orient., α	Axial ratio, R_f	$1/R_f$
265	8.537	0.117
077	8.080	0.124
069	3.600	0.278
090	3.500	0.286
073	2.684	0.373
075	2.600	0.385
090	2.593	0.386
076	3.867	0.259
082	6.133	0.163
082	5.952	0.168
084	6.609	0.151
083	3.071	0.326
074	6.522	0.153
075	6.867	0.146
094	2.300	0.435
096	2.818	0.355
081	2.250	0.444
072	4.095	0.244
081	8.000	0.125
077	3.500	0.286

$\Sigma 1/R_f = 5.204$

$N/(\Sigma 1/R_f) = 3.843$

$N = 20$

ACID VOLCANIC CLASTS

Long-axis orient., α	Axial ratio, R_f	$1/R_f$
082	9.750	0.103
084	6.000	0.167
083	4.478	0.223
079	4.828	0.207
076	6.000	0.167
080	12.308	0.081
075	7.700	0.130
078	7.583	0.132
078	7.391	0.135
078	9.194	0.109
080	8.667	0.115
078	7.300	0.137
082	20.000	0.050
082	8.786	0.114
083	11.500	0.087
078	7.125	0.140
077	10.846	0.092
076	7.500	0.133
077	17.000	0.059
078	11.750	0.085

$\Sigma 1/R_f = 2.466$

$N/(\Sigma 1/R_f) = 8.109$

$N = 20$

BASIC VOLCANIC CLASTS

Long-axis orient., α	Axial ratio, R_f	$1/R_f$
081	31.400	0.032
082	16.429	0.069
080	55.500	0.018
081	20.667	0.048
081	54.667	0.018

$\Sigma 1/R_f = 0.185$

$N/(\Sigma 1/R_f) = 26.998$

$N = 5$

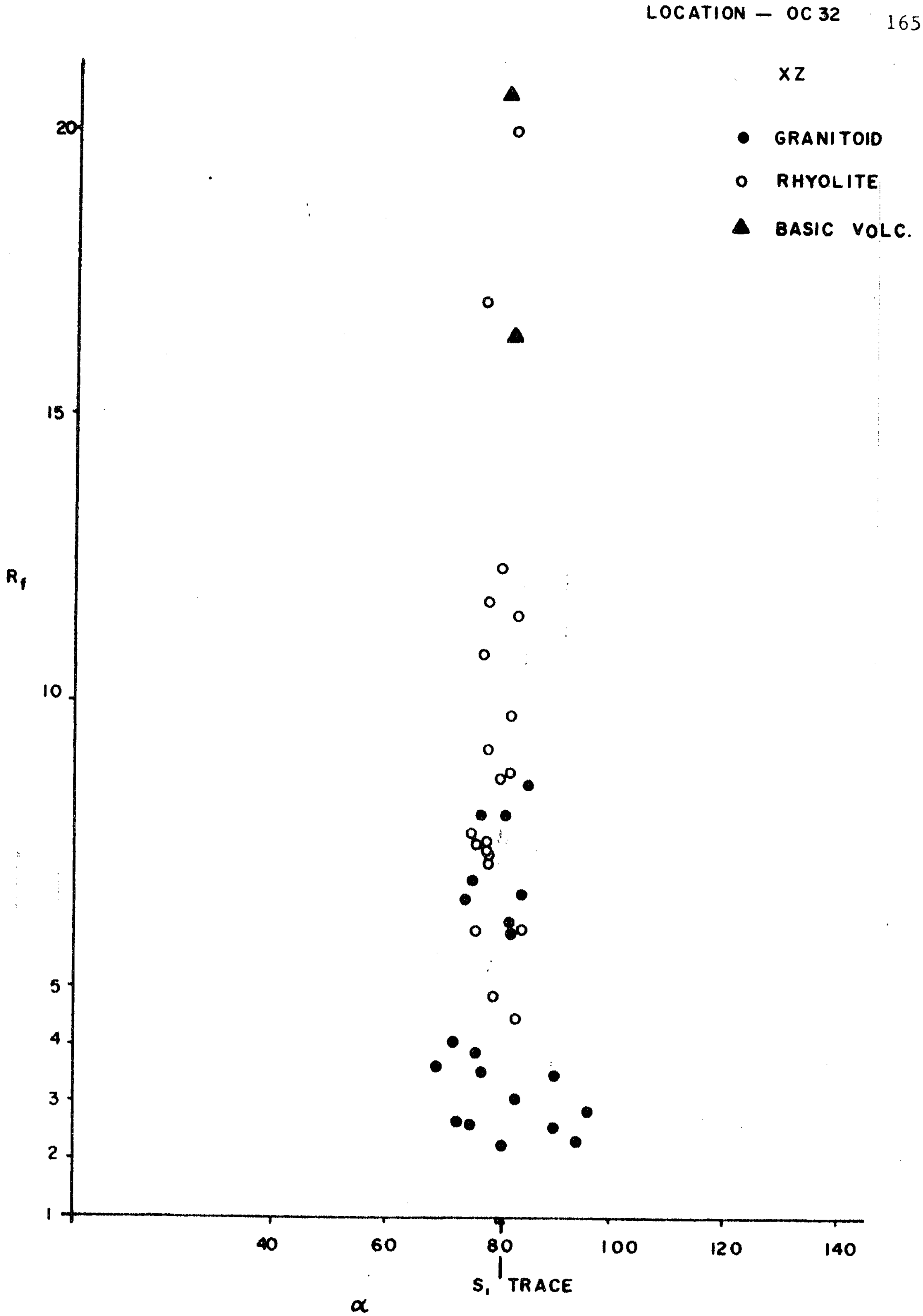
LOCATION — OC 32
XZ
GRANITOID
RHYOLITE
BASIC VOLC.
R_f
20
15
10
5
4
3
2
1
40
60
80
100
120
140
S_1 TRACE
α

Location - OC 32 YZ - surface

Orientation of joint surface = 165/45W

GRANITOID CLASTS

Long-axis orient., α	Axial ratio, R_f	$1/R_f$
102	2.385	0.419
098	1.364	0.733
107	2.000	0.500
145	1.656	0.604
087	5.280	0.189
106	3.158	0.317
086	3.146	0.318
097	3.857	0.259
117	1.500	0.667
097	5.600	0.179
112	3.500	0.286
090	2.895	0.345
084	2.313	0.432
093	2.467	0.405
079	2.583	0.387
063	1.950	0.513
104	2.308	0.433
089	2.500	0.400
090	2.667	0.375
083	3.286	0.304
093	1.400	0.714
097	2.692	0.371
108	1.417	0.706
080	1.789	0.559
079	1.556	0.643
106	2.156	0.464
067	1.550	0.645
095	1.588	0.630
087	4.458	0.224
087	4.800	0.208
096	2.719	0.368
132	1.421	0.704
120	1.500	0.667
097	1.471	0.680
095	1.900	0.526
100	3.397	0.294

$\Sigma 1/R_f$ = 16.468

$N/(\Sigma 1/R_f)$ = 2.186

N = 36

Location - OC 32 YZ - surface (cont.)

ACID VOLCANIC CLASTS

Long-axis orient., α	Axial ratio, R_f	$1/R_f$
083	4.176	0.239
103	6.091	0.164
091	7.500	0.133
088	9.000	0.111
086	8.500	0.118
101	5.000	0.200
093	9.636	0.104
098	7.545	0.133
094	4.778	0.209
091	5.818	0.172
091	6.400	0.156
102	8.632	0.116
112	4.077	0.245
092	4.154	0.241
095	5.250	0.190
093	2.955	0.338
078	2.563	0.390
095	5.333	0.188
093	6.000	0.167
089	8.500	0.118

$\Sigma 1/R_f = 3.732$

$N/(\Sigma 1/R_f) = 5.359$

$N = 20$

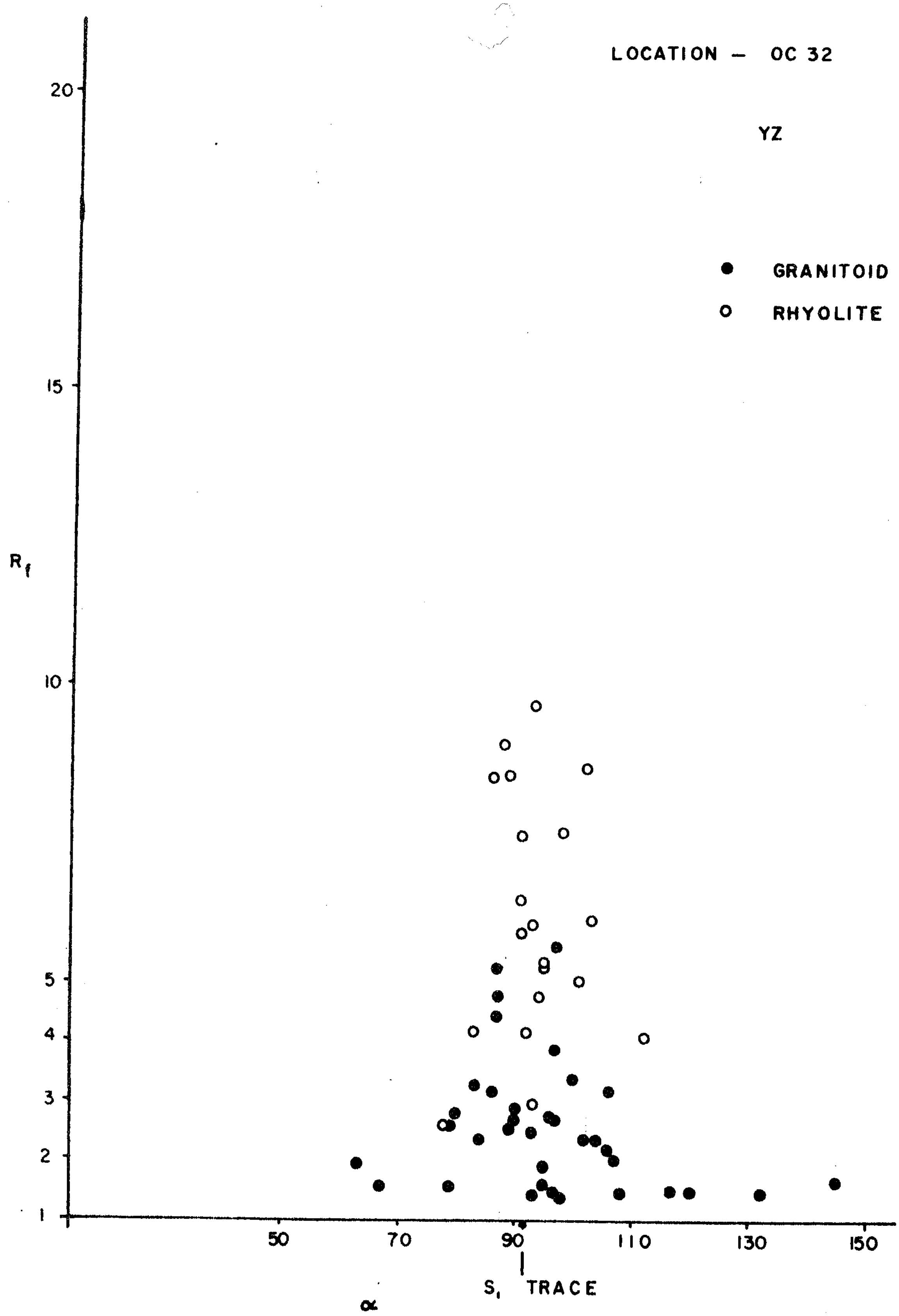

LOCATION — OC 32
YZ
GRANITOID
RHYOLITE
20
15
10
5
4
3
2
1
R_f
50
70
90
110
130
150
S_1 TRACE
α

Location - OC 36 XZ - surface

Orientation of S_1 = 082/74N
Orientation of stretching lineation = 081/28
Orientation of joint surface = 010/27E

GRANITOID CLASTS

Long-axis orient., α	Axial ratio, R_f	$1/R_f$
060	1.292	0.774
079	3.129	0.320
075	2.104	0.475
071	4.594	0.218
076	1.520	0.658
080	6.786	0.147
059	2.964	0.337
072	4.973	0.201
075	1.750	0.571
123	1.308	0.765
080	1.821	0.549
070	4.522	0.221
091	2.370	0.422
099	1.355	0.738
089	2.714	0.368
065	2.198	0.455
074	1.500	0.667
082	4.135	0.242
087	1.884	0.531
090	2.000	0.500
065	3.560	0.281
063	1.944	0.514
079	4.000	0.250
080	1.224	0.817
081	3.357	0.298
078	4.000	0.250
074	6.400	0.156

$\Sigma 1/R_f$ = 11.725

$N/(\Sigma 1/R_f)$ = 2.303

N = 27

Location - OC36 XZ - surface (cont.)

ACID VOLCANIC (RHYOLITE) CLASTS

Long-axis orient., α	Axial ratio, R_f	$1/R_f$
082	10.708	0.093
081	16.375	0.061
074	5.867	0.170
077	4.133	0.242
077	10.944	0.091
079	9.571	0.104
078	9.063	0.110
085	9.773	0.102
083	8.556	0.117
085	8.909	0.112
082	14.000	0.071
082	14.455	0.069
079	5.714	0.175
082	9.143	0.109
081	7.400	0.135

$\Sigma 1/R_f = 1.763$

$N/(\Sigma 1/R_f) = 8.511$

$N = 15$

BASIC VOLCANIC CLASTS

Long-axis orient., α	Axial ratio, R_f	$1/R_f$
085	12.182	0.082
081	8.500	0.118
082	36.333	0.028

$\Sigma 1/R_f = 0.228$

$N/(\Sigma 1/R_f) = 13.181$

$N = 3$

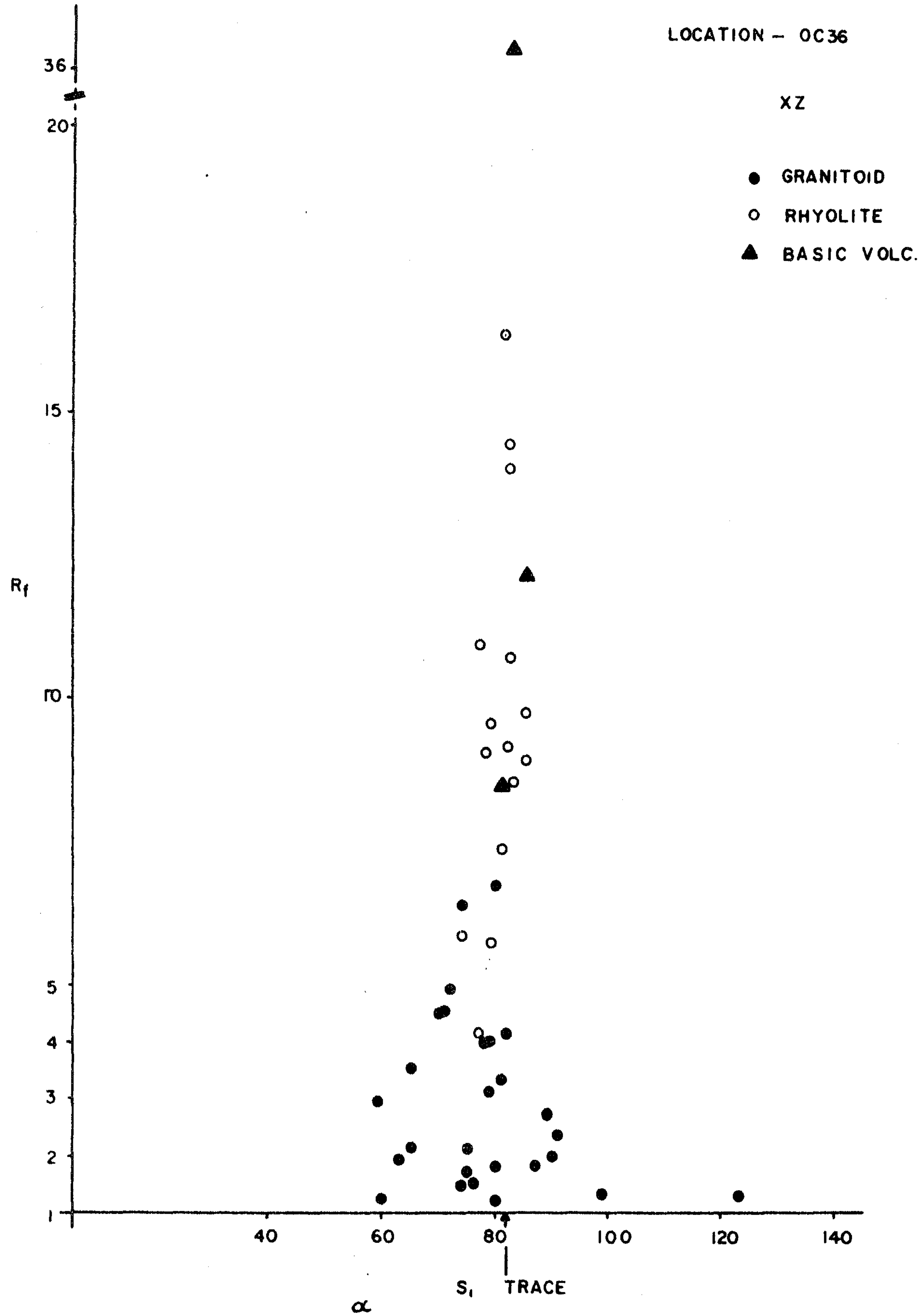
LOCATION – OC36
XZ
GRANITOID
RHYOLITE
BASIC VOLC.
R_f
36
20
15
10
5
4
3
2
1
40
60
80
100
120
140
S_1 TRACE
α

Location - OC36 YZ - surface

Orientation of joint surface = 167/69W

GRANITOID CLASTS

Long-axis pitch, α	Axial ratio, R_f	$1/R_f$
84S	2.185	0.458
83N	3.238	0.309
85N	3.500	0.286
83N	1.900	0.526
VERT.	2.595	0.385
87S	2.000	0.500
81N	3.237	0.309
78N	2.000	0.500
75N	3.000	0.333
89N	1.524	0.656
78N	3.523	0.284
89N	1.750	0.571
88S	1.229	0.814
81N	1.936	0.516
77N	2.850	0.351
76N	3.133	0.319
78N	1.625	0.615
62N	2.067	0.484
83N	1.522	0.657
73N	2.952	0.339
77N	1.568	0.638
89S	3.474	0.288
74N	2.520	0.397
83N	2.943	0.340
66N	2.294	0.426
62N	1.455	0.688

$\Sigma 1/R_f = 11.989$

$N/(\Sigma 1/R_f) = 2.169$

$N = 26$

Location - OC 36 YZ - surface (cont.)

ACID VOLCANIC (RHYOLITE) CLASTS

Long-axis pitch, α	Axial ratio, R_f	$1/R_f$
86N	5.920	0.169
86N	12.000	0.083
87N	5.267	0.190
78N	5.500	0.182
81N	7.600	0.132
79N	7.000	0.143
85N	4.081	0.245
88N	5.250	0.190
89N	9.444	0.106
85N	7.357	0.136
80N	13.000	0.077
75N	5.523	0.181
76N	9.424	0.106
74N	8.067	0.124
82N	3.158	0.317
80N	8.500	0.118
80N	6.273	0.159
82N	6.600	0.152
75N	5.962	0.168
77N	7.667	0.130
78N	4.080	0.245
78N	5.762	0.174
79N	10.750	0.093
78N	13.333	0.075
80N	3.500	0.286
	$\Sigma 1/R_f$ =	3.981
	$N/(\Sigma 1/R_f)$ =	6.280
	N =	25

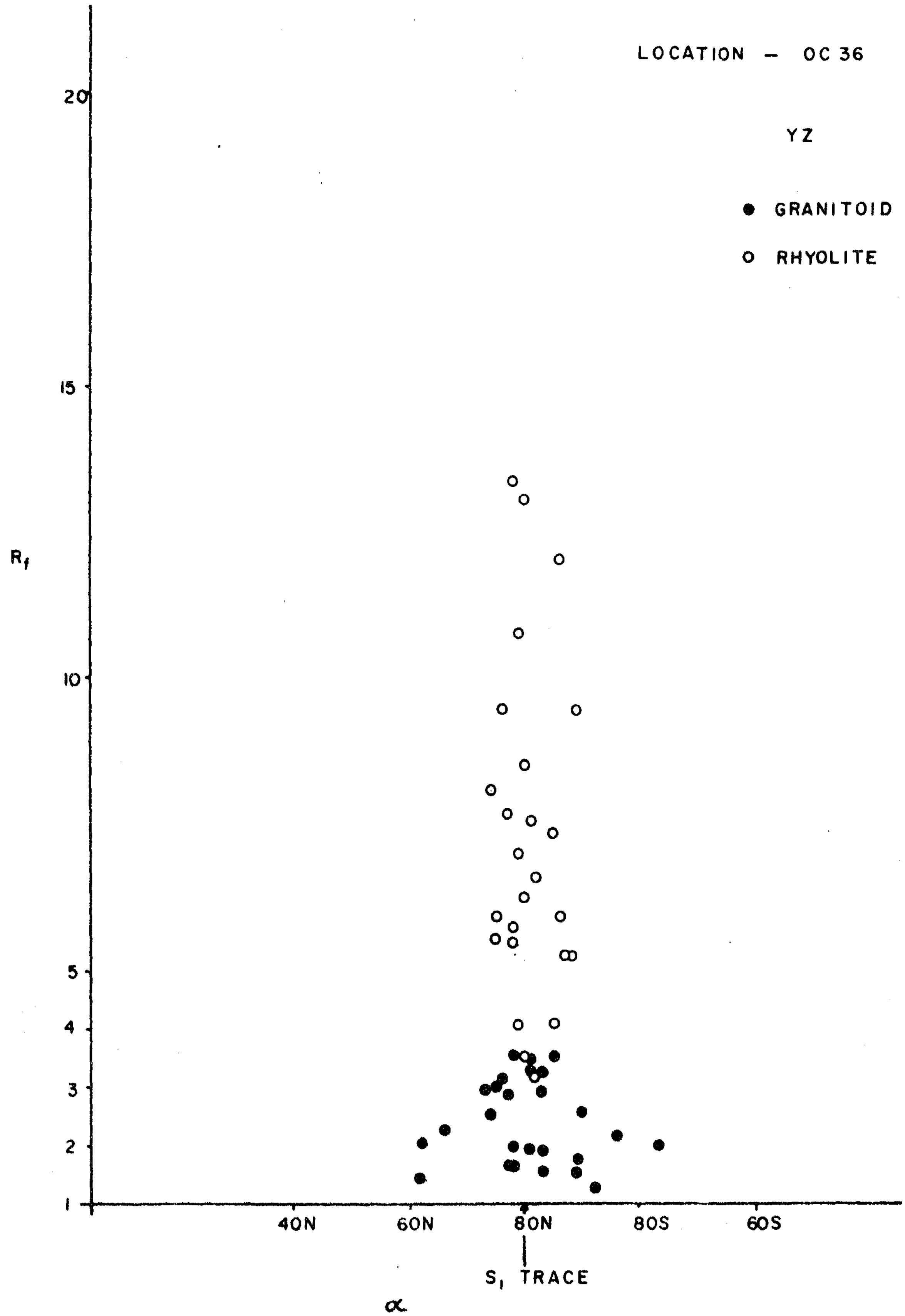
LOCATION – OC 36
YZ
GRANITOID
RHYOLITE
20
15
10
5
4
3
2
1
R_f
40N
60N
80N
80S
60S
S_1 TRACE
α

Location - OC 36A   XZ - surface

Orientation of S_1 = 080/75N
Orientation of stretching lineation = 077/22
Orientation of joint surface =015/7E

GRANITOID CLASTS

Long-axis orient., α	Axial ratio, R_f	$1/R_f$
076	1.053	0.949
091	2.089	0.479
105	1.203	0.831
088	1.389	0.720
086	1.333	0.750
093	2.660	0.376
071	2.476	0.404
107	1.590	0.629
072	1.247	0.802
076	1.241	0.806
079	1.575	0.635
090	2.200	0.455
080	1.667	0.600
076	1.845	0.542
111	1.393	0.718
137	1.333	0.750
106	1.471	0.680
089	2.048	0.488
070	2.600	0.385
077	1.854	0.539
095	2.375	0.421
081	2.278	0.439
076	1.509	0.663
077	1.470	0.680
081	1.630	0.613
072	1.667	0.600
070	2.167	0.462
105	1.351	0.740
082	4.000	0.250

$\Sigma 1/R_f$ = 17.406

$N/(\Sigma 1/R_f)$ = 1.666

N = 29

ACID VOLCANIC (RHYOLITE) CLASTS

Long-axis orient., α	Axial ratio, R_f	$1/R_f$
085	6.395	0.156
080	17.778	0.056
085	12.083	0.083
088	11.069	0.090
081	11.933	0.084
081	6.750	0.148
082	6.469	0.155
078	9.667	0.103
077	21.167	0.047
081	17.500	0.057

$\Sigma 1/R_f = 0.979$

$N/(\Sigma 1/R_f) = 10.215$

$N = 10$

INTERMEDIATE VOLCANIC CLASTS

Long-axis orient., α	Axial ratio, R_f	$1/R_f$
084	7.778	0.129
081	8.511	0.118
081	4.143	0.241
076	3.261	0.307
074	2.790	0.359

$\Sigma 1/R_f = 1.154$

$N/(\Sigma 1/R_f) = 4.333$

$N = 5$

BASIC VOLCANIC CLASTS

Long-axis orient., α	Axial ratio, R_f	$1/R_f$
084	17.400	0.058
076	16.875	0.059
080	16.857	0.059

$\Sigma 1/R_f = 0.176$

$N/(\Sigma 1/R_f) = 17.046$

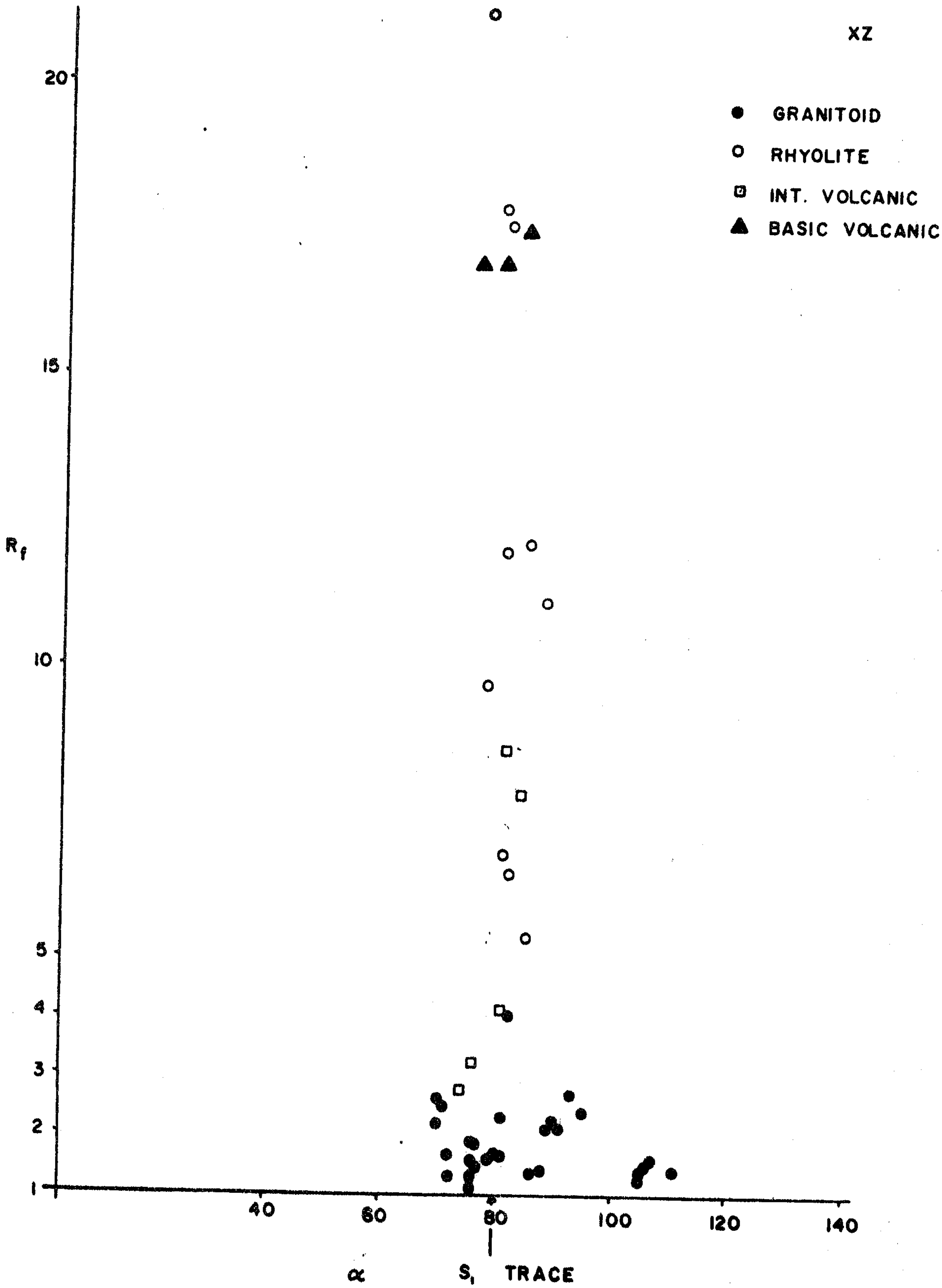
XZ
GRANITOID
RHYOLITE
INT. VOLCANIC
BASIC VOLCANIC
R_f
20
15
10
5
4
3
2
1
40
60
80
100
120
140
α
S_1 TRACE

Location - OC 36A YZ - surface

Orientation of joint surface = 163/63W

GRANITOID CLASTS

Long-axis pitch, α	Axial ratio, R_f	$1/R_f$
80N	2.059	0.486
67N	1.767	0.566
89N	1.625	0.615
77N	1.946	0.514
78S	1.367	0.732
81N	1.640	0.610
86S	2.046	0.489
83S	1.655	0.604
74N	1.194	0.837
87S	1.984	0.504
79N	1.360	0.735
86N	1.378	0.726
85N	2.392	0.418
87S	1.444	0.692
86N	3.031	0.330
75N	2.500	0.400
76N	3.063	0.327
77N	1.444	0.692
77N	1.700	0.588
89S	1.071	0.933
75N	1.086	0.921
89S	2.032	0.492
68N	1.196	0.836
62N	1.778	0.563
65N	2.619	0.382
89S	1.600	0.625

$\Sigma 1/R_f = 15.617$

$N/(\Sigma 1/R_f) = 1.665$

$N = 26$

ACID VOLCANIC (RHYOLITE) CLASTS

Long-axis pitch, α	Axial ratio, R_f	$1/R_f$
88N	8.250	0.121
82N	4.882	0.205
87N	4.714	0.212
82N	9.714	0.103
76N	2.875	0.378
75N	3.737	0.268
80N	5.300	0.187
80N	5.308	0.188
77N	5.308	0.188
79N	11.286	0.089
83N	8.091	0.124
74N	3.276	0.305
63N	2.793	0.358
72N	7.706	0.130
71N	2.625	0.381
73N	7.917	0.126
75N	12.429	0.081
62N	2.356	0.424
79N	1.781	0.561
76N	6.364	0.157

$\Sigma 1/R_f$ = 4.586

$N/(\Sigma 1/R_f)$ = 4.361

N = 20

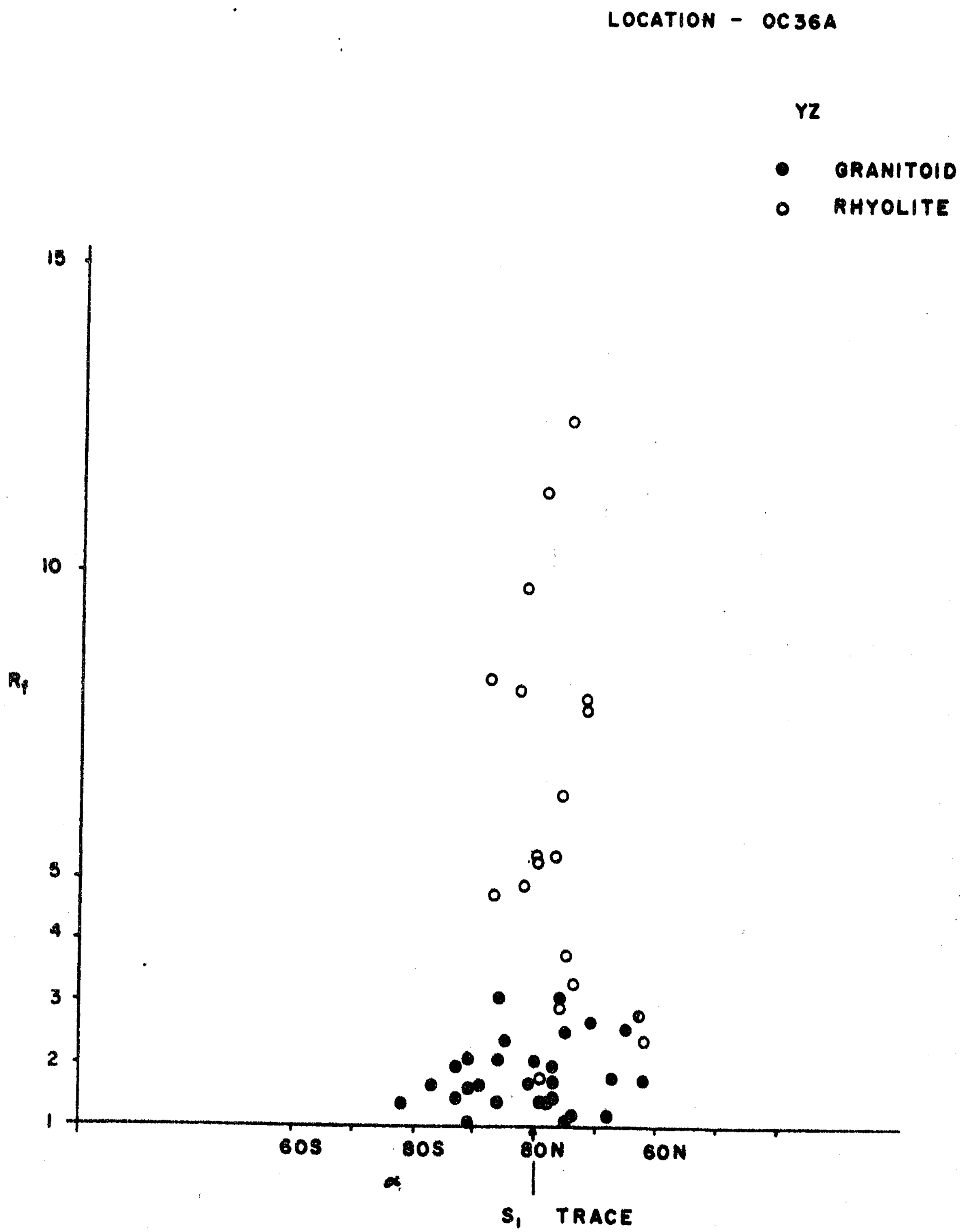
LOCATION - OC36A
YZ
GRANITOID
RHYOLITE
15
10
5
4
3
2
1
R_f
60S
80S
80N
60N
S_1 TRACE

Location - OC37 XZ - surface

Orientation of S_1 = 081/85N
Orientation of stretching lineation = 076/15
Orientation of joint surface = 048/11SE

GRANITOID CLASTS

Long-axis orient., α	Axial ratio, R_f	$1/R_f$
077	1.515	0.660
083	2.077	0.481
074	1.968	0.508
076	2.619	0.382
077	1.671	0.597
107	1.404	0.713
070	3.349	0.298
074	4.750	0.210
075	3.000	0.333
080	3.500	0.286
085	4.000	0.250
083	3.100	0.323
077	2.224	0.450
083	1.821	0.549
073	1.677	0.596
078	1.973	0.507
080	2.535	0.394
080	3.800	0.263
085	2.800	0.357
080	4.000	0.250
075	3.800	0.264
083	4.200	0.238
090	3.400	0.294
088	3.600	0.278
088	3.000	0.333
083	2.376	0.421
082	1.667	0.600
091	1.913	0.523
068	2.647	0.377
073	1.709	0.585
071	2.268	0.441
070	1.973	0.507
080	3.200	0.313
090	2.600	0.385
085	3.800	0.263
081	4.600	0.217
080	5.000	0.200
076	4.400	0.227
095	3.100	0.323
079	1.862	0.537
076	1.951	0.513
089	1.330	0.752
084	1.329	0.752
080	1.339	0.747

Location - OC 37 XZ - surface (cont.)

Long-axis orient., α	Axial ratio, R_f	$1/R_f$
093	1.926	0.519
085	3.400	0.294
075	3.600	0.277
073	4.200	0.238
071	4.000	0.250
060	1.364	0.733
094	1.561	0.641
075	2.464	0.406

$\Sigma 1/R_f = 21.804$

$N/(\Sigma 1/R_f) = 2.385$

$N = 52$

ACID VOLCANIC (RHYOLITE) CLASTS

Long-axis orient., α	Axial ratio, R_f	$1/R_f$
081	19.940	0.050
081	15.867	0.063
079	16.813	0.059
079	8.281	0.121
077	11.840	0.084
081	18.591	0.054
085	10.933	0.091
075	13.786	0.073
080	13.111	0.076
079	8.143	0.123
083	12.981	0.077
081	7.318	0.137
082	19.000	0.053
074	7.400	0.135
082	11.667	0.086
076	6.053	0.165
081	7.600	0.132
076	10.056	0.095
084	17.174	0.058
077	10.250	0.098

$\Sigma 1/R_f = 1.830$

$N/(\Sigma 1/R_f) = 10.929$

$N = 20$

Location - OC37 XZ - surface (cont.)

BASIC VOLCANIC CLASTS

Long-axis orient., α	Axial ratio, R_f	$1/R_f$
081	24.179	0.041
082	17.133	0.058
081	16.046	0.062
080	21.250	0.047
083	26.087	0.038

$\Sigma 1/R_f = 0.246$

$N/(\Sigma 1/R_f) = 20.325$

$N = 5$

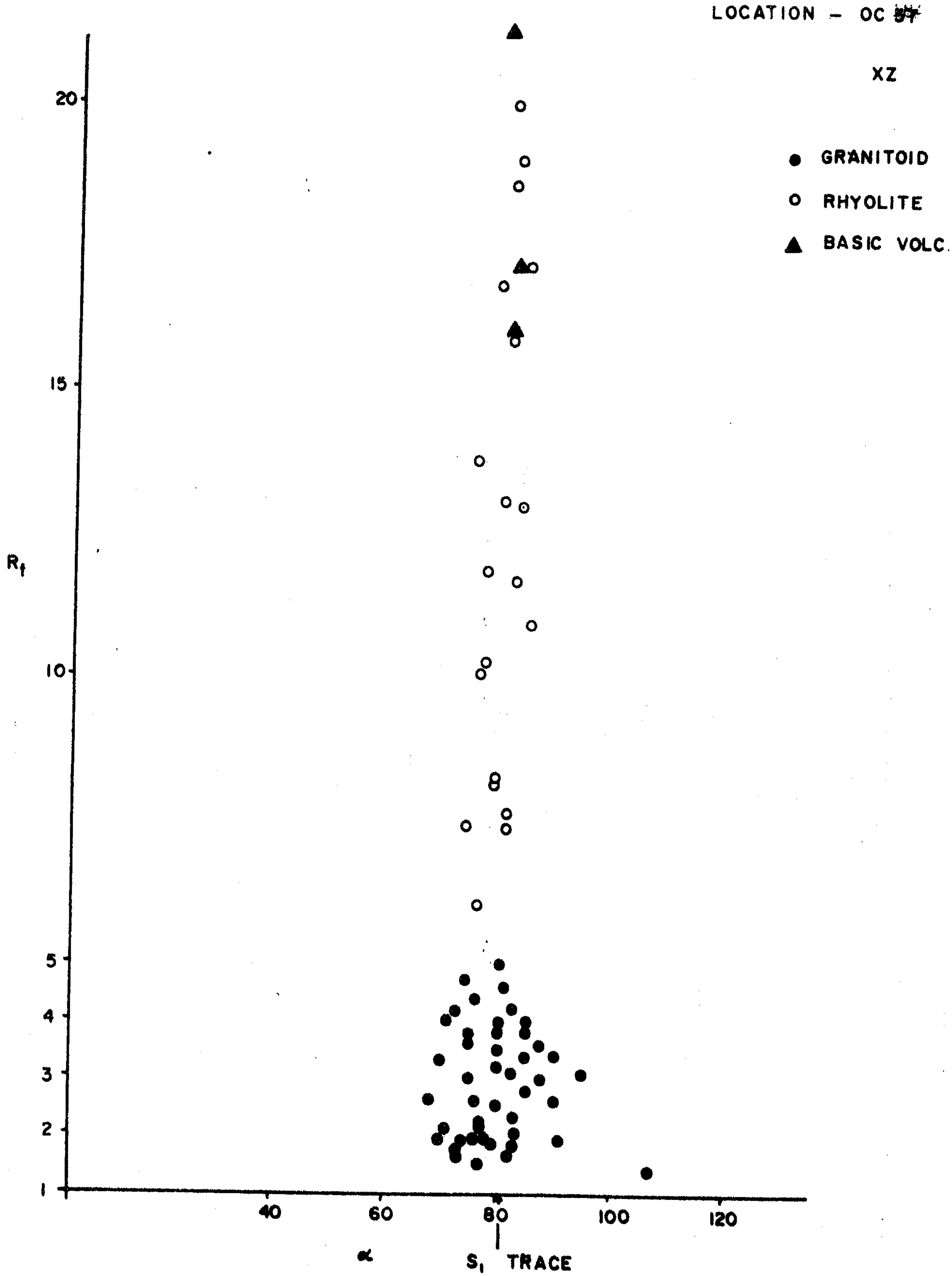
LOCATION – OC
XZ
GRANITOID
RHYOLITE
BASIC VOLC.
20
15
10
5
4
3
2
1
R_f
40
60
80
100
120
α
S_1 TRACE

Location - OC37 YZ - surface

Orientation of joint surface = 180/84W

GRANITOID CLASTS

Long-axis pitch, α	Axial ratio, R_f	$1/R_f$
72N	2.441	0.410
88S	2.647	0.378
74S	1.788	0.559
82N	2.439	0.410
80N	3.978	0.251
72N	5.658	0.177
73N	1.667	0.600
81S	1.825	0.548
68N	1.533	0.652
80N	1.857	0.538
76N	3.077	0.325
72N	2.520	0.397
78N	4.385	0.228
75N	6.571	0.152
80N	1.920	0.521
89S	2.712	0.369
80N	4.225	0.237
VERT.	2.320	0.431
82N	2.283	0.438
85S	1.522	0.657
76N	2.389	0.419
82N	1.867	0.536
84N	2.033	0.492

$\Sigma 1/R_f$ = 9.725

$N/(\Sigma 1/R_f)$ = 2.365

N = 23

ACID VOLCANIC (RHYOLITE) CLASTS

Long-axis pitch, α	Axial ratio, R_f	$1/R_f$
81N	12.000	0.083
77N	9.500	0.105
75N	7.200	0.139
80N	13.750	0.073
73N	17.571	0.057
78N	4.514	0.222
73N	15.625	0.064
77N	12.400	0.081
83N	11.200	0.089
77N	8.600	0.116
77N	38.500	0.026
73N	7.500	0.133
79N	16.923	0.059
75N	9.444	0.106
77N	5.571	0.179

Long-axis pitch, α	Axial ratio, R_f	$1/R_f$
82N	2.267	0.441
82N	6.000	0.167
74N	7.250	0.138
78N	11.684	0.086
79N	18.200	0.055
81N	18.889	0.053
	$\Sigma 1/R_f$ =	2.967
	$N/(\Sigma 1/R_f)$ =	7.078
	N =	21

INTERMEDIATE VOLCANIC CLASTS

Long-axis pitch, α	Axial ratio, R_f	$1/R_f$
78N	9.611	0.104
77N	7.108	0.141
74N	8.190	0.122
76N	5.873	0.170
77N	2.182	0.458
75N	7.278	0.137
77N	15.222	0.066
79N	3.756	0.266
72N	15.864	0.063
	$\Sigma 1/R_f$ =	1.527
	$N/(\Sigma 1/R_f)$ =	5.895
	N =	9

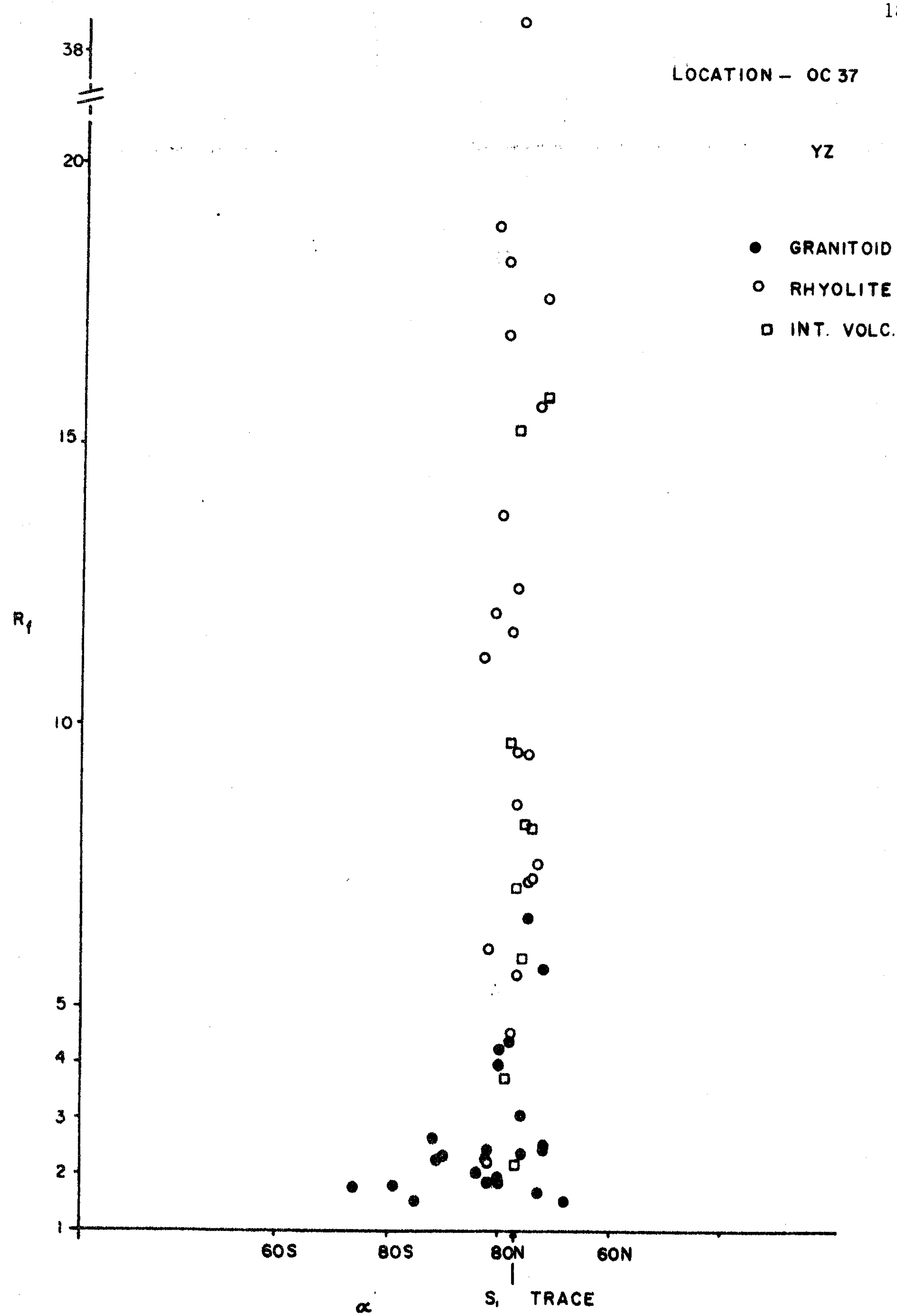
LOCATION – OC 37
YZ
GRANITOID
RHYOLITE
INT. VOLC.
38
20
15
10
5
4
3
2
1
R_f
60S
80S
80N
60N
α
S_1 TRACE

ARENITE

Sample PJ81-60 XZ-surface

Location - OC 9

Orientation of S_1 trace = 34.7

Long-axis orient., α	Axial ratio, R_f	$1/R_f$
47.3	1.944	0.514
40.2	1.650	0.610
37.2	3.250	0.308
27.8	2.000	0.500
27.4	2.538	0.394
34.6	2.300	0.435
79.8	1.600	0.625
23.3	2.778	0.360
39.8	2.222	0.450
34.8	2.353	0.425
28.9	1.853	0.540
38.5	2.778	0.360
38	2.818	0.355
31.5	2.966	0.337
27.1	3.813	0.262
33.6	1.583	0.632
37.8	3.214	0.311
31.9	2.000	0.500
33.2	1.733	0.577
33.5	3.588	0.279
32.3	2.292	0.436
35	3.056	0.327
32.6	1.917	0.522
38.8	2.714	0.368
71.7	1.286	0.778
33.3	2.167	0.462
35.5	3.867	0.259
30.5	2.143	0.467
23.3	2.762	0.362
32.5	4.857	0.206
32.2	2.333	0.429
31.4	2.600	0.385
22	4.714	0.212
34.6	2.464	0.406
23.2	3.554	0.281
31.2	3.724	0.269
30.9	2.400	0.417
48.1	1.148	0.871
33.5	3.364	0.297
30	2.667	0.375
32.9	2.333	0.429
31	5.833	0.171
31.8	3.900	0.256
22.1	2.245	0.445
29.6	1.708	0.585
36.2	3.500	0.286

Sample PJ81-60 XZ-surface (cont.)

Long-axis orient., α	Axial ratio, R_f	$1/R_f$
32.4	3.947	0.253
32.7	7.846	0.127
35.4	2.111	0.474
19.3	1.500	0.667
31.1	1.960	0.510
51.6	2.227	0.449
42.4	3.091	0.324
41.5	2.214	0.452
37.7	3.417	0.293
34.4	3.600	0.278
29.8	2.583	0.387
42.8	2.200	0.455
38	5.000	0.200
61	1.346	0.743
31.6	2.786	0.359
34.6	2.000	0.500
32.	2.550	0.392
29.6	2.192	0.456
31.1	3.750	0.267
30.3	4.067	0.246
37.2	3.048	0.328
30.7	3.250	0.308
38	1.741	0.575
34.5	3.381	0.296

$\Sigma 1/R_f = 28.414$

$N/(\Sigma 1/R_f) = 2.464$

$N = 70$

Sample PJ81-60 YZ-surface

Location - OC 9

Orientation of S_1 trace = 34.8

Long-axis orient., α	Axial ratio, R_f	$1/R_f$
26.4	2.750	0.364
57.7	1.400	0.714
13.8	3.500	0.286
29.6	1.750	0.571
11.3	1.455	0.688
27.3	2.500	0.400
346.3	1.818	0.550
41.2	2.000	0.500
36.6	2.067	0.484
48.9	3.111	0.321
43.9	1.909	0.534
26.3	2.375	0.421
31	2.273	0.440
36.8	1.692	0.591
356.7	1.625	0.615
39.8	4.750	0.211
12.5	2.143	0.467
15.4	2.778	0.360
31.3	2.571	0.389
38.7	1.500	0.667
38.9	2.400	0.417
46.7	2.667	0.375
48.2	2.100	0.476
34.5	2.000	0.500
50.5	1.696	0.590
38.5	2.300	0.435
32.3	4.000	0.250
18.5	1.600	0.625
14.9	2.083	0.480
31.4	1.308	0.765
71.3	1.417	0.706
66.2	1.143	0.875
349	1.200	0.833
34.7	2.400	0.417
26.2	1.875	0.533
36.7	2.800	0.357
12.1	2.517	0.397
33.5	2.429	0.412
37	2.385	0.419
38.4	3.500	0.286
29	2.714	0.368
17.2	1.739	0.575
33.6	6.333	0.158
111.6	1.176	0.850
26.3	1.929	0.519

Sample PJ81-60 YZ-surface (cont.)

Long-axis orient., α	Axial ratio, R_f	$1/R_f$
20.9	2.333	0.429
33.7	2.500	0.400
30.9	3.625	0.276
30	2.500	0.400
74.9	1.700	0.588
39.1	1.600	0.625
33.9	2.824	0.354
37.6	2.933	0.341
340.3	1.308	0.765
38.5	3.364	0.297
42.3	3.143	0.318
32.5	2.071	0.483
35.8	1.500	0.667
41.2	4.000	0.250
40	4.000	0.250
12.8	1.459	0.685
38.4	2.273	0.440
40.8	1.368	0.731
27	2.250	0.444
36.9	2.800	0.357
27.9	3.000	0.333
29.9	2.857	0.350
16.9	2.083	0.480
34	1.960	0.510
36.3	2.143	0.467

$\Sigma 1/R_f = 33.431$

$N/(\Sigma 1/R_f) = 2.094$

$N = 70$

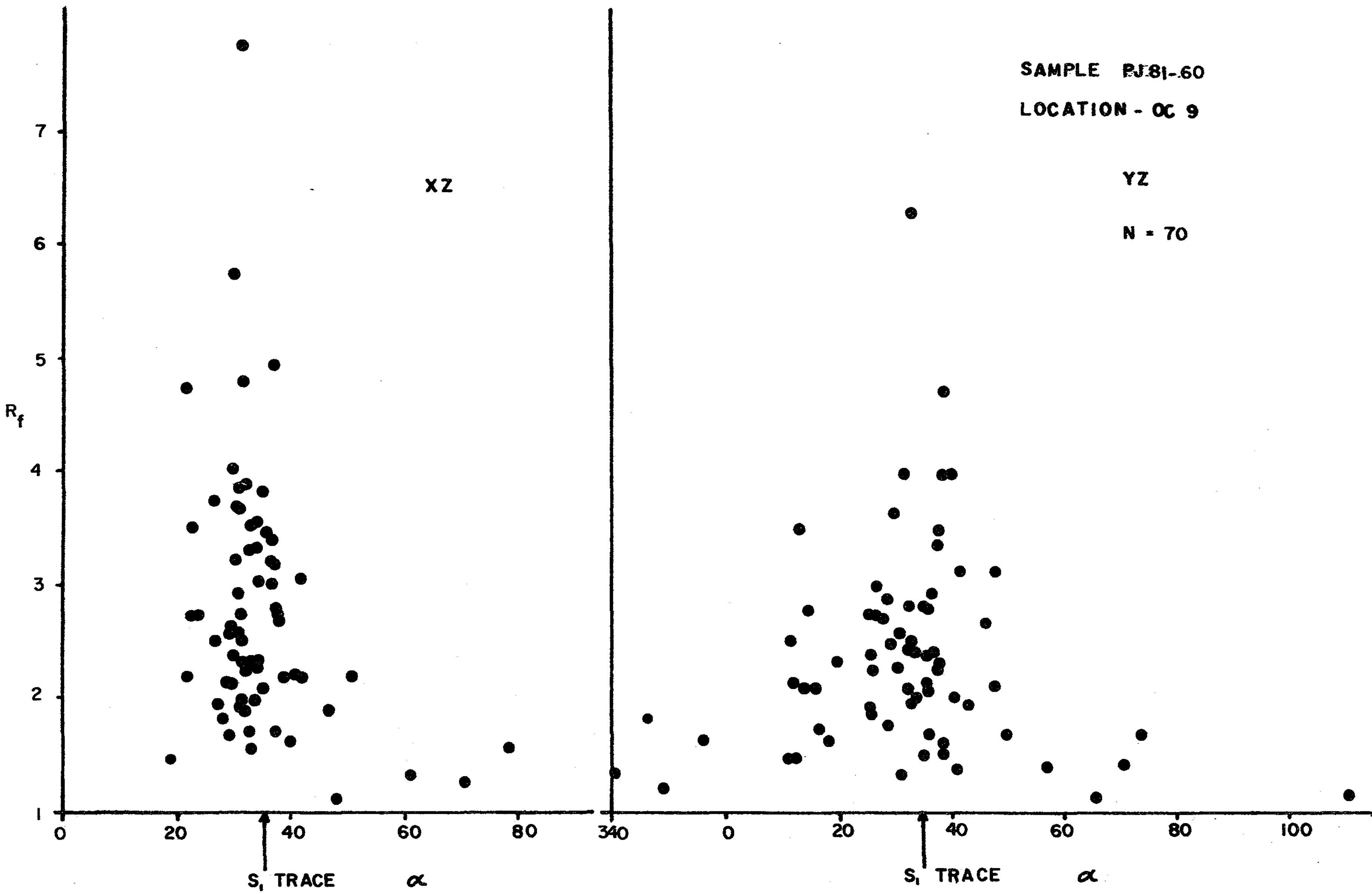

SAMPLE PJ 81-60
LOCATION - OC 9
XZ
YZ
N = 70
R_f
7
6
5
4
3
2
1
0
20
40
60
80
340
0
20
40
60
80
100
S_1 TRACE
α
S_1 TRACE
α

Sample PJ81-58 XZ-surface

Location - OC24

Orientation of S_1 trace = 254

Long axis orient., α	Axial ratio, R_f	$1/R_f$
268.3	1.167	0.857
252.8	3.765	0.266
326.5	1.154	0.867
256	4.348	0.230
265.7	2.889	0.346
255	1.278	0.783
236	1.818	0.550
287.6	1.346	0.743
259.5	3.100	0.323
272	3.438	0.291
256.4	10.250	0.098
255	1.898	0.527
247.7	1.889	0.529
251.8	6.625	0.151
249.6	3.231	0.310
263.5	5.333	0.188
249.8	2.111	0.474
255.5	2.667	0.375
257.6	2.147	0.466
244	3.000	0.333
248.3	4.000	0.250
255	2.625	0.381
255	5.111	0.196
242.6	2.875	0.348
255.5	2.000	0.500
258.5	4.286	0.233
253	3.762	0.266
253	3.375	0.296
251.6	2.966	0.337
244.7	5.500	0.182
264	4.250	0.235
252.6	2.273	0.440
253.7	4.500	0.222
251.8	3.375	0.296
251	3.125	0.320
246.2	10.692	0.094
254.3	7.333	0.136
256.4	4.200	0.238
254	4.278	0.234
224	1.321	0.757
255	2.000	0.500
255.7	3.556	0.281
204.4	1.300	0.769
245	1.795	0.557
252.3	2.231	0.448

Long axis orient., α	Axial ratio, R_f	$1/R_f$
260	2.462	0.406
262.4	5.000	0.200
261.4	3.111	0.321
252	6.000	0.167
257	3.875	0.258
251	2.727	0.367
246.6	3.154	0.317
267.3	2.077	0.481
257.6	5.400	0.185
256.2	4.000	0.250
251.4	3.474	0.288
261.6	2.645	0.378
264.6	2.364	0.423
250.8	4.929	0.203
253.6	8.250	0.121
251.7	3.286	0.304
258	4.267	0.234
251.5	2.818	0.355
259.5	1.909	0.524
265	2.077	0.481
245	3.222	0.310
255.5	5.400	0.185
260	2.533	0.395
254.4	3.333	0.300
265.5	2.394	0.418

$\sum 1/R_f = 25.472$

$N/(\sum 1/R_f) = 2.748$

$N = 70$

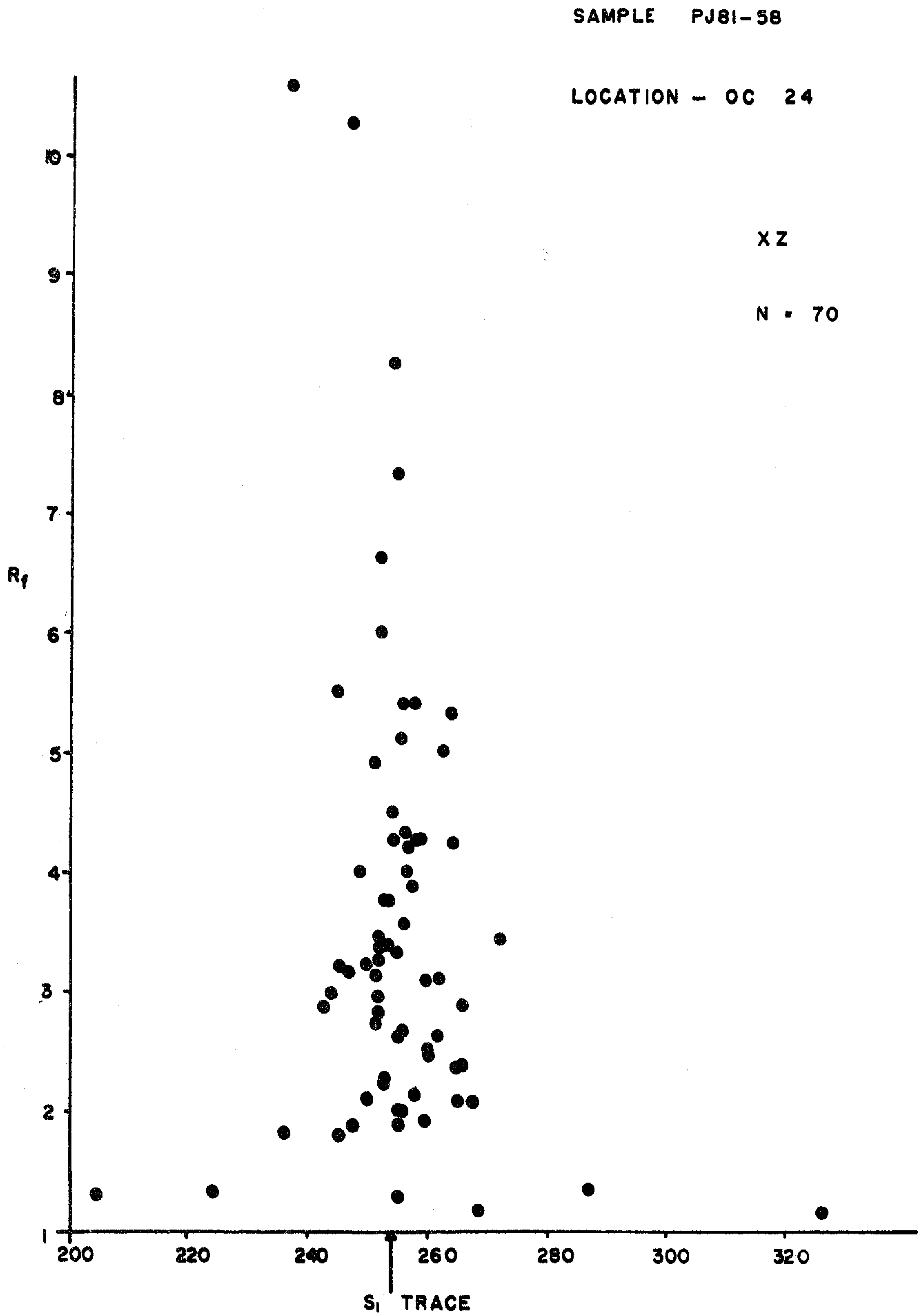
SAMPLE PJ81-58
LOCATION - OC 24
XZ
N = 70
R_f
1
2
3
4
5
6
7
8
9
10
200
220
240
260
280
300
320
S_1 TRACE

Sample PJ81-58 YZ-surface

Location - OC 24

Orientation of S_1 trace = 125.3

Long axis orient., α	Axial ratio, R_f	$1/R_f$
121.7	3.000	0.333
127.4	8.000	0.125
122	2.417	0.414
118.8	2.690	0.372
113.9	2.864	0.349
118	2.467	0.405
119.3	1.556	0.643
123	6.200	0.161
123.4	3.400	0.294
151	1.643	0.609
117	3.417	0.293
110.8	1.280	0.781
118.7	1.789	0.559
120	4.625	0.216
111	1.931	0.518
120.2	3.091	0.324
118.8	1.556	0.643
96.8	1.375	0.727
115.5	2.368	0.422
135	2.857	0.350
130.8	3.000	0.333
131.8	2.091	0.478
125.7	3.727	0.268
108.4	1.643	0.609
123	2.600	0.385
147	1.143	0.875
127.8	5.143	0.194
110.8	1.800	0.556
137.4	1.650	0.606
116	1.867	0.536
141	2.524	0.396
124.9	2.000	0.500
135.4	2.200	0.455
140.8	2.000	0.500
124.3	4.000	0.250
126.4	3.619	0.276
142.6	1.800	0.556
116.5	2.308	0.433
116	2.389	0.419
135	1.818	0.550
158	1.100	0.909
124.3	2.636	0.379
121.5	3.037	0.329
127	3.200	0.313
130.8	3.417	0.293

Sample PJ81-58 YZ-surface (cont.)

Long axis orient., α	Axial ratio, R_f	$1/R_f$
114.5	2.222	0.450
123.8	2.429	0.412
123.4	2.818	0.359
128.6	2.143	0.467
121	2.474	0.404
125	3.500	0.286
121.3	3.250	0.308
116.9	2.188	0.457
86.5	1.381	0.724
126.8	2.333	0.429
117.5	2.400	0.417
124.7	2.000	0.500
119	2.353	0.425
127.3	2.412	0.415
127.4	2.118	0.472
156	1.533	0.652
121.7	3.524	0.284
119	2.222	0.450
127	2.833	0.353
122	2.273	0.440
137.4	1.556	0.643
126.5	3.444	0.290
125	3.000	0.333
130.5	2.118	0.472
133.5	3.200	0.313

$\sum 1/R_f = 30.691$

$N/(\sum 1/R_f) = 2.281$

$N = 70$

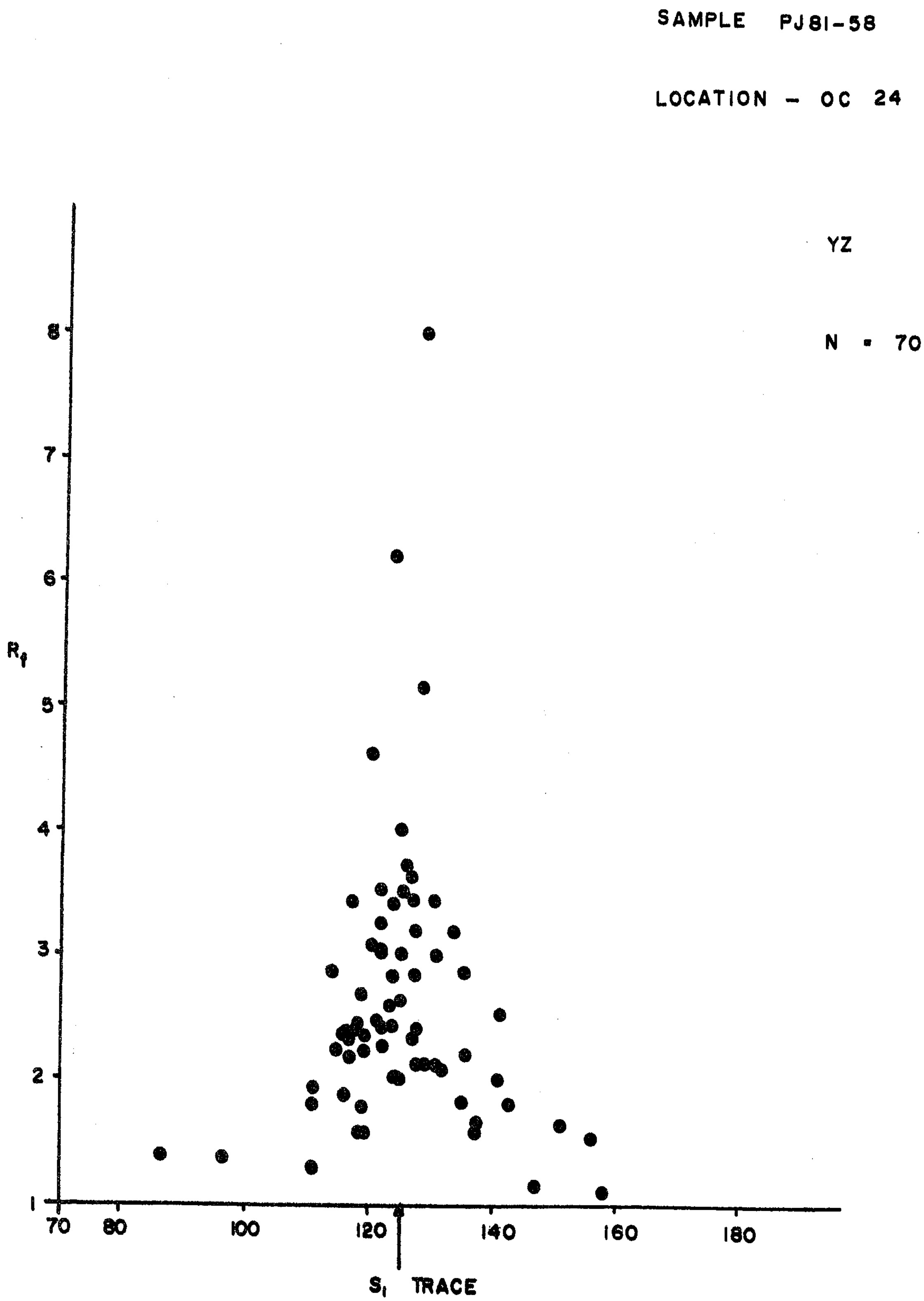
SAMPLE PJ81-58
LOCATION - OC 24
YZ
N = 70
R_f
8
7
6
5
4
3
2
1
70
80
100
120
140
160
180
S_1 TRACE

Sample PJ81-62 XZ-surface

Location - OC29

Orientation of S_1 trace = 92.4

Long axis orient., α	Axial ratio, R_f	$1/R_f$
73.1	1.615	0.619
93.5	5.538	0.181
90	9.200	0.109
101.1	2.000	0.500
92.3	7.889	0.127
98.2	2.000	0.500
79.6	1.667	0.600
92.3	11.667	0.086
109	1.286	0.778
76.8	2.286	0.438
93.4	7.714	0.130
87.4	1.816	0.551
56.7	1.222	0.182
89.2	7.250	0.138
90.3	4.833	0.207
90.4	7.692	0.130
74.1	1.929	0.519
67.3	3.500	0.286
92	6.400	0.156
93.7	5.286	0.189
87.4	5.625	0.178
89.4	5.807	0.172
97.2	4.636	0.216
95	5.750	0.174
85.8	1.600	0.625
102.3	1.375	0.727
94.9	6.444	0.155
91.8	7.429	0.135
81.8	2.000	0.500
94.5	6.375	0.157
85.9	6.300	0.159
96.1	1.556	0.643
93.5	8.100	0.123
95.4	5.000	0.200
101.4	2.154	0.464
78.5	2.316	0.432
87.2	3.250	0.308
39.1	1.923	0.520
93.8	7.143	0.140
105.2	2.375	0.421
99.5	2.200	0.455
60.9	1.700	0.588
96.2	1.250	0.800
61.4	1.625	0.615
100.8	1.200	0.833

Sample PJ81-62 XZ-surface (cont.)

Long axis orient., α	Axial ratio, R_f	$1/R_f$
71.5	1.500	0.667
92.4	1.526	0.655
98.5	2.000	0.500
101.9	1.250	0.800
55.3	1.600	0.625
97.2	2.600	0.385
87.7	2.750	0.364
84.1	1.857	0.538
88.8	2.100	0.476
76.5	2.235	0.447
84.5	2.364	0.423
90.4	2.000	0.500
88.9	4.333	0.231
80.8	2.143	0.467
70.2	1.344	0.744
127.4	1.286	0.778
83.4	1.556	0.643
104.1	1.500	0.667
80.4	2.000	0.500
71.8	1.571	0.636
88.5	3.200	0.313
92.4	4.000	0.250
94.2	2.000	0.500
103.5	3.000	0.333
90	2.333	0.429
89.4	2.250	0.444
52.8	1.500	0.667
92.4	2.750	0.364
86.8	2.800	0.357
76.3	1.706	0.586
73.1	2.250	0.444
84.3	1.447	0.691
93.8	2.400	0.417
93.8	2.154	0.464
89.2	4.375	0.229
82.5	2.235	0.447
75.8	1.643	0.609
89.6	2.000	0.500
94.1	3.250	0.308
83.2	3.500	0.286
24	1.111	0.900
99.6	2.667	0.375
92.4	5.467	0.183
30.5	1.333	0.750
92.4	2.333	0.429
147.1	1.429	0.700
91.5	4.133	0.242
108.8	1.444	0.692
102.5	2.419	0.413

Sample PJ81-62 XZ-surface (cont.)

Long axis orient., α	Axial ratio, R_f	$1/R_f$
91	2.444	0.409
70	2.222	0.450
44.4	1.071	0.933
112	2.118	0.472
93.8	2.933	0.341
97.5	1.200	0.833
105.5	1.786	0.560
42.5	1.313	0.762
80	1.545	0.647
90.6	5.000	0.200
92.4	2.333	0.429
85	1.818	0.550
92.4	3.000	0.333
96.4	3.091	0.324
83.5	1.818	0.550
95.4	2.400	0.417
24.6	1.222	0.818
109.5	1.667	0.600
114.3	1.700	0.588
96.8	1.769	0.565
102.1	2.444	0.409
92.4	2.333	0.429
92.4	3.200	0.313
99.6	2.222	0.450
114.6	1.222	0.818
59.5	1.412	0.708

$\sum 1/R_f = 54.342$

$N/(\sum 1/R_f) = 2.208$

$N = 120$

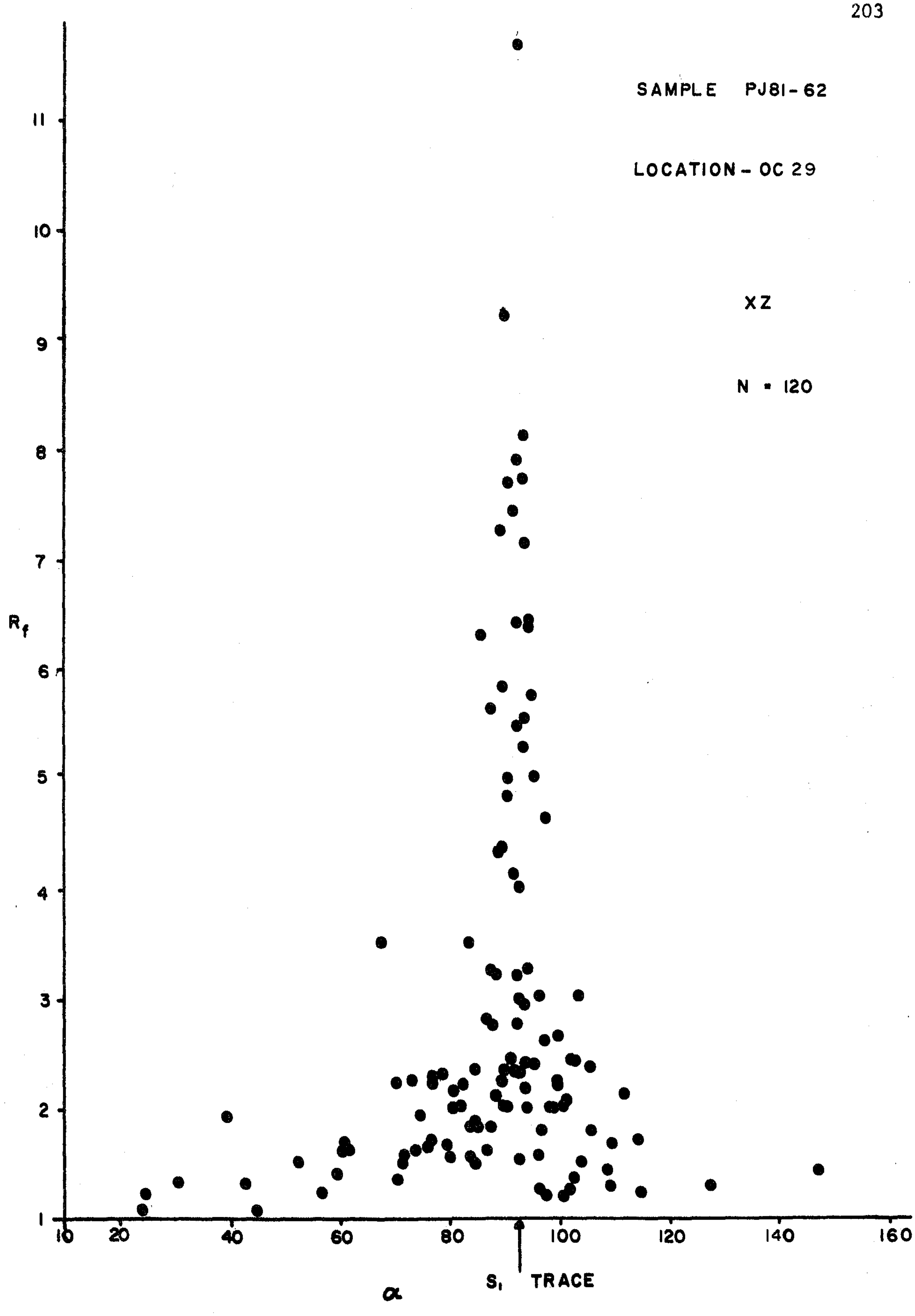
SAMPLE PJ81-62
LOCATION - OC 29
XZ
N = 120
R_f
α
S_1 TRACE
11
10
9
8
7
6
5
4
3
2
1
10
20
40
60
80
100
120
140
160

Sample PJ81-62 YZ-surface

Location - OC29

Orientation of S_1 trace = 84

Long axis orient., α	Axial ratio, R_f	$1/R_f$
92.4	2.000	0.500
72.5	1.714	0.583
92	2.667	0.375
97.2	1.545	0.647
87.5	2.083	0.480
88.3	2.000	0.500
79.6	2.000	0.500
84.4	4.211	0.238
42.8	1.448	0.690
71.2	2.105	0.475
85.8	2.200	0.455
82.8	1.500	0.667
85.6	2.833	0.353
98.4	1.875	0.533
23.2	1.417	0.706
47.4	1.750	0.571
88.5	2.500	0.400
74.5	2.667	0.375
78.5	2.125	0.471
95	2.154	0.464
84.2	1.429	0.700
86	2.357	0.424
92.4	1.455	0.688
92.4	2.400	0.417
82.9	3.200	0.313
82.5	4.667	0.214
82.8	3.200	0.313
89.2	2.154	0.464
78	2.714	0.368
83.7	2.667	0.375
96.5	2.000	0.500
168.8	1.381	0.724
82.5	5.250	0.190
84.5	3.857	0.259
92.4	1.727	0.579
74.1	1.222	0.450
70	2.125	0.471
92.4	4.000	0.250
83.5	3.333	0.300
105	1.909	0.524
91.5	2.444	0.409
103.4	1.833	0.545
105.4	1.778	0.563
73.2	1.500	0.668

Sample PJ81-62 YZ-surface (cont.)

Long axis orient., α	Axial ratio, R_f	$1/R_f$
76.5	3.000	0.333
96.1	2.182	0.458
84.5	3.905	0.256
92.4	1.818	0.550
87.1	5.000	0.200
79.8	3.250	0.308
80.7	2.333	0.429
64.4	2.714	0.368
54.6	1.333	0.750
44.1	2.286	0.438
88.2	2.364	0.423
117.4	1.692	0.591
74.8	2.667	0.375
77.3	2.200	0.455
67.7	1.900	0.526
92.4	2.667	0.375
106	1.429	0.700
86	1.500	0.667
114.6	1.313	0.762
73.5	1.800	0.556
82.5	1.586	0.630
69.2	1.348	0.742
132	1.316	0.760
98.8	1.458	0.686
53.9	1.500	0.667
80.7	1.737	0.576
86.3	1.704	0.587
88.6	1.522	0.657
70	1.200	0.833
95.5	1.500	0.667
91.2	1.643	0.609
51	1.455	0.688
91.8	1.286	0.778
69.3	1.214	0.824
93.6	1.833	0.545
111.3	1.500	0.667
35.3	1.115	0.897
110	1.071	0.933
88.9	3.300	0.303
97.5	1.850	0.541
61.8	1.667	0.600
84.5	1.733	0.577
86.8	1.577	0.634
74	2.500	0.400
90.5	1.667	0.600
54.7	1.474	0.679

$\sum 1/R_f = 47.290$

$N/(\sum 1/R_f) = 1.903$

$N = 90$

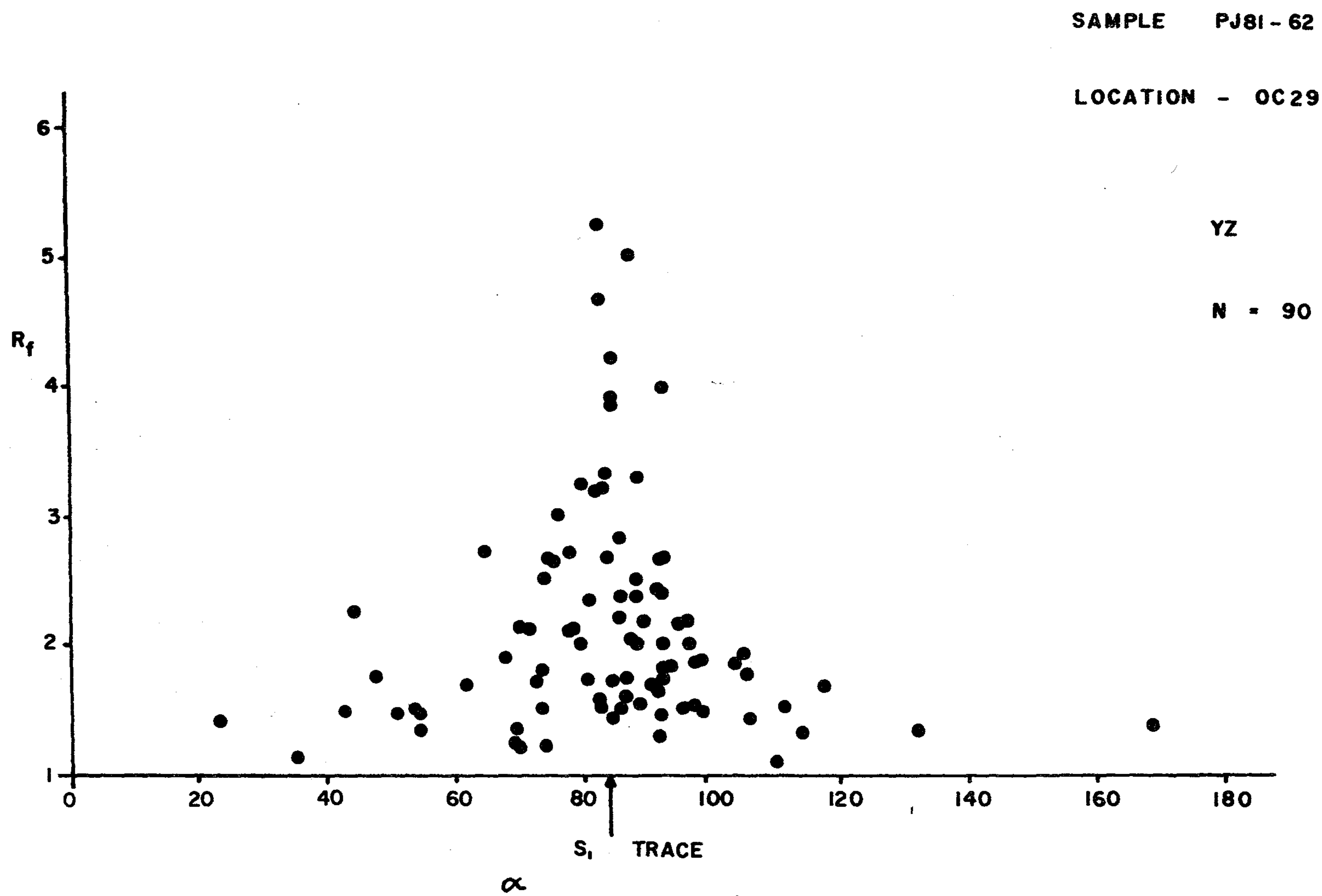
SAMPLE PJ81 - 62
LOCATION - OC29
YZ
N = 90
R_f
1
2
3
4
5
6
0
20
40
60
80
100
120
140
160
180
S_1 TRACE
α

Sample PJ81-57 XZ-surface

Location - OC 43

Orientation of S_1 trace = 125

Long-axis orient., α	Axial ratio, R_f	$1/R_f$
121	2.923	0.343
129.7	2.643	0.378
130.8	2.765	0.362
121.6	4.500	0.222
122.2	3.913	0.256
125.7	2.077	0.482
105	1.412	0.708
136.2	4.375	0.229
124	2.546	0.393
127.7	3.750	0.267
147	1.727	0.579
123.5	5.500	0.182
129	2.333	0.429
129.6	2.667	0.375
130.3	2.071	0.483
124.6	3.833	0.260
125.1	3.600	0.277
123.2	3.833	0.261
157.4	2.200	0.455
131.2	1.444	0.692
128.6	3.154	0.317
120.3	2.357	0.424
125.5	1.800	0.556
116.7	3.444	0.290
115	3.125	0.320
129.8	2.500	0.400
107.4	1.735	0.576
120.8	2.222	0.450
122.5	2.632	0.380
115.7	3.400	0.294
124	7.000	0.143
116	2.800	0.357
117.6	5.700	0.175
165.5	1.167	0.857
131	3.023	0.331
127.2	2.581	0.388
128.5	2.000	0.500
106.7	1.539	0.650
118.7	2.250	0.444
118.4	5.000	0.200
123.8	5.000	0.200
114.3	3.222	0.310
122.4	2.136	0.468
118.8	2.889	0.346

Sample PJ81-57 XZ-surface (cont.)

Long-axis orient., α	Axial ratio, R_f	$1/R_f$
133.8	2.308	0.433
122.5	3.316	0.302
120.6	4.167	0.240
182.3	1.355	0.738
132.7	4.500	0.222
112.3	1.667	0.600
116	3.286	0.304
119.4	4.222	0.237
116.8	2.147	0.466
106.5	1.333	0.750
140	1.529	0.654
123	3.000	0.333
117.3	2.833	0.353
113.3	1.833	0.546
120	2.296	0.435
122.7	2.833	0.353
129.3	2.000	0.500
79.2	1.278	0.783
122.4	3.125	0.320
119.7	2.125	0.471
125	5.000	0.200
125.9	4.400	0.227
123.3	4.462	0.224
121.3	5.111	0.196
131	2.833	0.353
115.1	2.545	0.393

$\Sigma 1/R_f$ = 27.642

$N/(\Sigma 1/R_f)$ = 2.532

N = 70

Sample PJ81-57 YZ-surface

Location - OC 43

Orientation of S_1 trace = 40.5

Long-axis orient., α	Axial ratio, R_f	$1/R_f$
51	2.077	0.482
28	2.529	0.395
50.4	1.368	0.731
40.8	1.613	0.620
25.4	1.333	0.750
27.5	1.870	0.535
3	1.444	0.692
43	1.500	0.667
57.6	1.486	0.673
19.3	1.235	0.810
356.5	1.765	0.567
34.2	2.125	0.471
33.3	2.643	0.378
41.6	1.704	0.587
356.2	1.316	0.760
28.5	2.125	0.471
56.2	1.333	0.750
60	1.316	0.760
39.4	1.263	0.792
98.6	1.240	0.807
15	1.560	0.641
38	1.674	0.597
27	1.429	0.700
42.1	1.643	0.609
353.3	1.692	0.591
43.8	1.379	0.725
36.5	1.813	0.552
50	1.478	0.677
50.6	1.455	0.688
24	2.000	0.500
45	1.525	0.656
38	2.133	0.469
27.8	1.765	0.567
53.6	1.233	0.811
46	1.680	0.595
78.4	1.118	0.895
40.6	1.591	0.629
49.8	2.046	0.489
64.7	1.579	0.633
49.6	1.125	0.889
28.8	1.818	0.550
59.6	1.541	0.649
5.8	1.235	0.809
4.7	1.031	0.970
44	2.818	0.355

Long-axis orient., α	Axial ratio, R_f	$1/R_f$
36.6	1.550	0.645
31.6	1.917	0.522
35.6	1.273	0.786
36.4	1.391	0.719
46.6	1.250	0.800
52.5	2.550	0.392
40	1.760	0.568
33.8	1.588	0.630
53	1.833	0.546
48.8	2.818	0.355
339.4	1.417	0.706
72.7	1.450	0.680
11.3	1.429	0.700
30	1.733	0.577
51.5	1.892	0.529
47.2	1.714	0.583
11	1.417	0.706
48	2.813	0.356
17.8	1.500	0.667
36.6	2.067	0.484
39.7	4.167	0.240
45.3	2.655	0.377
45	1.933	0.517
327	1.515	0.660
39.3	4.275	0.229

$\Sigma 1/R_f = 42.928$

$N/(\Sigma 1/R_f) = 1.631$

$N = 70$

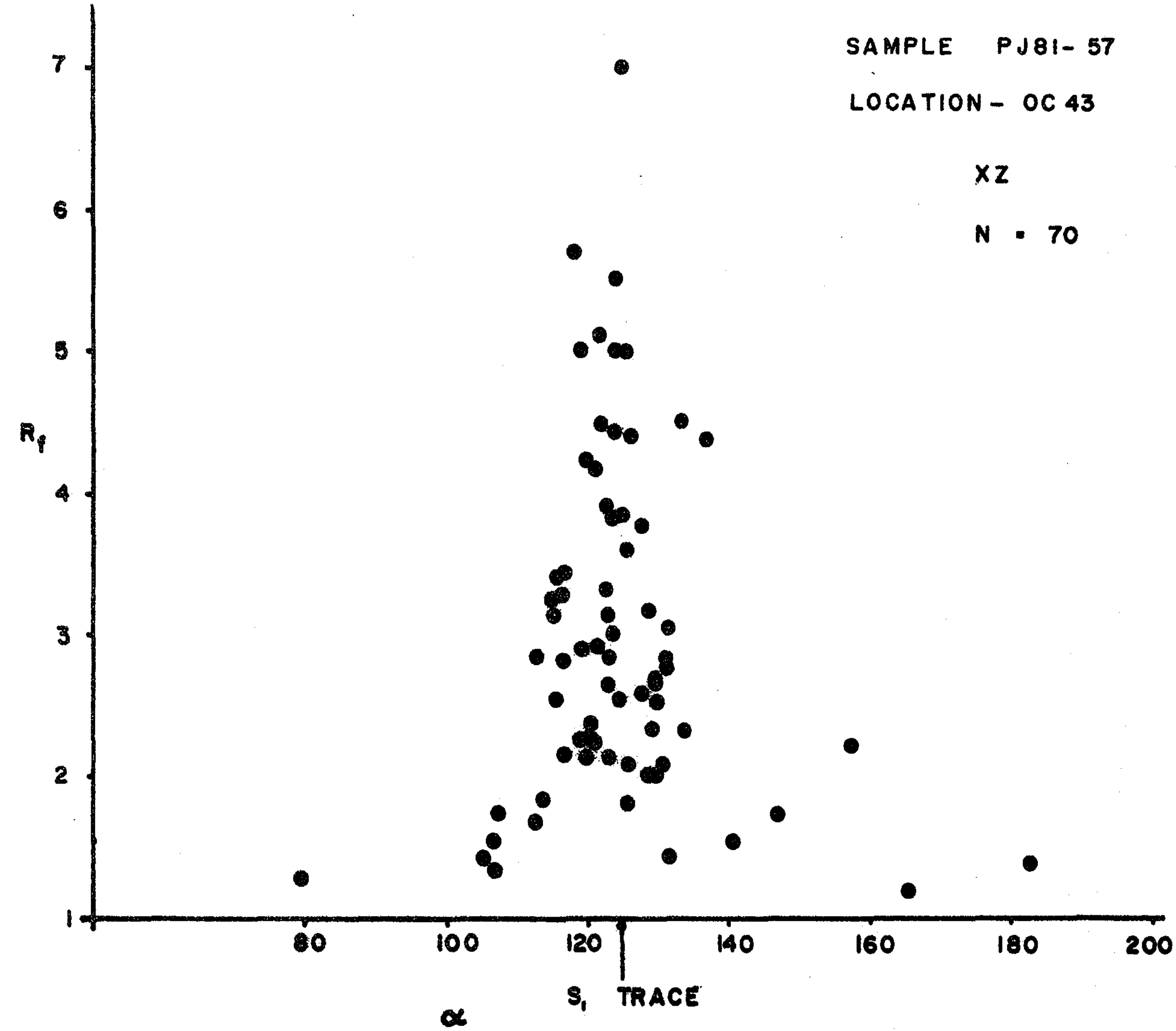

SAMPLE PJ81- 57
LOCATION - OC 43
XZ
N = 70
R_f
1
2
3
4
5
6
7
80
100
120
140
160
180
200
S_1 TRACE
α

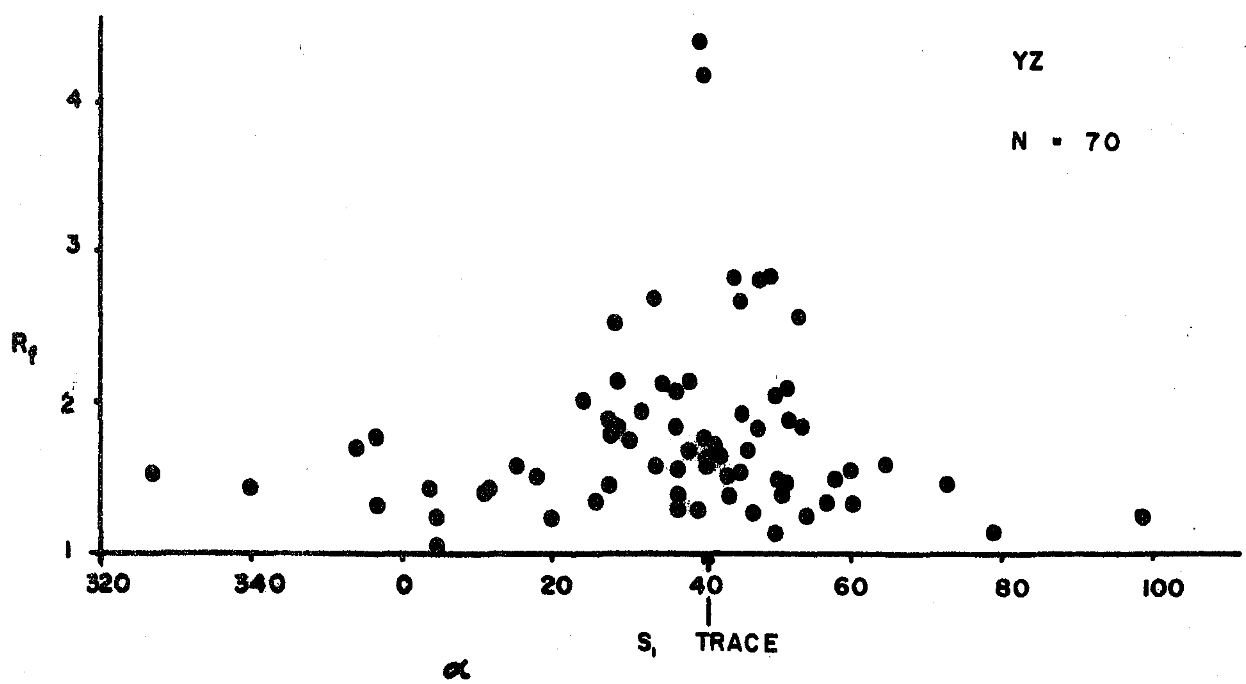

YZ
N = 70
R_f
1
2
3
4
320
340
0
20
40
60
80
100
S_1 TRACE
α

Sample PJ81-16 XZ-surface

Location- OC 64

Orientation of S_1 trace = 32.3

Long-axis orient., α	Axial ratio, R_f	$1/R_f$
28	5.091	0.196
40.8	2.933	0.341
45.5	1.778	0.563
6.6	2.067	0.484
37.5	5.167	0.194
37.6	4.857	0.206
42.2	4.000	0.250
33.2	5.636	0.177
34.8	3.429	0.292
32.9	1.870	0.535
30.2	10.833	0.092
37.9	1.542	0.649
31	8.000	0.125
30.6	4.400	0.227
34.8	4.500	0.222
31.1	5.000	0.200
40.6	1.667	0.600
22.3	1.714	0.583
23.6	1.571	0.636
28	5.143	0.194
66	1.250	0.800
28.2	1.174	0.852
40	1.786	0.560
30.5	4.250	0.235
27.3	2.400	0.417
31.4	2.044	0.489
28.7	2.125	0.471
38.8	1.625	0.615
46.6	2.333	0.429
26.3	1.857	0.539
34.3	2.727	0.366
33	4.042	0.247
29.7	6.115	0.164
22.7	4.500	0.222
31.4	5.400	0.185
23.8	2.071	0.483
11.9	3.000	0.333
48.4	1.941	0.515
16.7	2.842	0.352
9.6	1.435	0.697
20.8	2.125	0.471
36	3.500	0.286
16.7	2.567	0.390
34.7	4.800	0.208
39	4.000	0.250

Sample PJ81-16 XZ-surface (cont.)

Long-axis orient., α	Axial ratio, R_f	$1/R_f$
1.6	1.300	0.769
35.3	4.000	0.250
29.5	5.800	0.172
28	2.700	0.370
33.2	3.800	0.263
31.4	3.643	0.275
27.9	2.833	0.353
30.6	4.923	0.203
23	1.714	0.583
31	4.000	0.250
36	1.808	0.553
33.2	2.783	0.359
36.8	2.429	0.412
15.6	1.737	0.576
48	1.739	0.575
57.5	2.000	0.500
32.8	8.714	0.115
35.3	2.067	0.484
16.9	1.731	0.578
37.4	4.063	0.246
16.9	2.000	0.500
33	5.500	0.183
30	3.400	0.294
33.4	4.167	0.240
34.3	4.667	0.214

$\Sigma 1/R_f = 26.658$

$N/(\Sigma 1/R_f) = 2.625$

$N = 70$

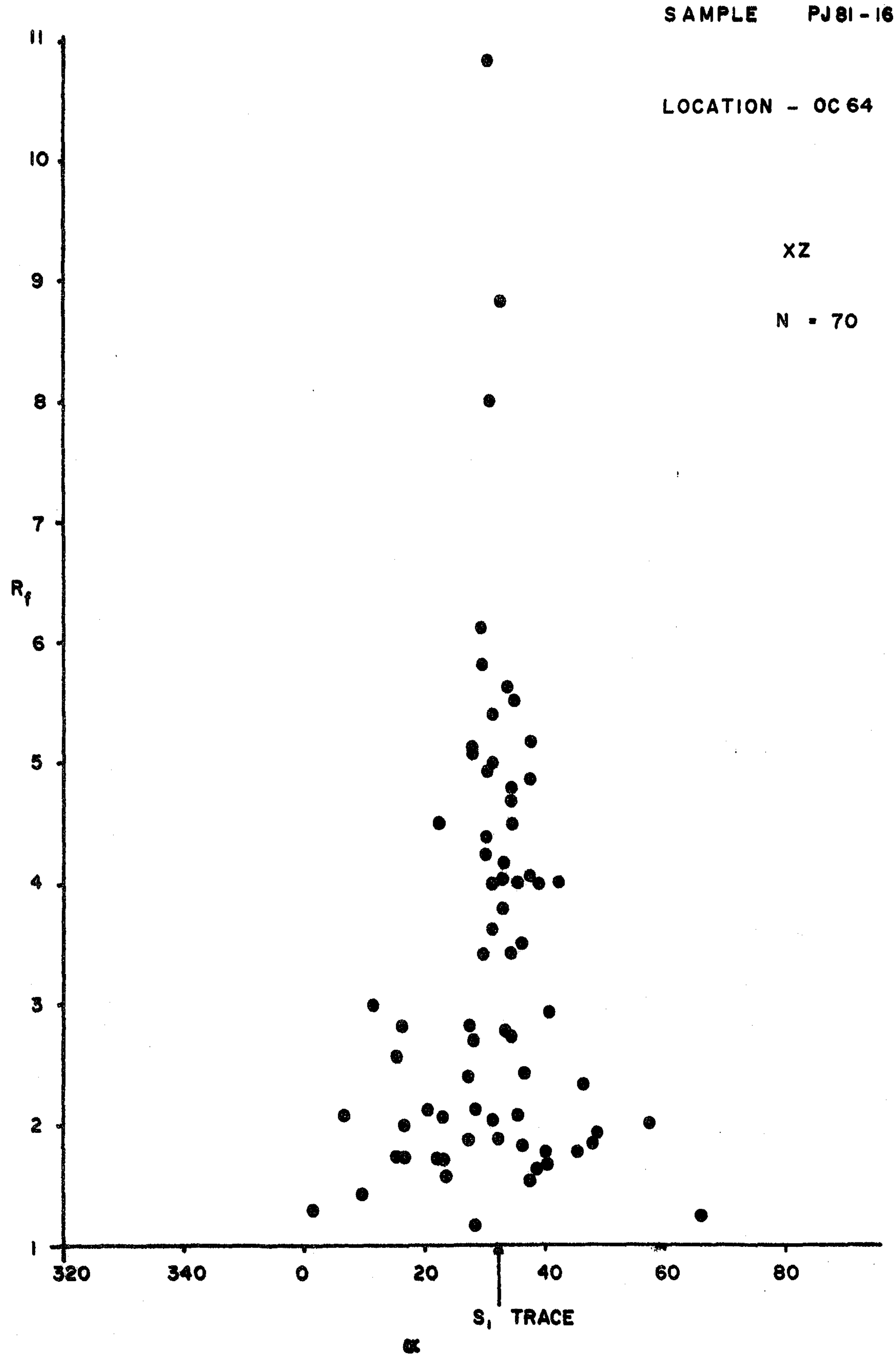
SAMPLE PJ 81-16
LOCATION - OC 64
XZ
N = 70
R_f
11
10
9
8
7
6
5
4
3
2
1
320
340
0
20
40
60
80
S_1 TRACE
α

Sample PJ81-16 YZ-surface

Location - OC 64

Orientation of S_1 trace = 267

Long-axis orient., α	Axial ratio, R_f	$1/R_f$
276	2.188	0.457
264.1	1.375	0.727
266.4	2.640	0.379
271.1	1.954	0.512
270.6	2.000	0.500
263.2	2.043	0.490
260.3	2.389	0.419
263	1.742	0.574
276	1.600	0.625
271	3.111	0.321
280.7	2.182	0.458
272	2.500	0.400
265.6	1.771	0.565
269.8	2.556	0.391
250	1.700	0.588
253.8	2.000	0.500
266.3	3.143	0.318
270	3.900	0.256
264	1.909	0.524
263.5	1.957	0.511
306.6	1.333	0.750
272.4	2.263	0.442
261.4	3.000	0.333
313	1.347	0.742
270	2.389	0.419
285.3	1.889	0.529
247.5	1.300	0.769
251.6	1.111	0.900
266	5.077	0.197
263	1.438	0.696
274	1.667	0.600
251.4	1.539	0.650
262.2	2.000	0.500
275.7	2.667	0.375
262	2.500	0.400
302.4	1.385	0.722
258	1.833	0.546
319	1.286	0.778
309.5	1.111	0.900
270.9	2.333	0.429
295	1.429	0.700
237	1.429	0.700
268	3.571	0.280
249	1.889	0.529

Long-axis orient., α	Axial ratio, R_f	$1/R_f$
267.7	3.143	0.318
268.7	2.833	0.353
246.5	1.385	0.722
258.6	2.000	0.500
243	1.333	0.750
263.2	2.250	0.444
267.8	3.167	0.316
275	2.500	0.400
262	2.357	0.424
233.2	1.667	0.600
229.8	1.500	0.667
271.4	3.250	0.308
284.3	2.200	0.455
282	2.333	0.429
281.6	2.136	0.468
270.6	1.500	0.667
269	1.429	0.700
239.7	1.875	0.533
258	1.455	0.688
271.3	2.727	0.367
262.6	2.125	0.472
268.7	2.000	0.500
295	1.600	0.625
264.4	5.000	0.200
263.3	2.833	0.353
271.2	2.857	0.350

$\Sigma 1/R_f = 36.009$

$N/(\Sigma 1/R_f) = 1.944$

$N = 70$

SAMPLE PJ81-16

LOCATION - OC 64

YZ

N = 70

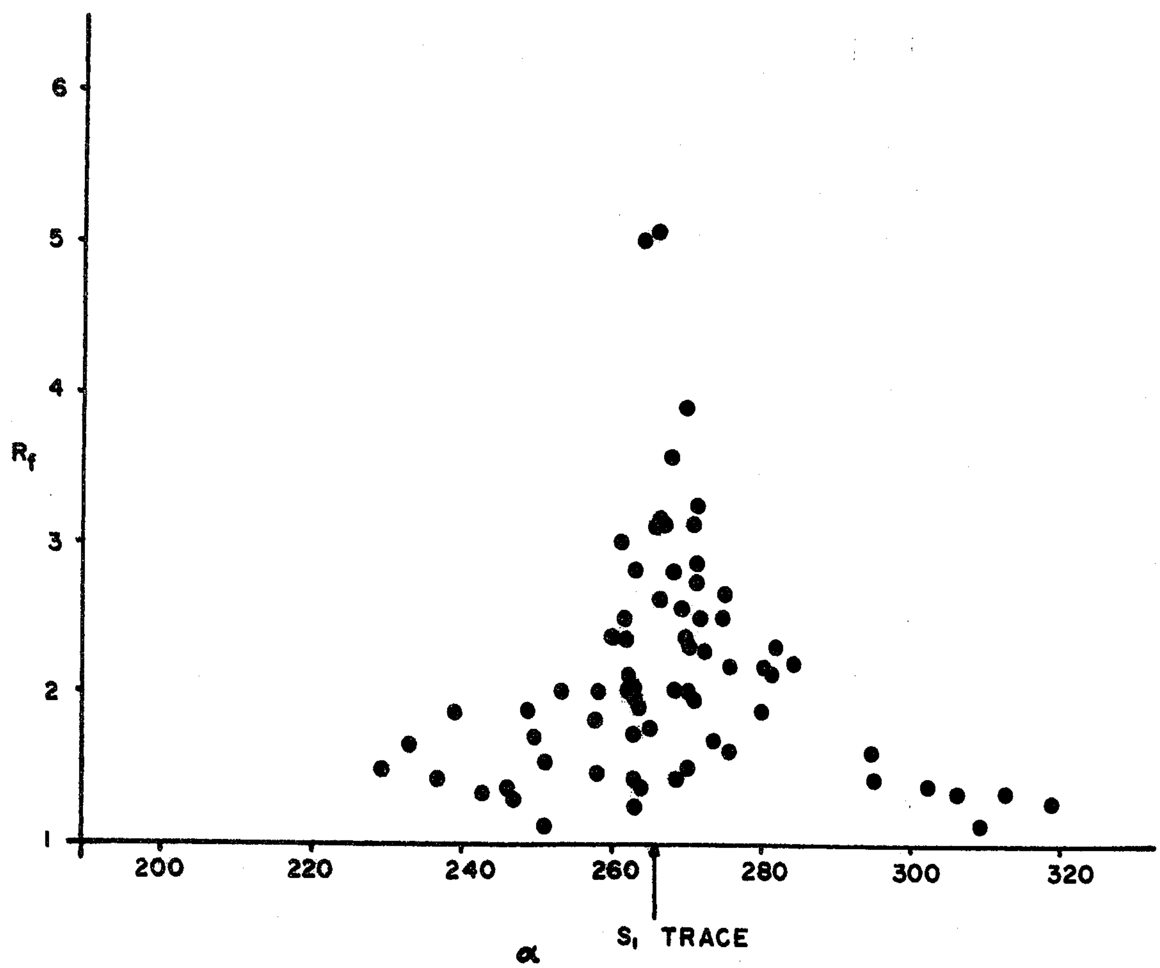

Sample PJ81-13B XZ-surface

Location - OC 65

Orientation of S_1 trace = 34

Long-axis orient., α	Axial ratio, R_f	$1/R_f$
45	1.450	0.690
28	2.778	0.360
25.8	2.286	0.438
19	1.724	0.580
33.8	3.259	0.307
47.7	2.222	0.450
24.5	1.482	0.675
36	2.000	0.500
22.9	1.818	0.550
49.5	1.517	0.659
36	2.703	0.370
31	4.250	0.235
339.6	1.875	0.533
18	1.409	0.710
27	1.364	0.733
51.2	2.200	0.455
44.8	2.200	0.455
45	2.636	0.379
29.6	1.818	0.550
40.5	1.600	0.625
25.7	3.231	0.310
29	1.529	0.654
30.8	1.929	0.519
22.4	1.818	0.550
36.8	3.118	0.321
64	1.485	0.674
31.6	2.000	0.500
45.5	1.250	0.800
34	4.087	0.245
31	3.364	0.297
21.7	2.267	0.441
21.8	2.177	0.460
26.2	2.875	0.348
21.5	1.923	0.520
27	2.333	0.429
18	1.405	0.712
49.6	2.556	0.391
38.7	2.308	0.433
34.3	3.188	0.314
30.8	2.000	0.500
30.9	2.250	0.444
31.3	3.788	0.264
28.7	2.313	0.432
38.6	1.760	0.568

Long-axis orient., α	Axial ratio, R_f	$1/R_f$
39.6	1.944	0.514
41.8	3.148	0.318
37.9	3.583	0.279
34.5	3.273	0.306
45	2.500	0.400
58.4	1.867	0.536

$\Sigma 1/R_f = 23.729$

$N/(\Sigma 1/R_f) = 2.107$

$N = 50$

Sample PJ81-13B YZ-surface

Location - OC 65

Orientation of S_1 trace = 124

Long-axis orient., α	Axial ratio, R_f	$1/R_f$
111.6	1.550	0.645
147.8	1.526	0.655
119.2	2.632	0.380
119.3	1.806	0.554
83.4	1.700	0.588
109	1.727	0.579
125	2.200	0.455
128.2	1.813	0.552
128	1.524	0.656
113.6	1.852	0.540
133.3	1.522	0.657
124.5	1.923	0.520
122.9	1.235	0.810
116.2	2.039	0.491
114.8	1.250	0.800
115.4	2.692	0.371
104.2	1.407	0.711
120	1.486	0.673
126.3	3.320	0.301
121.7	2.316	0.432
126	1.579	0.633
122.8	1.960	0.510
97.8	1.739	0.575
127.8	2.875	0.348
199.7	1.565	0.639
135.8	1.714	0.583
187.8	1.160	0.862
124.4	1.765	0.567
100.7	1.700	0.588
94.2	1.353	0.739
125.7	3.158	0.317
128.7	1.773	0.564
118.5	1.800	0.556
142.5	1.200	0.833
128.6	1.933	0.517
116.6	1.517	0.659
119.7	1.897	0.527
92	1.625	0.615
117.7	1.600	0.625
115	2.632	0.380
115.7	1.286	0.778
120.4	3.188	0.314
120	2.381	0.420
131.6	1.633	0.613

Sample PJ81-13B YZ-surface (cont.)

Long-axis orient., α	Axial ratio, R_f	$1/R_f$
112.9	1.600	0.625
136.2	1.833	0.546
115	1.586	0.630
105	1.857	0.539
123.6	1.769	0.565
120.5	3.044	0.329

$$\Sigma 1/R_f = 28.366$$

$$N/(\Sigma 1/R_f) = 1.763$$

$$N = 50$$

SAMPLE PJ81-13B

LOCATION - OC 65

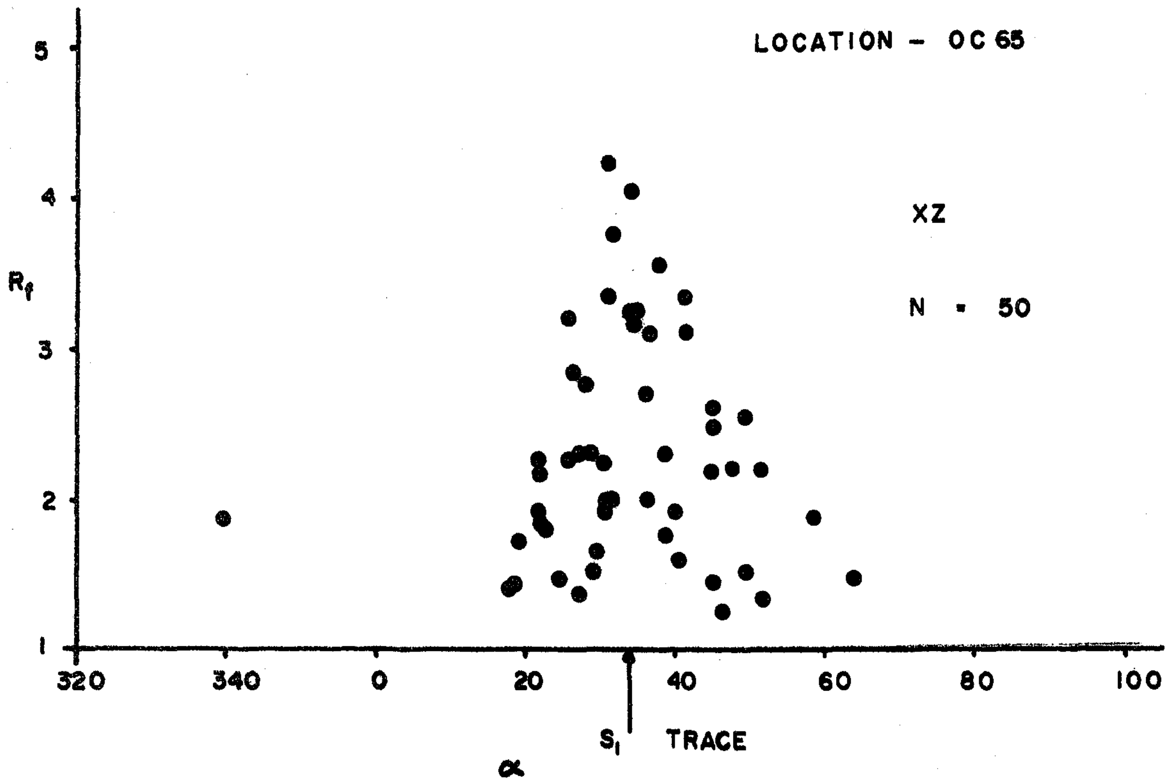

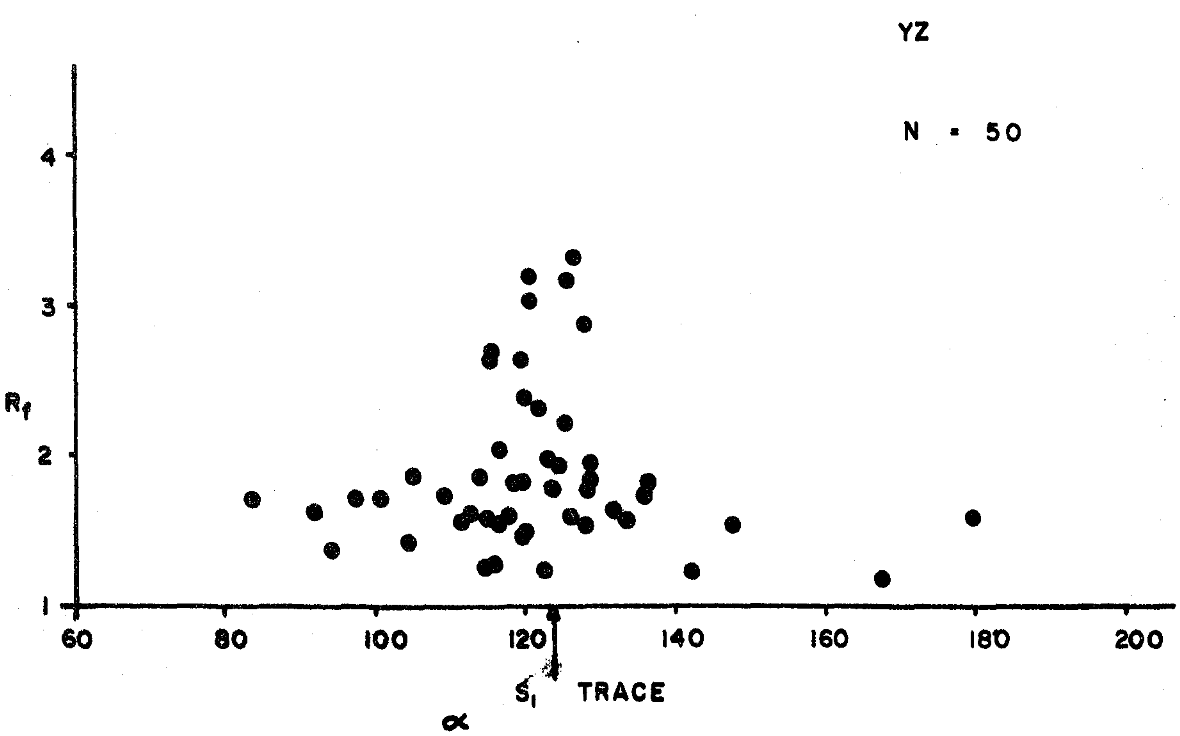

Sample PJ81-26 XZ-surface

Location - OC90

Orientation of S_1 trace = 121.4

Long axis orient., α	Axial ratio, R_f	$1/R_f$
117	3.692	0.271
118.4	5.273	0.180
126.8	3.400	0.294
132	2.500	0.400
125.8	2.556	0.391
122.5	7.923	0.126
122.7	3.333	0.300
128.9	3.667	0.273
124	2.678	0.378
130.7	1.680	0.595
114.3	2.500	0.400
122	1.938	0.516
123	4.688	0.213
127	4.071	0.246
145	2.130	0.499
125.1	1.588	0.630
124.8	3.267	0.306
121.2	4.640	0.216
118.3	2.200	0.455
121	3.143	0.318
133.7	1.574	0.635
123	8.800	0.114
119.2	5.455	0.183
116.7	2.526	0.396
120.8	2.308	0.433
121.7	4.148	0.241
120.3	3.000	0.333
122	6.250	0.160
129.8	1.364	0.733
124.2	5.857	0.171
123.5	2.267	0.440
124.6	5.190	0.193
122.5	12.111	0.083
125	5.813	0.172
121.5	3.333	0.300
147.5	1.857	0.538
113	1.130	0.885
126	2.391	0.418
126.7	4.267	0.234
125.6	5.667	0.176
130	1.515	0.660
133.7	2.077	0.481
129.6	6.250	0.160
123	2.444	0.409
121.5	7.067	0.142

Sample PJ81-26 XZ surface (cont.)

Long axis orient., α	Axial ratio, R_f	$1/R_f$
124.2	4.190	0.239
124.5	2.429	0.412
123	4.480	0.223
122.3	2.278	0.439
128	1.545	0.647
126.5	4.000	0.250
124.5	4.200	0.238
117.4	2.364	0.297
126.9	4.250	0.235
110.6	2.000	0.500
112	1.700	0.588
115.8	2.714	0.368
117	3.462	0.289
125	3.778	0.265
129.8	3.222	0.310
119.4	2.357	0.424
120	2.909	0.344
117	6.286	0.159
121.7	7.667	0.130
122.7	3.375	0.296
121	3.368	0.297
118	2.222	0.450
119.5	3.042	0.329
119.6	2.667	0.375
120	2.250	0.444

$\sum 1/R_f = 24.245$

$N/(\sum 1/R_f) = 2.887$

$N = 70$

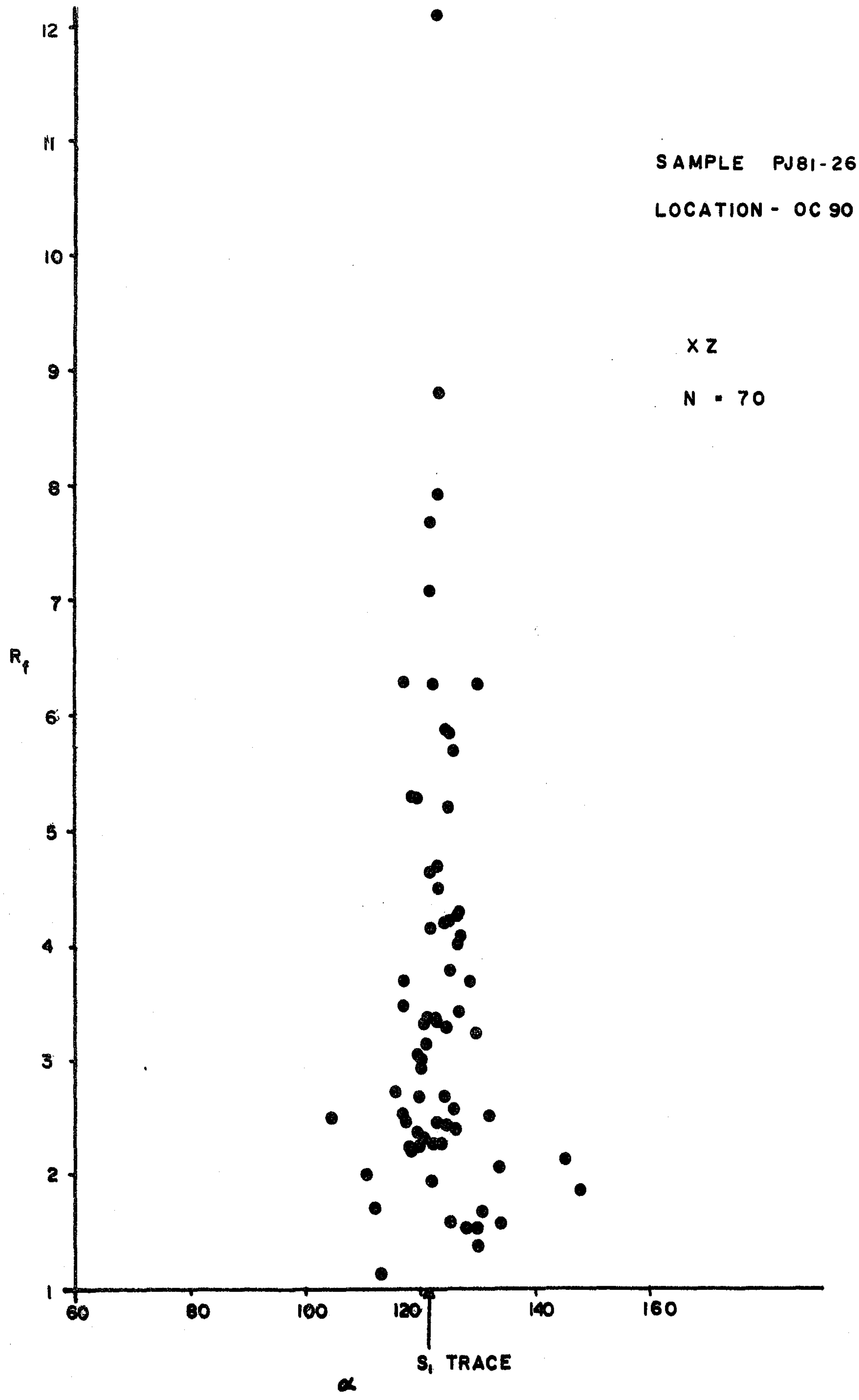
SAMPLE PJ81-26
LOCATION - OC 90
XZ
N = 70
R_f
12
11
10
9
8
7
6
5
4
3
2
1
60
80
100
120
140
160
S_1 TRACE
α

Sample PJ81-26 YZ- surface

Location - OC90

Orientation of S_1 trace = 123.6

Long axis orient., α	Axial ratio, R_f	$1/R_f$
158.6	1.478	0.676
122	1.833	0.545
125.2	3.500	0.286
101	1.676	0.597
131.9	1.821	0.549
121.6	2.667	0.375
45	1.556	0.643
154.4	2.222	0.450
125.8	2.167	0.462
127	3.158	0.317
133.8	3.231	0.310
115.3	1.733	0.577
114.4	2.000	0.500
132.8	1.056	0.947
139	2.045	0.489
135.3	1.522	0.657
196.7	1.308	0.765
102.2	1.684	0.594
128.8	1.700	0.588
141.7	2.813	0.355
98.8	2.333	0.429
131	3.308	0.302
119.9	5.000	0.200
183	1.375	0.727
149	1.500	0.667
110.3	2.050	0.488
54.6	1.846	0.542
123.5	2.435	0.411
136.4	2.579	0.388
88.7	1.833	0.545
119.7	1.949	0.513
124	4.276	0.234
124	3.067	0.326
130.2	3.207	0.312
123.9	2.571	0.389
161.4	1.500	0.667
121.3	2.077	0.482
124.7	4.188	0.239
114	1.929	0.519
118.8	2.462	0.406
117.6	1.556	0.643
141.5	1.950	0.513
116	2.143	0.467
126.7	5.429	0.184
145.8	3.000	0.333

Sample PJ81-26 YZ-surface (cont.)

Long axis orient., α	Axial ratio, R_f	$1/R_f$
114.3	1.714	0.583
127.9	3.306	0.303
114.1	1.667	0.600
160.9	1.417	0.706
144	1.364	0.733
126.3	1.577	0.634
129.4	1.900	0.526
119.7	2.600	0.385
68.7	1.536	0.651
124.8	2.000	0.500
142.3	2.400	0.417
116.5	2.056	0.486
111.6	1.364	0.733
113.3	2.214	0.452
121	2.933	0.341
114.4	1.867	0.536
146.5	1.278	0.783
154.6	1.938	0.515
125.7	1.923	0.520
121	2.200	0.455
135.7	1.917	0.522
123.8	1.800	0.556
116.8	1.467	0.491
144.3	1.467	0.682

$\sum 1/R_f = 34.969$

$N/(\sum 1/R_f) = 2.002$

$N = 70$

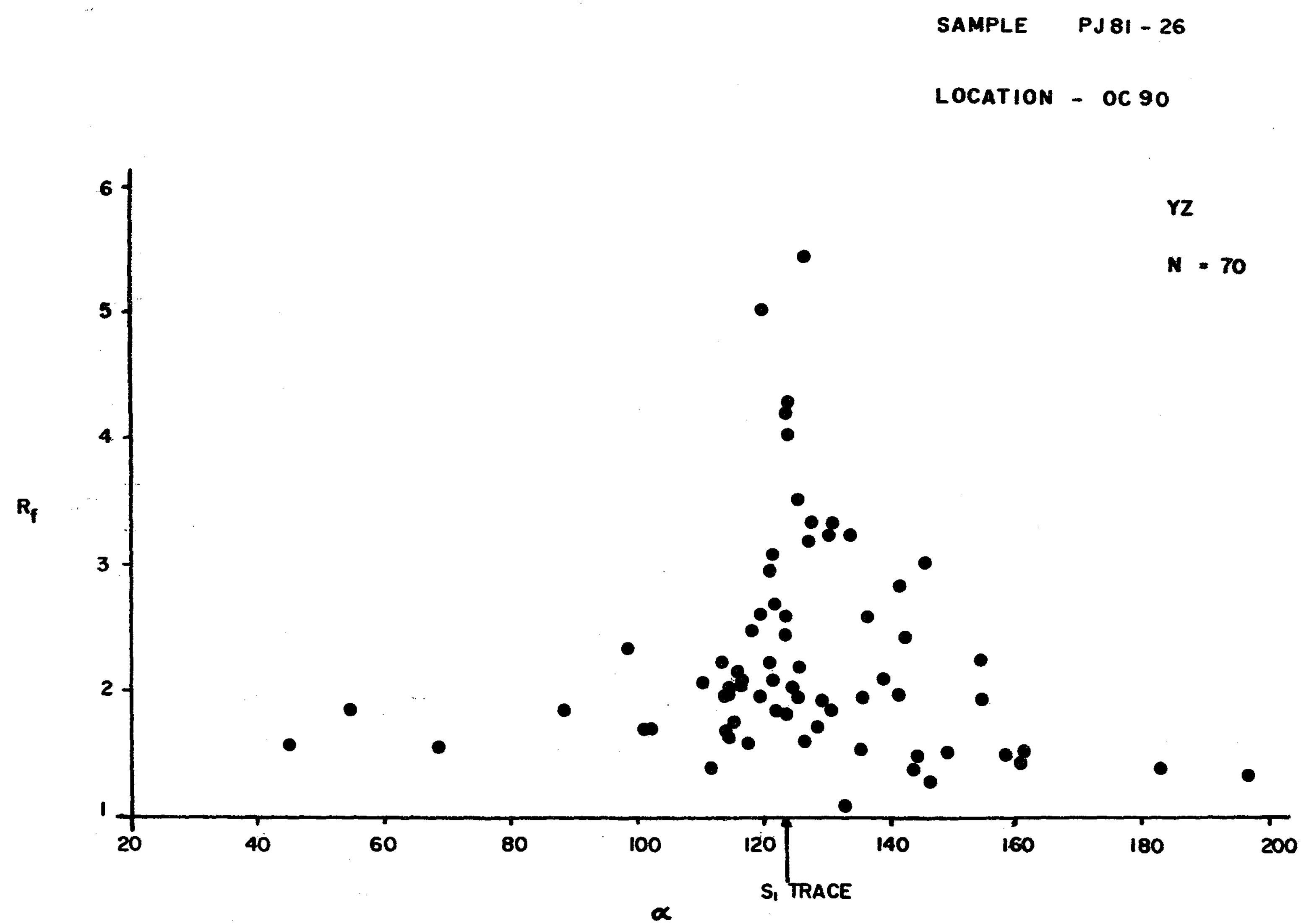
SAMPLE PJ81 - 26
LOCATION - OC 90
YZ
N = 70
R_f
6
5
4
3
2
1
20
40
60
80
100
120
140
160
180
200
S_1 TRACE
α

Sample PJ81-39 XZ-surface

Location - OC 94

Orientation of S_1 trace = 125.8

Long-axis orient., α	Axial ratio, R_f	$1/R_f$
131.2	3.727	0.268
150	1.667	0.600
127	2.571	0.389
110	1.375	0.727
125.7	6.250	0.160
126.8	3.563	0.281
122.5	4.500	0.222
129.5	3.818	0.262
125.3	2.857	0.350
125.4	4.667	0.214
125.7	4.667	0.214
133.7	2.308	0.433
125.4	2.625	0.381
119.7	2.462	0.406
124.4	4.000	0.250
116.8	2.286	0.438
127.5	8.000	0.125
123.4	5.429	0.184
122.5	3.167	0.318
125.4	10.000	0.100
90	1.212	0.825
126.3	6.200	0.161
137.8	2.200	0.455
124	9.455	0.106
120.5	1.857	0.538
129	5.700	0.175
126.7	4.786	0.209
124	3.500	0.286
117	3.250	0.308
125.6	7.000	0.143
113	1.462	0.684
113	2.050	0.488
120	3.000	0.333
136.5	1.600	0.625
102.8	2.263	0.442
142.8	1.455	0.688
129.8	4.286	0.233
121.4	2.857	0.350
99.5	1.375	0.727
138	2.000	0.500
122	4.455	0.225
120.2	2.857	0.350
119.7	4.444	0.225
122	4.273	0.234
114.5	1.692	0.591

Sample PJ81-39 XZ-surface (cont.)

Long-axis orient., α	Axial ratio, R_f	$1/R_f$
126.7	2.500	0.400
123.5	2.000	0.500
124.5	4.250	0.235
125	3.000	0.333
113.7	3.385	0.295
160	2.385	0.419
122.7	2.917	0.343
173	1.333	0.750
103.4	1.667	0.600
122.6	8.200	0.122
124.8	4.222	0.237
127	3.333	0.300
124.8	3.429	0.292
122.8	4.222	0.237
160	1.333	0.750
127.6	3.000	0.333
127	2.778	0.360
126.6	3.750	0.267
130	3.636	0.275
124.7	1.786	0.560
94.8	1.385	0.722
125.4	2.222	0.450
126.4	4.450	0.225
126.5	5.500	0.182
140	2.167	0.462

$\Sigma 1/R_f = 25.872$

$N/(\Sigma 1/R_f) = 2.706$

$N = 70$

SAMPLE PJ 81 - 39

LOCATION - OC 94

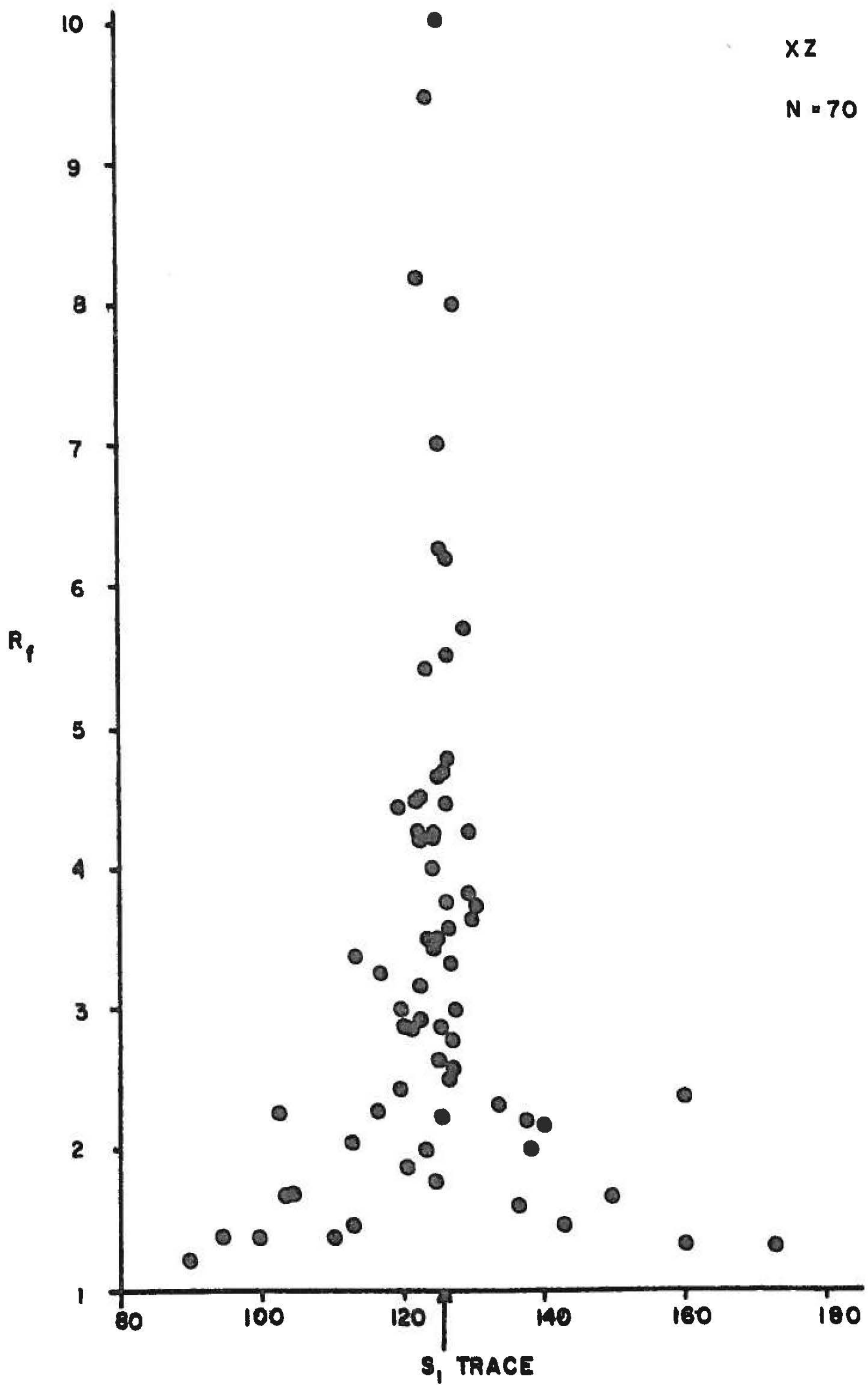

a

Sample PJ81-39 YZ surface

Location - OC 94

Orientation of S_1 trace = 125.7

Long axis orient., α	Axial ratio, R_f	$1/R_f$
116.7	1.400	0.714
159.7	1.250	0.800
46.4	1.500	0.667
89	1.733	0.577
40	1.500	0.667
136	1.840	0.544
43	1.800	0.556
75.6	1.250	0.800
133.5	3.000	0.333
130.7	1.789	0.559
184.3	1.556	0.643
96	1.400	0.714
92	1.583	0.632
168.8	1.857	0.538
137.4	1.167	0.857
114.5	1.778	0.563
159.4	2.600	0.385
88	1.364	0.733
119.6	2.143	0.467
132.2	1.231	0.813
135.6	1.900	0.526
98	1.333	0.750
101.5	1.250	0.800
143	1.429	0.700
125.8	1.875	0.533
153	1.800	0.556
150	1.227	0.815
103.3	1.250	0.800
204	1.533	0.652
149	2.000	0.500
139	1.733	0.577
112	1.583	0.632
161	2.500	0.400
113.2	1.778	0.563
151.4	2.182	0.458
123	1.320	0.758
120.5	1.263	0.792
123	1.800	0.556
135.7	1.333	0.750
84.5	1.538	0.650
80.7	1.333	0.750
113.4	2.080	0.481
103	1.733	0.577
124.7	3.200	0.313
142	1.615	0.619
124.4	2.667	0.375

Sample PJ81-39 YZ surface (cont.)

Long axis orient., α	Axial ratio, R_f	$1/R_f$
140	1.667	0.600
83	1.833	0.545
156.6	1.429	0.700
169.8	1.733	0.577
85.3	1.375	0.727
85.7	1.733	0.577
202	1.462	0.684
71.5	1.727	0.579
130.5	2.000	0.500
141.2	2.200	0.455
92	1.556	0.643
146.7	2.231	0.448
129	1.739	0.575
149.6	1.706	0.586
106	1.611	0.621
69	1.588	0.630
114.5	2.222	0.450
66	1.600	0.625
54	1.120	0.893
84	1.643	0.609
184.5	1.154	0.867
173	2.333	0.429
146.5	1.926	0.519
44.4	1.250	0.800

$\Sigma 1/R_f = 43.084$

$N/(\Sigma 1/R_f) = 1.625$

$N = 70$

SAMPLE PJ81 - 39

LOCATION - OC 94

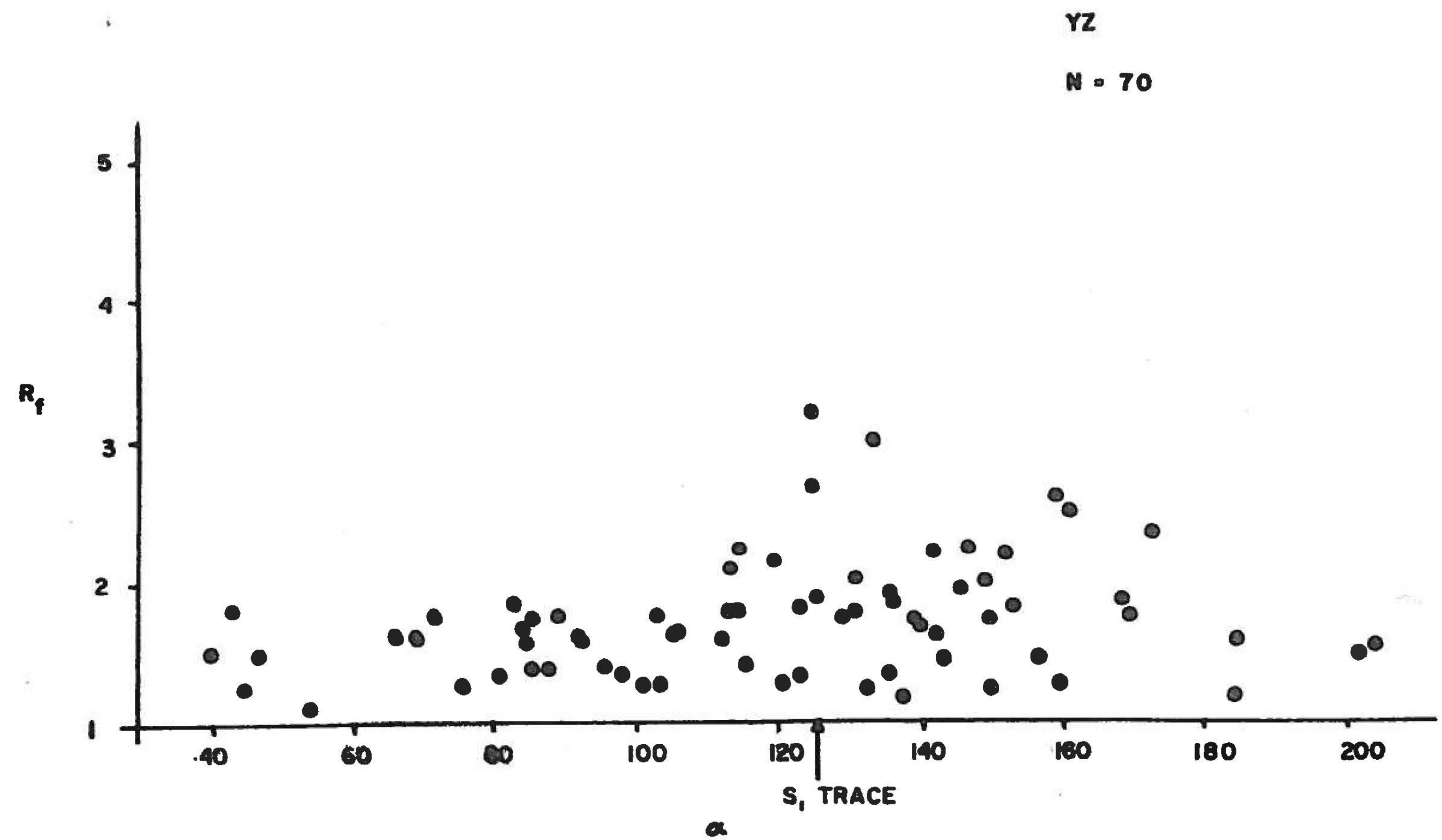

Sample PJ81-42 XZ-surface

Location - OC 97

Orientation of S_1 trace = 126.2

Long-axis orient., α	Axial ratio, R_f	$1/R_f$
121.7	2.857	0.350
120.2	1.846	0.542
114.5	2.313	0.432
126	7.778	0.129
124.5	4.000	0.250
125.9	9.053	0.110
126	7.000	0.143
124.4	4.000	0.250
125.8	6.500	0.154
131	8.375	0.119
123.7	4.867	0.205
131	2.909	0.344
134.4	5.500	0.182
123	3.667	0.273
124.6	3.571	0.280
152	2.375	0.421
132.3	3.636	0.275
125.3	12.000	0.083
125.6	6.188	0.162
135	2.000	0.500
129	8.000	0.125
130	3.714	0.269
124	3.733	0.268
123.7	3.100	0.323
126.1	5.625	0.178
129.5	3.722	0.269
129.3	2.222	0.450
127.3	6.889	0.145
121.4	2.435	0.411
131.5	3.571	0.280
105.5	1.333	0.750
124	7.000	0.143
125	4.333	0.231
116.8	3.800	0.263
123.7	8.250	0.121
128	4.800	0.208
127.6	6.333	0.158
126.7	8.250	0.121
129	4.444	0.225
121	2.909	0.344
115.8	1.467	0.682
120.7	6.375	0.157
127.3	3.800	0.263
119	2.667	0.375
123.2	2.288	0.438

Sample PJ81-42 XZ-surface (cont.)

Long-axis orient., α	Axial ratio, R_f	$1/R_f$
128.5	3.444	0.290
113.6	2.286	0.438
130	2.000	0.500
132	1.852	0.540
117.8	2.000	0.500
124.4	2.815	0.355
116.4	1.957	0.511
130	5.792	0.173
119.8	4.231	0.236
132.7	4.571	0.219
132	3.167	0.316
124.8	2.875	0.348
120	4.615	0.217
117	3.833	0.261
83.5	1.471	0.680
122.4	2.000	0.500
121	8.769	0.144
123.4	4.375	0.229
121.7	6.125	0.163
116.8	2.868	0.349
125.4	2.320	0.431
119.5	4.000	0.250
125.5	2.923	0.342
119.5	4.636	0.216
117.9	2.059	0.486

$\Sigma 1/R_f = 21.065$

$N/(\Sigma 1/R_f) = 3.323$

$N = 70$

SAMPLE PJ81-42

LOCATION - OC97

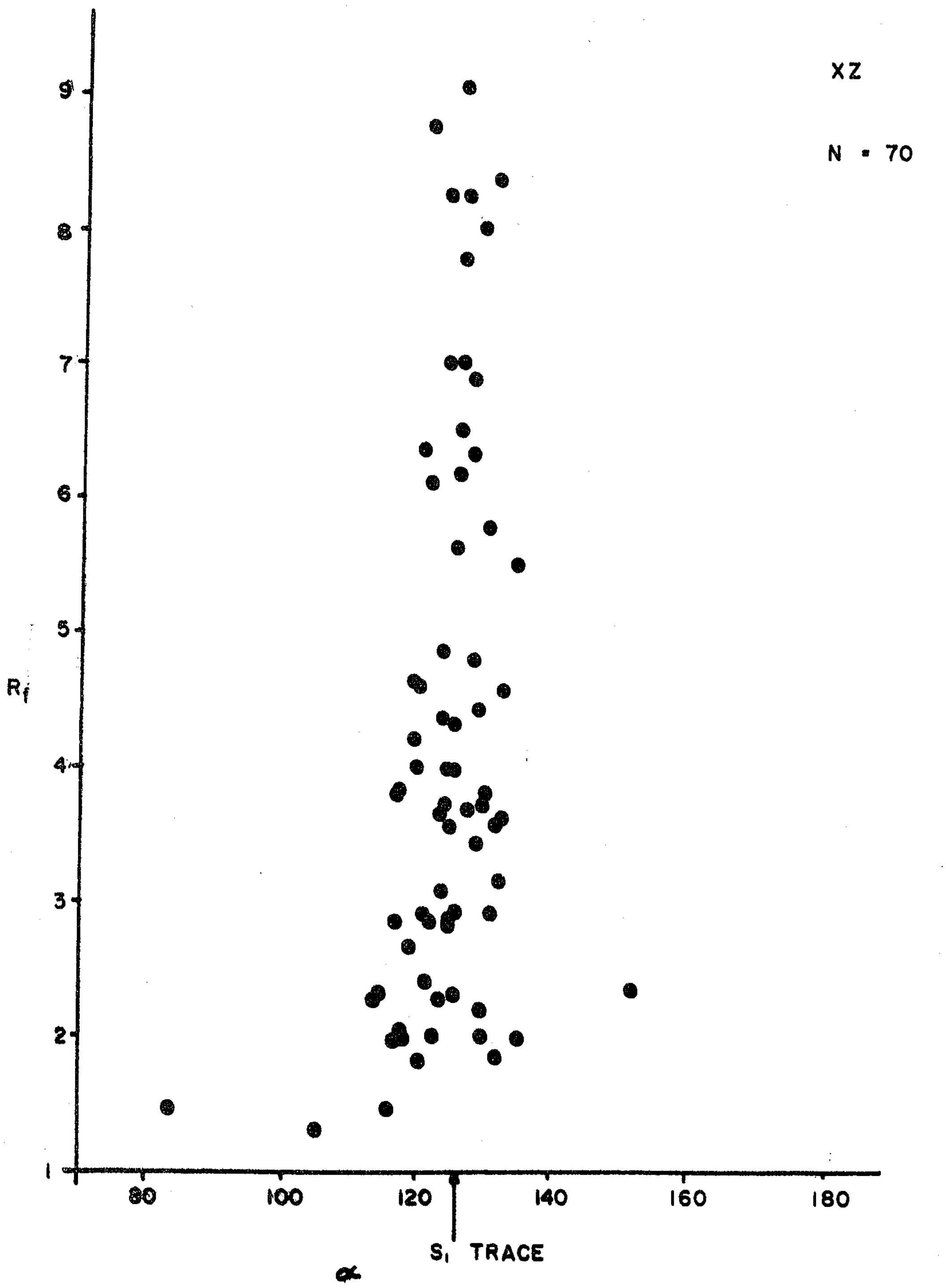

Sample PJ81-42 YZ-surface

Location - OC 97

Orientation of S_1 trace = 120

Long-axis orient., α	Axial ratio, R_f	$1/R_f$
110.8	1.423	0.703
102.9	1.600	0.625
117.9	4.071	0.246
116.7	3.308	0.302
128	1.250	0.800
121.5	11.667	0.086
118.6	6.583	0.152
120.7	3.375	0.296
119.6	3.200	0.313
117.3	2.447	0.409
118.3	2.818	0.355
122	3.900	0.256
116.3	3.154	0.317
120	8.167	0.122
118.7	4.200	0.238
111.5	1.933	0.517
120	3.077	0.325
117	2.550	0.392
120	2.409	0.415
171.4	1.083	0.923
117.5	1.929	0.519
116.5	2.222	0.450
142.4	1.400	0.714
120	7.667	0.130
124.3	3.000	0.333
119.6	3.778	0.265
117.4	3.053	0.328
100	1.625	0.615
120.5	3.429	0.292
120.4	2.286	0.438
115.5	2.571	0.389
109.4	1.667	0.600
122.5	2.333	0.429
117.8	4.000	0.250
119.4	5.214	0.192
118.3	2.077	0.481
111.4	2.083	0.480
105.8	2.000	0.500
117	5.200	0.192
120.4	4.250	0.235
119.6	4.125	0.242
105	1.545	0.647
120	1.615	0.619
120.4	1.556	0.643
130	2.216	0.451

Sample PJ81-42 YZ-surface (cont.)

Long-axis orient., α	Axial ratio, R_f	$1/R_f$
117	2.174	0.460
115	1.545	0.647
118	2.857	0.350
123.2	7.188	0.139
118.4	2.313	0.432
119.3	3.950	0.253
200	1.400	0.714
116.7	1.500	0.667
108.7	2.083	0.480
116.4	2.857	0.350
120	2.571	0.389
129	1.926	0.519
95.8	1.636	0.611
124	3.143	0.318
122	9.333	0.107
109.6	2.000	0.500
113.4	1.385	0.722
116	1.500	0.667
124.7	3.000	0.333
89	1.667	0.600
124.3	2.889	0.346
123	3.667	0.273
157	1.467	0.682
118.3	4.125	0.242
126.7	2.900	0.345

$\Sigma 1/R_f$ = 29.368

$N/(\Sigma 1/R_f)$ = 2.384

N = 70

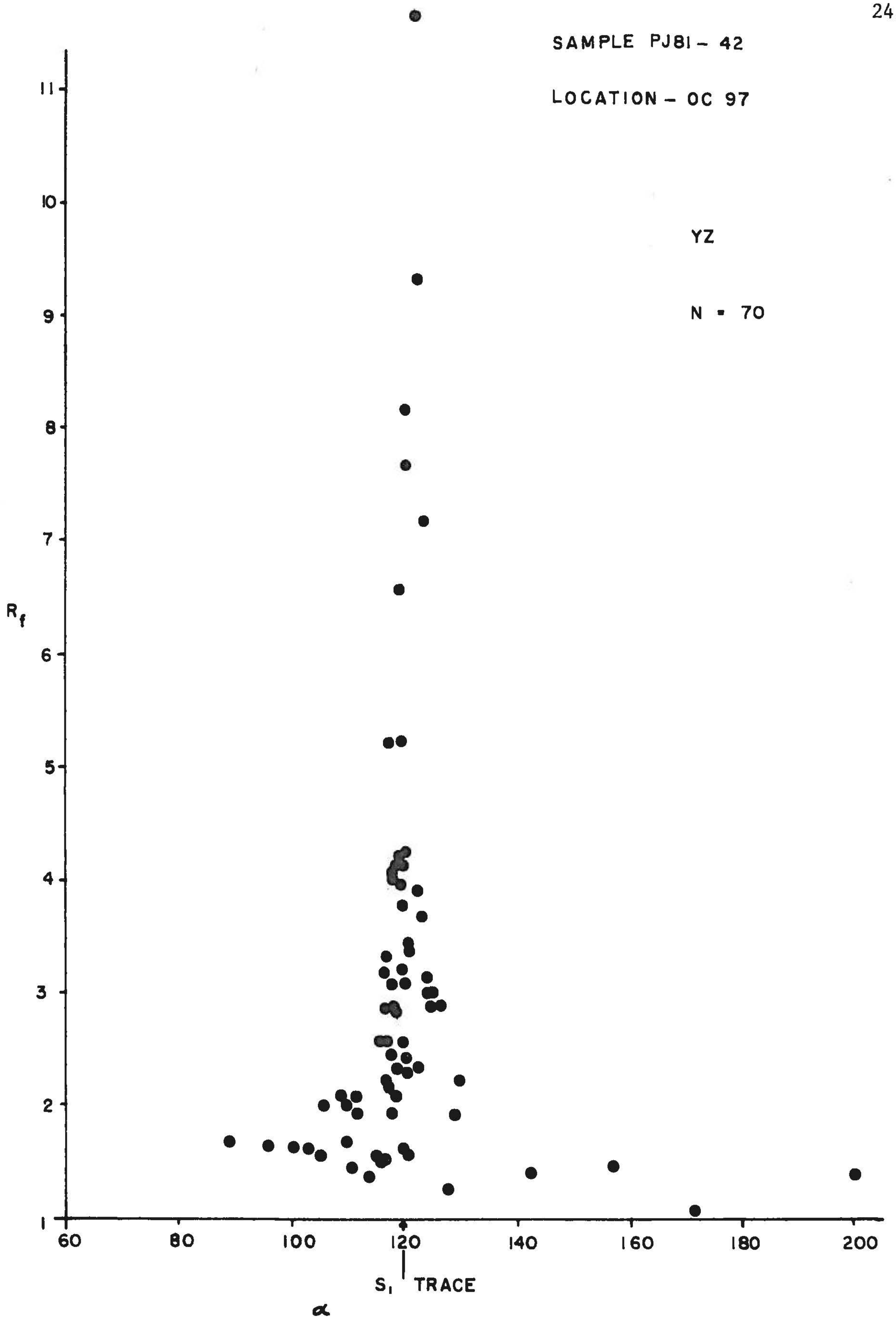

SAMPLE PJ81 - 42
LOCATION - OC 97
YZ
N = 70
R_f
α
S_1 TRACE
1
2
3
4
5
6
7
8
9
10
11
60
80
100
120
140
160
180
200

Sample PJ81-43 XZ-surface

Location - OC 98

Orientation of S_1 trace = 122.5

Long-axis orient., α	Axial ratio, R_f	$1/R_f$
122.3	3.231	0.310
127.7	1.850	0.541
124.6	3.273	0.306
123	2.462	0.406
120	2.375	0.421
111.2	2.818	0.355
189.4	1.571	0.636
118	2.583	0.387
116.7	2.111	0.474
124	3.444	0.290
119.6	4.000	0.250
122.8	3.500	0.286
123.3	5.136	0.195
124.7	1.650	0.606
123.5	8.250	0.121
125.4	1.800	0.556
122	4.471	0.224
124.5	3.905	0.256
114.7	3.400	0.294
126.5	2.750	0.364
117.4	2.500	0.400
128.9	2.154	0.464
116.6	3.923	0.255
108.4	1.941	0.515
121.7	3.667	0.273
116.8	7.143	0.140
137.3	2.462	0.406
120	2.905	0.344
121.3	2.077	0.481
128.5	2.000	0.500
94.3	1.735	0.576
112.6	2.250	0.444
122	8.941	0.112
114.7	2.471	0.405
114.3	5.333	0.188
120.8	5.105	0.196
120.5	5.889	0.170
114.6	3.267	0.306
120	4.933	0.203
114	2.500	0.400
125.3	2.300	0.435
120.7	3.579	0.279
118.2	3.750	0.267
125	2.625	0.381
124.4	5.500	0.182

Sample PJ81-43 XZ-surface (cont.)

Long-axis orient., α	Axial ratio, R_f	$1/R_f$
116	3.179	0.315
119	3.000	0.333
124.4	3.333	0.300
125	2.500	0.400
119	2.538	0.394
124.6	2.647	0.378
112	2.750	0.364
122.2	8.000	0.125
115.3	2.765	0.362
114.7	3.500	0.286
125.4	2.533	0.395
120.5	6.800	0.147
121.6	3.875	0.258
121.8	10.667	0.094
120	3.250	0.308
113.8	2.276	0.439
124.3	7.900	0.127
111	1.444	0.692
121.4	3.739	0.267
119.3	3.333	0.300
130	6.000	0.167
123.8	5.000	0.200
123.7	4.182	0.239
127.3	1.619	0.618
123.5	4.233	0.236

$$\Sigma 1/R_f = 23.344$$

$$N/(\Sigma 1/R_f) = 2.999$$

$$N = 70$$

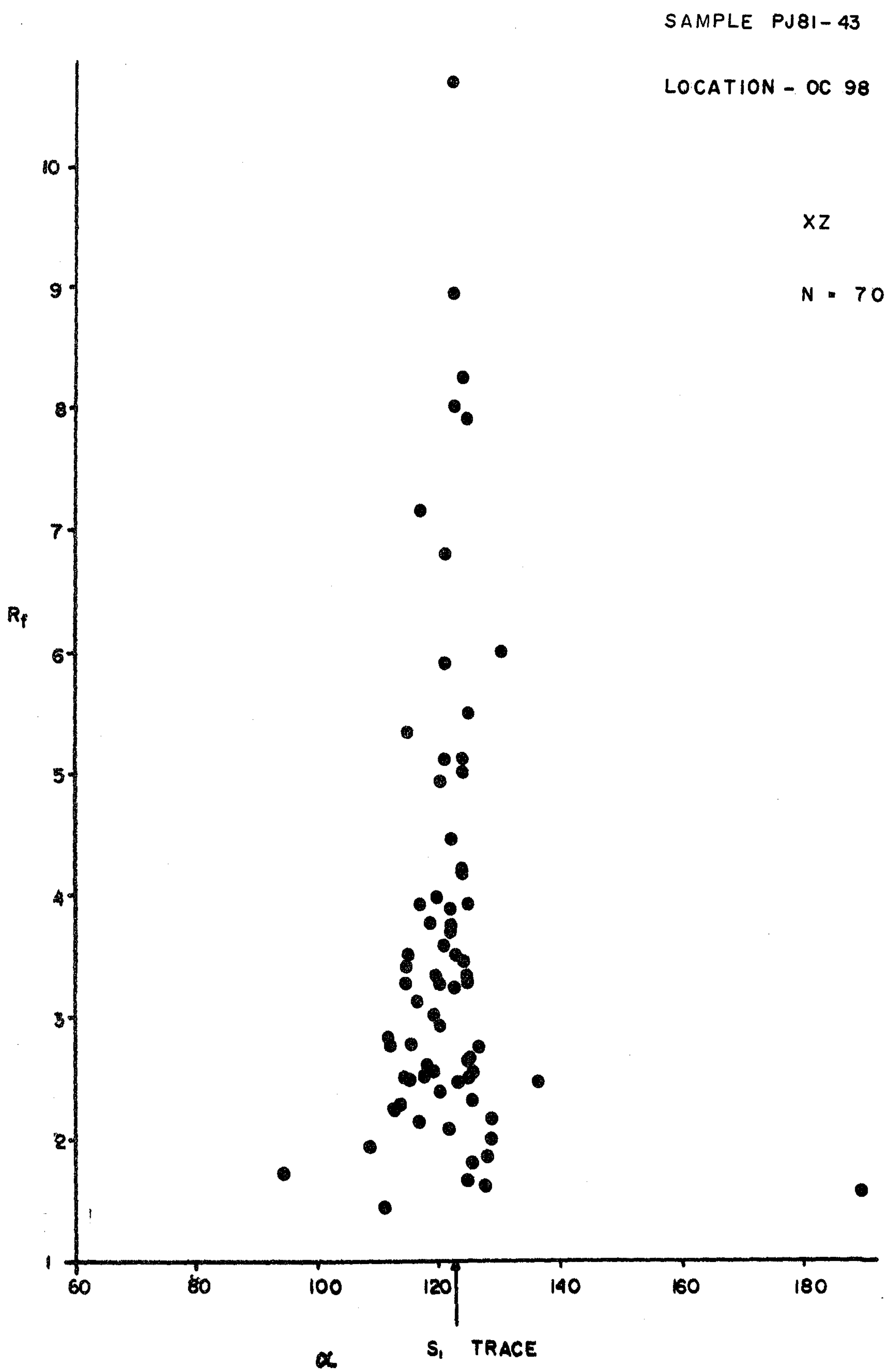
SAMPLE PJ81-43
LOCATION - OC 98
XZ
N = 70
R_f
10
9
8
7
6
5
4
3
2
1
60
80
100
120
140
160
180
α
S_1 TRACE

Sample PJ81-43 YZ-surface

Location - OC 98

Orientation of S_1 trace = 137

Long-axis orient., α	Axial ratio, R_f	$1/R_f$
95	1.786	0.560
138.7	1.542	0.649
120.8	1.667	0.600
147	2.893	0.346
154	1.394	0.717
115.4	1.538	0.650
125.3	1.917	0.522
63.4	1.167	0.857
121.6	2.138	0.468
210.3	1.313	0.762
145	2.953	0.339
128.5	2.933	0.341
150	2.150	0.465
142.8	2.333	0.429
134	3.250	0.308
137	1.800	0.556
132.5	2.833	0.353
125	1.619	0.618
123	1.786	0.560
127.8	1.692	0.591
148.4	2.250	0.444
99	1.917	0.522
144	2.227	0.449
131	1.833	0.545
132.4	2.053	0.487
137	2.412	0.415
153	2.120	0.472
133.3	1.167	0.857
139	1.905	0.525
121.4	2.778	0.360
129.2	1.833	0.545
128	5.333	0.188
125.3	2.000	0.500
155.5	1.148	0.871
137	2.188	0.457
138	1.793	0.558
151.8	1.300	0.769
145.8	2.484	0.403
125.5	1.778	0.563
130.3	3.583	0.279
133	1.857	0.538
105	1.667	0.600
133.6	2.316	0.432
134.5	2.786	0.359
126.3	2.308	0.433

Long-axis orient., α	Axial ratio, R_f	$1/R_f$
103.8	1.833	0.545
124.5	2.000	0.500
131	2.154	0.464
137.3	1.346	0.743
139	1.455	0.688
80.8	1.458	0.686
138.4	2.143	0.467
129.5	2.700	0.370
140.7	2.750	0.364
122	1.500	0.667
138.3	1.250	0.800
119	1.600	0.625
125.6	1.750	0.571
125.3	3.100	0.323
115	1.421	0.704
117.4	2.833	0.353
173.3	1.667	0.600
129	1.875	0.533
136	3.962	0.252
121.3	1.765	0.567
127	2.500	0.400
137.5	2.727	0.367
128.3	1.588	0.630
135.5	1.600	0.625
134.8	2.138	0.468

$\Sigma 1/R_f = 36.574$

$N/(\Sigma 1/R_f) = 1.914$

$N = 70$

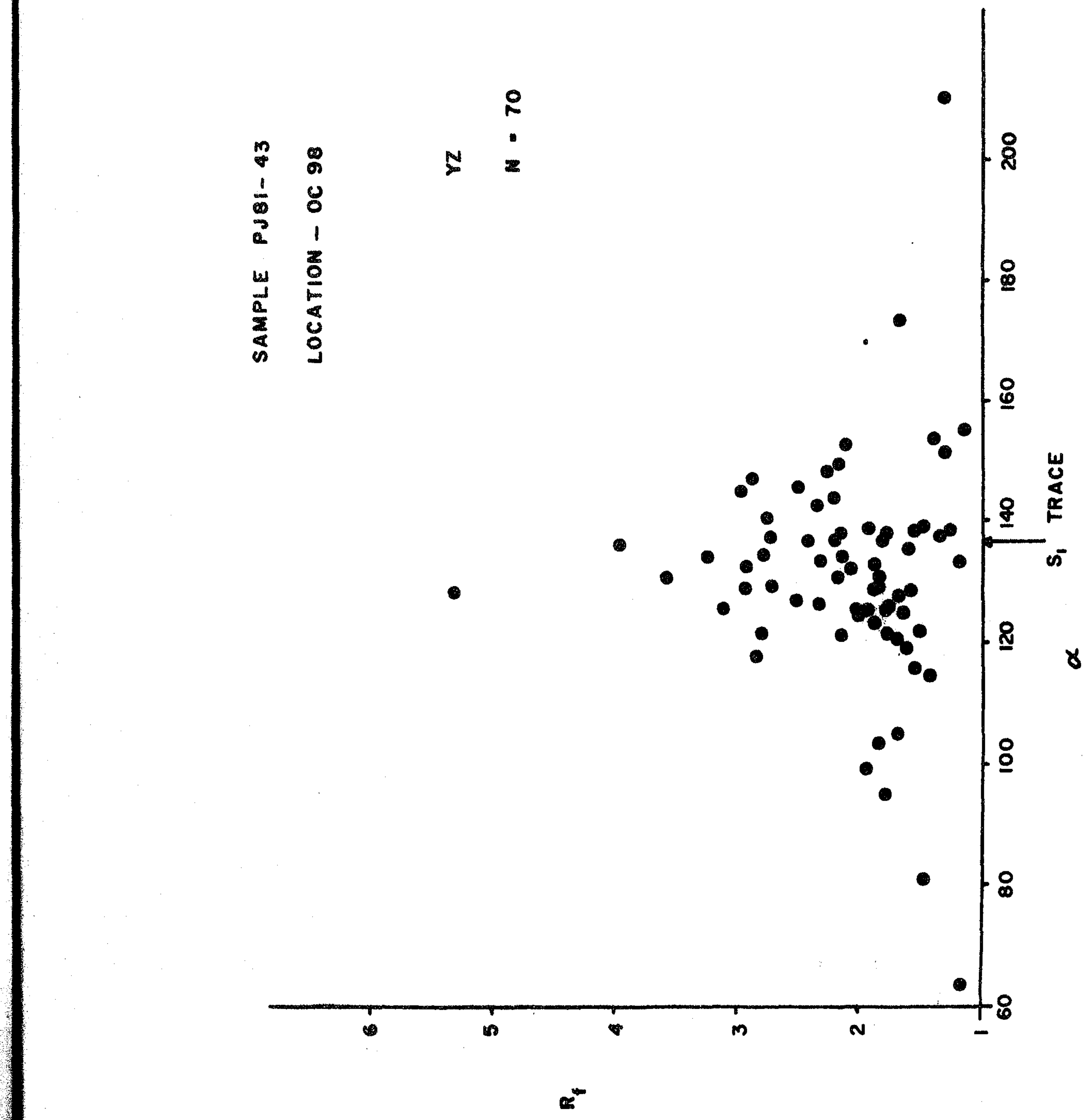

SAMPLE PJ81- 43
LOCATION – OC 98
YZ
N = 70
R_f
1
2
3
4
5
6
60
80
100
120
140
160
180
200
α
S_1 TRACE

Sample PJ81-47 XZ-surface

Location - OC 103

Orientation of S_1 trace = 37.6

Long-axis orient., α	Axial ratio, R_f	$1/R_f$
41.8	3.267	0.306
34.5	2.353	0.425
46	2.000	0.500
44.6	2.267	0.441
40.3	4.500	0.222
41.9	2.750	0.364
38.8	2.381	0.420
38	2.643	0.378
35	4.154	0.241
40.4	2.533	0.395
34.4	2.875	0.348
77.5	1.222	0.818
40.3	9.125	0.110
53.9	1.118	0.895
39.8	2.800	0.357
38.7	2.467	0.405
37	2.833	0.353
30.5	1.867	0.536
40.4	1.917	0.572
41.4	3.000	0.333
39.2	1.529	0.654
34.6	2.545	0.393
38	3.250	0.308
43.3	3.250	0.308
35.8	2.444	0.409
37.3	3.000	0.333
38.2	2.471	0.405
34.9	2.136	0.468
28.5	2.111	0.474
50.7	1.706	0.586
45.8	2.667	0.375
38.2	2.000	0.500
33.7	3.125	0.320
45.3	2.667	0.375
323.2	1.100	0.909
38.7	4.889	0.205
41.7	2.750	0.364
32.8	3.200	0.313
38.5	2.368	0.422
43.6	2.867	0.349
34.6	1.462	0.684
111.3	1.190	0.840
35.9	3.462	0.289
43.8	3.111	0.321
39.6	2.500	0.400

Sample PJ81-47 XZ-surface (cont.)

Long-axis orient., α	Axial ratio, R_f	$1/R_f$
38.7	7.111	0.141
38.2	6.857	0.146
35.1	2.733	0.366
37	8.167	0.122
32.6	2.636	0.379
31.3	2.000	0.500
37	2.043	0.489
116.6	1.182	0.846
38.8	1.692	0.591
29.3	1.750	0.571
44.3	2.360	0.424
39.3	2.500	0.400
40.6	2.500	0.400
37.8	2.083	0.480
37.4	1.833	0.545
41.8	1.824	0.548
41.7	3.000	0.333
31.8	2.700	0.370
36.1	2.571	0.389
27.3	1.727	0.579
41.5	4.143	0.241
52	2.714	0.368
40.9	2.625	0.381
64.6	3.385	0.295
40.5	3.000	0.333

$\Sigma 1/R_f = 29.660$

$N/(\Sigma 1/R_f) = 2.360$

$N = 70$

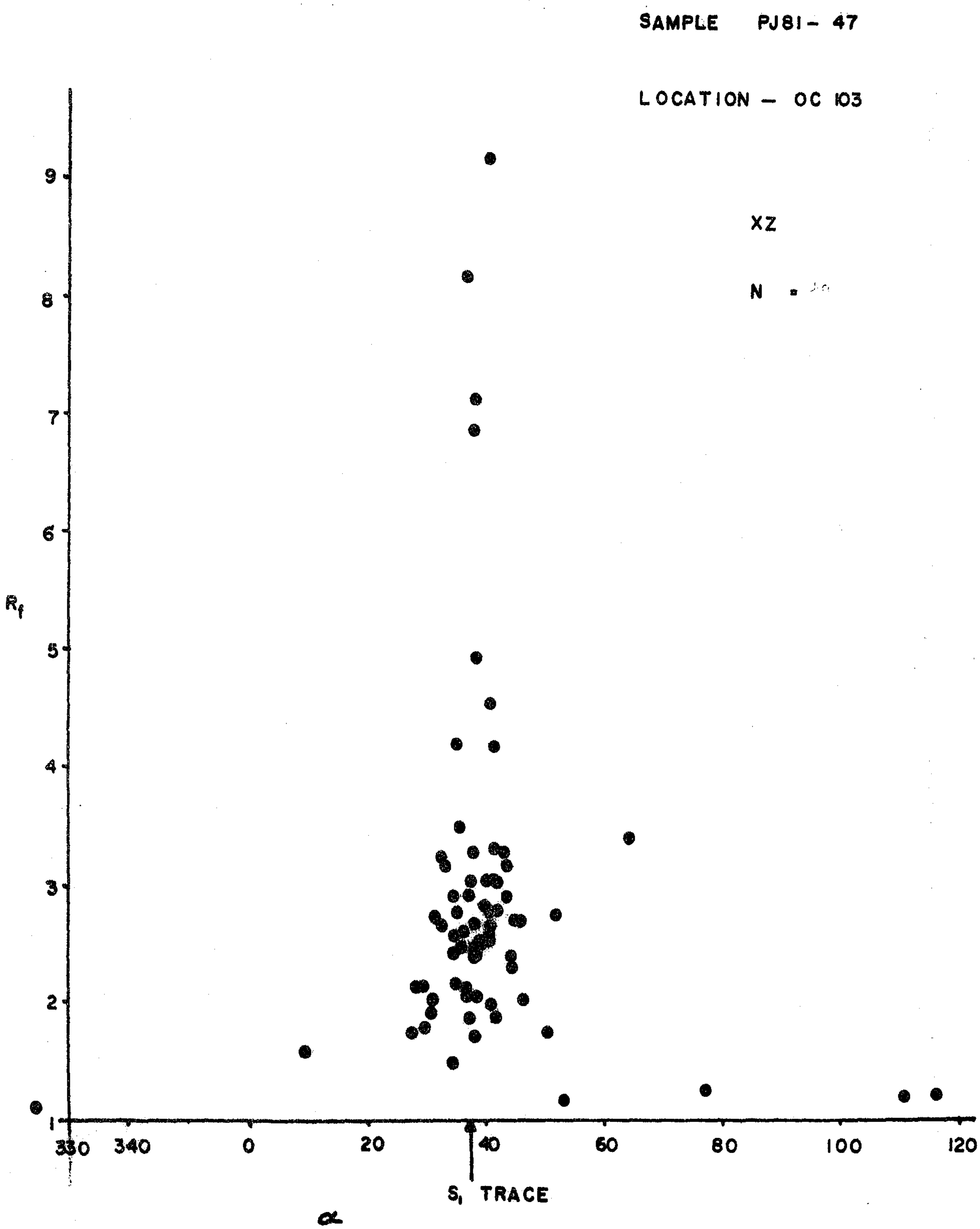
SAMPLE PJ81- 47
LOCATION — OC 103
XZ
N =
9
8
7
6
5
4
3
2
1
R_f
330
340
0
20
40
60
80
100
120
S_1 TRACE
α

Sample PJ81-47 YZ-surface

Location - OC103

Orientation of S_1 trace = 4

Long axis orient., α	Axial ratio, R_f	$1/R_f$
49.7	1.925	0.519
6.3	1.600	o.625
304.1	1.563	0.640
7.6	3.900	0.256
358.5	2.400	0.417
56.5	2.267	0.441
56.8	1.125	0.889
356.2	2.000	0.500
9.5	1.769	0.565
2.4	2.118	0.472
15.8	1.750	0.571
23.3	1.800	0.556
21.2	1.862	0.537
14.8	1.100	0.909
15	1.478	0.676
2.4	2.667	0.375
48.3	1.333	0.750
8	3.300	0.303
85.9	1.727	0.579
2.4	2.700	0.370
13	2.625	0.381
14.6	1.429	0.700
10.8	3.000	0.333
347	2.286	0.438
27.4	3.000	0.333
2.4	2.375	0.421
6.9	3.133	0.319
24.8	1.500	0.667
317.4	1.450	0.690
2.4	2.875	0.348
359	1.778	0.563
0.7	2.000	0.500
11.7	2.375	0.421
356.6	2.667	0.375
352	1.667	0.600
0	2.000	0.500
13.1	1.875	0.533
356.4	1.917	0.522
4.2	2.364	0.423
343	3.500	0.286
357.4	2.875	0.348
8.2	2.000	0.500
355.1	2.500	0.400
18	3.125	0.320

Sample PJ81-47 YZ-surface (cont.)

Long axis orient., α	Axial ratio, R_f	$1/R_f$
352.5	1.875	0.533

$$\sum 1/R_f = 22.404$$

$$N/(\sum 1/R_f) = 2.009$$

$$N = 45$$

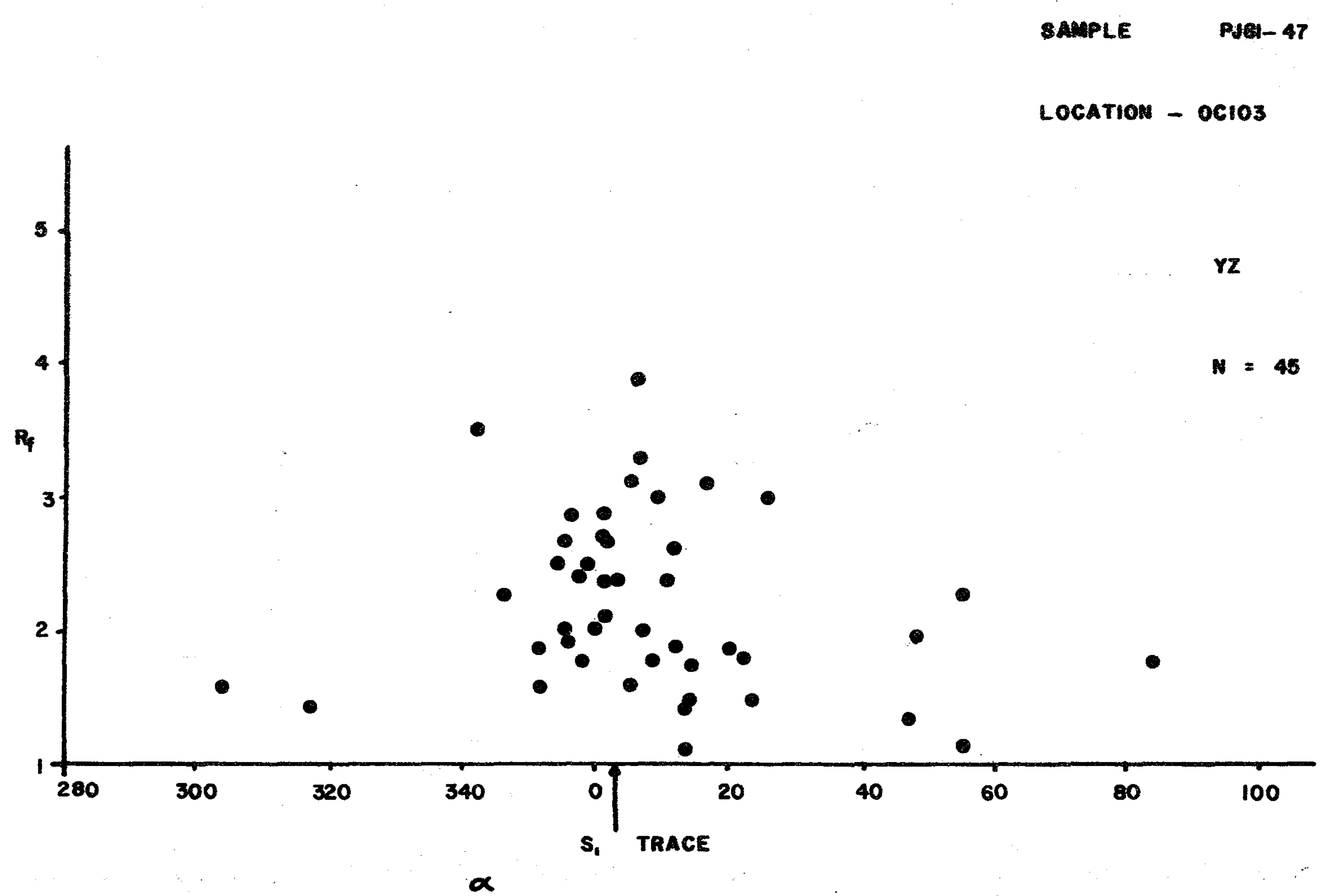
SAMPLE PJGI-47
LOCATION - OC103
YZ
N = 45
R_f
1
2
3
4
5
280
300
320
340
0
20
40
60
80
100
S_1 TRACE
α

REFERENCES

Bathurst, R.G.C., 1975. Carbonate sediments and their diagenesis, Sedimentology Ser., no. 12 (second edition), 677 pp., Elsevier Scientific Publ. Co.

Bishop, D.G. and Force, E.R., 1969. The reliability of graded bedding as an indicator of the order of superposition. J. Geol., v. 77, 346-352.

Borradaile, G.J., 1976. "Structural Facing" (Shackleton's Rule) and the palaeozoic rocks of the Malaguide Complex near Velez Rubio, SE Spain. Koninklijke Nederlandse Akademie van Wetenschappen, Amsterdam, Ser. B, v. 79, 330-336.

Borradaile, G.J., 1978. Transected folds: a study illustrated with examples from Canada and Scotland . Geological Soc. of America Bulletin, v. 89, 481-493.

Borradaile, G.J., 1981. Minimum strain from conglomerates with a ductility constrast. J. Structural Geol., v. 3, 295-298.

Borradaile and Jackson, In Borradaile, G.J., Bayly, B. and Powell, C. McA., 1982. Atlas of deformational and metamorphic rock fabrics. Springer Verlag, Heidelberg, 583 pp.

Borradaile, G.J. and Poulsen, K.H., 1981. Tectonic deformation of pillow lava. Tectonophysics, v. 79, T17-T26.

Cloos, E., 1947. Oolite deformation in South Mountain Fold, Maryland. Geol. Soc. America Bull., v. 58, 843-918.

Cummins, W.A. and Shackleton, R.M., 1955. The Ben Lui Recumbent Syncline (S.W. Highlands). Geol. Mag., v. 92, 353-363.

Dunnet, D., 1969. A technique of finite strain analysis using elliptical particles. Tectonophysics, v. 7, 117-136.

Dunnet, D. and Siddans, A.W.B., 1971. Non-random sedimentary fabrics and their modification by strain. Tectonophysics, v. 12, 307-325.

Durney, D.W., 1972. Solution-transfer, an important geological deformation mechanism. Nature, v. 235, 315-317.

Durney, D.W., 1976. Pressure-solution and crystallization deformation. Phil. Trans. R. Soc. Lond. Ser. A., v. 283, 229-240.

Durney, D.W. and Ramsay, J.G., 1973. Incremental strains measured by syntectonic crystal growth. In Gravity and Tectonics, de Jong, C.A. and Scholten, R. (editors). Van Bemmelan Volume, Wiley, N.Y., 67-96.

Flinn, D., 1962. On folding during three-dimensional progressive deformation. Q. Jl. Geol. Soc. Lond., v. 118, 385-428.

Fumerton, S.L., 1980. Calm Lake area, District of Rainy River. In summary of fieldwork 1980 by the Ont. Geol. Survey, Report No. 8. Milne, V.G., White, O., Barlow, R. and Colvine, S. (editors), 32-35.

Gay, N.C., 1968a. The motion of rigid particles embedded in a viscous fluid during pure shear deformation of the fluid. Tectonophysics, v. 5(2), 81-88.

Gay, N.C., 1968b. Pure shear and simple shear deformation of inhomogeneous viscous fluids. 1. Theory. Tectonophysics, v. 5, 211-234.

Gay, N.C., 1968c. Pure shear and simple shear deformation of inhomogeneous viscous fluids. 2. The determination of the total finite strain in a rock from objects such as deformed pebbles. Tectonophysics, v. 5, 295-302.

Gay, N.C. and Jaeger, J.C., 1975. Cataclastic deformation of geological materials in matrices of differing composition: 1. Pebbles and conglomerates. Tectonophysics, v. 27, 303-322.

Greensmith, J.T., 1978. Petrology of the Sedimentary Rocks. Textbook of Petrology, v. 2, 6th ed., Gorge Allen and Unwin, London, 241 pp.

Hsu, M.Y., 1971. Analysis of strain, shape and orientation of the deformed pebbles in the Seine River area, Ontario. Unpubl. Ph.D. thesis, McMaster University, 167 pp.

Lawson, A.C., 1888. Report on the geology of the Rainy Lake Region. Annual Report, Geol. Surv. Can., Vol. III, 1888, Report F.

Lawson, A.C., 1913. The Archean Geology of Rainy Lake Re-studied. Geol. Survey of Canada, Memoir 40, 115 pp. Accompanied by Map 98A, Scale 1 inch to 1 mile.

Lisle, R.J., 1977a. Clastic grain shape and orientation in relation to cleavage from the Aberystwyth Grits, Wales. Tectonophysics, v. 39, 381-395.

Lisle, R.J., 1977b. Estimation of the tectonic strain ratio from the mean shape of deformed elliptical markers. Geologie en Mijnbouw, v. 56, 140-144.

Lisle, R.J., 1979. Strain analysis using deformed pebbles: the influence of initial shape. Tectonophysics, v. 60, 263-277.

McClay, K.R., 1977. Pressure solution and coble creep in rocks. Jl. Geol. Soc. Lond., v. 134, 71-75.

McEwen, T.J., 1978. Diffusional mass transfer processes in pitted pebble conglomerates. Contrib. Mineral. Petr., v. 67, 405-415.

Mosher, S., 1981. Pressure solution deformation of the Purgatory conglomerate from Rhode Island. J. Geol., v. 89, 37-55.

Poulsen, K.H., Borradaile, G.J. and Kenhlenbeck, M.M., 1980. An inverted Archean succession at Rainy Lake. Can. J. E. Sci., v. 17, 1358-1369.

Powell, C. McA., 1974. Timing of slaty cleavage during folding of precambrian rocks, Northwest Tasmania. Bull. Geol. Soc. Am., v. 85, 1043-1060.

Ramsay, J.G., 1967. Folding and fracturing of rocks. McGraw-Hill, New York, 568 pp.

Robin, P-Y.F., 1977. Determination of geologic strain using randomly oriented strain markers of any shape. Tectonophysics, v. 12, T7-T16.

Schwerdtner, W.M., Stone, D., Osadetz, K., Morgan, J. and Stott, G.M., 1979. Granitoid complexes and the Archean tectonic record in the Southern part of Northwestern Ontario. Can. J. E. Sci., v. 16, 1965-1977.

Shackleton, R.M., 1958. Downward facing structures of the Highland Border. J. Geol. Soc. Lond., v. 113, 361-392.

Shrock, R.R., 1948. Sequence in layered rocks. New York.

Sorby, H.C., 1865. On impressed limestone pebbles, as illustrating a new principle in chemical geology. West Yorks, Geol. Soc. Proc., v. 14, 458-461.

Sorby, H.C., 1908. On the application of quantitative methods to the study of the structure and history of rocks. Quast. J. Geol. Soc., v. 64, 171-232.

Streckeisen, A.L., 1976. To each plutonic rock its proper name. Earth Sci. Rev., v. 12, 1-33.

Turner, F.J. and Weiss, L.E., 1963. Structural analysis of metamorphic tectonites. McGraw-Hill, Toronto, 545 pp.

Wood, J., 1980. Epiclastic sedimentation and stratigraphy in the North Spirit Lake and Rainy Lake areas: a comparison. Precambrian Research, v. 12, 227-256.

Young, W.L., 1960. Geology of the Bennett-Tanner area. Ontario Dept. Mines, Vol. 69, pt. 4, 17 p. Accompanied by map 1960b, Scale 1 inch to 1/2 mile.

FIG. AP-6

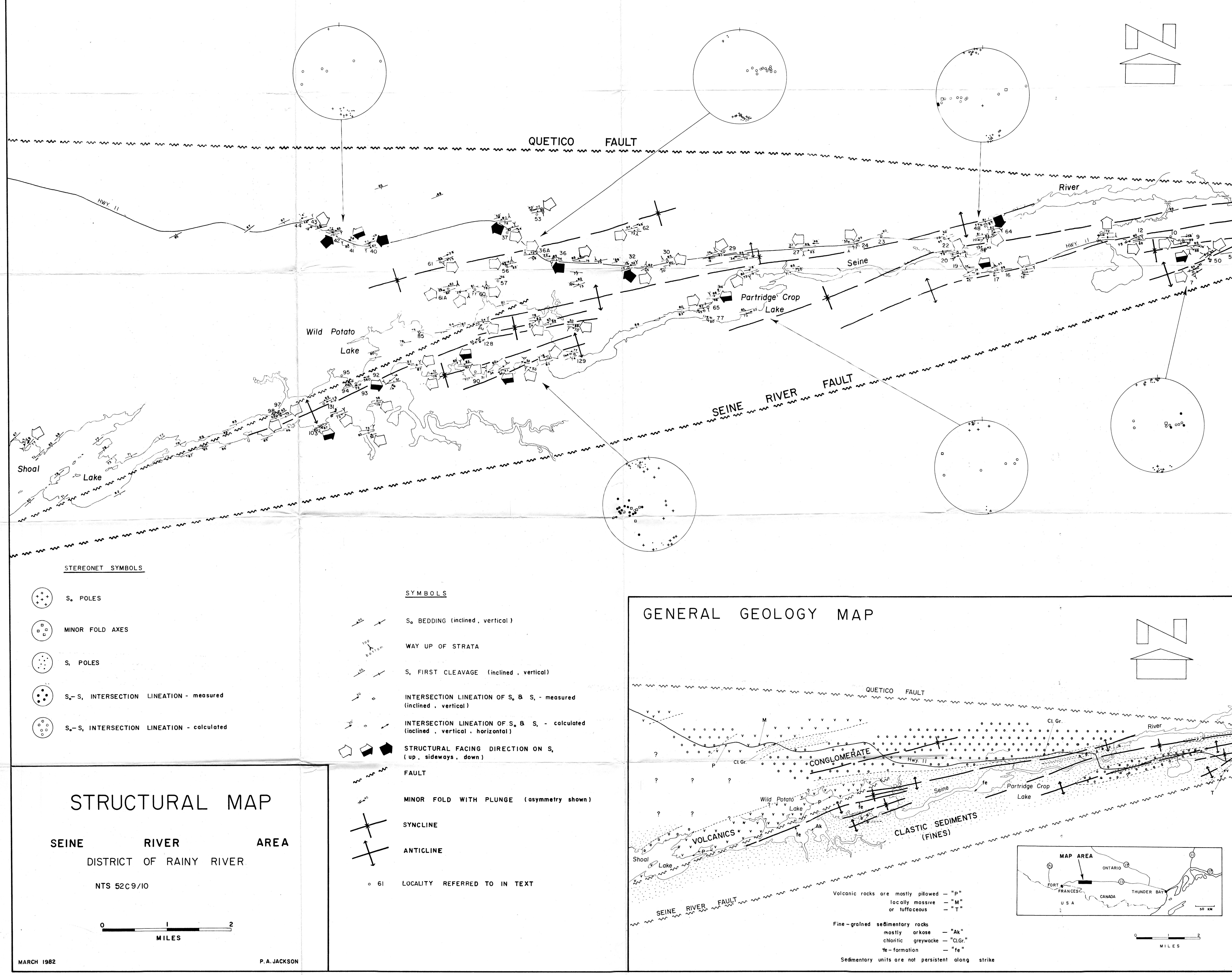

STRUCTURAL MAP

SEINE RIVER AREA

DISTRICT OF RAINY RIVER

NTS 52C9/10

0 1 2 MILES

MARCH 1982

P.A. JACKSON

FIG. AP-7

SCHEMATIC STRUCTURAL DIAGRAM

SEINE RIVER AREA

DISTRICT OF RAINY RIVER

NTS 52C 9/10

MARCH 1982

P.A. JACKSON